

MODELING NONADIABATIC DYNAMICS AT MOLECULE-METAL INTERFACES

Wenjie Dou

A DISSERTATION

in

Chemistry

Presented to the Faculties of the University of Pennsylvania

in

Partial Fulfillment of the Requirements for the

Degree of Doctor of Philosophy

2018

Supervisor of Dissertation

---

Joseph E. Subotnik, Professor of Chemistry

Graduate Group Chairperson

---

Gary A. Molander, Hirschmann-Makineni Professor of Chemistry

Dissertation Committee

Andrew M. Rappe, Blanchard Professor of Chemistry

Marsha I. Lester, Edmund J. Kahn Distinguished Professor

Jessica M. Anna, Professor of Chemistry

MODELING NONADIABATIC DYNAMICS AT MOLECULE-METAL INTERFACES

© COPYRIGHT

2018

Wenjie Dou

This work is licensed under the  
Creative Commons Attribution  
NonCommercial-ShareAlike 3.0  
License

To view a copy of this license, visit

## ACKNOWLEDGEMENT

Graduate school has been very confusing. I would not have gone through graduate school eventually without lots of helps and guidances from many people. Particularly, many thanks to my research advisor Joe Subotnik, who is a great advisor. With great kindness and being very very supportive, he teaches me everything, from writing, communication, presentation all the way to science. I would not have gone that far without he being role model of how to approach science. I would also like to thank Abe Nitzan, who is our close collaborator and effectively my secondary advisor. He is very very patient and has great physical intuition. I will remember his famous saying/question: small (or large parameter) compared to what? Also he got me interested in metal surface during my first year, which becomes the topic of this dissertation. I am very grateful to have such a tremendous pair of advisors in graduate school.

I also want to thank our collaborators Prof. Michael Thoss and his student Christian Schinabeck on electron transport properties study. It was a good collaboration and resulted in fruitful outcomes. I would also like to thank my committee members: Prof. Andrew Rappe, Prof. Marsha Lester and Prof. Jessica Anna. Many thanks to them for providing valuable feedback and special thanks to Prof. Rappe for also being helpful during my postdoc searching.

I would also like to thank students and postdocs in Subotnik Group that provide friendship and helps (though this list is not exhaustive): Brian Landry, Kousik Samanta, Andrew Petit, Amber Jain, Ethan Alguire, Greg Medders, Xinle Liu, Qi Ou, Wenjun Ouyang, Nicole Bellonzi, Gaohan Miao, Zuxin Jin, Theta Chen, Alec Coffman, Tao Li, Hung-Hsuan Teh. All members of Rappe Group and Nitzan group during my time as well as all my friends in graduate school also have my appreciation.

Finally very sincere thanks to my family, who have been caring me so much but also give me freedom to work on my goal.

# ABSTRACT

## MODELING NONADIABATIC DYNAMICS AT MOLECULE-METAL INTERFACES

Wenjie Dou

Joseph E. Subotnik

The coupled electronic-nuclear dynamics at molecule-metal interfaces are fundamental processes that underlie many distinct areas of science: from electrochemistry, chemisorption, heterogeneous catalysis, quantum dots, all the way to molecular conduction. Simulating these coupled dynamics at molecule-metal interfaces is very challenging, due to the breakdown of the Born-Oppenheimer approximation and the inclusion of a manifold of electrons from the metal. Two methods are presented to investigate these nonadiabatic dynamics: a) In the outer sphere regime (weak electronic coupling between molecule and metal), a surface hopping approach is developed to treat nuclear motion classically with electronic motion captured by hopping between different potential energy surfaces; b) In the inner sphere regime (strong electronic coupling between molecule and metal), electronic dynamics are incorporated into a frictional force (i.e. electronic friction) together with a random force. In addition, a natural combination of these two methods called a broadened classical master equation (BCME) is developed. As benchmarked against numerical exact solutions, the BCME works well in both inner and outer sphere regimes. Finally, a universal form of electronic friction is derived. Such a formula unifies many different forms of electronic friction in the literature and allows the inclusion of electron-electron interactions, and can demonstrate interesting Kondo resonances at low temperature.

## TABLE OF CONTENTS

ACKNOWLEDGEMENT . . . . .	ii
ABSTRACT . . . . .	iii
LIST OF ILLUSTRATIONS . . . . .	xvii
CHAPTER 1 : Introduction . . . . .	1
1.1 The Born-Oppenheimer approximation . . . . .	1
1.2 Nonadiabatic dynamics: Tully’s fewest switch surface hopping . . . . .	3
1.3 Nonadiabatic dynamics at molecule-metal interfaces . . . . .	5
1.4 Theory . . . . .	8
1.5 Overview of this dissertation . . . . .	12
CHAPTER 2 : Surface Hopping with A Manifold of Electronic States II: Application to the Many-Body Anderson-Holstein Model . . . . .	14
2.1 Introduction . . . . .	14
2.2 Theory . . . . .	16
2.3 Results and Discussion . . . . .	26
2.4 Conclusions . . . . .	35
2.5 Appendix . . . . .	37
CHAPTER 3 : Surface hopping with a manifold of electronic states, III: transients, broadening and the Marcus picture . . . . .	40
3.1 Introduction . . . . .	40
3.2 Transient dynamics . . . . .	42
3.3 ET rate for the AH model . . . . .	47
3.4 Broadening by the Marcus rate . . . . .	52

3.5	Steady state current . . . . .	53
3.6	Conclusions . . . . .	58
CHAPTER 4 : Frictional effects near a metal surface . . . . .		61
4.1	Introduction . . . . .	61
4.2	Electronic friction . . . . .	63
4.3	Results . . . . .	69
4.4	Conclusions . . . . .	77
4.5	Appendix . . . . .	78
CHAPTER 5 : A broadened classical master equation approach for nonadiabatic dy-		
	namics at metal surfaces: beyond the weak molecule-metal coupling	
	limit . . . . .	83
5.1	Introduction . . . . .	83
5.2	Theory . . . . .	86
5.3	Modified surface hopping procedure . . . . .	91
5.4	Results . . . . .	93
5.5	Conclusions . . . . .	97
5.6	Appendix . . . . .	101
CHAPTER 6 : A broadened classical master equation approach for treating electron-		
	nuclear coupling in non-equilibrium transport . . . . .	109
6.1	Introduction . . . . .	109
6.2	Broadened classical master equation (BCME) . . . . .	111
6.3	QME and bQME . . . . .	117
6.4	Hierarchical Quantum Master Equation (HQME) . . . . .	119
6.5	Results . . . . .	122
6.6	Conclusions . . . . .	127
6.7	Appendix . . . . .	128

CHAPTER 7 : A generalized surface hopping algorithm to model non-adiabatic dynamics near metal surfaces: The case of multiple electronic orbitals	130
7.1 Introduction . . . . .	130
7.2 Equation of motion . . . . .	132
7.3 Surface hopping algorithms . . . . .	135
7.4 Results and Discussion . . . . .	144
7.5 Conclusions . . . . .	148
7.6 Appendix . . . . .	148
CHAPTER 8 : Born-Oppenheimer Dynamics, Electronic Friction, and the Inclusion of Electron-Electron Interactions . . . . .	154
8.1 Introduction . . . . .	154
8.2 Theory . . . . .	157
8.3 Anderson-Holstein model . . . . .	160
8.4 Conclusions . . . . .	162
CHAPTER 9 : Universality of electronic friction I: the equivalence of von Oppen's nonequilibrium Green's function approach and the Head-Gordon-Tully model at equilibrium . . . . .	165
9.1 Introduction . . . . .	165
9.2 Non-Equilibrium Green's Function . . . . .	169
9.3 A model with system-bath separation . . . . .	174
9.4 Discussion . . . . .	178
9.5 Conclusions . . . . .	179
CHAPTER 10 : The universality of electronic friction II: Equivalence of the quantum-classical Liouville equation approach with von Oppen's nonequilibrium Green's function methods out of equilibrium . . . . .	181
10.1 Introduction . . . . .	181
10.2 Quadratic Hamiltonian . . . . .	184

10.3 Agreement of QCLE friction and NEGF friction . . . . .	186
10.4 System-bath separation and Non-Condon effects . . . . .	189
10.5 Conclusions . . . . .	193
10.6 Appendix . . . . .	194
CHAPTER 11 : Conclusions . . . . .	199
BIBLIOGRAPHY . . . . .	200

## LIST OF ILLUSTRATIONS

- FIGURE 1 : NO gas molecule scattering event. When a NO molecule comes near to a Au or Ag metal surface, a free electron can be pulled out from the Fermi sea of the metal, such that NO becomes  $\text{NO}^-$ . Before  $\text{NO}^-$  leaves the interaction region, an electron is pushed back to the metal, and  $\text{NO}^-$  becomes NO again. Such an electron transfer mechanism results in a huge vibrational energy loss for the NO molecule during the scattering event. . . . . 7
- FIGURE 2 : Molecular junctions. When a single molecule is connected to two leads, with a voltage bias applied between the metals, there is an electronic current going through the molecule. The interplay between electron transfer and nuclear motion gives rise to a host of interesting phenomena, such as Frank-Condon blockades in current-voltage curves and heating of the molecule induced by electronic currents. . . . . 8
- FIGURE 3 : Surface hopping view of nonadiabatic dynamics at molecule-metal interfaces. Blue and red curves correspond to two PESs for the diatomic molecule (neutral and charged). By exchanging electrons with the metal surface, a diatomic molecule jumps back and forth between the two potential surfaces. . . . . 11

FIGURE 4 :	How to run SH: We assume that the oscillator (blue ball) has been moving along on the red potential energy surface. (a) At the start of each time step, we generate a random number $\xi$ . If $\xi > \gamma_{red \rightarrow blue}(x)dt$ , (b), the oscillator will continue to move along the red potential energy surface for the next time interval $dt$ . Otherwise, (c), the oscillator will jump and move along the blue surface for the next time interval $dt$ . . . . .	22
FIGURE 5 :	Phonon relaxation: $\Gamma = 0.003$ , $kT = 0.03$ , $\hbar\omega = 0.003$ , $E_d = 0$ , $\mu = 0$ . 10000 trajectories are used. . . . .	27
FIGURE 6 :	Velocity distribution (a) and position distribution (b): $\Gamma = 0.003$ , $kT = 0.03$ , $g = 0.01$ , $\hbar\omega = 0.003$ , $E_d = 0$ , $\mu = 0$ . Red dots represents averages over 10000 trajectories. The blue line is the analytic result from Eqn. 2.19 for (a) and from Eqn. 2.20 for (b). . . . .	28
FIGURE 7 :	Electronic population as a function of impurity energy level: $kT = 0.01$ , $\hbar\omega = 0.003$ . For NRG calculation, band width $D=1$ , and the basis is initialized with 30 boson states, the maximum number of eigenstates kept is $N_s = 512$ , and the logarithmic discretizing parameter is $\Lambda = 2$ . . . . .	29
FIGURE 8 :	Electronic population as a function of renormalized impurity energy level: $kT = 0.2\Gamma$ , $\Gamma = 1$ . The line represents SH results (Eqns. 2.43), and the dots represent NRG results. For the NRG calculation, we set $D = 84\Gamma$ , where $D$ is the band width. The basis is initialized with 40 boson states, the maximum number of eigenstates kept is $N_s = 1500$ , and the logarithmic discretizing parameter is $\Lambda = 2$ . . . . .	30

FIGURE 9 : I-V curves in the limit of small e-ph coupling. For the QME and SH, we take a small value for the e-ph coupling,  $g = 0.02$ . The other parameters are:  $kT = 0.2$ ,  $\hbar\omega = 5$ ,  $\Gamma = 2\Gamma_L = 2\Gamma_R = 1$ ,  $\mu_L = V/2$ ,  $\mu_R = -V/2$ . The Landauer results are for  $g = 0$  as in Eqn. 2.44. . . . . 31

FIGURE 10 : I-V curves. The QME (as given by Eqns. 2.30-2.39 and broadened by Eqns. 2.42,2.45) is represented by lines. Real time path integral results<sup>[1,2]</sup> are represented by dots.  $kT = 0.2$ .  $\Gamma = 2\Gamma_L = 2\Gamma_R = 1$ ,  $\mu_L = V/2$ ,  $\mu_R = -V/2$ ,  $E_d = g^2/\hbar\omega$ . This choice of parameters represents the quantum regime, as can be seen by the non-linear steps in the I-V curve that arise from nuclear quantization. Our classical SH simulations will not be accurate in this regime. . . . 33

FIGURE 11 : I-V curves. Observe the agreement between SH (dots) and QME (lines) in the classical, high temperature limit. At low T, these two approaches disagree (as the QME predicts I-V steps, which SH ignores).  $g = 2$ ,  $\Gamma = 2\Gamma_L = 2\Gamma_R = 1$ ,  $E_d = g^2/\hbar\omega$ ,  $\mu_L = V/2$ ,  $\mu_R = -V/2$ . . . . . 33

FIGURE 12 : I-V curves demonstrating the results from the different formalisms. The other parameters are:  $\Gamma = 2\Gamma_L = 2\Gamma_R = 1$ ,  $\mu_L = V/2$ ,  $\mu_R = -V/2$ ,  $g = 2$ . . . . . 34

FIGURE 13 : Transient dynamics: the impurity electron population as a function of time.  $\Gamma = 1$ ,  $\hbar\omega = 0.3$ , e-ph coupling  $g = 0.75$ ,  $\bar{E}_d = 0$ . Note that SH and nQME agree at high temperatures. The sQME does not show any oscillations in electronic population, whereas the nQME shows transient oscillations which are (empirically) close to the frequency  $\omega$ . At time zero, the phonon is prepared to be equilibrated thermally (assuming the impurity is unoccupied).<sup>[3]</sup> . . . 48

FIGURE 14 :	Transient dynamics: the impurity electron population as a function of time. $kT = 1$ , $\hbar\omega = 0.3$ , e-ph coupling $g = 0.75$ , $\bar{E}_d = 0$ . Note that SH and nQME agree in small $\Gamma$ limit. The sQME does not show any oscillations in electronic population, whereas the nQME shows transient oscillations which are (empirically) close to the frequency $\omega$ . At time zero, the phonon is prepared to be equilibrated thermally (assuming the impurity is unoccupied). <sup>[3]</sup> . . . . .	49
FIGURE 15 :	The equilibrium electron population as a function of the impurity energy level, when $\Gamma$ depends on nuclear coordinate, $\Gamma = \Gamma_0 e^{-Dx^2}$ , $\Gamma_0 = 0.01$ , $kT = 0.01$ , $\hbar\omega = 0.003$ , e-ph coupling $g = 0.0025$ . The Marcus rates appear to be good estimate for a broadening rate. NRG data can be considered nearly exact. <sup>[4,5]</sup> . . . . .	54
FIGURE 16 :	The equilibrium electron population as a function of the impurity energy level, when $\Gamma$ depends on nuclear coordinate, $\Gamma = \Gamma_0 e^{-Dx^2}$ , $\Gamma_0 = 0.01$ , $kT = 0.01$ , $\hbar\omega = 0.003$ , e-ph coupling $g = 0.0075$ . The Marcus rates appear to be good estimate for a broadening rate. NRG data can be considered nearly exact. <sup>[4,5]</sup> . . . . .	55
FIGURE 17 :	The equilibrium electron population as a function of (a) e-ph coupling $g$ and (b) temperature $kT$ . The other parameters are $D = 0$ , $\Gamma_0 = 0.01$ , $\hbar\omega = 0.003$ , $\bar{E}_d = -0.018$ . Note that broadening by the Marcus rate gives the qualitatively correct behavior. NRG data can be considered nearly exact. <sup>[4,5]</sup> . . . . .	56
FIGURE 18 :	I-V curves for different values of $D$ (see Eq. 3.46). Lines from SH, dots from the sQME. $g = 0.005$ , $\hbar\omega = 0.003$ , $kT = 0.01$ , $\Gamma = 2\Gamma_0 = 0.01$ , $\bar{E}_d = 0$ . For large $D$ , we observe negative differential resistance. . . . .	59

FIGURE 19 :	(a) I-V curves with and without an extra phonon bath, (b) the average kinetic energy (effective temperature) of the oscillator as a function of bias. $kT = 0.01$ , $\Gamma_0 = 0.01$ , $D = 0.5$ , $\hbar\omega = 0.003$ , $\bar{E}_d = 0$ , e-ph coupling $g = 0.0075$ , the damping term $\gamma_p = 0.02$ . For weak phonon damping, negative differential resistance goes hand in hand with a voltage-dependent heating. For strong phonon damping, however, the average kinetic energy is independent of voltage and we find no negative differential resistance. . . . .	59
FIGURE 20 :	Potential of mean force (PMF, Eq. 4.24) and electronic friction (Eq. 4.22) as a function of position for the AH model; $V_0$ (Eq. 4.6) and $V_1$ (Eqs. 4.7 and 4.25) are the two diabatic PES's. $g = 0.02$ , $\hbar\omega = 0.003$ , $\Gamma = 0.01$ , $\bar{E}_d = 0$ , $kT = 0.02$ . In Ref. <sup>[6]</sup> , $kT = 0.01$ by mistake, which should be $kT = 0.02$ . Here, the electronic friction is plotted in units of $\frac{g^2\omega}{\Gamma kT}$ . . . . .	68
FIGURE 21 :	Electronic population in the impurity from EF-LD (circles) and SH (lines): (a) long time dynamics, (b) short time dynamics. $g = 0.02$ , $\hbar\omega = 0.003$ , $\Gamma = 0.01$ , $kT = 0.05$ . Note that EF-LD and SH agree only at long times; at short times, EF-LD is unreliable. . . . .	71
FIGURE 22 :	The effect of electronic friction on phonon relaxation. Here, we plot the average kinetic energy as a function of time. $kT = 0.05$ , $\hbar\omega = 0.003$ , $g = 0.02$ , $\bar{E}_d = 0$ . We prepare the initial states satisfying a Boltzmann distribution with a temperature $5kT$ . Note that EF-LD agrees with SH increasingly well as $\Gamma$ increases. . . .	72
FIGURE 23 :	The effect of electronic friction on the momentum-momentum correlation function. $kT = 0.05$ , $\hbar\omega = 0.003$ , $g = 0.02$ , $\bar{E}_d = 0$ . 100 trajectories have been used to calculate the momentum-momentum correlation function. Note that EF-LD agrees better with SH for large $\Gamma$ . . . . .	73

FIGURE 24 :	The effect of electronic friction on the momentum-momentum correlation function. $kT = 0.05$ , $\Gamma = 0.01$ , $\hbar\omega = 0.003$ , $\bar{E}_d = 0$ . 100 trajectories have been used to calculate the momentum-momentum correlation function. Note that EF-LD agrees better with SH when $g$ is smaller. . . . .	74
FIGURE 25 :	(a): Electron transfer rate as a function of $\Gamma$ ; (b): A zoomed in picture of (a) in the range $\Gamma \in [0, 0.01]$ . $g = 0.02$ , $\hbar\omega = 0.003$ , $\bar{E}_d = 0$ , $kT = 0.01$ . The electronic friction varies as $1/\Gamma$ , so that over damped dynamics occur as $\Gamma \rightarrow 0$ . . . . .	75
FIGURE 26 :	Electronic population in the impurity as a function of time with different phonon frictions. $g = 0.02$ , $\hbar\omega = 0.003$ , $\Gamma = 0.01$ , $\bar{E}_d = 0$ , $kT = 0.01$ . . . . .	76
FIGURE 27 :	ET forward rates as function of phonon friction $\gamma$ from SH and EF-LD. $g = 0.02$ , $\hbar\omega = 0.003$ , $\bar{E}_d = 0$ , $kT = 0.01$ . Note the agreement between EF-LD and SH. For large $\gamma$ , we fit the ET rates as $A/\gamma$ (where $A$ is a fitting parameter), which indicates that ET decays as $1/\gamma$ for large friction. . . . .	77
FIGURE 28 :	The energy regimes for different theoretical approaches. All methods treat the nuclei classically, hence $kT > \hbar\omega$ . Depending on how strong the electron-metal coupling ( $\Gamma$ ) is, different methods will be applicable. A broadened CME (BCME) will have the largest range of applicability, connecting the domains of the standard CME and broadened FP (BFP) equation. . . . .	86

FIGURE 29 : Potential surfaces (diabatic and adiabatic, with and without broadening) for the AH model.  $\hbar\omega = 0.003$ ,  $g = 0.015$ ,  $\Gamma = 0.03$ ,  $kT = 0.01$ ,  $\bar{E}_d = 0$  ( $\bar{E}_d \equiv E_d - g^2/\hbar\omega$  is the renormalized energy level). We also plot minus the log of equilibrium total density,  $-kT \ln(A)$ ,  $A(x) = \int dp (P_0(x, p) + P_1(x, p))$  from surface hopping simulation (black dots); the latter quantity agrees with the broadened potential of mean force  $\tilde{V}_{adia}^0$  very well. Diabat 1 corresponds to the molecular level being occupied. Diabat 0 corresponds to the molecular level being unoccupied. . . . . 97

FIGURE 30 : Electronic population as a function of (a) shorter time (b) longer time:  $\Gamma = 0.02$ ,  $\omega = 0.003$ ,  $g = 0.0075$ ,  $kT = 0.01$ ,  $\bar{E}_d = 0.01$  ( $\bar{E}_d \equiv E_d - g^2/\hbar\omega$  is the renormalized energy level). We set  $\hbar = 1$ . We prepare the initial temperature as  $T_i = 5T$  for symmetry with Fig. 31. For notation, FP=Fokker-Planck (unbroadened), BFP=broadened Fokker-Planck, CME=classical master equation (unbroadened), BCME=broadened classical master equation. See Fig. 28. Note that the BCME results agree with CME at short time and BFP at long time; as one would hope. . . . . 98

FIGURE 31 : Average kinetic energy as a function of real time:  $\omega = 0.003$ ,  $g = 0.0075$ ,  $kT = 0.01$ ,  $\bar{E}_d = 0.01$  ( $\bar{E}_d \equiv E_d - g^2/\hbar\omega$  is the renormalized energy level). We set  $\hbar = 1$ . We prepare the initial temperature as  $T_i = 5T$ . Note that the BCME agrees with the CME for small  $\Gamma$ . Same notation as in Fig. 28. . . . . 99

FIGURE 32 : Average position of the oscillator as a function of time.  $\omega = 0.003$ ,  $g = 0.015$ ,  $kT = 0.01$ ,  $\bar{E}_d = 0$  ( $\bar{E}_d \equiv E_d - g^2/\hbar\omega$  is the renormalized energy level). We have set  $\hbar = 1$ . We prepare the initial temperature as  $T_i = T$ .  $x_1$  corresponds to the position that minimizes the energy of the occupied diabat,  $x_1 = -\sqrt{2}g/\hbar\omega$ . The nuclei are initialized either to be in quasi-equilibrium with the electron (Eqs. 5.25-5.26) or to be photoexcited and out of equilibrium with the electron (Eq. 5.35-5.36). Note that the BCME correctly agrees with the CME for small  $\Gamma$  ( $\Gamma \ll kT$ ) and with the BFP for large  $\Gamma$  ( $\Gamma \gg \hbar\omega$ ). Same notation as in Fig. 28. . . . . 100

FIGURE 33 : I-V curves in the classical limit:  $k_B T = 0.01$ ,  $\hbar\omega = 0.003$ . The bQME and bCME agree with HQME almost exactly, whereas the QME and CME fail in the limit of large  $\Gamma$ . Other parameters:  $g = 0.0075$ ,  $\tilde{E}_d = 0$ .  $\mu_L = -\mu_R = \Phi/2$ ,  $\Gamma_L = \Gamma_R = \Gamma/2$ . . . . . 123

FIGURE 34 : Phonon excitation-voltage curves in the classical limit:  $k_B T = 0.01$ ,  $\hbar\omega = 0.003$ . bQME and bCME agree with HQME almost exactly, whereas QME and CME fail in the limit of large  $\Gamma$ . Other parameters:  $g = 0.0075$ ,  $\tilde{E}_d = 0$ .  $\mu_L = -\mu_R = \Phi/2$ ,  $\Gamma_L = \Gamma_R = \Gamma/2$ . . . . . 124

FIGURE 35 : Quantum regime:  $k_B T = 0.005$ ,  $\hbar\omega = 0.02$ . In this limit, a classical treatment fails. Overall the bQME performs well. Other parameters:  $g = 0.03$ ,  $\tilde{E}_d = 0$ .  $\mu_L = -\mu_R = \Phi/2$ ,  $\Gamma_L = \Gamma_R = \Gamma/2$ . . . . . 126

FIGURE 36 : Low temperature:  $\Gamma = 0.01$ ,  $k_B T = 0.004$ . Data from the QME (dashed lines) and bQME (solid lines) is benchmarked against HQME (squares, diamonds, triangles). The QME data shows very sharp step-like features. By contrast, the bQME data shows step-like features that are much less sharp. The current from the bQME data is in closer overall agreement with the HQME, but neither the bQME or the QME is quantitatively accurate here.  $\tilde{E}_d = 0$ ,  $\mu_L = -\mu_R = \Phi/2$ ,  $\Gamma_L = \Gamma_R = \Gamma/2$ . . . . . 127

FIGURE 37 : Diabatic electronic population on the donor ( $\langle \hat{d}_D^+ \hat{d}_D \rangle$ ) and the kinetic energy ( $E_k$ ) as a function of time. The QME results can be considered nearly exact (see Appendix 7.6.4). All the SH algorithms (SH, sec-SH, A-SH) agree well with the QME. In the adiabatic limit (large  $W$  and  $\Gamma$ ), EF-LD works for long-time dynamics.  $kT = 0.01$ ,  $\hbar\omega = 0.003$ ,  $g = 0.0075$ ,  $\epsilon_D = 2E_r$ ,  $E_r = g^2/\hbar\omega$ . . . . . 145

FIGURE 38 : Diabatic electronic population on the donor ( $\langle \hat{d}_D^+ \hat{d}_D \rangle$ ) and the kinetic energy ( $E_k$ ) as a function of time. SH fails to recover the correct equilibrium. Sec-SH does recover the correct equilibrium but fails for early dynamics. Overall, A-SH performs the best among different SH methods.  $kT = 0.01$ ,  $\hbar\omega = 0.003$ ,  $g = 0.0075$ ,  $\epsilon_D = 2E_r$ ,  $E_r = g^2/\hbar\omega$ . . . . . 146

FIGURE 39 : (a) Electronic friction as function of position  $x$  according to both NRG and MFT<sup>[7,8]</sup> calculations at temperature  $T=0.005$ . Note that MFT fails to recover two peaks in the friction. (b) Electronic friction according to NRG at low temperature; note that the two peaks in friction become four peaks in friction at low temperature. (c) The Kondo temperature  $T_K(x)$  as a function of position and the physical temperature  $T(x)$  for which find a peak in friction at position  $x$ . Note that these two temperatures are in rough agreement, as predicted by Langreth<sup>[9]</sup>. (d) The height of the Kondo peak  $\gamma_K$  as a function of temperature; note that these peaks decrease exponentially and vanish at zero Kelvin, in disagreement with Ref.<sup>[9]</sup>. Other parameters  $U = 0.1$ ,  $\Gamma = 0.01$ ,  $E_d = -0.05$ ,  $g = 0.0075$ , bandwidth  $D = 1$ . We have set  $k_B = \hbar = 1$ . . . . . 161

FIGURE 40 : Electronic friction as a function of  $x$  for a single level coupled linearly to a harmonic oscillator. For the nonequilibrium case ( $eV \neq 0$ ), when the Condon approximation holds ( $z = 0$ ), the electronic friction exhibits two peaks corresponding to the resonance of the dot level with each of the two different Fermi levels for the leads:  $\epsilon_b(x) = \mu_L$  and  $\epsilon_b(x) = \mu_R$ . With non-Condon effects ( $z = 1$ ), the electronic friction exhibits a dip at the position  $x = 0$ , where  $V_{k\alpha}(x)$  is maximum. Thus, when we go out of equilibrium and break the Condon approximation, we effectively find three peaks.  $kT = 0.01$ ,  $\lambda = 0.01$ ,  $\Gamma_0^L = \Gamma_0^R = 0.01$ ,  $\hbar\omega = 0.003$ ,  $\epsilon_0 = 0.015$ ,  $\mu_L = -\mu_R = eV/2$ . . . . . 193

## CHAPTER 1 : Introduction

### 1.1. The Born-Oppenheimer approximation

To model molecule-metal interfaces, we consider all electrons and nuclei in the molecule as well as the metal surface, where the total Hamiltonian  $\hat{H}_{tot}$  can be split into the nuclear kinetic energy operator plus the electronic Hamiltonian  $\hat{H}$ :

$$\hat{H}_{tot} = - \sum_{\alpha} \frac{\hbar^2}{2m_{\alpha}} \frac{\partial^2}{\partial R_{\alpha}^2} + \hat{H} \quad (1.1)$$

Here, we use  $\alpha$  to denote nuclear degrees of freedoms, with  $\mathbf{R} = \{R_{\alpha}\}$  being the nuclear configuration. The electronic Hamiltonian  $\hat{H}$  consists of the electronic kinetic energy operator  $\hat{T}_e$ , the electron-electron interaction operator  $\hat{V}_{ee}$ , the electron-nuclei interaction operator  $\hat{V}_{en}$ , and the nuclei-nuclei interaction operator  $\hat{V}_{nn}$ :

$$\hat{H} = \hat{T}_e(\mathbf{r}) + \hat{V}_{ee}(\mathbf{r}) + \hat{V}_{en}(\mathbf{R}, \mathbf{r}) + \hat{V}_{nn}(\mathbf{R}) \quad (1.2)$$

From ab initio point of view, all the interaction terms ( $\hat{V}_{ee}$ ,  $\hat{V}_{en}$  and  $\hat{V}_{nn}$ ) are naturally taken to be Coulombic. We have used  $\mathbf{r}$  to denote electronic coordinates.

According to the Born-Oppenheimer approximation<sup>[10,11]</sup>, because electrons are much lighter and move much faster than nuclei, we should consider electronic dynamics for fixed nuclear configuration  $\mathbf{R}$ . Through ab initio electronic structure calculation, by diagonalizing the electronic Hamiltonian  $\hat{H}$  for fixed nuclear configuration  $\mathbf{R}$ , we get a bunch of electronic states:

$$\hat{H}(\mathbf{R})|\Phi_I\rangle = E_I(\mathbf{R})|\Phi_I\rangle \quad (1.3)$$

Here  $|\Phi_I\rangle$  is the  $I$ th eigenstate of  $\hat{H}$ , which is often called adiabatic state with  $E_I$  being the corresponding adiabatic potential energy surface (PES). The adiabatic states  $|\Phi_I\rangle$  are

orthogonal

$$\langle \Phi_I | \Phi_J \rangle = \delta_{IJ}, \quad (1.4)$$

and  $|\Phi_I\rangle$  represents a complete basis for the electronic wave function, such that when nuclear motion is considered, we can expand the total electron-nuclear wave function  $|\Psi\rangle$  as a series of product of nuclear states  $|\chi_I\rangle$  and electronic states  $|\Phi_I\rangle$ :

$$|\Psi\rangle = \sum_I |\chi_I\rangle |\Phi_I\rangle \quad (1.5)$$

Consider now the total electron-nuclear wave function  $|\Psi\rangle$  that diagonalizes the total Hamiltonian  $\hat{H}_{tot}$ ,

$$\hat{H}_{tot}|\Psi\rangle = E|\Psi\rangle \quad (1.6)$$

Using the orthogonality of the electronic states  $|\Phi_I\rangle$ ,  $|\Psi\rangle$  must satisfy<sup>[12]</sup>

$$-\sum_{\alpha} \frac{\hbar^2}{2m_{\alpha}} \frac{\partial^2}{\partial R_{\alpha}^2} |\chi_I\rangle + E_I |\chi_I\rangle - E |\chi_I\rangle = -\frac{\hbar^2}{2} \sum_J D_{IJ} |\chi_J\rangle + \sum_{\alpha, J \neq I} \frac{\hbar^2}{m_{\alpha}} d_{IJ}^{\alpha} \frac{\partial}{\partial R_{\alpha}} |\chi_J\rangle \quad (1.7)$$

Here,  $d_{IJ}^{\alpha}$  and  $D_{IJ}$  are first and second derivative coupling matrix elements respectively:

$$d_{IJ}^{\alpha} = \langle \Phi_I | \frac{\partial}{\partial R_{\alpha}} | \Phi_J \rangle \quad (1.8)$$

$$D_{IJ} = \sum_{\alpha} \frac{1}{m_{\alpha}} \langle \Phi_I | \frac{\partial^2}{\partial R_{\alpha}^2} | \Phi_J \rangle \quad (1.9)$$

The right hand side (RHS) of the Eq. 1.7 couples different states  $I$  and  $J$ . Under the Born-Oppenheimer approximation, assuming very slow nuclear motion, we can ignore such nonadiabatic coupling and Eq. 1.7 is greatly simplified

$$\hat{H}_{BO}|\chi_I\rangle = E|\chi_I\rangle \quad (1.10)$$

Here, the Born-Oppenheimer Hamiltonian  $\hat{H}_{BO}$  is simply

$$\hat{H}_{BO} = \sum_{\alpha} \frac{\hat{P}_{\alpha}^2}{2m_{\alpha}} + E_I, \quad (1.11)$$

where  $\hat{P}_{\alpha} = i\hbar \frac{\partial}{\partial R_{\alpha}}$  is the momentum operator.

Furthermore, for very heavy nuclei, it is sufficient to assume that the nuclear dynamics are classical, such that we can approximate the Schrodinger equation (Eqs. 1.10-1.11) by the Newtonian equation:

$$m_{\alpha} \ddot{R}_{\alpha} = -\frac{\partial}{\partial R_{\alpha}} E_0 \quad (1.12)$$

In the above equation, we have assumed the nuclei simply move on the ground state PES ( $E_0$ ).

## 1.2. Nonadiabatic dynamics: Tully's fewest switch surface hopping

As shown above, the Born-Oppenheimer (BO) approximation is valid for very slow nuclear dynamics, which ignores derivative couplings between different electronic states entirely. Now let us look at the first derivative coupling closely, which can be rewritten as (using the Hellmann-Feynman theorem),

$$d_{IJ}^{\alpha} = \frac{\langle \Phi_I | \frac{\partial \hat{H}}{\partial R_{\alpha}} | \Phi_J \rangle}{E_J - E_I} \quad (1.13)$$

Note that  $d_{IJ}^{\alpha}$  can be very large when state  $I$  and  $J$  are degenerate,  $E_J = E_I$ . In fact, near a conical intersection<sup>[13-15]</sup>, the derivative coupling diverges, such that the BO approximation breaks down dramatically. Developing reliable and efficient methods to go beyond the BO approximation is one of the central goal in chemical dynamics.

Probably the most commonly used approach to handle nonadiabatic dynamics is fewest switch surface hopping (FSSH) developed by Tully in 1990.<sup>[16]</sup> Generally speaking, according

to Tully's FSSH, one runs classical trajectories on adiabatic PESs. Nonadiabatic effects are realized by stochastic hopping between different PESs through the derivative coupling. To be specific, nuclei are treated classically moving on one PES:

$$m_\alpha \ddot{R}_\alpha = -\frac{\partial}{\partial R_\alpha} E_\lambda \quad (1.14)$$

We have used  $\lambda$  to denote the PES that nuclei move along, which is usually called the active PES.

For the electronic part, using the time dependent coefficient  $c_I(t)$ , we expand the total electronic wave function as

$$|\Psi_e\rangle = \sum_I c_I(t) |\Phi_I\rangle \quad (1.15)$$

We can recover the equation of motion (EOM) for the coefficients  $c_I(t)$  by plugging  $|\Psi_e\rangle$  into the time dependent Schrodinger equation,

$$\dot{c}_I = -\frac{i}{\hbar} E_I c_I - \sum_{\alpha J} \dot{R}_\alpha d_{IJ}^\alpha c_J \quad (1.16)$$

It is convenient to define the electronic density as  $\sigma_{IJ} = c_I c_J^*$ . From Eq. 1.16, the EOM for  $\sigma_{IJ}$  is

$$\dot{\sigma}_{IJ} = -\frac{i}{\hbar} (E_I - E_J) \sigma_{IJ} - \sum_{\alpha K} \dot{R}_\alpha (d_{IK}^\alpha \sigma_{KJ} - \sigma_{IK} d_{KJ}^\alpha) \quad (1.17)$$

Note that the derivative coupling matrix element  $d_{IK}^\alpha$  naturally appears. Obviously, the derivative coupling causes electronic transitions between the two adiabatic states  $|\Phi_I\rangle$  and  $|\Phi_J\rangle$ ; for instance, if we look at the population of the electronic density, we find

$$\dot{\sigma}_{II} = -\sum_{\alpha J} \dot{R}_\alpha (d_{IJ}^\alpha \sigma_{JI} - \sigma_{IJ} d_{JI}^\alpha) \quad (1.18)$$

Assuming the nuclei is moving on state  $I$  ( $\lambda = I$ ), the decay rate of  $\sigma_{II}$  (Eq. 1.18) yields the hopping rate  $k_{I \rightarrow J}$  from state  $|\Phi_I\rangle$  to state  $|\Phi_J\rangle$ . Tully guessed the hopping rate to be

$$k_{I \rightarrow J} = \Theta \left( -2\text{Re} \sum_{\alpha} \dot{R}_{\alpha} d_{JI}^{\alpha} \frac{\sigma_{IJ}}{\sigma_{II}} \right) \quad (1.19)$$

Here we define  $\Theta(x)$  function as:

$$\Theta(x) = \begin{cases} x, & \text{if } x \geq 0 \\ 0, & \text{if } x < 0 \end{cases} \quad (1.20)$$

Finally, when hops occur, Tully postulated to rescale momentum to conserve energy. See Refs. [16, 17] for details.

Since 1990, Tully's FSSH has been widely used to study a host of nonadiabatic effects in gas phase or in solution, e.g. photochemistry, electron and energy transfer, proton coupled electron transfer. In spite of these successes, however, a few more words on FSSH are appropriate. First, note that when Tully originated the FSSH ansatz, such a scheme was not rigorously derived. Later, after the quantum-classical Liouville equation (QCLE) was introduced<sup>[18–20]</sup>, several groups found a deep connection between the QCLE and FSSH,<sup>[17,21,22]</sup> especially involving the momentum rescaling. Second, Tully's FSSH suffers decoherence issues due to the use of pure electronic states. In fact, Tully was clearly aware of this issue even in his original paper. Over the years, great efforts have been made to resolve the decoherence issue. In particular, our group came up with an Augmented FSSH (AFSSH) algorithm, which is parameter free and well connected to the QCLE. With such decoherence scheme, AFSSH can recover the renowned Marcus rate for electron transfer between a donor and acceptor.<sup>[23]</sup>

### 1.3. Nonadiabatic dynamics at molecule-metal interfaces

FSSH is a very efficient way to handle nonadiabatic dynamics with a handful of electronic states, such as molecules in gas phase or in solution. However, the computational cost of

FSSH dramatically increases when number of electronic states becomes large. Obviously, since a metal contains  $\sim 10^{23}$  electrons, a naive implementation of FSSH would be useless for modeling nonadiabatic dynamics at molecule-metal interfaces. That being said, many experiments already indicate that nonadiabatic effects can be very significant at molecule-metal interfaces, and so we need new methods.

### *1.3.1. One example: NO molecules scattering from metal surface*

One example of nonadiabatic effects at molecule-metal interfaces can be seen from vibrational relaxation during a scattering event. In a series of experiments, Wodtke and co-workers have managed to measure the vibrational relaxation of an NO molecule after scattering from metal surfaces.<sup>[24]</sup> Before scattering with the metal, they prepare NO molecules in highly vibrationally excited states. After scattering from the gold metal surface, they find that reflected NO molecules have a much lower vibrational energy. The energy loss is about 1.5eV. They postulate that this huge amount of energy loss is due to electronic effects instead of interactions with surface atoms, as there is an energy mismatch between the Debye frequency of the surface atoms and the NO's energy loss. Such a hypothesis can be further confirmed by scattering NO off an insulator, LiF, as in this case, Wodtke et al find that most of NO molecules stay in their initial vibrational states, i.e. no large amount of vibrational loss is found.

One mechanism that explains the energy loss during the scattering events is based on an electron transfer process. A metal contains many free electrons. When a NO molecule approaches a metal, an electron can be easily pulled out of the metal, such that NO becomes  $\text{NO}^-$ . Before  $\text{NO}^-$  leaves the interaction region, an electron is extracted back to the metal, and  $\text{NO}^-$  becomes NO again. Such an electron transfer process can result in a huge vibrational energy loss for the NO molecule during the scattering event. Moreover, unlike a metal, an insulator does not contain free electrons; no electron transfer is allowed during the scattering event, such that there is no huge amount of energy loss.<sup>[25]</sup> Thus, this interpretation is consistent with the experiments.

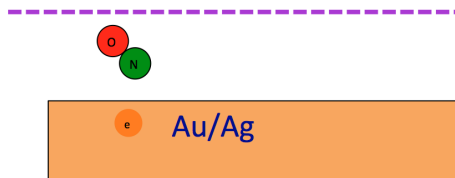


Figure 1: NO gas molecule scattering event. When a NO molecule comes near to a Au or Ag metal surface, a free electron can be pulled out from the Fermi sea of the metal, such that NO becomes  $\text{NO}^-$ . Before  $\text{NO}^-$  leaves the interaction region, an electron is pushed back to the metal, and  $\text{NO}^-$  becomes NO again. Such an electron transfer mechanism results in a huge vibrational energy loss for the NO molecule during the scattering event.

Given this interpretation, NO scattering is a nonadiabatic process as there is electron transfer between the molecule and metal surface. Beside vibrational DoFs, nonadiabatic effects can also be seen from the translation energy loss when  $H$  atoms scatter from metal surface. This nonadiabatic translation energy loss promotes  $H$  atoms adsorbing on metal surfaces. See Ref. [26] for details.

### 1.3.2. Other examples: heterogeneous catalysis, molecular junctions and electrochemistry

The scattering events mentioned above involve molecules interacting with one metal, which can be seen as a case of dynamics under equilibrium conditions. Similarly, nonadiabatic effects at molecule-metal interfaces are very important for many other chemical reactions, e.g. chemisorption, heterogeneous catalysis, etc.

Under nonequilibrium conditions, i.e multiple metals at different temperatures and/or with voltage bias, nonadiabatic effects can be even more dramatic. One such an example is a molecular junction, where a single molecule is connected to two metals. A voltage bias can be applied between the metals, resulting in a nonequilibrium electronic current running through the molecule. The interplay between the electronic transfer and nuclear motion gives rise to a host of interesting nonadiabatic phenomena. For example, on the one hand, the vibrational DoFs of the molecule can affect electronic tunneling, i.e. leading to a Frank-Condon blockade in the current-voltage curve.<sup>[27–29]</sup> On the other hand, an electronic

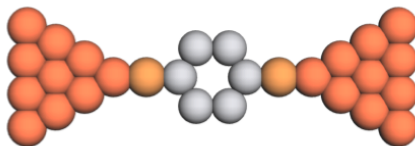


Figure 2: Molecular junctions. When a single molecule is connected to two leads, with a voltage bias applied between the metals, there is an electronic current going through the molecule. The interplay between electron transfer and nuclear motion gives rise to a host of interesting phenomena, such as Frank-Condon blockades in current-voltage curves and heating of the molecule induced by electronic currents.

current can directly affect the vibrational DoFs of the molecules, such as heating or photo emission.<sup>[30–33]</sup>

Another out of equilibrium application is electrochemistry, which convert electrical energy into chemical energy or vice versa. In case of electrochemistry, things are much more complicated than in the gas phase, because different species of molecules or ions are not only interacting with the metal surface but also interacting with each other. Typically BO adiabatic molecule dynamics are used to study the electrochemical solvents. Electron transfer processes are then studied afterwards using free energy curves and Marcus theory.<sup>[34–36]</sup> Treating nonadiabatic electron transfer and solvent molecular dynamics on equal footing is not available yet.

## 1.4. Theory

In this dissertation, I have made early strides as far as generating models for studying nonadiabatic dynamics at metal surfaces. Here, the work horse is the Anderson-Holstein model.

### 1.4.1. Anderson-Holstein model

The Anderson-Holstein (AH) model gives the simplest possible description of the molecule-metal interfaces. According to the AH model, the electronic Hamiltonian  $\hat{H}$  is divided into

the system Hamiltonian  $\hat{H}_s$ , bath Hamiltonian  $\hat{H}_b$ , and interaction Hamiltonian  $\hat{H}_I$ :

$$\hat{H} = \hat{H}_s + \hat{H}_I + \hat{H}_b \quad (1.21)$$

$$\hat{H}_s = \epsilon_d(\mathbf{R})\hat{d}^+\hat{d} + U_0(\mathbf{R}) \quad (1.22)$$

$$\hat{H}_b = \sum_k \epsilon_k \hat{c}_k^+ \hat{c}_k \quad (1.23)$$

$$\hat{H}_I = \sum_k V_k(\mathbf{R})(\hat{d}^+ \hat{c}_k + \hat{d} \hat{c}_k^+) \quad (1.24)$$

Here,  $\hat{H}_s$  describes a molecule with an orbital  $d$  and an nuclear potential  $U_0(\mathbf{R})$ .  $\hat{H}_b$  describe the metal with a manifold of electronic orbital  $k$ . The interaction  $\hat{H}_I$  between the molecule and metal is bilinear.

The AH model is very difficult to solve. One reason is that the metal (bath) consists of a manifold of electronic states with typically  $\sim 10^{23}$  electrons. Tully’s FSSH cannot be applied to study that many electronic states. Another reason is that the AH model has multiple energy scales, e.g. the energy scale of electronic motion, the energy scale of nuclear motion, temperature  $kT$  et al. Treating multiple energy scales on equal footing can be very challenging.

To study such nonadiabatic dynamics at molecule-metal interfaces, in this dissertation, we develop and implement two main methods: classical master equation/surface hopping and electronic friction.

#### 1.4.2. *Electronic friction*

The most commonly used method to treat nonadiabatic dynamics at molecule-metal interface is so-called “electronic friction”. As we can see from the NO scattering experiments above, nonadiabatic electronic transfer results in energy relaxation of vibrational DOFs. Such energy relaxation can be effectively seen as a frictional effect on nuclear motion. Hence, electronic friction and associated random force are added to the Newtonian equation, acting effectively as a correction to the BO approximation, resulting in a Langevin

equation:

$$-m_\alpha \ddot{R}_\alpha = -\bar{F}_\alpha + \sum_\nu \gamma_{\alpha\nu} \dot{R}_\nu - \zeta_\alpha(t) \quad (1.25)$$

Here,  $\bar{F}_\alpha$  is the mean force (or the BO force, see Eq. 1.12),  $\gamma_{\alpha\nu}$  is the friction tensor, and  $\zeta_\alpha(t)$  denotes a random force. At equilibrium, the random force satisfies the following statistics:

$$\langle \zeta_\alpha(t) \rangle = 0, \quad \langle \zeta_\alpha(t) \zeta_\nu(t') \rangle = kT \gamma_{\alpha\nu} \delta(t - t') \quad (1.26)$$

The above relationships are also called the second fluctuation-dissipation theorem. In the equilibrium case, at zero temperature and without electron-electron interaction, the friction tensor can be rewritten as<sup>[8]</sup>

$$\gamma_{\alpha\nu} = \pi \hbar \sum_{pq} d_{pq}^\alpha d_{qp}^\nu (\epsilon_q - \epsilon_p) \delta(\epsilon_F - \epsilon_p) \delta(\epsilon_F - \epsilon_q) \quad (1.27)$$

Here  $p$  and  $q$  are self consistent field (SCF) orbitals on (a mean-field level) that diagonalizes electronic Hamiltonian  $\hat{H}$  effectively, and  $\epsilon_F$  is the Fermi levels.

Electronic friction, as a first order correction to the BO approximation, can be used to describe not very strong nonadiabatic coupling. For many experiments, this assumption of weak nonadiabaticity is not valid. For example, electronic friction cannot be used to describe NO scattering experiments quantitatively correctly. Furthermore, in a set of following experiments, Wodtke and co-workers have shown that when Cs atoms are used to lower the work function of a gold surface, hot electrons emerge depending on the energy of the incoming NO molecules.<sup>[37]</sup> Such strong nonadiabatic effects must be treated within an electron transfer picture, which leads us to a separate, classical master equation/surface hopping approach.

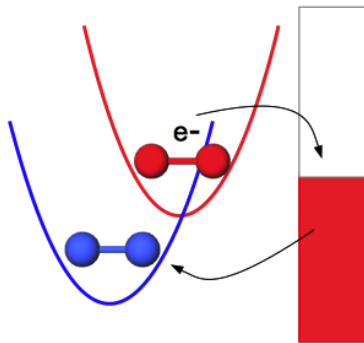


Figure 3: Surface hopping view of nonadiabatic dynamics at molecule-metal interfaces. Blue and red curves correspond to two PESs for the diatomic molecule (neutral and charged). By exchanging electrons with the metal surface, a diatomic molecule jumps back and forth between the two potential surfaces.

#### 1.4.3. Classical master equation/surface hopping

Our second method is a classical master equation/surface hopping. As mentioned above, the NO scattering experiments are well described within an electron transfer picture. Combined with the AH model Eqs. 1.21-1.24, with the  $d$  orbital in the molecule being the empty orbital (NO) or occupied orbital ( $\text{NO}^-$ ), there are two different diabatic potential energy surfaces  $U_0(\mathbf{R})$  and  $U_0 + \epsilon_d(\mathbf{R})$ . When NO becomes  $\text{NO}^-$  or vice versa, the nuclear dynamics can be described as hopping between the two PESs. In such a picture, we can derive a classical master equation, where such hopping effects are given explicitly. And in the end, just as for Tully's FSSH, we find ourselves running trajectories on two PESs, with stochastic hops between them. Different from Tully's FSSH, however, our hopping is due to molecule-metal interaction instead of the derivative coupling. Furthermore, when hops occur, we do not rescale momentum to conserve energy. Physically, this difference is because we are dealing with an open quantum system.

Throughout this dissertation, we will use classical master equation/surface hopping as well as electronic friction to tackle nonadiabatic dynamics at molecule-metal interfaces. We will also show the connections between as well as the strengths and weaknesses possessed by the two methods. Finally, we propose a method that merge the two methods together.

## 1.5. Overview of this dissertation

In Chapter 2, starting from the Anderson-Holstein model, in the weak coupling regime, we derive a classical master equation to describe the coupled electron-nuclear dynamics of a molecule with a single level near metal surfaces. We further propose a surface hopping like method to solve the CME, i.e. we evolve nuclei on one of the two diabatic PESs with stochastic hops between the two PESs. We find that, no matter how we prepare initial states, the surface hopping solution admits a unique steady state solution that obeys detailed balance. We also propose a simple broadening scheme that go beyond weak coupling regime. The surface hopping scheme can be easily extended to out of equilibrium case with electronic current running through the molecule.

In Chapter 3, we further explore the transit dynamics of a surface hopping solution. Such a surface hopping scheme agrees well with a quantum solution at relatively high temperatures. We find that surface hopping recovers the Marcus rate for electron transfer at a metal surface. By incorporating a position dependent molecule-metal interaction, surface hopping can further yield negative differential resistance.

In Chapter 4, we map the CME onto a Fokker-Planck equation, with a potential of mean force and electronic friction. The corresponding dynamics are Langevin dynamics, i.e. a Newtonian equation with a velocity dependent force and random force. Effectively, the fast electron transition can be replaced by a frictional effect and a fluctuating force. The frictional force and random force naturally obey detailed balance, guaranteeing that nuclear motion will reach thermal equilibrium. We also explore the effect of phonon friction on the electron transfer rate. Furthermore, we make a connection between our form of friction and other forms of electronic friction, particularly the Head-Gordon Tully (HGT) friction.

In Chapter 5, motivated by the mapping in Chapter 4, by modifying the potential of mean force, we incorporate broadening effects into our CME, resulting in a broadened CME (bCME) that works well in both weak and strong coupling regimes. In the weak coupling

regime, the BCME reduces to the CME. and in the strong coupling regime, the BCME reduces to a FP equation moving on a broadened potential of mean force.

In Chapter 6, we apply the BCME to study electron transport properties. As benchmarked by numeral exact solution, the BCME agrees with HEOM in both strong and weak coupling limits, in adiabatic and nonadiabatic limit. Such a broadening scheme works very well even in the low temperature case.

In Chapter 7, we go beyond a single molecular level, dealing with multiple levels. We embed the quantum-classical Liouville equation into a classical master equation, resulting in a QCLE-CME. Such a QCLE-CME is naturally a combination of Tully's FSSH with our surface hopping. We also include decoherence. Such a surface hopping scheme is a very powerful means to model electronic transfer within a molecule and electron transfer between the molecule and metal.

In Chapter 8, from the QCLE, we derive a very general form of electronic friction. This form of electronic friction unifies a variety of different frictional forms found in the literature. As shown later, almost all other forms reduce to this very general QCLE form, which allows us to include the effects of electron-electron interactions. At low temperature, we show that the electronic friction can exhibit interesting Kondo resonances.

In Chapter 9, we further compare our form of electronic friction with other forms in the literature and we demonstrate a single uniform of electronic friction at equilibrium.

In Chapter 10, we further study the QCLE expression for electronic friction, and now we focus on the out of equilibrium case. We compare our form of electronic friction to von Oppen's nonequilibrium Green's function results, and obtain complete equivalence, confirming the existence of a single unique electronic friction tensor.

We conclude in Chapter 11.

## CHAPTER 2 : Surface Hopping with A Manifold of Electronic States II: Application to the Many-Body Anderson-Holstein Model

This chapter was adapted from Ref. [38]

### 2.1. Introduction

Surface hopping (SH) has proven to be a very successful approach for treating nuclear-electronic coupling<sup>[16,39]</sup>. When it began in 1971, the most basic idea of Tully-Preston surface hopping was to propagate classical nuclei, while switching the active force field whenever nuclei move through avoided crossings<sup>[39]</sup>. Later, Tully extended the notion of hopping at crossings to a continuous probability of hopping that was calculated at every time step (e.g., the so-called “Fewest Switches Surface Hopping” (FSSH)<sup>[16]</sup>). More recently, there has been a great deal of theoretical work trying to fix up the decoherence failures of the FSSH algorithm<sup>[23,40–58]</sup>, and to extract spectroscopic information from SH trajectories<sup>[59–63]</sup>. There has also been a great of work exploring the foundations of the SH approach<sup>[17]</sup> vis-a-vis the quantum classical Liouville equation<sup>[18,20,22,64]</sup>.

As applied in the literature, SH has been used to model a host of experimental systems, including energy transfer<sup>[65]</sup>, proton-coupled electron transfer<sup>[66]</sup>, and electronic relaxation<sup>[67]</sup>. Of particular interest to this article are recent studies by Tretiak<sup>[68]</sup> and Prezhdo<sup>[69]</sup>, who have studied energy transfer in extended organic chromophores and electron transfer to semiconductors, respectively. For both cases, one must deal with a manifold of electronic states. In general, however, the FSSH algorithm has usually been restricted to studying isolated molecules in solvents with only a handful of electronic states.<sup>1</sup> Thus far, the most important exception to this general rule was the pioneering “Independent Electron Surface Hopping (IESH)” model of Shenvi, Roy and Tully<sup>[71–73]</sup>, who studied NO scattering off of a gold surface. Shenvi *et al* suggested discretizing a continuum of adiabatic electronic levels to simulate electronic friction in a metal; and by running FSSH on a large number of

---

<sup>1</sup>Li *et al* recently explored a scheme for mixing FSSH dynamics with mean-field Ehrenfest dynamics to handle the particular case of one well-defined ground state interacting with a manifold of excited states.<sup>[70]</sup>

electronic states, Shenvi *et al* were able to correctly describe vibrational relaxation of the NO molecule. In a slightly different context, Preston and Cohen also proposed a “surface leaking” approach for treating the decay of an electronic state into a continuum of electronic levels but, to our knowledge, surface leaking has thus far only been applied to study loosely bound anions.<sup>[74,75]</sup>

In a companion paper, we have discussed a straightforward extension of FSSH to treat model one-electron systems. In the present paper, we focus on a many-body problem and offer a simple (but generalizable) SH approach describing a molecule absorbed on a metal surface. We will study the simplest case: a single impurity level coupled to a single phonon as well as one or two electronic (fermionic) baths (which is known as the Anderson-Holstein model<sup>[76,77]</sup>). For the case of one electronic bath, we study relaxation to equilibrium. For the case of two electronic baths, with different Fermi levels, we will study the steady state transport, where some features of inelastic scattering are visible<sup>[78,79]</sup>. The approach in this paper will not rely on the assumption of small electron-phonon couplings and, as such, should go beyond standard models of electronic friction acting on molecules at metal surfaces<sup>[80–82]</sup>. Furthermore, in the future, it will be important to include a bath of external vibrations as well, which can be achieved easily through a random force in our surface (or, more formally, through a Fokker-Planck equation<sup>[83]</sup>). For the present article, we will restrict ourselves to the simple Anderson-Holstein model (without any explicit nuclear friction) and we will demonstrate the power of a SH approach to recover many dynamical phenomena for this simple system.

An outline of this paper is as follows. In Section 2.2, we will present the necessary theory. First, we will motivate and justify our SH approach based on a classical master equation (CME) for the nuclear-electronic subsystem. We will do this both for the cases of equilibrium (one electronic bath) and out-of-equilibrium (two electronic baths) dynamics. Second, for concreteness, we will then give a step-by-step flowchart for our SH algorithm. Third, we will discuss briefly quantum master equations (QME) and numerical renormalization group

(NRG) theory, which represent alternative formalisms against which we can benchmark our dynamics. In section 2.3, we will present results showing the power of this simple model. We conclude in section 2.4.

## 2.2. Theory

### 2.2.1. Model Hamiltonian

The Anderson-Holstein Hamiltonian involves an electronic impurity level coupled to (i) a phonon degree of freedom, and (ii) a continuum of electronic levels. One can think of the impurity level as an atomic or molecular orbital that can give an electron to or get an electron from a metal surface. A common example would be an anion near a charged metal surface, e.g. an electrochemical interface. We group the impurity and phonon together as the system ( $H_s$ ), and the continuous levels of electrons to be the bath ( $H_b$ ). The interaction between them ( $H_c$ ) is bilinear:

$$H = H_s + H_b + H_c \quad (2.1)$$

$$H_s = E_d d^\dagger d + g(a^\dagger + a)d^\dagger d + \hbar\omega(a^\dagger a + \frac{1}{2}) \quad (2.2)$$

$$H_b = \sum_k (\epsilon_k - \mu) c_k^\dagger c_k \quad (2.3)$$

$$H_c = \sum_k V_k (c_k^\dagger d + d^\dagger c_k) \quad (2.4)$$

Here,  $d^\dagger$  ( $d$ ),  $a^\dagger$  ( $a$ ),  $c_k^\dagger$  ( $c_k$ ) are creation (annihilation) operators on the impurity electron, phonon and metal electrons respectively.  $E_d$  is the impurity energy level,  $\omega$  is the frequency of the phonon,  $g$  is the coupling between the impurity and the phonon.  $\epsilon_k$  is an energy level of the bath, which has Fermi level  $\mu$ , and  $V_k$  is the coupling between the impurity and the bath. The interaction between the impurity and bath determines the hybridization function  $\Gamma$ ,

$$\Gamma(\epsilon) = 2\pi \sum_k |V_k|^2 \delta(\epsilon - \epsilon_k) \quad (2.5)$$

In the following, we will assume that  $\Gamma$  is a constant (the wide band approximation). In developing a SH model of the Anderson-Holstein model, it will be convenient to replace  $a^+$  and  $a$  with the (dimensionless) position  $x$  and momentum  $p$  coordinates, so that the system Hamiltonian is written as,

$$H_s = E_d d^+ d + \sqrt{2} g x d^+ d + \frac{1}{2} \hbar \omega (x^2 + p^2) \quad (2.6)$$

### 2.2.2. Classical Master Equation

In a surface-hopping based description of semiclassical dynamics, the critical input is the choice of classical potential surfaces and the implementation of the surface hopping algorithm. Here we work in the diabatic representation of the electronic state of the system. In this representation  $d^+ d$  is either 0 or 1, that is, the impurity can be either unoccupied (denoted as state 0) or occupied (state 1). The corresponding diabatic potential surfaces for the nuclei are

$$V_0(x) = \frac{1}{2} \hbar \omega x^2 \quad (2.7)$$

$$V_1(x) = \frac{1}{2} \hbar \omega x^2 + \sqrt{2} g x + E_d \quad (2.8)$$

The basic premise of our SH approach is to model the electronic bath implicitly; all of the information required about it are the rate  $\Gamma$  and the Fermi distribution. Furthermore, we treat the phonon degree of freedom classically. The classical motion is carried on the diabatic surfaces (Eqn. 2.7 or Eqn. 2.8) while, in the spirit of the Franck-Condon picture (vertical transitions), the hopping events are assumed to take place at fixed nuclear position and momentum and are controlled by rates  $\gamma_{0 \rightarrow 1}(x, p)$  and  $\gamma_{1 \rightarrow 0}(x, p)$  as described below. The ensuing dynamics is encoded in a CME for the probability density of the system<sup>[83]</sup>:

$$\frac{\partial P_0(x, p)}{\partial t} = \frac{\partial H_0(x, p)}{\partial x} \frac{\partial P_0(x, p)}{\partial p} - \frac{\partial H_0(x, p)}{\partial p} \frac{\partial P_0(x, p)}{\partial x} - \gamma_{0 \rightarrow 1} P_0(x, p) + \gamma_{1 \rightarrow 0} P_1(x, p) \quad (2.9)$$

$$\frac{\partial P_1(x, p)}{\partial t} = \frac{\partial H_1(x, p)}{\partial x} \frac{\partial P_1(x, p)}{\partial p} - \frac{\partial H_1(x, p)}{\partial p} \frac{\partial P_1(x, p)}{\partial x} + \gamma_{0 \rightarrow 1} P_0(x, p) - \gamma_{1 \rightarrow 0} P_1(x, p) \quad (2.10)$$

where the potential on each surface (in dimensionless coordinates) are:

$$H_\alpha = V_\alpha(x) + \frac{1}{2}\hbar\omega p^2, \alpha = 0, 1 \quad (2.11)$$

Here,  $P_0(x, p)$  ( $P_1(x, p)$ ) is the probability density for the impurity level to be unoccupied (occupied) with the position and momentum of the oscillator to be  $x$  and  $p$ ;  $P_0$  and  $P_1$  satisfy the obvious normalization condition  $\int dx dp (P_1(x, p) + P_0(x, p)) = 1$ .

Next, consider the hopping rates. When the classical system interacts with a single electronic bath (a free electron metal), it is expected to reach at long time thermal equilibrium compatible with the temperature and chemical potential of this metal. The simplest choice of hopping rates compatible with this requirement is

$$\gamma_{0 \rightarrow 1} = \frac{\Gamma}{\hbar} f(\Delta V) \quad (2.12)$$

$$\gamma_{1 \rightarrow 0} = \frac{\Gamma}{\hbar} (1 - f(\Delta V)) \quad (2.13)$$

$$\Delta V(x) = V_1(x) - V_0(x) \quad (2.14)$$

where  $f$  is the Fermi function of the bath

$$f(z) = \frac{1}{1 + e^{\beta(z-\mu)}} \quad (2.15)$$

Eqns. 2.9-2.15 recover the correct equilibrium in the limit of small  $\Gamma$  (shown below). (The restriction to small  $\Gamma$  reflects the fact that level broadening is disregarded in the dynamics postulated above. In Section 2.2.5, we describe a way to incorporate level broadening properly.)

Before solving the CME at equilibrium, we note that according to Eqns. 2.9-2.10, the unoccupied ( $P_0(x, p)$ ) and occupied ( $P_1(x, p)$ ) probability densities evolve under two processes: (*i*) motion of a nucleus along its respective surface and (*ii*) hopping between two potential surfaces. Eqns. 2.12-2.14 imply that the latter is determined by both (*i*) the potential

difference between the two potential surfaces and (ii) the time scale  $\Gamma$  for electron transfer between the impurity and the bath. Thus, according to the CME, there is never any explicit damping of the oscillator's velocity.

Let us now return the question of an analytical steady state. An equilibrium solution to Eqns. 2.9-2.10 is given by

$$P_0(x, p) = C \exp\left(-\frac{1}{2}\beta\hbar\omega(x^2 + p^2)\right) \quad (2.16)$$

$$\begin{aligned} P_1(x, p) &= C \exp\left(-\frac{1}{2}\beta\hbar\omega(x^2 + p^2) - \sqrt{2}\beta gx - \beta E_d\right) \\ &= C \exp\left(-\frac{1}{2}\beta\hbar\omega\left((x + \sqrt{2}g/\hbar\omega)^2 + p^2\right) - \beta(E_d - g^2/\hbar\omega)\right) \end{aligned} \quad (2.17)$$

$C$  is a normalization factor, determined by  $\int \int dx dp (P_0(x, p) + P_1(x, p)) = 1$ ,

$$C = \frac{\beta\hbar\omega}{2\pi} \frac{1}{1 + \exp(-\beta(E_d - g^2/\hbar\omega))} \quad (2.18)$$

These solutions are just the simple Boltzmann distributions that one would expect in the limit of small  $\Gamma$ . The reduced distribution functions for the position  $x$  and momentum  $p$  of the oscillator, then take the forms

$$P(p) = \int dx (P_0(x, p) + P_1(x, p)) = \sqrt{\frac{\beta\hbar\omega}{2\pi}} \exp\left(-\frac{1}{2}\beta\hbar\omega p^2\right) \quad (2.19)$$

$$\begin{aligned} P(x) &= \int dp (P_0(x, p) + P_1(x, p)) \\ &= C \sqrt{\frac{2\pi}{\beta\hbar\omega}} \left( \exp\left(-\frac{1}{2}\beta\hbar\omega x^2\right) + \exp\left(-\frac{1}{2}\beta\hbar\omega x^2 - \sqrt{2}\beta gx - \beta E_d\right) \right) \end{aligned} \quad (2.20)$$

Thus, assuming there is only one fixed point, we conclude that the CME with the rates Eqns. 2.12-2.13 does capture the correct equilibrium for the case of one oscillator coupled to one bath <sup>2</sup>.

---

<sup>2</sup> Interestingly, for standard Tully style FSSH, detailed balance is also recovered, but only approximately (usually up to a small factor) <sup>[84,85]</sup>. The detailed balance here is in fact exact in the limit of  $\Gamma \rightarrow 0$ .

Obviously, Eqns. 2.12-2.15 can be generalized in a straightforward way to situations where the system is coupled to many electronic baths, each in its own equilibrium. For example, for a conduction junction comprising two metals,  $L$  and  $R$ , Eqns. 2.12-2.13 are replaced by

$$\gamma_{0 \rightarrow 1} = \frac{\Gamma_L}{\hbar} f^L(\Delta V) + \frac{\Gamma_R}{\hbar} f^R(\Delta V) \quad (2.21)$$

$$\gamma_{1 \rightarrow 0} = \frac{\Gamma_L}{\hbar} (1 - f^L(\Delta V)) + \frac{\Gamma_R}{\hbar} (1 - f^R(\Delta V)) \quad (2.22)$$

where  $f^L$  ( $f^R$ ) is the Fermi function for left (right) bath with chemical potential  $\mu_L$  ( $\mu_R$ ) and  $\Gamma_L$  ( $\Gamma_R$ ) represents the corresponding left (right) hybridization.

Once the probability densities  $P_\alpha(x, p; t)$  ( $\alpha = 0, 1$ ) have been determined, we can calculate just about any quantity of interest. For example, the population of the impurity level  $N$  and the kinetic energy of the oscillator  $E_k$  are:

$$N = \int dx dp P_1(x, p) \quad (2.23)$$

$$E_k = \int dx dp \left( P_1(x, p) + P_0(x, p) \right) \frac{1}{2} \hbar \omega p^2 \quad (2.24)$$

For a biased conduction junction with  $f^L \neq f^R$ , the long time dynamics will converge to a non-equilibrium steady state characterized by the electronic current

$$I = \int dx dp \left( \gamma_{0 \rightarrow 1}^L(x) P_0(x, p) - \gamma_{1 \rightarrow 0}^L(x) P_1(x, p) \right) \quad (2.25)$$

with,

$$\gamma_{0 \rightarrow 1}^L = \frac{\Gamma_L}{\hbar} f^L(\Delta V) \quad (2.26)$$

$$\gamma_{1 \rightarrow 0}^L = \frac{\Gamma_L}{\hbar} (1 - f^L(\Delta V)) \quad (2.27)$$

### 2.2.3. Surface Hopping Algorithm

The dynamics of Eqns. 2.9-2.10 can be solved directly using a simple SH approach. The algorithm is as follows:

1. Prepare the initial velocities and positions of the oscillators according to the relevant initial conditions. Note that these initial conditions will be irrelevant if one seeks only a description of equilibrium or steady state (and transient dynamics are not important). As discussed above, we believe the CME yields a unique fixed point at long times. In the present paper we initialize all velocities and positions so that they satisfy a Boltzmann distribution at a given initial temperature on one potential surface,

$$P_0(x, p) = \frac{\beta\hbar\omega}{2\pi} \exp\left(-\frac{1}{2}\beta\hbar\omega(x^2 + p^2)\right) \quad (2.28)$$

$$P_1(x, p) = 0 \quad (2.29)$$

2. At the beginning of every time step, if the oscillator is moving along surface  $\alpha$  and has position  $x$ , determine the possibility of hopping  $\gamma_{\alpha\rightarrow\alpha'}(x)$  in Eqns. 2.12-2.13 (or Eqns. 2.21-2.22 for two baths), and generate a random number  $\xi \in [0, 1]$ . If  $\xi < \gamma_{\alpha\rightarrow\alpha'}(x)dt$ , then we switch surfaces (and the active surface becomes  $\alpha'$ ); otherwise, we keep the same active surface.
3. Propagate the position  $x$  and momentum  $p$  along the active diabatic potential surface for a time step  $dt$ .
4. Repeat step 2 and sample over as long a trajectory as is desired until convergence. For dynamical averages, it will be necessary to sample over many independent trajectories.

The scheme above is visualized in Fig. 4. We emphasize again that, at step 2, if the oscillator hops, the momentum is not rescaled to conserve total nuclear energy. This variability in the energy of the oscillator is different from standard FSSH<sup>[16]</sup> (and resembles more “surface

leaking”<sup>[74,75]</sup>); as will be shown, this naive hopping scheme allows the nucleus to relax to the temperature of the electronic bath.

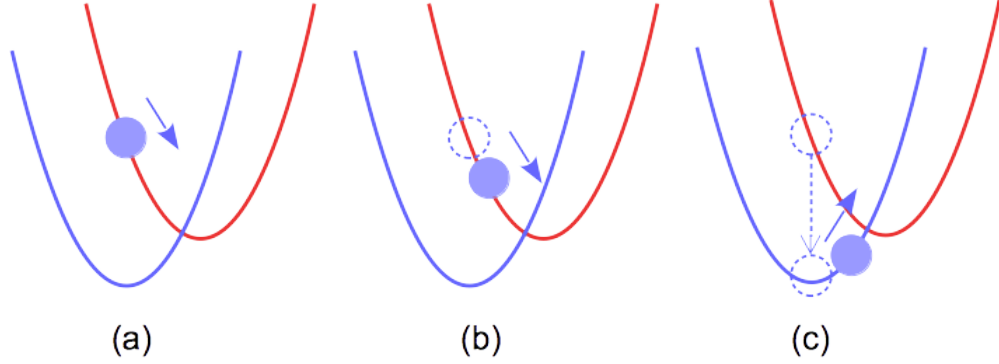


Figure 4: How to run SH: We assume that the oscillator (blue ball) has been moving along on the red potential energy surface. (a) At the start of each time step, we generate a random number  $\xi$ . If  $\xi > \gamma_{red \rightarrow blue}(x)dt$ , (b), the oscillator will continue to move along the red potential energy surface for the next time interval  $dt$ . Otherwise, (c), the oscillator will jump and move along the blue surface for the next time interval  $dt$ .

#### 2.2.4. Quantum Master Equation

The CME (Eqns. 2.9-2.10) will not be adequate at low temperature where  $kT < \hbar\omega$ , and a quantum description of the oscillator is needed. In the limit of small  $\Gamma$ , such a description is provided by the quantum master equation (QME)<sup>[32,86]</sup>,

$$\frac{dP_q^n}{dt} = \sum_{n', q'} [P_{q'}^{n'} W_{q' \rightarrow q}^{n' \rightarrow n} - P_q^n W_{q \rightarrow q'}^{n \rightarrow n'}] \quad (2.30)$$

Here,  $P_q^n$  is the probability density for the impurity to be in electronic state  $n$  ( $|n\rangle = |0\rangle, |1\rangle$ ) and for the phonon to be in state  $q$  ( $|q\rangle = |0\rangle, |1\rangle, |2\rangle, \dots$ ).  $W_{q \rightarrow q'}^{n \rightarrow n'}$  is the transition possibility from  $n$  to  $n'$  and  $q$  to  $q'$ . For the case of one bath,  $W_{q \rightarrow q'}^{n \rightarrow n'}$  is given by

$$W_{q \rightarrow q'}^{0 \rightarrow 1} = \frac{\Gamma}{\hbar} |M_{q \rightarrow q'}|^2 f\left(E_d - \frac{g^2}{\hbar\omega} + \hbar\omega(q' - q)\right) \quad (2.31)$$

$$W_{q \rightarrow q'}^{1 \rightarrow 0} = \frac{\Gamma}{\hbar} |M_{q \rightarrow q'}|^2 \left(1 - f\left(E_d - \frac{g^2}{\hbar\omega} + \hbar\omega(q - q')\right)\right) \quad (2.32)$$

$$W_{q \rightarrow q'}^{n \rightarrow n'} = 0, n = n' \quad (2.33)$$

Here,  $E_d - \frac{g^2}{\hbar\omega}$  represents the renormalized energy level of the impurity (i.e. the energy of the impurity level minus the reorganization energy).  $M_{q \rightarrow q'}$  is the Frank-Condon factor, which is the overlap between eigenstates  $q$  and  $q'$  of the harmonic oscillator with the origin shifted by  $\sqrt{2}\lambda \equiv \sqrt{2}g/\hbar\omega$ ,

$$M_{q \rightarrow q'} = \int dx \phi_{q'}(x) \phi_q(x - \sqrt{2}\lambda) \quad (2.34)$$

The Franck-Condon factor can be expressed as<sup>[32,86]</sup>

$$M_{q \rightarrow q'} = (p!/Q!)^{1/2} \lambda^{Q-p} e^{-\lambda^2/2} L_p^{Q-p}(\lambda^2) \text{sgn}(p-Q)^{p-Q} \quad (2.35)$$

Here,  $Q(p)$  is the maximum (minimum) of  $q$  and  $q'$ ,  $L_n^m$  is generalized Laguerre polynomial.

For the case of one bath, there is an analytical solution to Eqns. 2.30-2.33:

$$P_q^0 = C \exp(-\beta\hbar\omega(q + \frac{1}{2})) \quad (2.36)$$

$$P_q^1 = C \exp(-\beta\hbar\omega(q + \frac{1}{2})) \exp(-\beta(E_d - g^2/\hbar\omega)) \quad (2.37)$$

where  $C$  is the normalized factor that satisfies  $\sum_q (P_q^0 + P_q^1) = 1$ . This solution captures one oscillator in the presence of two possible electronic states (with small coupling  $\Gamma$  between the states). Thus, the QME impurity population agrees exactly with the CME (compare Eqns. 2.36-2.37 with Eqns. 2.16-2.17).

For the case of two baths, the hopping probability is the sum of the left and right hopping probabilities:

$$W_{q' \rightarrow q}^{n \rightarrow n'} = W_{q' \rightarrow q}^{n \rightarrow n' R} + W_{q' \rightarrow q}^{n \rightarrow n' L} \quad (2.38)$$

where  $W_{q' \rightarrow q}^{n \rightarrow n' R}$  ( $W_{q' \rightarrow q}^{n \rightarrow n' L}$ ) depend on the Fermi functions  $f^R$  ( $f^L$ ). At steady state, the impurity and the phonon can be collectively be described by  $P_q^{n,eq}$ , which is the normalized nontrivial solution to  $\frac{dP_q^n}{dt} = 0 \Big|_{P_q^n = P_q^{n,eq}}$ .  $P_q^{n,eq}$  can be used to calculate any and all steady-

state observables. For example, current is given by

$$I = \sum_{qq'} W_{q' \rightarrow q}^{0 \rightarrow 1L} P_{q'}^{0,eq} - W_{q' \rightarrow q}^{1 \rightarrow 0L} P_{q'}^{1,eq} \quad (2.39)$$

When discussing our SH results below, we will compare with the QME results. For a QME simulation, we must truncate the infinite set of phonon states, including only a finite number, while making sure that the result is converged.

### 2.2.5. Implementing Level Broadening

In conjunction with the equilibrium distribution Eqns. 2.16-2.17, Eqn. 2.23 yields the equilibrium electron population of the impurity level predicted by the SH scheme in the form

$$N = \int dx dp P_1(x, p) = f(\tilde{E}_d) \quad (2.40)$$

where  $\tilde{E}_d = E_d - g^2/\hbar\omega$  is impurity level energy renormalized by the reorganization energy  $g^2/\hbar\omega$ . Eqn. 2.40 is just a Fermi function at a well defined impurity energy, and thus Eqn. 2.40 disregards level broadening. Indeed, in the case of no oscillators, the exact expression for the population of an impurity level (at energy  $E_d$ ) interacting with an equilibrium Fermi distribution is given by<sup>[87]</sup>

$$N = \int dE \frac{1}{2\pi} \frac{\Gamma}{(E - E_d)^2 + (\Gamma/2)^2} f(E) \quad (2.41)$$

Consequently, Eqn. 2.40 is a good approximation only in the limit of small impurity-bath coupling (  $kT \gg \Gamma$  ). To improve upon this answer, one must fully account for the level broadening of the impurity by the electronic bath. Within the context of our SH calculations, we can include broadening as follows. For each trajectory in our simulation, we initialize the relative energy level of the impurity  $E_d$  according to a Lorentzian distribution,

$$\rho(E) = \frac{1}{2\pi} \frac{\Gamma}{(E - E_d)^2 + (\Gamma/2)^2} \quad (2.42)$$

Thereafter, we run many simulations, evaluating physical observables by averaging over all trajectories. For the electronic population of the impurity, we get

$$N = \int dE \rho(E) f(E - g^2/\hbar\omega) = \int dE \frac{1}{2\pi} \frac{\Gamma}{(E - \tilde{E}_d)^2 + (\Gamma/2)^2} f(E) \quad (2.43)$$

Except for the shift of the impurity energy level ( $\tilde{E}_d = E_d - g^2/\hbar\omega$  instead of  $E_d$ ), Eqn. 2.43 is the same as Eqn. 2.41.

In the appendix 2.5.1, we show how the level broadening changes the position  $x$  and momentum  $p$  distribution (Eqns. 2.19-2.20). Furthermore, we define a mean potential and a potential of mean force, and show that, without taking the broadening into account ( $\Gamma \ll kT$ ), these two potentials give the same result.

### 2.2.6. Numerical Renormalization Group

Finally, it is important to remember that both the CME and QME methods above treat the electronic bath implicitly (and are derived only by assuming that  $\Gamma$  is very small). In the end, the validity of our SH results needs to be justified. At equilibrium this can be done by comparing with results of a numerical renormalization group (NRG)<sup>[4,88]</sup> calculation, which, at low enough temperatures can yield very accurate results when converged properly<sup>[89]</sup>. This method is particularly suited for a system with small number of degrees of freedom interaction with a microscopic bath. By logarithmically discretizing the continuum representing the bath, the NRG approach transforms a Hamiltonian with a continuous number of system-bath couplings into a semi-infinite chain, where each site of the chain only couples with its nearest neighbors. Furthermore, because the couplings along the chain decrease exponentially, one can easily truncate the infinite Hilbert space representing the bath, and recover very accurate answers. Details about NRG for bosons and fermions can be found in Ref. [4, 88].

## 2.3. Results and Discussion

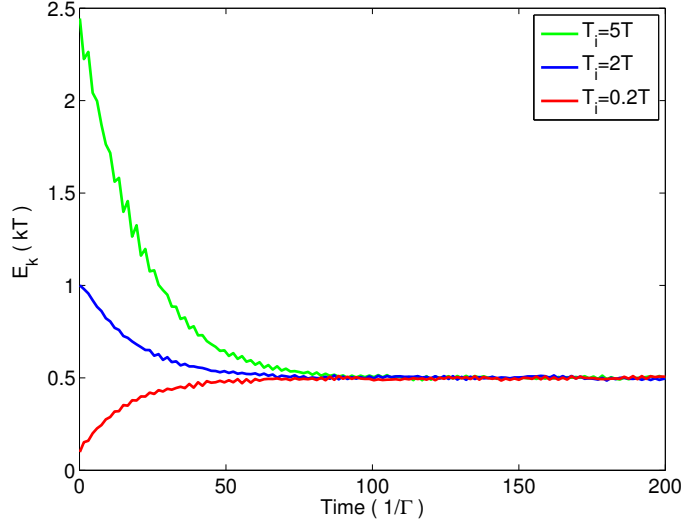
### 2.3.1. One Electronic Bath–Relaxation to Equilibrium

For the problem of one electronic bath, we first investigate the relaxation of the oscillator towards equilibrium using the simplest SH scheme with rates given by Eqns. 2.12-2.15. Figure 5(a) shows the time evolution of the average kinetic energy of the oscillator for a variety of initial temperatures. For each initial condition, we find that the kinetic energy of the system inevitably reaches its classical thermal limit  $E_K = \frac{1}{2}kT$  where  $kT$  is the temperature of the electronic bath. The same long-time limit is obtained (Figure 5(b)) for different choices of the e-ph couplings  $g$ . Increasing the e-ph coupling causes faster relaxation but the final equilibrium state is unchanged.

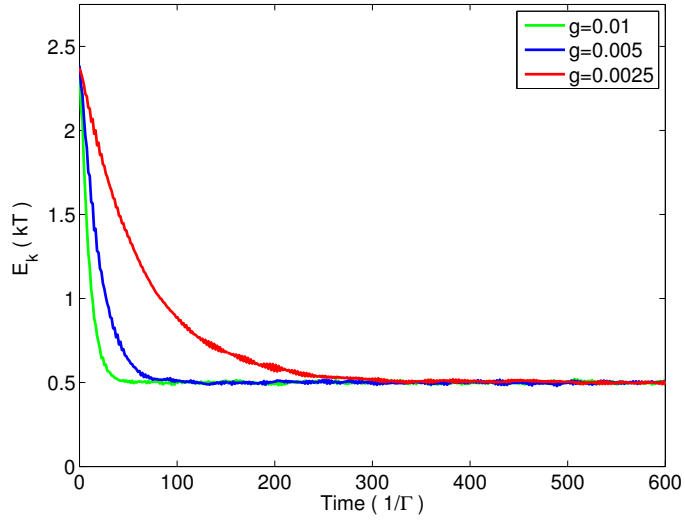
In Figure 6, we plot the numerical distributions of the oscillator position  $x$  and momentum  $p$  that are obtained from the SH trajectories, as well as the analytical  $x$  and  $p$  distributions given by Eqns. 2.19-2.20. We find perfect agreement, thus reinforcing our intuition that Eqns. 2.9-2.10 admit only one long time solution.

The results displayed in Figures 5 and 6 have used the SH algorithm that disregarded level broadening. Figure 7 shows the effect of including broadening as described in Section 2.2.5. With broadening, we find perfect agreement of the computed impurity equilibrium population between SH/QME results and NRG results. (Recall that SH and QME yield identical impurity populations; see Eqns. 2.36-2.37 and Eqns. 2.16-2.17.)

Finally, in Figure 8, we plot SH (Eqn. 2.43) vs. NRG results for a difficult (nonclassical) quantum regime, where  $\Gamma, \hbar\omega, g^2/\hbar\omega > kT$ . Not surprisingly, in this regime, SH cannot quite recover the correct electron population as a function of the renormalized impurity energy level ( $\tilde{E}_d$ ). This figure should be a reminder that there are equilibrium regimes where SH is not applicable. In general, for many problems of interest, the agreement between SH and NRG is quite strong.

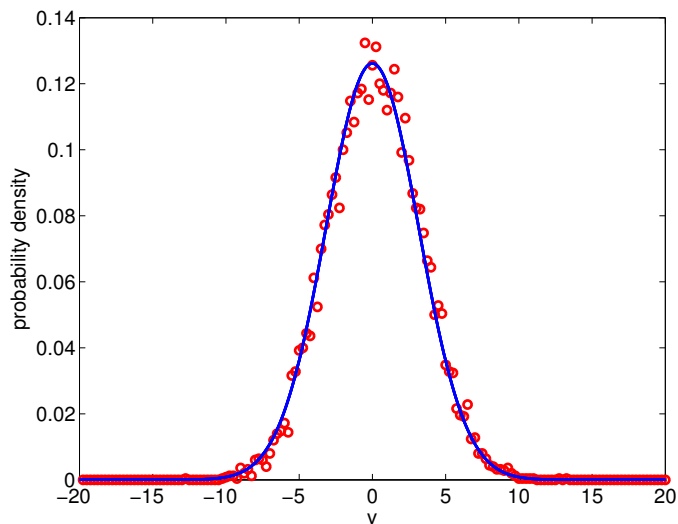


(a) Phonon relaxation with different initial conditions,  $g=0.005$ .  $T_i$  represents the temperature at which the oscillator is initialized.

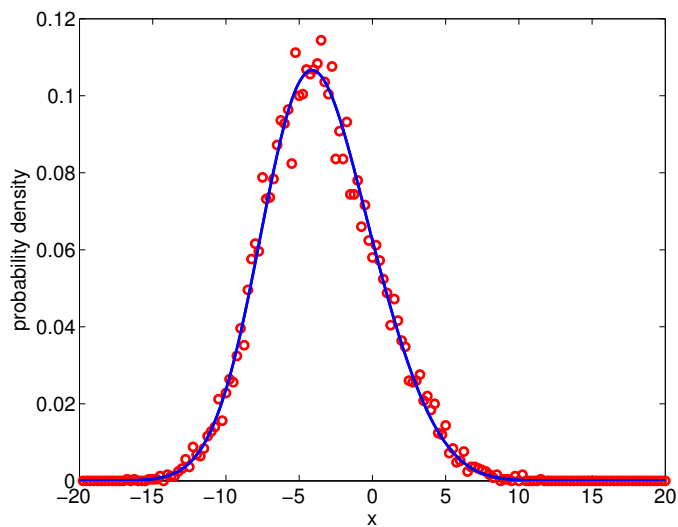


(b) Phonon relaxation with different e-ph couplings,  $g$ .

Figure 5: Phonon relaxation:  $\Gamma = 0.003$ ,  $kT = 0.03$ ,  $\hbar\omega = 0.003$ ,  $E_d = 0$ ,  $\mu = 0$ . 10000 trajectories are used.

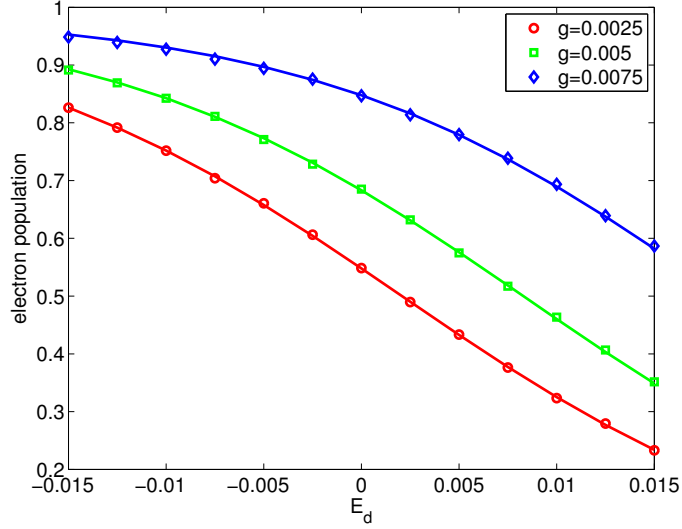


(a) Velocity distribution

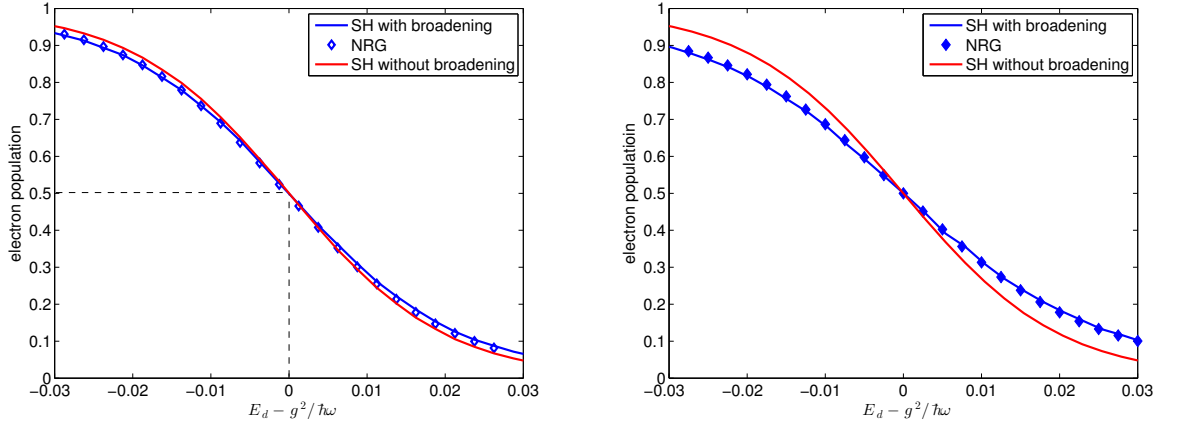


(b) Position distribution

Figure 6: Velocity distribution (a) and position distribution (b):  $\Gamma = 0.003$ ,  $kT = 0.03$ ,  $g = 0.01$ ,  $\hbar\omega = 0.003$ ,  $E_d = 0$ ,  $\mu = 0$ . Red dots represents averages over 10000 trajectories. The blue line is the analytic result from Eqn. 2.19 for (a) and from Eqn. 2.20 for (b).



(a) Electron population of the impurity as a function of  $E_d$ . Dots represent the NRG results, the line represents the SH results when we include broadening. The agreement serves confirm the validity of our SH approach.  $\Gamma = 0.003$



(b) Electron population as a function of shifted  $E_d$ , with  $g = 0.0075$ ,  $\Gamma = 0.003$ . Note that, by including broadening, we do improve the SH results.

(c) Electron population as a function of shifted  $E_d$ , with  $g = 0.0025$ ,  $\Gamma = 0.01$ .

Figure 7: Electronic population as a function of impurity energy level:  $kT = 0.01$ ,  $\hbar\omega = 0.003$ . For NRG calculation, band width  $D=1$ , and the basis is initialized with 30 boson states, the maximum number of eigenstates kept is  $N_s = 512$ , and the logarithmic discretizing parameter is  $\Lambda = 2$

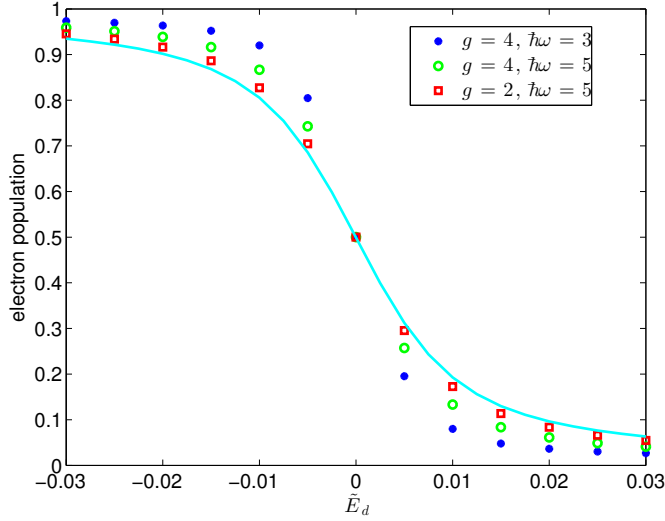


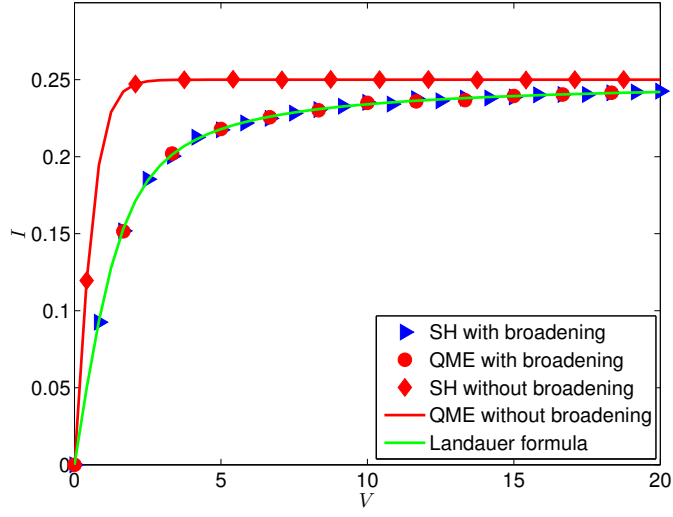
Figure 8: Electronic population as a function of renormalized impurity energy level:  $kT = 0.2\Gamma$ ,  $\Gamma = 1$ . The line represents SH results (Eqns. 2.43), and the dots represent NRG results. For the NRG calculation, we set  $D = 84\Gamma$ , where  $D$  is the band width. The basis is initialized with 40 boson states, the maximum number of eigenstates kept is  $N_s = 1500$ , and the logarithmic discretizing parameter is  $\Lambda = 2$ .

### 2.3.2. Two Electronic Baths–Bias and Current

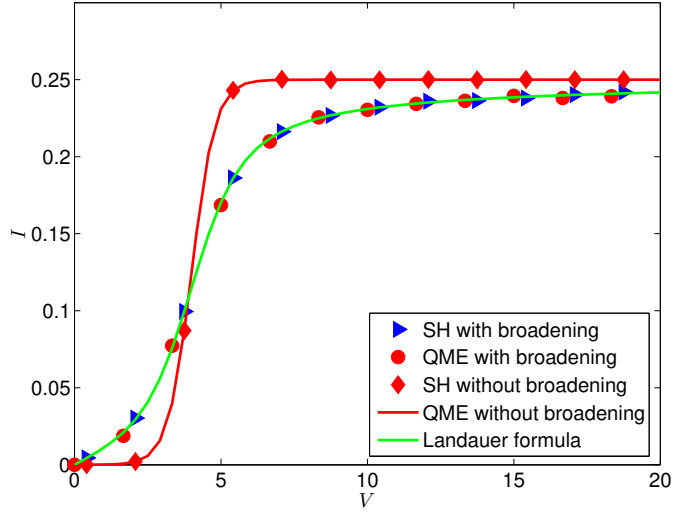
The next system we investigated was the out of equilibrium case, where the Fermi levels of the two electronic baths have a bias between them. We calculated the current ( $I$ ) as a function of bias ( $V$ ). In the absence of e-ph coupling, the result is well known as single level Landauer formula from nonequilibrium Green Function approaches<sup>[90,91]</sup> and other frameworks<sup>[92]</sup>,

$$I = \int dE \frac{\Gamma_L \Gamma_R}{(E - E_d)^2 + (\Gamma/2)^2} (f^L(E) - f^R(E)) \quad (2.44)$$

In Figure 9, we plot the QME and SH results for current vs. voltage in the limit of very small e-ph coupling. For comparison, we also plot the Landauer current (Eqn. 2.44, for which  $g = 0$ ). For the SH results, we show both broadened and unbroadened results. In fact, it can be shown that, after broadening, SH gives the correct result compared with Eqn. 2.44 (see Appendix 2.5.2).



(a)  $E_d = 0$



(b)  $E_d = 2$

Figure 9: I-V curves in the limit of small e-ph coupling. For the QME and SH, we take a small value for the e-ph coupling,  $g = 0.02$ . The other parameters are:  $kT = 0.2$ ,  $\hbar\omega = 5$ ,  $\Gamma = 2\Gamma_L = 2\Gamma_R = 1$ ,  $\mu_L = V/2$ ,  $\mu_R = -V/2$ . The Landauer results are for  $g = 0$  as in Eqn. 2.44.

In Figure 9, we also show results from the QME, which should extend SH results into the limit of low temperature. According to Eqns. 2.31-2.32, just as for SH, the straightforward QME transition rates do not include broadening of the impurity levels. Just as for SH, however, we can include broadening by working with a series of different QME's (rather than just one), each with different impurity level energies sampled from Lorentzian distribution with half width

$$\Gamma = \Gamma_L + \Gamma_R \tag{2.45}$$

Having done so, we compute the current by averaging the QME results over the Lorentzian distribution of the impurity energy level  $E_d$  (we sample over 5000 initial conditions for the simulation).

Note that all broadened methods (Landauer, QME, SH) agree with each other in Fig. 9. Note also that, without broadening, neither the SH nor QME can reproduce the correct I-V curve. Thus, we may now have some confidence that, when broadening is included, SH can be extended to out of equilibrium case. We will next investigate the performance of the SH algorithm in the limits of larger electron-phonon couplings (which is the most interesting case).

In Figure 10, we calculate I-V curves at low temperature, comparing both the QME and real path integral results from Ref. [1]. In this region, the quantum nature of the boson is paramount and SH must break down. We observe that the QME gets the correct overall form of the current in the quantum region, whereby the current should increase in steps at intervals of roughly  $2\omega$ <sup>[78]</sup>. From this agreement, we may conclude that the QME is valid at low or high temperatures.

In Figure 11, we compare our SH results with QME results as the temperature is raised. We observe that, in transitioning from the quantum (low T) region to the classical (high T) region, SH achieves better and better agreement with the QME. Although SH never

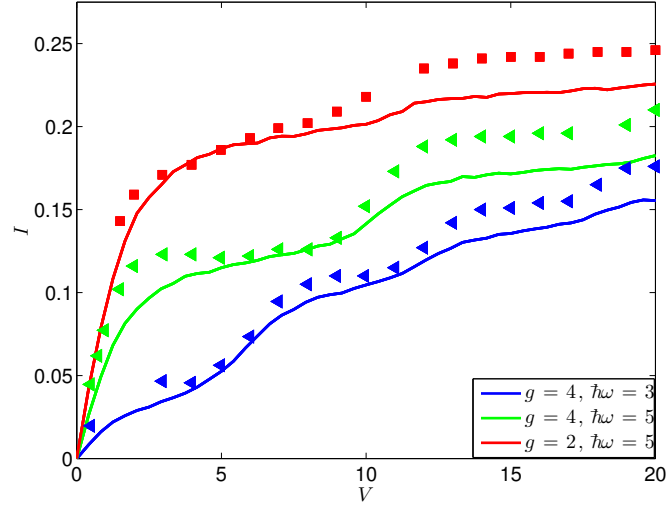


Figure 10: I-V curves. The QME (as given by Eqns. 2.30-2.39 and broadened by Eqns. 2.42,2.45) is represented by lines. Real time path integral results<sup>[1,2]</sup> are represented by dots.  $kT = 0.2$ .  $\Gamma = 2\Gamma_L = 2\Gamma_R = 1$ ,  $\mu_L = V/2$ ,  $\mu_R = -V/2$ ,  $E_d = g^2/\hbar\omega$ . This choice of parameters represents the quantum regime, as can be seen by the non-linear steps in the I-V curve that arise from nuclear quantization. Our classical SH simulations will not be accurate in this regime.

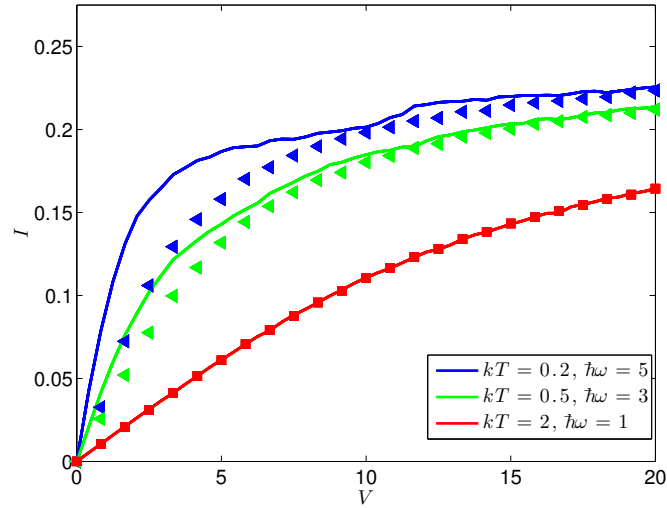
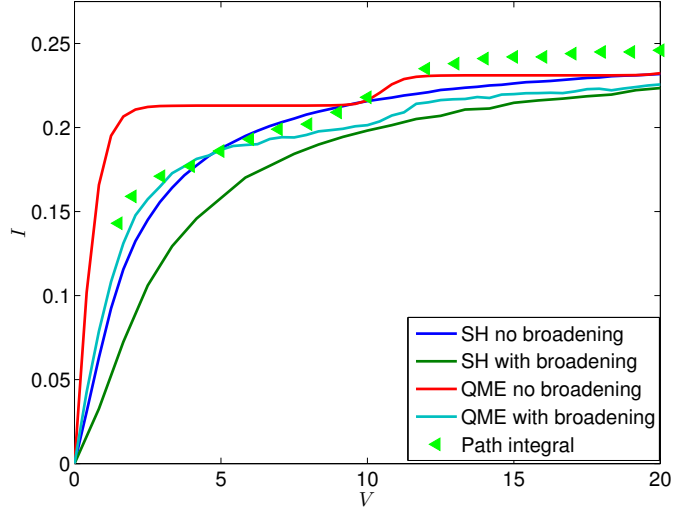
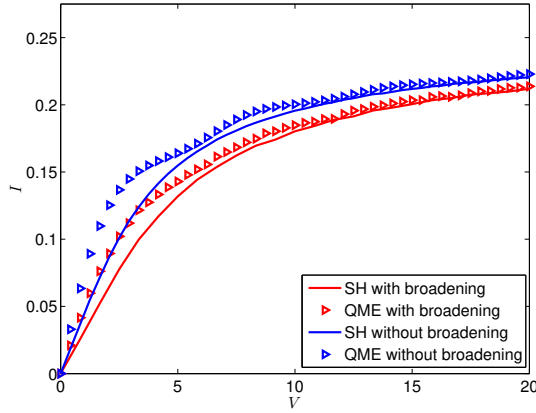


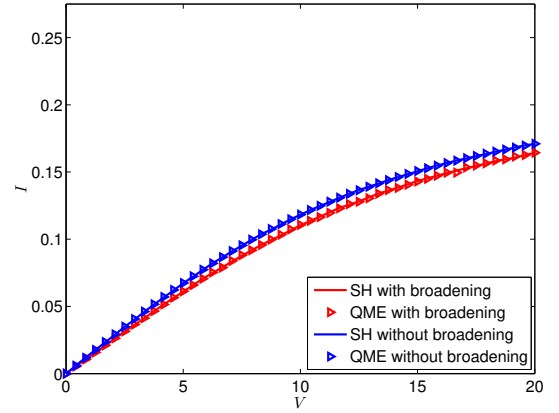
Figure 11: I-V curves. Observe the agreement between SH (dots) and QME (lines) in the classical, high temperature limit. At low T, these two approaches disagree (as the QME predicts I-V steps, which SH ignores).  $g = 2$ ,  $\Gamma = 2\Gamma_L = 2\Gamma_R = 1$ ,  $E_d = g^2/\hbar\omega$ ,  $\mu_L = V/2$ ,  $\mu_R = -V/2$ .



(a)  $\hbar\omega = 5, kT = 0.2$



(b)  $\hbar\omega = 3, kT = 0.5$



(c)  $\hbar\omega = 1, kT = 2$

Figure 12: I-V curves demonstrating the results from the different formalisms. The other parameters are:  $\Gamma = 2\Gamma_L = 2\Gamma_R = 1, \mu_L = V/2, \mu_R = -V/2, g = 2$ .

captures a step feature at low temperature limit ( $kT < \hbar\omega$ ) (where the energy levels of the nuclei are discretized), the SH approach is quite reliable at large temperatures.

Finally, Figure 12 compares I-V curves over a range of parameters going from the quantum limit to classical limit with and without broadening using different methods. Two general conclusions are apparent. First, broadening clearly reduces the step feature in the quantum limit. Second, with or without broadening, the QME and SH approaches agree in the classical limit. Overall, for future simulations of charge injection between classical fluids and metal surfaces, we expect that the SH approach discussed here should be quite reliable. In particular, even for systems with reasonable strong molecular-metal coupling, we are hopeful that SH can be applied, provided that we use the broadening protocol discussed above.

#### 2.4. Conclusions

We have proposed a simple and effective way to treat coupled nuclear-electronic problems, and we have focused on the Anderson-Holstein model. The rules of our simulation are very simple: nuclear degree of freedom are treated classically and evolve according to Newton's equation. Occasional hops between diabatic potential surfaces are promoted at a rate proportional to the hybridization coupling between the system and the electronic bath.

For an impurity and phonon coupled to one electronic bath, we find that the system (impurity and phonon) recovers the correct thermal equilibrium regardless of any initial condition; the phonon learns about the temperature of the electronic bath indirectly (but effectively) through the hopping rate on and off. Interestingly, by broadening the energy level of the impurity (as induced by its interaction with the bath), we are able to recover the exact population of the impurity for all hybridizations in the limit of no electron-phonon coupling. Furthermore, with electron-phonon coupling, our results for the impurity electron population still yield good agreement with NRG calculations. As such, our final approach here would seem to go beyond any second order perturbation treatment of the impurity,

for which there is not even any exact agreement without electron phonon coupling. That being said, we are aware, of course, that the standard CME or QME is derived from such a second-order perturbative treatment, and so the effect of our broadening will need to be tested more generally in the future.

For the out of equilibrium case, we have investigated both the CME and QME, and explored high and low temperature regimes. As before, we have found improved results by broadening our master equation results. With broadening, both the CME and QME recover the Landauer formula (in the limit of zero e-ph coupling). At low temperature and for strong e-ph couplings, we have found that the QME recovers the correct step features in the I-V curves, whereas the CME fails. At high temperatures (in the classical limit), the SH and QME agree with each other.

Overall, we may conclude that the master equations presented here can be applied to physical problems that are either at equilibrium or out of equilibrium. In the future, we will aim to study a host of other interesting transport effects, including instability<sup>[30–32]</sup> and hysteresis<sup>[78]</sup>. Of course, in terms of cost, the SH approach is the least computationally demanding, followed by the QME, and then followed by NRG. Moreover, NRG would require a very large cost to propagate dynamics at high temperature<sup>[93]</sup>. Given the simplicity and efficiency of the SH approach here, one might expect that these dynamics will be very useful for simulating large systems of coupled classical nuclear degrees interacting with a reservoir of electrons, e.g. an electrochemical interface<sup>[94]</sup>. While further benchmarking of this method is undoubtedly needed, we believe the stochastic dynamics advocated in this paper will be a strong extension of the standard SH methodology.

## 2.5. Appendix

### 2.5.1. Dynamics with a broadened impurity level: the mean potential and the potential of mean force

The probability densities established in Eqns. 2.19-2.20 were computed without taking into account the broadening of the impurity energy level. After taking broadening into account as suggested above (section 2.2.5), we must average over  $E_d$ , which is considered a variable with a Lorentzian distribution.  $P(x)$  becomes

$$P(x) = \sqrt{\frac{2\pi}{\beta\hbar\omega}} \left( (1-N) \exp\left(-\frac{1}{2}\beta\hbar\omega x^2\right) + N \exp\left(-\frac{1}{2}\beta\hbar\omega(x + \sqrt{2}g/\hbar\omega)^2\right) \right) \quad (2.46)$$

with  $N$  defined in Eqn. 2.43. After averaging,  $P(p)$  remains unchanged, as in Eqn. 2.19, which indicates the average kinetic energy is still  $\frac{1}{2}kT$ . Using  $P(x)$  above, we can define the mean potential,

$$P(x) = \exp(-\beta V_{MP}) \quad (2.47)$$

which gives  $V_{MP}$

$$V_{MP} = V_0 - \frac{1}{\beta} \log \left( (1-N) \exp\left(-\frac{1}{2}\beta\hbar\omega x^2\right) + N \exp\left(-\frac{1}{2}\beta\hbar\omega(x + \sqrt{2}g/\hbar\omega)^2\right) \right) \quad (2.48)$$

with  $V_0 = -\frac{1}{\beta} \log \sqrt{\frac{2\pi}{\beta\hbar\omega}}$  is a constant. Also, according to Ref. [80], the potential of mean force is defined as,

$$V_{PMF} = \frac{1}{2}\hbar\omega x^2 - \int_{x_0}^x dx' F(x') \quad (2.49)$$

Here the mean force  $F(x)$  on the oscillator (as induced by the electrons) is defined as,

$$F(x) = -\sqrt{2}g \langle d^+ d \rangle |x\rangle = -\sqrt{2}g \int \frac{dE}{\pi} \frac{\Gamma}{(E - \sqrt{2}gx - E_d)^2 + \Gamma^2} f(E) \quad (2.50)$$

Let us now show that, if we exclude level broadening, Eqn. 2.47 and Eqn. 2.49 give same result. Without broadening, using Eqns. 2.20 and 2.47 the mean potential is,

$$\begin{aligned} V_{MP} &= V_1 - \frac{1}{\beta} \log \left( \exp(-\frac{1}{2}\beta\hbar\omega x^2) + \exp(-\frac{1}{2}\beta\hbar\omega x^2 - \sqrt{2}\beta gx - \beta E_d) \right) \\ &= V_1 + \frac{1}{2}\hbar\omega x^2 - \frac{1}{\beta} \log(1 + \exp(-\beta\sqrt{2}gx - \beta E_d)) \end{aligned} \quad (2.51)$$

where  $V_1$  is a constant. Furthermore the mean force defined in Eqn. 2.50 (without broadening) becomes,

$$F(x) = -\sqrt{2}g \langle d^\dagger d \rangle |x = -\sqrt{2}gf(\sqrt{2}gx + E_d) \quad (2.52)$$

The integral over  $x$  gives the extra potential felt by the oscillator,

$$\begin{aligned} - \int_{x_0}^x dx' F(x') &= \int_{x_0}^x \sqrt{2}gf(\sqrt{2}gx + E_d) \\ &= V_2 - \frac{1}{\beta} \log(1 + \exp(-\beta\sqrt{2}gx - \beta E_d)) \end{aligned} \quad (2.53)$$

$V_2$  is another constant reference potential. Thus, the potential of mean force is,

$$V_{PMF} = V_2 + \frac{1}{2}\hbar\omega x^2 - \frac{1}{\beta} \log(1 + \exp(-\beta\sqrt{2}gx - \beta E_d)) \quad (2.54)$$

Within a constant,  $V_{PMF} = V_{MP}$ .

### 2.5.2. Current from SH in absent of e-ph coupling

In this appendix, we show that (with broadening), our SH approach (as well as the QME) recovers the correct Landauer current in the limit of no electron-phonon coupling. In such a case,  $P_1(x, p) = P_1, P_0(x, p) = P_0$ . Both the CME (Eqns. 2.9-2.10) and QME become

$$\frac{\partial P_0}{\partial t} = -\gamma_{0 \rightarrow 1} P_0 + \gamma_{1 \rightarrow 0} P_1 \quad (2.55)$$

$$\frac{\partial P_1}{\partial t} = \gamma_{0 \rightarrow 1} P_0 - \gamma_{1 \rightarrow 0} P_1 \quad (2.56)$$

Plugging in Eqns. 2.21-2.22, where now  $\Delta V = E_d$ , we find steady state solutions

$$P_0 = \frac{\Gamma_L(1 - f^L(E_d)) + \Gamma_R(1 - f^R(E_d))}{\Gamma} \quad (2.57)$$

$$P_1 = \frac{\Gamma_L f^L(E_d) + \Gamma_R f^R(E_d)}{\Gamma} \quad (2.58)$$

The current (Eqn. 2.25) is given by

$$\begin{aligned} I &= \Gamma_L f^L(E_d) P_0 - \Gamma_L (1 - f^L(E_d)) P_1 \\ &= \frac{\Gamma_L \Gamma_R}{\Gamma} (f^L(E_d) - f^R(E_d)) \end{aligned} \quad (2.59)$$

Finally, when  $E_d$  is broadened by a Lorentzian of width  $\Gamma = \Gamma^L + \Gamma^R$ , the result after averaging is

$$I = \int \frac{dE}{2\pi} \frac{\Gamma_L \Gamma_R}{(E - E_d)^2 + (\Gamma/2)^2} (f^L(E) - f^R(E)) \quad (2.60)$$

This is the correct Landauer current.

## CHAPTER 3 : Surface hopping with a manifold of electronic states, III: transients, broadening and the Marcus picture

This chapter was adapted from Refs. [95, 96]

### 3.1. Introduction

Electron transfer between a molecule and a metal electrode is a fundamental reaction that underlies all electrochemical and molecular electronic processes as well as many phenomena involved in corrosion and heterogeneous catalysis. The Anderson-Holstein (AH) model (see Eqs. 3.1-3.4) is a simple model to describe such a system, where an electronic impurity level couples both to an electronic bath and to nuclear motion<sup>[77]</sup>. For simplicity, in this paper we will not consider electron-electron (el-el) repulsion which is a source of rich physics that must be treated carefully<sup>[97]</sup>. Even without el-el repulsion, the AH model has so many degrees of freedom (DOF) that it admits no simple solution. Numerical Renormalization Group (NRG)<sup>[4,88,98]</sup>, Multi-Configuration Time-Dependent Hartree (MCTDH)<sup>[99]</sup> and Path Integral Monte Carlo (PIMC)<sup>[1]</sup> can produce numerical exact solutions, but likely none of these methods is feasible if we seek to extend the AH model to more complicated, realistic Hamiltonians. If we are interested in approximate solutions, which do not treat the bath explicitly, Influence Functionals (IF)<sup>[81]</sup> and Nonequilibrium Green functions (NEGF)<sup>[78,80,100–102]</sup> offer alternative tools whereby one focuses on a subsystem with a handful of DOF.

Besides the methods above, historically surface hopping (SH)<sup>[16,39]</sup> has been a widely used tool for treating electron-phonon (e-ph) couplings for molecules or atoms if there are only a few electronic DOF. In the presence of a manifold of electronic DOF—for instance, the case of a loosely bound anion—Preston’s surface leaking algorithm<sup>[74,103]</sup> is one possible approach. More generally, near a metal surface, Shenvi *et al* have suggested discretizing the electronic bath, and running SH on a large number of independent potential energy surfaces (PES’s)<sup>[71–73]</sup>. A nonequilibrium version of the Shenvi algorithm might be possible

in the vein of Refs. [91, 104–108].

In a previous paper<sup>[38]</sup>, which we refer to as Paper II, we have analyzed an alternative approach based on a classical master equation (CME) that describes the dynamics of the AH impurity subsystem. This CME is solved by a SH approach—basically one runs trajectories on two diabatic PES's with stochastic hops between them. By further implementing level broadening, we have shown that equilibrium and out of equilibrium observables agree well with the results from NRG and the secular quantum master equation (sQME) in a classical regime (i.e. high temperature).

In the present paper, we address some interesting aspects of the CME/SH approach that were not discussed in Paper II. First, we will look at transient dynamics of the impurity electronic population. Second, we will show how our SH approach recovers the Marcus rate analytically. Third, we will generalize the AH model to the case where the impurity hybridization function depends on the nuclear coordinate, which is very relevant for processes dominated by the dynamics of the impurity-surface distance such as chemisorption<sup>[109]</sup> and surface scattering<sup>[24,71]</sup>. Fourth, in the latter case, we will investigate how to implement level broadening and show that the Marcus rate is an appealing approximation for this broadening. Fifth and finally, we will study a set of out of equilibrium I-V curves, and we will demonstrate interesting turnover effects that involve inelastic electron transport properties<sup>[78,79]</sup>.

We organize the paper as follows. In Sec. 3.2, we outline how to derive the CME and discuss the transient observables. In Sec. 3.3 we show that SH recovers a Marcus rate, and then we use that Marcus rate to include level broadening. We compare our results with NRG results for electron population in Sec. 3.4. In Sec. 3.5, we show how one can find I-V curves that exhibit negative differential resistance according to SH and the QME. We conclude in Sec. 3.6.

## 3.2. Transient dynamics

### 3.2.1. Classical Master Equation

We begin our study with the AH model Hamiltonian:

$$H = H_s + H_b + H_c, \quad (3.1)$$

$$H_s = E_d d^\dagger d + g(a^\dagger + a)d^\dagger d + \hbar\omega(a^\dagger a + \frac{1}{2}), \quad (3.2)$$

$$H_b = \sum_k (\epsilon_k - \mu) c_k^\dagger c_k, \quad (3.3)$$

$$H_c = \sum_k V_k (c_k^\dagger d + d^\dagger c_k). \quad (3.4)$$

$H_s$  is the system Hamiltonian, consisting of an impurity level with energy  $E_d$  coupled to an oscillator with frequency  $\omega$ . The bath Hamiltonian,  $H_b$ , describes an electrode which is assumed to be in equilibrium characterized by the temperature  $T$  and the electronic chemical potential  $\mu$ .  $H_c$  is the coupling between the impurity and the electrode.

The key quantity of interest is the reduced density matrix of the system. Starting with the quantum Liouville equation in the interaction picture, we find the total density matrix evolves as<sup>[83]</sup>,

$$\frac{d\rho(t)}{dt} = -\frac{i}{\hbar}[H_c(t), \rho(0)] - \frac{1}{\hbar^2} \int_0^t dt' [H_c(t), [H_c(t'), \rho(t')]], \quad (3.5)$$

where

$$H_c(t) = \exp(i(H_s + H_b)t/\hbar) H_c \exp(-i(H_s + H_b)t/\hbar). \quad (3.6)$$

In the Born-Markovian approximation, we replace  $\rho(t')$  by  $\rho_b^{eq} \otimes \rho_s(t)$  in the integrand that relies on the assumptions that the bath remains in equilibrium throughout the process and that bath correlation functions decay fast on the system timescale. This leads to (setting

$\tau = t - t')$

$$\frac{d\rho(t)}{dt} = -\frac{i}{\hbar}[H_c(t), \rho(0)] - \frac{1}{\hbar^2} \int_0^\infty d\tau [H_c(t), [H_c(t - \tau), \rho_b^{eq} \otimes \rho_s(t)]]. \quad (3.7)$$

Next, we assume the initial total density matrix is a direct product of the system density matrix and the equilibrium bath density matrix, i.e.  $\rho(0) = \rho_b^{eq} \otimes \rho_s(0)$  and take the trace of Eq. 3.7 over the bath degrees of freedom. This yields

$$\frac{d\rho_s(t)}{dt} = -\frac{1}{\hbar^2} \int_0^\infty d\tau \text{Tr}_b [H_c(t), [H_c(t - \tau), \rho_b^{eq} \otimes \rho_s(t)]]. \quad (3.8)$$

In Eq. 3.8, we have used  $\text{Tr}_b(H_c(t)\rho_b^{eq}) = 0$ . We can further write  $H_s$  as

$$H_s = H_0|0\rangle\langle 0| + H_1|1\rangle\langle 1|, \quad (3.9)$$

where  $|0\rangle$  ( $|1\rangle$ ) denotes the unoccupied (occupied) state of the impurity electron:

$$H_0 = \frac{1}{2}\hbar\omega(x^2 + p^2), \quad (3.10)$$

$$H_1 = E_d + \sqrt{2}gx + \frac{1}{2}\hbar\omega(x^2 + p^2), \quad (3.11)$$

with  $x = \frac{1}{\sqrt{2}}(a^+ + a)$  and  $p = \frac{i}{\sqrt{2}}(a^+ - a)$ .

In what follows we will consider processes in which the impurity initial state is either state 0 or state 1, that is,

$$\rho_s(t=0) = \rho_0|0\rangle\langle 0| + \rho_1|1\rangle\langle 1|, \quad (3.12)$$

which ensures that there will be no coherence between occupied and unoccupied states at later time (with this Hamiltonian). Thus, we can write

$$\rho_s(t) = \rho_0|0\rangle\langle 0| + \rho_1|1\rangle\langle 1|. \quad (3.13)$$

After plugging Eq. 3.13 into Eq. 3.8, one can show that, in the Schrödinger picture, the

reduced density matrix for state 0 and state 1 evolves as<sup>[83]</sup>,

$$\begin{aligned} \frac{d\rho_0}{dt} = & -\frac{i}{\hbar}[H_0, \rho_0] - \sum_k \frac{|V_k|^2}{\hbar^2} \int_0^\infty d\tau e^{i\epsilon_k\tau/\hbar} f(\epsilon_k) e^{-iH_1\tau/\hbar} e^{iH_0\tau/\hbar} \rho_0 \\ & - e^{i\epsilon_k\tau/\hbar} (1 - f(\epsilon_k)) \rho_1 e^{-iH_1\tau/\hbar} e^{iH_0\tau/\hbar} + h.c. \end{aligned} \quad (3.14)$$

$$\begin{aligned} \frac{d\rho_1}{dt} = & -\frac{i}{\hbar}[H_1, \rho_1] - \sum_k \frac{|V_k|^2}{\hbar^2} \int_0^\infty d\tau e^{-i\epsilon_k\tau/\hbar} (1 - f(\epsilon_k)) e^{-iH_0\tau/\hbar} e^{iH_1\tau/\hbar} \rho_1 \\ & - e^{-i\epsilon_k\tau/\hbar} f(\epsilon_k) \rho_0 e^{-iH_0\tau/\hbar} e^{iH_1\tau/\hbar} + h.c. \end{aligned} \quad (3.15)$$

Here  $h.c$  denotes Hermitian conjugate. Eqs. 3.14 and 3.15 constitute a quantum master equation (QME). The CME is obtained by taking the Wigner transform of Eqs. 3.14 and 3.15, and throwing out all terms that are linear or higher in  $\hbar$ . This corresponds to a classical approximation for the nuclear motion (note that we are using dimensionless  $x$  and  $p$  here)<sup>[83]</sup>,

$$\frac{\partial P_0(x,p)}{\partial t} = \frac{1}{\hbar} \frac{\partial H_0(x,p)}{\partial x} \frac{\partial P_0(x,p)}{\partial p} - \frac{1}{\hbar} \frac{\partial H_0(x,p)}{\partial p} \frac{\partial P_0(x,p)}{\partial x} - \gamma_{0 \rightarrow 1} P_0(x,p) + \gamma_{1 \rightarrow 0} P_1(x,p), \quad (3.16)$$

$$\frac{\partial P_1(x,p)}{\partial t} = \frac{1}{\hbar} \frac{\partial H_1(x,p)}{\partial x} \frac{\partial P_1(x,p)}{\partial p} - \frac{1}{\hbar} \frac{\partial H_1(x,p)}{\partial p} \frac{\partial P_1(x,p)}{\partial x} + \gamma_{0 \rightarrow 1} P_0(x,p) - \gamma_{1 \rightarrow 0} P_1(x,p), \quad (3.17)$$

where,

$$\gamma_{0 \rightarrow 1} = \frac{\Gamma}{\hbar} f(\Delta V), \quad (3.18)$$

$$\gamma_{1 \rightarrow 0} = \frac{\Gamma}{\hbar} (1 - f(\Delta V)), \quad (3.19)$$

$$\Delta V = H_1 - H_0 = E_d + \sqrt{2}gx. \quad (3.20)$$

Here,  $\Gamma$  is the hybridization function,

$$\Gamma(\epsilon) = 2\pi \sum_k |V_k|^2 \delta(\epsilon_k - \epsilon). \quad (3.21)$$

In the wide band limit,  $\Gamma$  is a constant.  $f$  represents the Fermi function of the relevant

electronic bath. Eqs. 3.16 and 3.17 can be solved using the SH methodology as described in Paper II.

### 3.2.2. The Quantum Master Equation: the full QME vs. the secular approximation

To assess the validity of the CME, we will compute exact QME dynamics according to Eqs. 3.14 and 3.15. To do so, we assume that  $\Gamma$  is a constant (i.e. does not change with  $\epsilon$  [Eq. 3.21] or  $x$ ) and we expand the reduced density matrix in a basis of harmonic oscillator eigenstates:

$$\begin{aligned}
\frac{d\rho_0(i, j)}{dt} &= -\frac{\mathbf{i}}{\hbar}(\epsilon_0(i) - \epsilon_0(j))\rho_0(i, j) \\
&\quad -\frac{\Gamma}{2\hbar} \sum_{i', k} f(\epsilon_1(i') - \epsilon_0(k)) F_{i \rightarrow i'} F_{k \rightarrow i'} \rho_0(k, j) \\
&\quad -\frac{\Gamma}{2\hbar} \sum_{i', k} \rho_0(i, k) f(\epsilon_1(i') - \epsilon_0(k)) F_{j \rightarrow i'} F_{k \rightarrow i'} \\
&\quad +\frac{\Gamma}{2\hbar} \sum_{i', j'} (1 - f(\epsilon_1(j') - \epsilon_0(j))) F_{i \rightarrow i'} F_{j \rightarrow j'} \rho_1(i', j') \\
&\quad +\frac{\Gamma}{2\hbar} \sum_{i', j'} \rho_1(i', j') (1 - f(\epsilon_1(i') - \epsilon_0(i))) F_{i \rightarrow i'} F_{j \rightarrow j'}, \tag{3.22}
\end{aligned}$$

$$\begin{aligned}
\frac{d\rho_1(i', j')}{dt} &= -\frac{\mathbf{i}}{\hbar}(\epsilon_1(i') - \epsilon_1(j'))\rho_1(i', j') \\
&\quad -\frac{\Gamma}{2\hbar} \sum_{i, k'} (1 - f(\epsilon_1(k') - \epsilon_0(i))) F_{i \rightarrow i'} F_{i \rightarrow k'} \rho_1(k', j') \\
&\quad -\frac{\Gamma}{2\hbar} \sum_{i, k'} \rho_1(i', k') (1 - f(\epsilon_1(k') - \epsilon_0(i))) F_{i \rightarrow j'} F_{i \rightarrow k'} \\
&\quad +\frac{\Gamma}{2\hbar} \sum_{i, j} f(\epsilon_1(j') - \epsilon_0(j)) F_{i \rightarrow i'} F_{j \rightarrow j'} \rho_0(i, j) \\
&\quad +\frac{\Gamma}{2\hbar} \sum_{i, j} \rho_0(i, j) f(\epsilon_1(i') - \epsilon_0(i)) F_{i \rightarrow i'} F_{j \rightarrow j'}. \tag{3.23}
\end{aligned}$$

where  $\epsilon_0(i) = \hbar\omega(i + \frac{1}{2})$ , and  $\epsilon_1(i') = \hbar\omega(i' + \frac{1}{2}) + \bar{E}_d$ .  $\bar{E}_d$  is the renormalized impurity energy level,

$$\bar{E}_d \equiv E_d - E_r, \quad (3.24)$$

where  $E_r \equiv g^2/\hbar\omega$  is the reorganization energy.  $i$  ( $i'$ ) labels a phonon mode centered at  $x=0$  ( $x = -\sqrt{2}g/\hbar\omega$ ).  $F$  is the Franck-Condon factor,

$$F_{i \rightarrow i'} = \langle i' | i \rangle = \int dx \phi_{i'}(x + \sqrt{2}\lambda) \phi_i(x), \lambda \equiv g/\hbar\omega, \quad (3.25)$$

where  $\phi_i(x)$  is the  $i$ th eigenfunction of the harmonic oscillator. The Franck-Condon factor can be expressed as<sup>[32,86]</sup>,

$$F_{i \rightarrow i'} = (p!/Q!)^{1/2} \lambda^{Q-p} e^{-\lambda^2/2} L_p^{Q-p}(\lambda^2) [\text{sgn}(i' - i)]^{i-i'}. \quad (3.26)$$

$p$  ( $Q$ ) is the minimum (maximum) of  $i$  and  $i'$ , and  $L_n^m$  is generalized Laguerre polynomial. Eqs. 3.22 and 3.23 represent full, nonsecular QME dynamics which we will abbreviate “nQME”. Often in the literature, when solving the QME, one makes a secular approximation—whereby one eliminates the fast oscillating off-diagonal terms of the reduced density matrix and focuses only on the diagonal matrix elements. In this case, the secular approximation of the QME (sQME) dynamical equations of motion are

$$\frac{dP_i^n}{dt} = \sum_{n', i'} [P_{i'}^{n'} W_{i' \rightarrow i}^{n' \rightarrow n} - P_i^n W_{i \rightarrow i'}^{n \rightarrow n'}], \quad (3.27)$$

with

$$W_{i \rightarrow i'}^{0 \rightarrow 1} = \frac{\Gamma}{\hbar} |F_{i \rightarrow i'}|^2 f(\bar{E}_d + \hbar\omega(i' - i)), \quad (3.28)$$

$$W_{i' \rightarrow i}^{1 \rightarrow 0} = \frac{\Gamma}{\hbar} |F_{i \rightarrow i'}|^2 (1 - f(\bar{E}_d + \hbar\omega(i' - i))), \quad (3.29)$$

$$W_{i \rightarrow i'}^{n \rightarrow n'} = 0, n = n'. \quad (3.30)$$

Eqs. 3.27-3.30 were studied in Paper II. It is easy to show that, for the case of one bath, the nQME (Eqs. 3.22-3.26) and the sQME (Eqs. 3.27-3.30) yield the same equilibrium density matrix.

Figures 13 and 14 compare the transient dynamics for electron population according to sQME, nQME and CME for different parameters (for all the plots here and below, we have set  $\hbar = 1$ ). We prepare the system initially with the phonon equilibrated thermally assuming that the impurity state (or level) is unoccupied (state 0). For both sQME and nQME, we use 4th order Runge-Kutta to integrate the real time dynamics, and 60 vibrational states are included to achieve converged results. For SH, we average the results over 10000 trajectories. Clearly, without including coherence of the phonon states, sQME does not capture the oscillations of the electronic population at short times. By contrast, nQME populations do show transient oscillations and CME agrees well with nQME in the limit of high temperature and small  $\Gamma$ . Interestingly, whereas Ref. [83] suggests that the CME can be accurate only when  $\hbar\omega \ll \Gamma$ , we find empirically that the CME is accurate in our simulations provided only that  $\hbar\omega, \Gamma \ll kT$ .

### 3.3. ET rate for the AH model

Even though the transient populations of the impurity level exhibit oscillations at short times, after reaching equilibrium, one finds equal and opposite fluxes in population from one diabat to the other. These fluxes will now be shown to be those derived from the corresponding Marcus rates.

#### 3.3.1. Standard electron transfer: Marcus theory for the spin-boson model

For a spin-boson model with two electronic states D and A that correspond to the system states before and after an electron transfer (ET) step, the ET rate is given by the Marcus rate

$$k_{D \rightarrow A} = \frac{2\pi}{\hbar} |V_{DA}|^2 \mathcal{F}(E_{AD}). \quad (3.31)$$

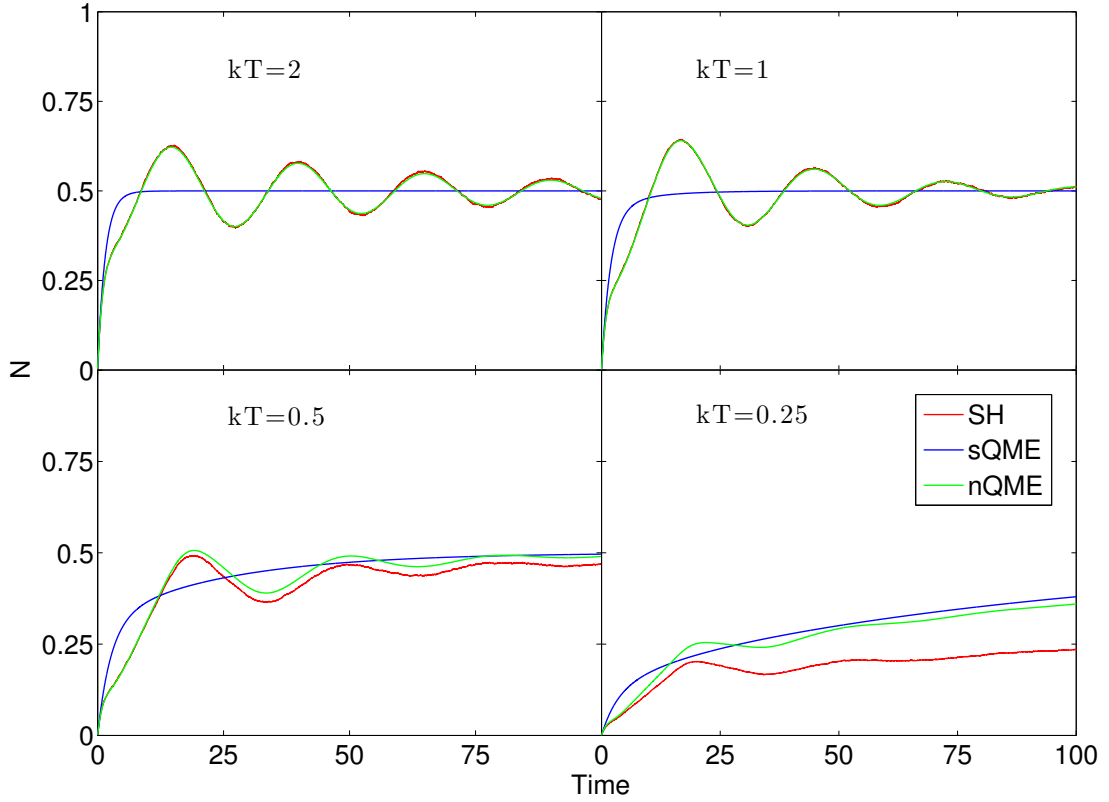


Figure 13: Transient dynamics: the impurity electron population as a function of time.  $\Gamma = 1$ ,  $\hbar\omega = 0.3$ , e-ph coupling  $g = 0.75$ ,  $E_d = 0$ . Note that SH and nQME agree at high temperatures. The sQME does not show any oscillations in electronic population, whereas the nQME shows transient oscillations which are (empirically) close to the frequency  $\omega$ . At time zero, the phonon is prepared to be equilibrated thermally (assuming the impurity is unoccupied).<sup>[3]</sup>

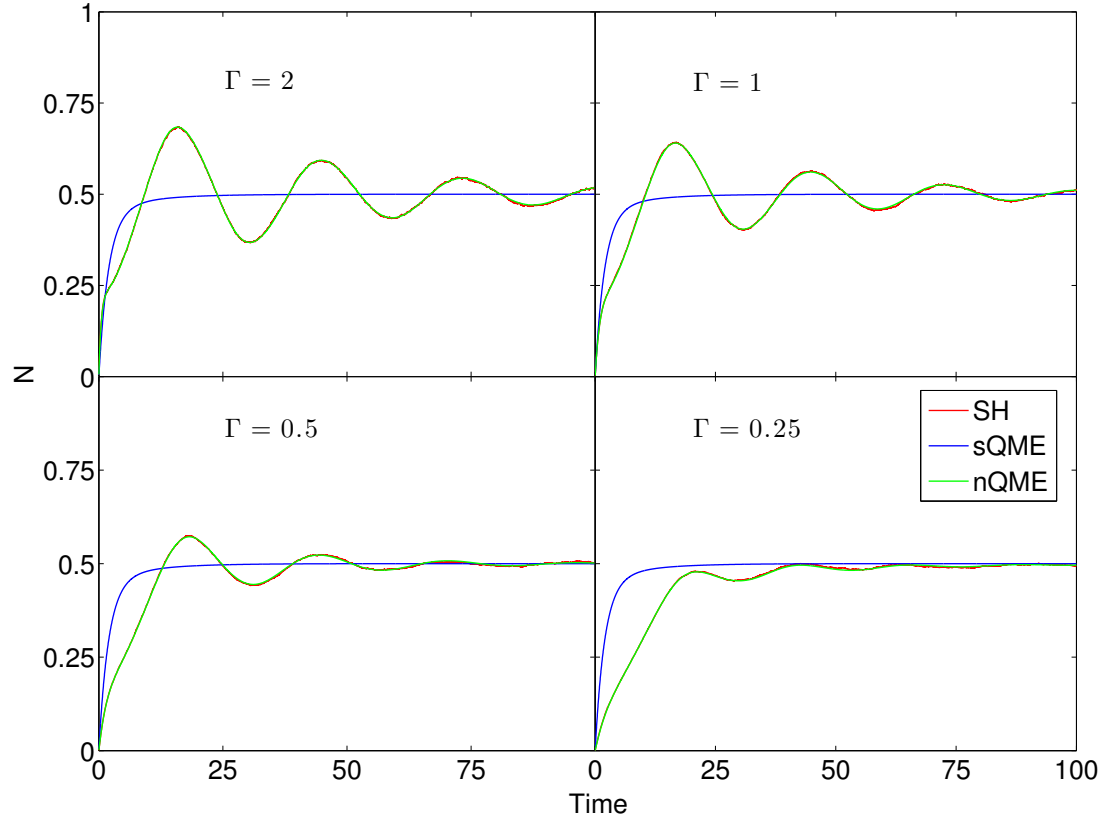


Figure 14: Transient dynamics: the impurity electron population as a function of time.  $kT = 1$ ,  $\hbar\omega = 0.3$ , e-ph coupling  $g = 0.75$ ,  $\bar{E}_d = 0$ . Note that SH and nQME agree in small  $\Gamma$  limit. The sQME does not show any oscillations in electronic population, whereas the nQME shows transient oscillations which are (empirically) close to the frequency  $\omega$ . At time zero, the phonon is prepared to be equilibrated thermally (assuming the impurity is unoccupied).<sup>[3]</sup>

Here  $E_{AD} \equiv E_A - E_D$  is the difference in energy between relaxed donor and acceptor (i.e. the “driving force”), and  $\mathcal{F}$  is the density weighted Frank-Condon factor which, in the classical limit, takes the form

$$\mathcal{F}(E_{AD}) = \frac{e^{-(E_r + E_{AD})^2/4E_r kT}}{\sqrt{4\pi E_r kT}}. \quad (3.32)$$

$E_r$  is the reorganization energy. In the corresponding electrode process, taking the process  $D \rightarrow A$  to imply an electron given from the impurity to the metal, the initial and final states are replaced by manifolds of system-metal states and the rate is obtained by averaging over the thermal distribution of initial states and summing over all final states. This leads to<sup>[110]</sup>

$$k_{D \rightarrow A} = \int d\epsilon \Gamma(\epsilon) (1 - f(\epsilon)) \mathcal{F}(E_{AD} + \epsilon) \quad (3.33)$$

$$k_{A \rightarrow D} = \int d\epsilon \Gamma(\epsilon) f(\epsilon) \mathcal{F}(E_{DA} - \epsilon) \quad (3.34)$$

where  $\Gamma(\epsilon) = 2\pi \sum_k |V_k|^2 \delta(\epsilon_k - \epsilon)$ , is the hybridization function defined in Eq. 3.21, taken below to be energy independent. Finally note that in the AH model,  $E_{DA} = -E_{AD} = \bar{E}_d$  is the renormalized single electron energy defined by Eq. 3.24.

### 3.3.2. Agreement with the SH picture

Let us now show that the CME yields the same Marcus rate in the long time (equilibrium) limit.<sup>1</sup>

In Paper II, we have shown that at equilibrium, the probability densities  $P_1(x, p)$  and  $P_0(x, p)$  reach a Boltzmann distribution. Thus the normalized reduced probability densities

---

<sup>1</sup>To understand why CME rates should agree with Marcus rates at equilibrium, we observe that Marcus theory is a transition state theory (TST) for the electron transfer rate, that relies on the two standard TST assumptions: (a) The reactant state is in thermal equilibrium, and (b) Back-scattering processes may be disregarded in the rate calculation. The second assumption is already implemented in the second order rates that enter the master equation 3.16-3.19

for position will be,

$$P_1(x) = \sqrt{\frac{\hbar\omega}{2\pi kT}} e^{-\frac{1}{2}\hbar\omega(x+\sqrt{2}g/\hbar\omega)^2/kT}, \quad (3.35)$$

$$P_0(x) = \sqrt{\frac{\hbar\omega}{2\pi kT}} e^{-\frac{1}{2}\hbar\omega x^2/kT}. \quad (3.36)$$

From the CME (Eqs. 3.16-3.20), the ET rate from state 1 to state 0 (representing an electron hopping from the impurity to the bath) at position  $x$  is determined as  $\Gamma(1 - f(\sqrt{2}gx + E_d))$ .

On average, the rate is

$$k_{1\rightarrow 0} = \int dx \Gamma(1 - f(\sqrt{2}gx + E_d)) \sqrt{\frac{\hbar\omega}{2\pi kT}} e^{-\frac{1}{2}\hbar\omega(x+\sqrt{2}g/\hbar\omega)^2/kT}. \quad (3.37)$$

Now, if we define  $\sqrt{2}gx + E_d \equiv \epsilon$  and change variables from  $x$  to  $\epsilon$  (using  $E_r = g^2/\hbar\omega$ , and  $\bar{E}_d = E_d - E_r$ ), the above equation becomes

$$k_{1\rightarrow 0} = \int d\epsilon \Gamma(1 - f(\epsilon)) \frac{e^{-(E_r+\epsilon-\bar{E}_d)^2/4E_r kT}}{\sqrt{4\pi E_r kT}}, \quad (3.38)$$

which agrees with Eq. 3.33. Similarly, one can show the backward rate from SH is given by

$$k_{0\rightarrow 1} = \int dx \Gamma f(\sqrt{2}gx + E_d) P_0(x). \quad (3.39)$$

Eq. 3.39 can be rewritten to recover the standard ET result (Eq. 3.34),

$$k_{0\rightarrow 1} = \int d\epsilon \Gamma f(\epsilon) \frac{e^{-(E_r-\epsilon+\bar{E}_d)^2/4E_r kT}}{\sqrt{4\pi E_r kT}}. \quad (3.40)$$

This proves the equivalence we hypothesized.

Moreover, in the SH picture, these ET rates can be easily extended to the case where  $\Gamma$  is not a constant, but depends on the nuclear position  $x$ . Below, we consider the case where  $\Gamma = \Gamma_0 \exp(-Dx^2)$ . This is equivalent to replacing  $d^+$  ( $d$ ) with  $d^+ e^{-Dx^2/2}$  ( $d e^{-Dx^2/2}$ ) in the system-bath coupling Hamiltonian (Eq. 3.4)

### 3.4. Broadening by the Marcus rate

From Eqs. 3.37-3.40, one can show that the forward and backward Marcus rates satisfy detailed balance

$$k_{1 \rightarrow 0} = e^{\bar{E}_d/kT} k_{0 \rightarrow 1}, \quad (3.41)$$

where  $\bar{E}_d$  is defined in Eq. 3.24. Eq. 3.41 proves that the equilibrium impurity electron population is a Fermi function,

$$N = \frac{k_{0 \rightarrow 1}}{k_{0 \rightarrow 1} + k_{1 \rightarrow 0}} = \frac{1}{1 + e^{\bar{E}_d/kT}} = f(\bar{E}_d), \quad (3.42)$$

which follows from detailed balance (Eq. 3.41).

It is important to remember that Eq. 3.42 is correct only in the limit of vanishingly small  $\Gamma$ . This expression does not include any broadening of the impurity level. To incorporate such broadening, in Paper II, we broadened all electronic observables using a Lorentzian function of width  $\Gamma$ . This worked well in certain regimes. However, this ansatz is not general and it is not clear how to define a broadening width if  $\Gamma$  is not a constant, but rather depends on nuclear coordinates. For instance,  $\Gamma(x) = \Gamma_0 e^{-Dx^2}$ .

Numerical tests described below indicate that a convolution of all electronic observables with a Lorentzian whose width is given by the sum of forward and backward Marcus rates

$$\gamma_t = k_{0 \rightarrow 1} + k_{1 \rightarrow 0}, \quad (3.43)$$

provides a good approximation as compared with numerically exact NRG results. This observation is intuitively appealing, since Eq. 3.43 is the inverse lifetime of an electron (hole) in an occupied (unoccupied) molecular level. Applying such broadening to Eq. 3.42, the impurity level occupation takes the form

$$N = \int dE \frac{1}{2\pi} \frac{\gamma_t}{(\gamma_t/2)^2 + (E - \bar{E}_d)^2} f(E), \quad (3.44)$$

that can be compared to the NRG-calculated value. As shown in Figures 15 and 16, the results from Eq. 3.44 agree well with Numerical Renormalization Group (NRG). For comparison, we also plot results either (i) without broadening or (ii) after broadening by  $\Gamma_0$ :

$$N = \int dE \frac{1}{2\pi} \frac{\Gamma_0}{(\Gamma_0/2)^2 + (E - \bar{E}_d)^2} f(E). \quad (3.45)$$

Note when  $D = 0$ ,  $\Gamma = \Gamma_0$ .

To highlight some of the nuances we face in estimating broadening rates, in Figures 17(a)-(b), we plot the electron population as a function of (a) e-ph coupling  $g$  and (b) temperature  $T$ . In Figure 17(a), we find that, even though results from Marcus rate broadening are not perfect (as compared to the NRG results), Marcus rate broadening clearly captures the feature that increasing  $g$  reduces the effective broadening. In Figure 17(b), we note that Marcus rate broadening agrees with NRG for both high and low temperatures.

Overall, Eq. 3.44 is the best approximation among all broadening approaches we have tested thus far. Future work will likely explore further the data in Figures 15-17 and seek either a better approach or an improved theoretical foundation for this empirical broadening behavior.

### 3.5. Steady state current

Thus far, we have shown that, when impurity-bath coupling depends strongly on nuclear coordinates, SH shows good agreement with NRG for equilibrium quantities (i.e. population). With this in mind we will now study out of equilibrium quantities; in particular we will compare I-V curves from SH and sQME in case of two electronic baths.<sup>[1,111]</sup><sup>2</sup> Our interest is exploring the rich nonequilibrium physics possible when  $\Gamma$  strongly depends on

---

<sup>2</sup>In the future, we intend to benchmark some time dependent calculation against exact results from Path Integral Monte Carlo<sup>[1,111]</sup>

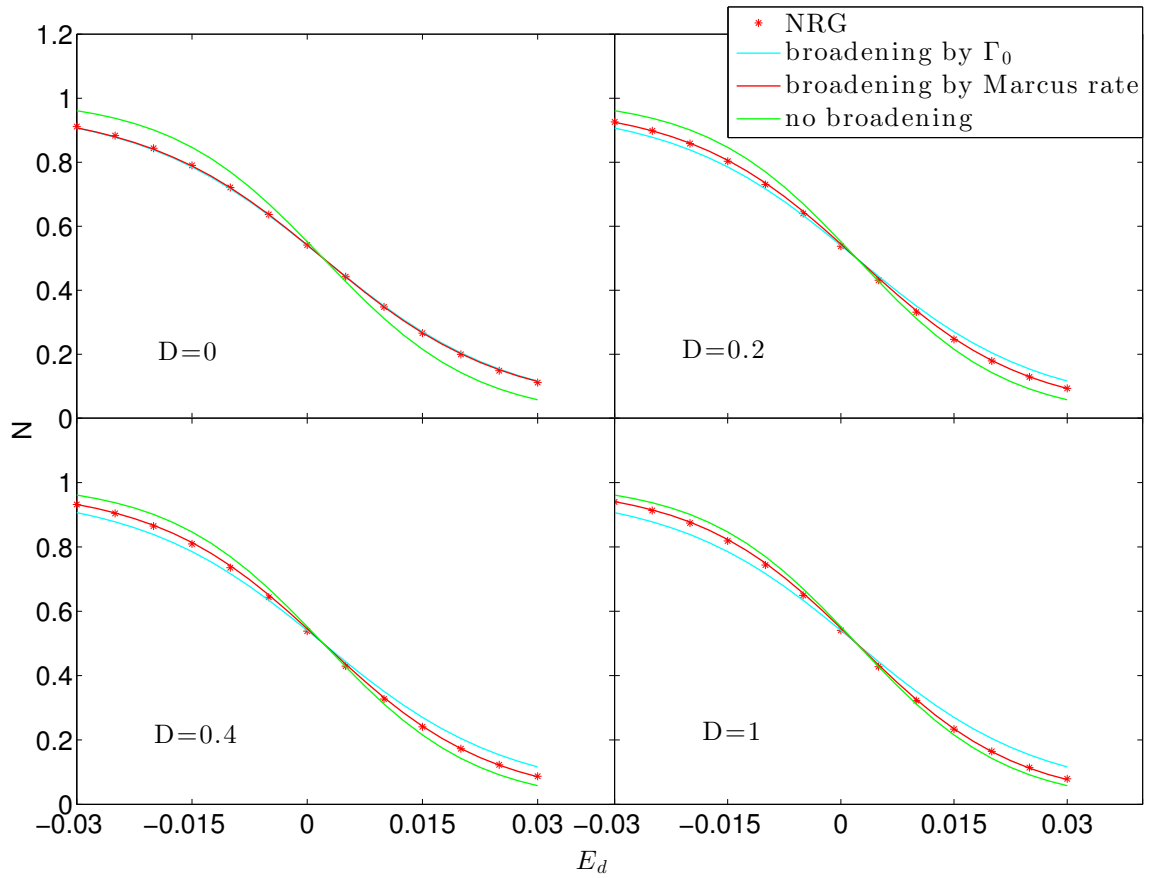


Figure 15: The equilibrium electron population as a function of the impurity energy level, when  $\Gamma$  depends on nuclear coordinate,  $\Gamma = \Gamma_0 e^{-Dx^2}$ ,  $\Gamma_0 = 0.01$ ,  $kT = 0.01$ ,  $\hbar\omega = 0.003$ , e-ph coupling  $g = 0.0025$ . The Marcus rates appear to be good estimate for a broadening rate. NRG data can be considered nearly exact.<sup>[4,5]</sup>

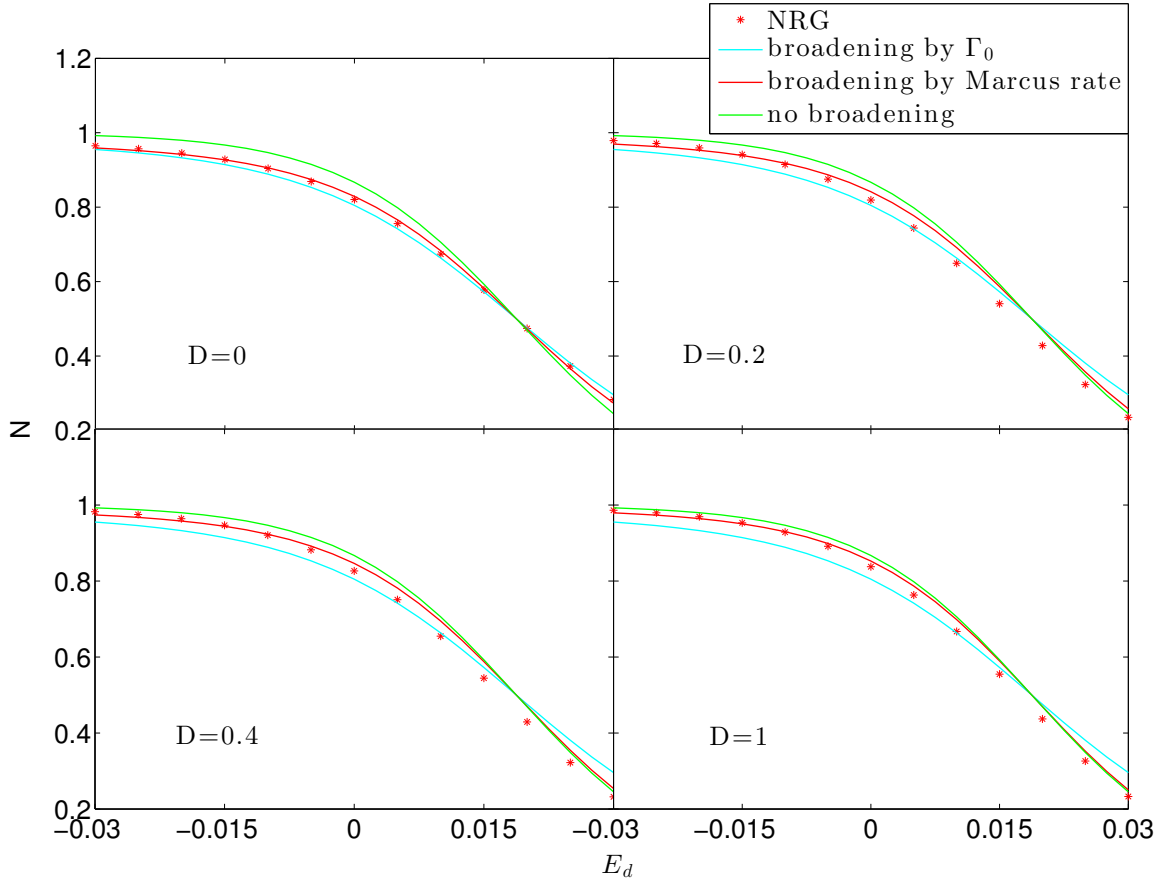


Figure 16: The equilibrium electron population as a function of the impurity energy level, when  $\Gamma$  depends on nuclear coordinate,  $\Gamma = \Gamma_0 e^{-Dx^2}$ ,  $\Gamma_0 = 0.01$ ,  $kT = 0.01$ ,  $\hbar\omega = 0.003$ , e-ph coupling  $g = 0.0075$ . The Marcus rates appear to be good estimate for a broadening rate. NRG data can be considered nearly exact.<sup>[4,5]</sup>

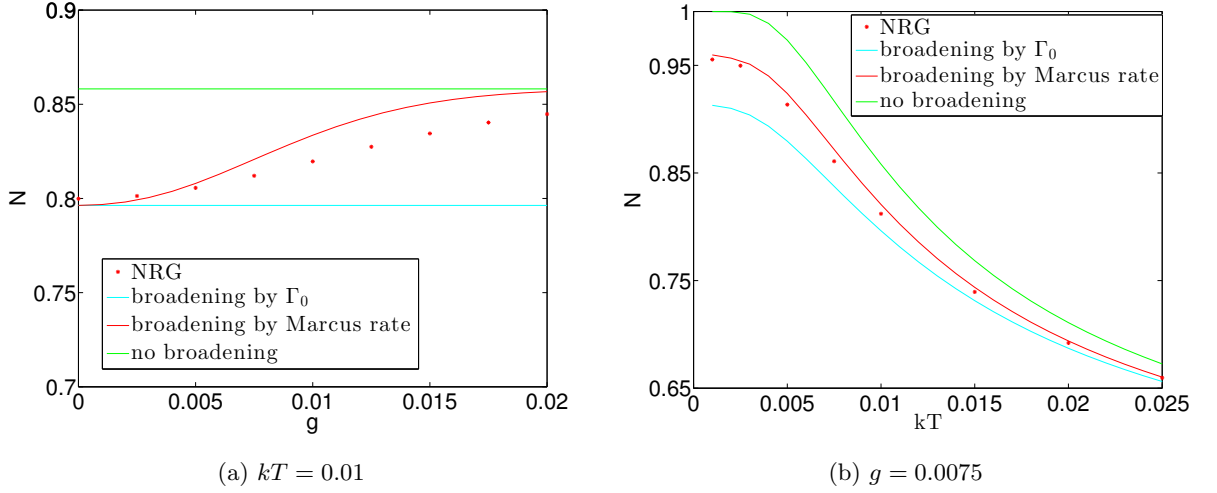


Figure 17: The equilibrium electron population as a function of (a) e-ph coupling  $g$  and (b) temperature  $kT$ . The other parameters are  $D = 0$ ,  $\Gamma_0 = 0.01$ ,  $\hbar\omega = 0.003$ ,  $\bar{E}_d = -0.018$ . Note that broadening by the Marcus rate gives the qualitatively correct behavior. NRG data can be considered nearly exact.<sup>[4,5]</sup>

$x$ , which might be called “non-Condon” behavior. Our choice here of hybridization is

$$\Gamma_L = \Gamma_0 e^{-Dx^2}, \quad (3.46)$$

$$\Gamma_R = \Gamma_0. \quad (3.47)$$

The procedure for calculating I-V curves for SH and QME can be found in Paper II. In short, with two electronic baths (with Fermi levels  $\mu_L$  and  $\mu_R$ ), the hopping rates of the CME (compared with the case of one electronic bath [Eqs. 3.18-3.19]) will be,

$$\gamma_{0 \rightarrow 1} = \frac{\Gamma_L}{\hbar} f^L(\Delta V) + \frac{\Gamma_R}{\hbar} f^R(\Delta V) \quad (3.48)$$

$$\gamma_{1 \rightarrow 0} = \frac{\Gamma_L}{\hbar} (1 - f^L(\Delta V)) + \frac{\Gamma_R}{\hbar} (1 - f^R(\Delta V)) \quad (3.49)$$

$\Gamma_L$  ( $\Gamma_R$ ) is the hybridization function of the impurity coupled to the left (right) electronic bath. The CME (Eqs.3.16-3.17) will be unchanged. The current can be calculated using

the steady states probability densities  $P_0(x, p)$  and  $P_1(x, p)$ ,

$$I = \int dx dp \left( \gamma_{0 \rightarrow 1}^L(x) P_0(x, p) - \gamma_{1 \rightarrow 0}^L(x) P_1(x, p) \right) \quad (3.50)$$

with,

$$\gamma_{0 \rightarrow 1}^L = \frac{\Gamma_L}{\hbar} f^L(\Delta V) \quad (3.51)$$

$$\gamma_{1 \rightarrow 0}^L = \frac{\Gamma_L}{\hbar} (1 - f^L(\Delta V)) \quad (3.52)$$

For the sQME (secular QME), when  $\Gamma_L = \Gamma_0 e^{-Dx^2}$ , it is easy to show that the transition rates between the impurity and the left electrode become (compared to Eqs. 3.28-3.30),

$$W_{i \rightarrow i'}^{0 \rightarrow 1^L} = \frac{\Gamma_0}{\hbar} |\langle i | e^{-Dx^2/2} | i' \rangle|^2 f^L(\bar{E}_d + \hbar\omega(i' - i)), \quad (3.53)$$

$$W_{i' \rightarrow i}^{1 \rightarrow 0^L} = \frac{\Gamma_0}{\hbar} |\langle i | e^{-Dx^2/2} | i' \rangle|^2 (1 - f^L(\bar{E}_d + \hbar\omega(i' - i))), \quad (3.54)$$

$$W_{i \rightarrow i'}^{n \rightarrow n'^L} = 0, n = n', \quad (3.55)$$

where again  $i$  ( $i'$ ) labels a phonon mode centered at  $x=0$  ( $x = -\sqrt{2}g/\hbar\omega$ ). The transition rates between the impurity and the right electrode are unchanged; one just sets  $f = f^R$  in Eqs. 3.28-3.30. As implemented in the sQME, the final on and off rates are the sum of the left and right rates,

$$W_{i' \rightarrow i}^{n' \rightarrow n} = W_{i' \rightarrow i}^{n' \rightarrow n^L} + W_{i' \rightarrow i}^{n' \rightarrow n^R}. \quad (3.56)$$

Similar to Eq. 3.50, with the steady states probabilities densities  $P_i^n$ , we can calculate the steady current

$$I = \sum_{ii'} P_i^0 W_{i \rightarrow i'}^{0 \rightarrow 1^L} - P_{i'}^1 W_{i' \rightarrow i}^{1 \rightarrow 0^L}. \quad (3.57)$$

To obtain converged results for the current, 300 phonon states are kept for the sQME. Here we do not incorporate any level broadening for either the sQME or SH data (which is valid

when  $\Gamma$  is small).

In Figure 18, we plot I-V curves for different values of D from SH and sQME, and we find good agreement between them.

The most interesting observation in Figure 18 is that, when D is nonzero, the I-V curve shows a peak. In words, increasing the voltage across the impurity can lower the current. This peak can be explained by the (unbroadened) Landauer formula,

$$I = \frac{\Gamma_L \Gamma_R}{\Gamma_L + \Gamma_R} (f^L - f^R). \quad (3.58)$$

In the normal region, when the bias between the two fermi levels becomes larger ( $f^L - f^R$  becomes larger), current increases. However, in addition to this primary effect, increasing the bias will also heat the oscillator to a higher temperature than the bath<sup>[30-32]</sup>. Thus, on average, the root of mean square displacement  $\langle x^2 \rangle$  should increase, which reduces the average of  $\Gamma_L$ , due to the factor  $e^{-Dx^2}$ . From the Landauer formula, when  $\Gamma_L$  becomes smaller, the current decreases.

As evidence for this explanation, in our SH calculations, we have added an external phonon bath coupled to the oscillator both through a Langevin force and a damping term<sup>[23]</sup>. Figure 19(b) shows that if the damping term  $\gamma_p$  is set to be  $\gamma_p=0.02$ , the temperature of the oscillator will not change with the voltage. In this case, observe that there are now no peaks in the I-V curves (Figure 19(a)). By contrast, without friction, the temperature of the oscillator changes dramatically with bias, and the I-V curves do show a peak.

### 3.6. Conclusions

We have investigated the transient dynamics of the CME, which include interesting oscillations at short times. For large enough temperature  $T$ , our dynamics agree with the full, nonsecular QME at most times. The secular QME provides a good approximation to the full QME at steady states.

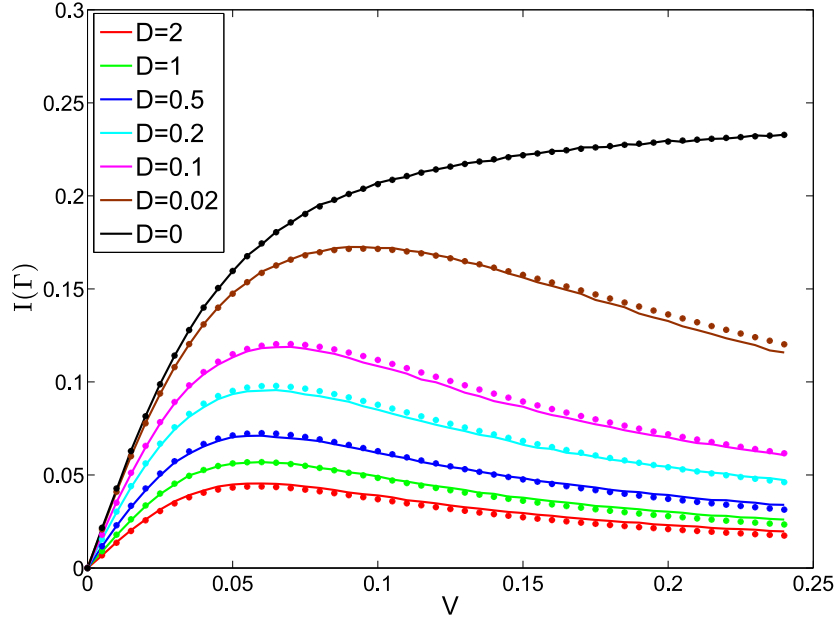


Figure 18: I-V curves for different values of  $D$  (see Eq. 3.46). Lines from SH, dots from the sQME.  $g = 0.005$ ,  $\hbar\omega = 0.003$ ,  $kT = 0.01$ ,  $\Gamma = 2\Gamma_0 = 0.01$ ,  $\bar{E}_d = 0$ . For large  $D$ , we observe negative differential resistance.

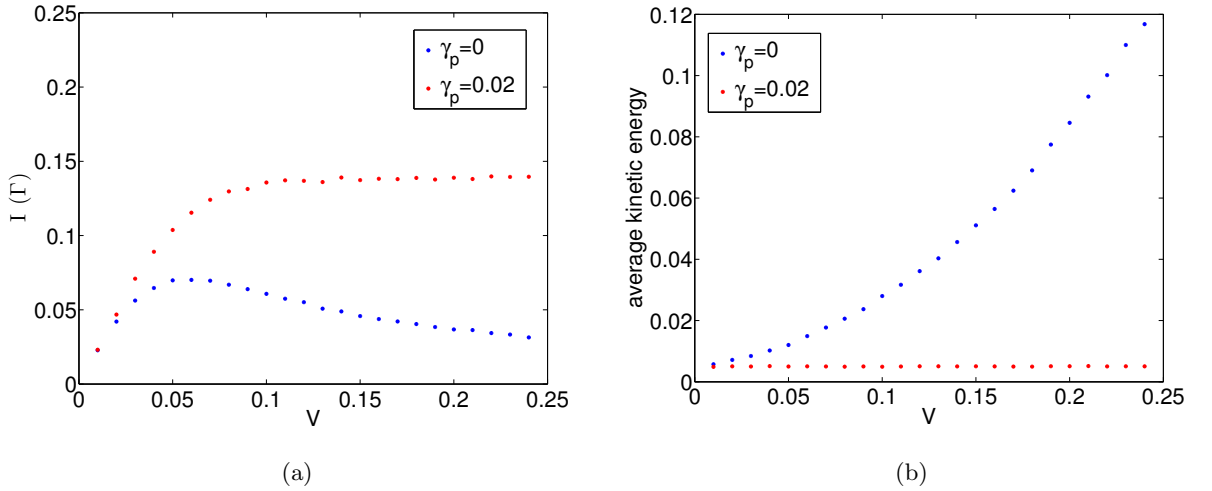


Figure 19: (a) I-V curves with and without an extra phonon bath, (b) the average kinetic energy (effective temperature) of the oscillator as a function of bias.  $kT = 0.01$ ,  $\Gamma_0 = 0.01$ ,  $D = 0.5$ ,  $\hbar\omega = 0.003$ ,  $\bar{E}_d = 0$ , e-ph coupling  $g = 0.0075$ , the damping term  $\gamma_p = 0.02$ . For weak phonon damping, negative differential resistance goes hand in hand with a voltage-dependent heating. For strong phonon damping, however, the average kinetic energy is independent of voltage and we find no negative differential resistance.

To connect with standard nonadiabatic quantum dynamics, we have shown analytically that our SH approach recovers the celebrated Marcus rate when  $\Gamma$  is a constant. Moreover, SH can be extended easily to the case where the hybridization function depends on the nuclear coordinate. In such a case, the Marcus rate gives us an easy, approximate way to incorporate level broadening, which has been verified by comparing with NRG for equilibrium populations (and with secular QME for out of equilibrium I-V curves). If possible, further benchmarking against exact dynamics will be useful. For now, we believe it is promising to apply the CME to a real condensed phase system—for example, the interaction between an adsorbate and a metal surface, which depends strongly on position. This work is ongoing.

Finally, we have studied I-V curves for the case where  $\Gamma = \Gamma_0 e^{-Dx^2}$ , and we have found an interesting turnover effect. This turnover can be explained as the result of heating from a steady state current and offers yet another example of inelastic scattering (which can lead to instability<sup>[30,32]</sup>, and I-V step features<sup>[78,79]</sup>). With coupling to an external phonon bath, however, the turnover effect disappears.

Overall, given the fact that  $\Gamma$  will hardly ever be a constant in practice, we believe the paper represents an important step forward towards understanding SH and implementing an algorithm to simulate a realistic condensed phase system.

## CHAPTER 4 : Frictional effects near a metal surface

This chapter was adapted from Ref. [6]

### 4.1. Introduction

When nuclei interact nonadiabatically with a manifold of electronic states, e.g. an adsorbate at a metal surface, there is a drastic breakdown of the Born-Oppenheimer approximation. For a closed system, with only a few degrees of freedom (DoFs), there exist some exact methodologies for studying this breakdown, including numerical exact approaches, such as Numerical Renormalization Group (NRG)<sup>[4,88,98]</sup>, Multi-Configuration Time-Dependent Hartree (MCTDH)<sup>[99]</sup>, and Path Integral Monte Carlo (PIMC)<sup>[1]</sup>. These methods are very powerful tools for solving model problems, but are difficult to apply to large, realistic (atomistic) systems.

A much simpler (but more approximate) approach for treating large-scale (atomistic) nonadiabatic dynamics near a metal surface is via a generalized Langevin dynamics (LD), whereby one runs effectively adiabatic molecular dynamics by including friction and a random force from the bath<sup>[112,113]</sup>. One such stochastic model of friction has been given by Head-Gordon and Tully, based on a smeared view of nonadiabatic couplings<sup>[82]</sup>. This model of electronic friction was derived for small electron-phonon (el-ph) couplings and zero temperature, and can be extended to the finite temperature case somewhat naturally<sup>[114]</sup>. Another stochastic model of Langevin dynamics was derived by von Oppen and coworkers based on a nonequilibrium Green function formalism and scattering matrix approaches that are applicable in and out of equilibrium.<sup>[80,115]</sup> Similar results were achieved using Influence Functionals<sup>[81,116]</sup>.

For large systems, surface hopping (SH) is yet another appealing approach for modeling (approximately) dynamics with el-ph couplings<sup>[16,39]</sup>. Now, traditionally, SH has been restricted to the case that molecules interact with a limited (i.e. a handful) of electronic states.

To go beyond this limited case and treat an (infinite) manifold of electronic states—e.g. the case of a molecule near a metal surface—Shenvi *et al* have proposed an independent electron surface hopping (IESH).<sup>[71]</sup> According to the IESH scheme, one discretizes the continuum and, by assuming independent one electron states, one can run reasonably large simulations that can capture vibrational relaxation.<sup>[72]</sup>

In a series of recent papers<sup>[38,95]</sup>, we have explored still another SH methodology—based on a classical master equation (CME)—to describe the dynamics of a molecule near a metallic system. According to this CME approach, the influence of the metal surface enters as hopping rates between two potential energy surfaces (PES’s). Essentially, if the molecule is charged, the nuclei move on one potential surface; and if the molecule is uncharged, the nuclei move on another. This method is valid when two conditions are met. First, as usual for SH methods, classical mechanics must be a good approximation for the nuclear motion, that is,  $\hbar\omega \ll kT$ , where  $\omega$  is a characteristic nuclear frequency and  $T$  is the temperature. Second, the CME should provide a good approximation for the kinetics of the electron transfer between molecule and metal. The CME is a perturbative expansion in metal-molecule coupling and will be accurate when the effect of molecular level broadening associated with the metal-molecule charge-transfer interaction can be disregarded, i.e.  $kT \gg \Gamma$ , where  $\Gamma$  is the corresponding width. (However, see Ref. [95] for an approximate workaround to incorporate broadening approximately.)

By using such a SH approach to construct and solve the CME, we have shown that an ensemble of SH trajectories admit a unique steady state solution no matter how we prepare the initial states. This solution is a manifestation of relaxation associated with the repeated electron exchange with a thermal electronic bath, similar in nature to the frictional effects described in Refs. [80, 81, 115, 116]. Now, the latter works consider the case of strong molecule-metal couplings ( $\hbar\omega \ll \Gamma$ ), where the nuclear motion loses its surface hopping character and can be described as motion on a single potential of mean force accompanied by electronic thermal noise and friction. By contrast, the CME is valid (see above) both

in the limit of strong metal-molecule coupling ( $\Gamma \gg \hbar\omega$ ) and weak metal-molecule coupling ( $\Gamma \ll \hbar\omega$ ). It is therefore of interest to compare SH dynamics versus mean field LD both in the weak and the strong metal-molecule coupling regime, both numerically and analytically.

In this paper, we show that in the strong molecule-metal coupling limit the CME can indeed be mapped onto a Fokker-Planck (FP) equation with (electronic) frictional damping and a random force. This FP equation can be formulated easily as an equivalent Langevin equation. Furthermore, the fluctuation-dissipation theorem is satisfied automatically for the case of a molecule near one equilibrium metallic bath. Our results are identical to those obtained in Ref. [80] in the limit  $kT \gg \Gamma$ .

The final objective of this paper is to study the effect of friction on the ET rate. This can be done in two ways: either (i) changing the metal-molecule coupling or (ii) adding a nuclear phonon bath. In either case, we find a Kramer turnover effect.

The structure of this paper is as follows. In Sec. 4.2, we derive a FP equation from the CME. In Sec. 4.3.1, we compare dynamical observables from a FP equation versus those from a CME. In Sec. 4.3.2, we analyze the effect of friction on electron transfer (ET). We conclude in Sec. 4.4.

A word about notation is in order. Below, we use dimensionless position  $x$  ( $X = x\sqrt{\frac{\hbar}{m\omega}}$ ) and momentum  $p$  ( $P = p\sqrt{m\omega\hbar}$ ). Here  $X$  and  $P$  are the usual position and momentum operators.  $m$  and  $\omega$  are the mass and frequency of an oscillator respectively.

## 4.2. Electronic friction

### 4.2.1. Classical Master Equation

For this paper, we will restrict ourselves to a generalized version of the Anderson-Holstein (AH) model. Our model Hamiltonian describes an impurity energy level (molecule) coupled

both to a vibrational DoF and a continuum of electronic states:

$$H = H_s + H_b + H_c, \quad (4.1)$$

$$H_s = E(x)d^+d + \frac{1}{2}\hbar\omega(x^2 + p^2), \quad (4.2)$$

$$H_b = \sum_k(\epsilon_k - \mu)c_k^+c_k, \quad (4.3)$$

$$H_c = \sum_k V_k(c_k^+d + d^+c_k), \quad (4.4)$$

where  $d$  ( $d^+$ ) and  $c_k$  ( $c_k^+$ ) are the annihilation (creation) operators for an electron in the impurity (subsystem) and in the continuum (bath),  $x$  and  $p$  are (dimensionless) position and momentum operators for the nuclei. For now,  $E(x)$  can be an arbitrary function of nuclear position. For the original AH model,  $E(x) = \sqrt{2}gx + E_d$ .

In the diabatic picture, there are two classes of PES's—those with the impurity occupied (denoted as 1) and those with the impurity unoccupied (denoted as 0),

$$H_\alpha = V_\alpha + \frac{1}{2}\hbar\omega p^2, \alpha = 0, 1 \quad (4.5)$$

$$V_0 = \frac{1}{2}\hbar\omega x^2, \quad (4.6)$$

$$V_1 = \frac{1}{2}\hbar\omega x^2 + E(x). \quad (4.7)$$

In a CME, we define the classical phase space probability densities  $P_0(x, p, t)$  ( $P_1(x, p, t)$ ) for the nuclear DoFs at time  $t$ , assuming that the impurity is unoccupied (occupied) and the nuclei is at position  $x$  with momentum  $p$ . The time evolution of phase space probability densities is governed by<sup>[83,95]</sup>,

$$\frac{\partial P_0(x, p, t)}{\partial t} = \{H_0(x, p), P_0(x, p, t)\} - \gamma_{0 \rightarrow 1}P_0(x, p, t) + \gamma_{1 \rightarrow 0}P_1(x, p, t), \quad (4.8)$$

$$\frac{\partial P_1(x, p, t)}{\partial t} = \{H_1(x, p), P_1(x, p, t)\} + \gamma_{0 \rightarrow 1}P_0(x, p, t) - \gamma_{1 \rightarrow 0}P_1(x, p, t), \quad (4.9)$$

where  $\{\}$  is the Poisson bracket,

$$\{A, B\} = \frac{1}{\hbar} \left( \frac{\partial A}{\partial x} \frac{\partial B}{\partial p} - \frac{\partial B}{\partial x} \frac{\partial A}{\partial p} \right). \quad (4.10)$$

$\gamma_{0 \rightarrow 1}$  and  $\gamma_{1 \rightarrow 0}$  are the hopping rates. In the case of one electronic bath,

$$\gamma_{0 \rightarrow 1} = \frac{\Gamma}{\hbar} f(E), \quad (4.11)$$

$$\gamma_{1 \rightarrow 0} = \frac{\Gamma}{\hbar} (1 - f(E)). \quad (4.12)$$

Here,  $f$  is the Fermi function, and  $\Gamma$  is the hybridization function,

$$\Gamma(\epsilon) = 2\pi \sum_k |V_k|^2 \delta(\epsilon_k - \epsilon), \quad (4.13)$$

which is assumed to be a constant (i.e. the wide band approximation).

#### 4.2.2. Fokker-Planck Equation

Let us now write down the CME explicitly for the case of one bath:

$$\begin{aligned} \hbar \frac{\partial P_0(x, p, t)}{\partial t} = & - \hbar \omega p \frac{\partial P_0(x, p, t)}{\partial x} + \hbar \omega x \frac{\partial P_0(x, p, t)}{\partial p} - \Gamma f(E) P_0(x, p, t) \\ & + \Gamma (1 - f(E)) P_1(x, p, t), \end{aligned} \quad (4.14)$$

$$\begin{aligned} \hbar \frac{\partial P_1(x, p, t)}{\partial t} = & - \hbar \omega p \frac{\partial P_1(x, p, t)}{\partial x} + \left( \hbar \omega x + \frac{dE}{dx} \right) \frac{\partial P_1(x, p, t)}{\partial p} + \Gamma f(E) P_0(x, p, t) \\ & - \Gamma (1 - f(E)) P_1(x, p, t). \end{aligned} \quad (4.15)$$

We define new densities  $A(x, p, t)$  and  $B(x, p, t)$  as follows,

$$P_0(x, p, t) = (1 - f(E)) A(x, p, t) + B(x, p, t), \quad (4.16)$$

$$P_1(x, p, t) = f(E) A(x, p, t) - B(x, p, t). \quad (4.17)$$

Note that  $A(x, p, t) = P_0(x, p, t) + P_1(x, p, t)$ , which is the total probability density. We would like to find a FP equation describing the time evolution of  $A(x, p, t)$ .

To that end, if we plug Eqs. 4.16 and 4.17 into Eqs. 4.14 and 4.15 and add them up, we find,

$$\hbar \frac{\partial A(x, p, t)}{\partial t} = -\hbar\omega p \frac{\partial A(x, p, t)}{\partial x} + (\hbar\omega x + \frac{dE}{dx} f(E)) \frac{\partial A(x, p, t)}{\partial p} - \frac{dE}{dx} \frac{\partial B(x, p, t)}{\partial p}. \quad (4.18)$$

Next, using  $B(x, p, t) = f(E)P_0(x, p, t) - (1 - f(E))P_1(x, p, t)$ , together with Eqs. 4.14 and 4.15, we find

$$\begin{aligned} \hbar \frac{\partial B(x, p, t)}{\partial t} &= -\hbar\omega p \frac{\partial B(x, p, t)}{\partial x} + \hbar\omega p A \frac{\partial f(E)}{\partial x} + \hbar\omega x \frac{\partial B(x, p, t)}{\partial p} \\ &- \frac{dE}{dx} f(E)(1 - f(E)) \frac{\partial A(x, p, t)}{\partial p} + \frac{dE}{dx} (1 - f(E)) \frac{\partial B(x, p, t)}{\partial p} - \Gamma B(x, p, t). \end{aligned} \quad (4.19)$$

Eqs. 4.18-4.19 are valid under the CME assumptions  $kT \gg \hbar\omega, \Gamma$ . We now further make the strong coupling assumption that the inverse lifetime of the impurity is much larger than the oscillator frequency,  $\Gamma \gg \hbar\omega$ , which implies that the oscillator reaches local equilibrium quickly. Thus,  $B(x, p, t)$  should be small relative to  $A(x, p, t)$ , and one might hope that  $B(x, p, t)$  should change slowly with respect to  $x, p, t$ . (The validity of these assumptions can be inferred from the data below.) These assumptions allow us to ignore several terms in Eq. 4.19, and we find

$$B(x, p, t) \approx -\frac{dE}{dx} \frac{1}{\Gamma} (1 - f(E)) f(E) \frac{\partial A(x, p, t)}{\partial p} + \frac{\hbar\omega}{\Gamma} p A \frac{\partial f(E)}{\partial x}. \quad (4.20)$$

If we substitute Eq. 4.20 back into Eq. 4.18, we arrive at a FP equation (using the fact that  $\frac{\partial f(E)}{\partial x} = -\frac{dE}{dx} f(E)(1 - f(E)) \frac{1}{kT}$ ),

$$\begin{aligned} \hbar \frac{\partial A(x, p, t)}{\partial t} &= -\hbar\omega p \frac{\partial A(x, p, t)}{\partial x} + \frac{\partial U(x)}{\partial x} \frac{\partial A(x, p, t)}{\partial p} \\ &+ \hbar\gamma_e \frac{\partial}{\partial p} (pA(x, p, t)) + \hbar\gamma_e \frac{kT}{\hbar\omega} \frac{\partial^2 A(x, p, t)}{\partial p^2}. \end{aligned} \quad (4.21)$$

Here  $\gamma_e$  is the electronic friction

$$\gamma_e = \frac{1}{\Gamma} \frac{\omega}{kT} f(E)(1 - f(E)) \left( \frac{dE}{dx} \right)^2, \quad (4.22)$$

and  $\frac{\partial U(x)}{\partial x}$  is the mean force

$$\frac{\partial U(x)}{\partial x} = \hbar\omega x + \frac{dE}{dx} f(E). \quad (4.23)$$

We can write the potential of mean force explicitly (up to a constant),

$$U(x) = \frac{1}{2} \hbar\omega x^2 - \frac{1}{\beta} \log(1 + \exp(-\beta E(x))). \quad (4.24)$$

Eqs. 4.21-4.23 are the main results of this paper. In Appendix 4.5.1 we show that these equations are consistent with those of Ref. [80] in the limit  $kT \gg \Gamma$ . Also in Appendix 4.5.1, we give a very rough sketch about how our model might connect with the Head-Gordon/Tully electronic friction model. Note that our results are not restricted to a harmonic approximation for the nuclear motion (see Appendix 4.5.2 for the general form of the FP equation in standard units).

To better understand Eqs. 4.21-4.23, we will consider here and below the original AH model, where  $E(x)$  is chosen to linearly depend on  $x$ ,

$$E(x) = \sqrt{2}gx + E_d. \quad (4.25)$$

We define the renormalized energy as  $\bar{E}_d \equiv E_d - E_r$ , where  $E_r = g^2/\hbar\omega$  is the reorganization energy. In Fig. 20, we plot the potential of mean force and electronic friction as a function of  $x$  for the AH model. Note that the friction shows a peak where the two PES's cross and multiple surface effects are important. At this point, electrons are exchanged near the metal Fermi energy, where the partial occupation of the metal single-electron levels facilitates this exchange.

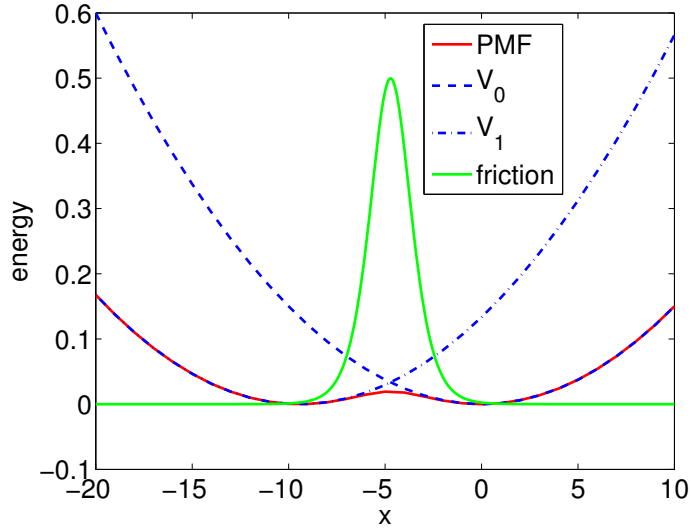


Figure 20: Potential of mean force (PMF, Eq. 4.24) and electronic friction (Eq. 4.22) as a function of position for the AH model;  $V_0$  (Eq. 4.6) and  $V_1$  (Eqs. 4.7 and 4.25) are the two diabatic PES's.  $g = 0.02$ ,  $\hbar\omega = 0.003$ ,  $\Gamma = 0.01$ ,  $\bar{E}_d = 0$ ,  $kT = 0.02$ . In Ref.<sup>[6]</sup>,  $kT = 0.01$  by mistake, which should be  $kT = 0.02$ . Here, the electronic friction is plotted in units of  $\frac{g^2\omega}{\Gamma kT}$ .

#### 4.2.3. Equilibrium Solution

Before we analyze numerically the behavior of the electronic friction model in Eqs. 4.21-4.23, a few analytical results about the equilibrium are appropriate.

The electronic friction in the FP equation (Eq. 4.21) guarantees that the total system density  $A(x, p, t)$  reaches thermal equilibrium. Let us show that this equilibrium (with Eqs. 4.20-4.21) will be identical to the equilibrium distribution from the CME.

As shown previously, the simple equilibrium solution for the CME is (for the case of one bath),

$$P_0^{CME}(x, p) = C \exp\left(-\frac{1}{2}\beta\hbar\omega(x^2 + p^2)\right), \quad (4.26)$$

$$P_1^{CME}(x, p) = C \exp\left(-\frac{1}{2}\beta\hbar\omega(x^2 + p^2) - \beta E(x)\right). \quad (4.27)$$

$C$  is a normalization factor, determined by  $\int \int dx dp (P_0^{CME}(x, p) + P_1^{CME}(x, p)) = 1$ .

Now, from Eq. 4.21, one can show easily that the equilibrium solution for the FP equation is,

$$A(x, p) = C \exp \left( -\frac{1}{2} \beta \hbar \omega p^2 - \beta U(x) \right). \quad (4.28)$$

From Eq. 4.20, moreover, we find that  $B(x, p)$  vanishes at equilibrium. Thus Eqs. 4.16 and 4.17 are reduced to

$$P_0(x, p) = (1 - f(E))A(x, p), \quad (4.29)$$

$$P_1(x, p) = f(E)A(x, p). \quad (4.30)$$

With the explicit form for the potential of mean force in Eq. 4.24, it is straightforward to show that Eqs. 4.29-4.30 give the same results as Eqs. 4.26-4.27.

### 4.3. Results

#### 4.3.1. *Electronic friction-Langevin dynamics*

Finally, we will now study the dynamics of the electronic friction/FP model and compare these dynamics with dynamics from the CME.

For the CME, phase space densities can be propagated using a SH algorithm in real time<sup>[38]</sup>. In short, we use a swarm of trajectories to sample phase space densities. For each trajectory, we assume the oscillator moves on one potential surface 1 (or 0). At each time step, we generate a random number  $\zeta \in [0, 1]$ . If  $\zeta > \gamma_{1 \rightarrow 0} dt$  (or  $\zeta > \gamma_{0 \rightarrow 1} dt$ ), the oscillator will continue moving on potential surface 1 (or 0) for a single time step of length  $dt$ . Otherwise, the oscillator will hop to potential surface 0 (or 1), and move a single time step on potential surface 0 (or 1). If the oscillator hops, the position and momentum are **not** adjusted.

For the FP equation, we use electronic friction-Langevin dynamics (EF-LD),

$$\hbar\dot{p} = -\frac{\partial U}{\partial x} - \hbar\gamma_e p + \xi, \quad (4.31)$$

$$\hbar\dot{x} = \hbar\omega p, \quad (4.32)$$

where  $\xi$  is the random force that is assumed to be a Gaussian variable with a norm  $\sigma = \sqrt{2\hbar\gamma_e kT/(\omega dt)}$  (which satisfies the fluctuation-dissipation theorem<sup>[23,110]</sup>). Again,  $dt$  is the time step interval. We use 4th order Runge-Kutta to integrate Eqs. 4.31-4.32. Below, unless stated otherwise, we use 10000 trajectories for SH and EF-LD simulations.

### Electronic population

First we look at the electronic population in the impurity as a function of time. For EF-LD, to calculate the electronic population, we make the following approximation,

$$N(t) = \int dx dp P_1(x, p, t) \approx \int dx dp f(E) A(x, p, t) \equiv \langle f(E) \rangle. \quad (4.33)$$

At long times, when  $B(x, p, t)$  vanishes, Eq. 4.33 gives the same population as the CME, as shown in Sec. 4.2.3. That being said, for short times, SH dynamics and FP dynamics can be extremely different.

In Fig. 21, we simulate electronic population in the impurity for both SH and EF-LD, where we prepare the initial states of the oscillators in one well with a Boltzmann distribution at temperature  $kT$ . Note that, because the potential of mean force is a mixture of two diabatic PES's, the initial ( $t = 0$ ) electronic populations from EF-LD are not equal to 1. Furthermore, observe that SH and EF-LD dynamics disagree strongly at short times; agreement occurs only at long times. Clearly, EF-LD is not reliable for calculating electronic population in general. In fact, EF-LD would be useless for simulating the early time dynamics of a photoexcited system where the nuclear distribution was completely uncorrelated with electronic population.

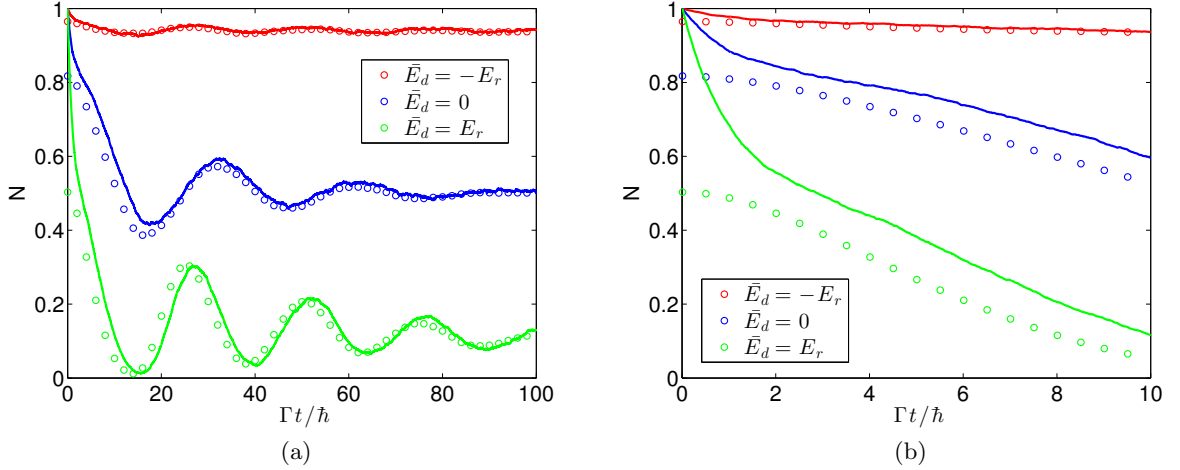


Figure 21: Electronic population in the impurity from EF-LD (circles) and SH (lines): (a) long time dynamics, (b) short time dynamics.  $g = 0.02$ ,  $\hbar\omega = 0.003$ ,  $\Gamma = 0.01$ ,  $kT = 0.05$ . Note that EF-LD and SH agree only at long times; at short times, EF-LD is unreliable.

### Kinetic energies and momentum-momentum correlation functions

Whereas EF-LD does not yield a robust treatment of impurity population, the model is much more reliable for measuring nuclear observables.

In Fig. 22, we look at the average kinetic energy as the oscillator relaxes after being prepared initially with an inflated temperature of  $5kT$  (in a Boltzmann distribution). Fig. 23 plots the momentum-momentum correlation. Both plots show that, with increased  $\Gamma$ , EF-LD agrees with SH. Lastly, Fig. 24 shows that, for the AH model, EF-LD works best when  $g$  (the el-ph coupling) is not too large.

Overall, our conclusions are as follows. On the one hand, Ref. [95] shows our SH approach agrees well with quantum master equation (QME), both when  $\Gamma \ll \hbar\omega$ , or  $\Gamma \gg \hbar\omega$ . On the other hand, we have shown the EF-LD agrees well with SH only in the limit that  $\Gamma \gg \hbar\omega$  and when the initial conditions are quasi-equilibrium. Because both SH and EF-LD are computationally inexpensive with roughly the same cost, for now we presume SH approach will be more useful than EF-LD in the limit  $kT \gg \Gamma$ . For now, EF-LD would appear

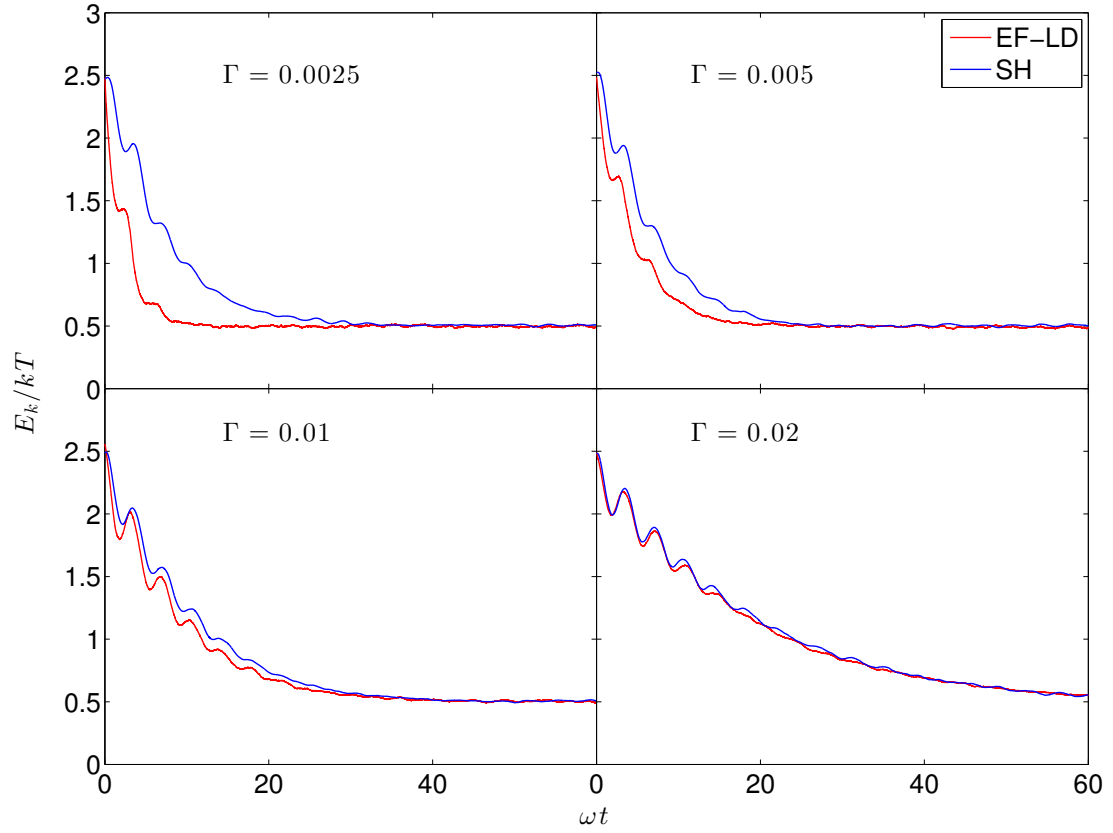


Figure 22: The effect of electronic friction on phonon relaxation. Here, we plot the average kinetic energy as a function of time.  $kT = 0.05$ ,  $\hbar\omega = 0.003$ ,  $g = 0.02$ ,  $\bar{E}_d = 0$ . We prepare the initial states satisfying a Boltzmann distribution with a temperature  $5kT$ . Note that EF-LD agrees with SH increasingly well as  $\Gamma$  increases.

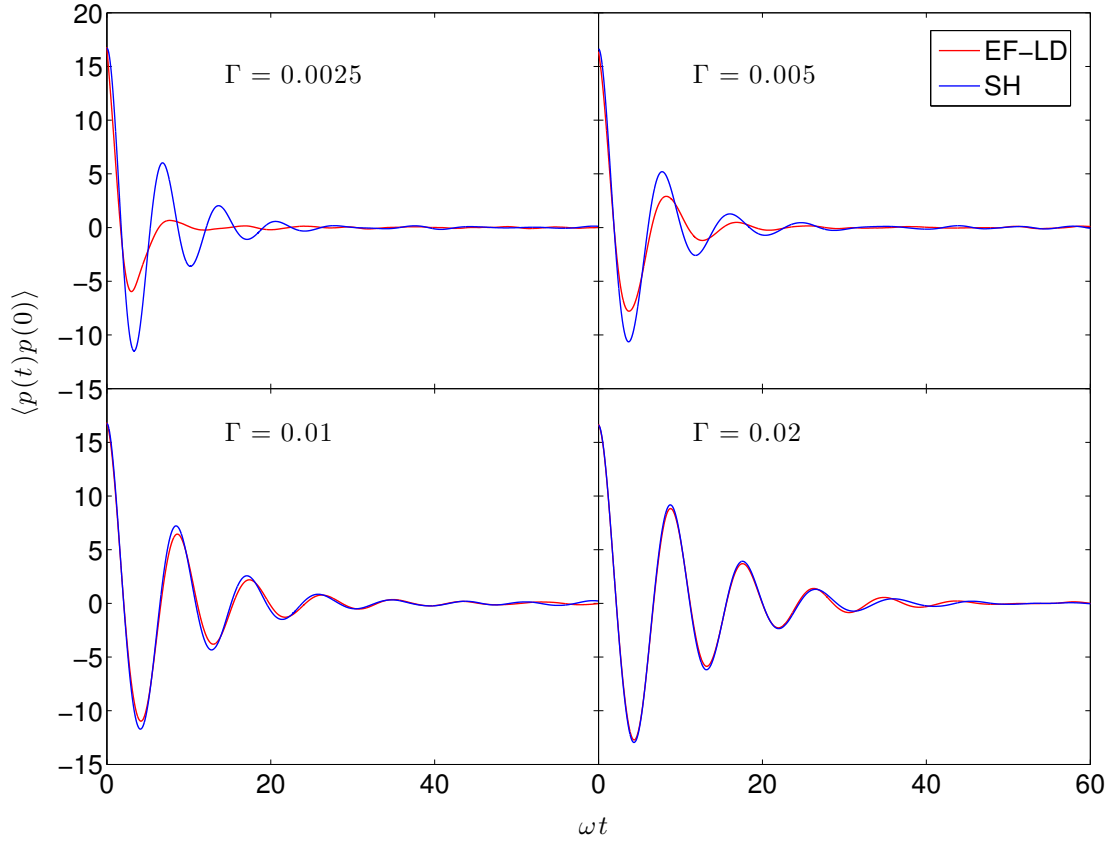


Figure 23: The effect of electronic friction on the momentum-momentum correlation function.  $kT = 0.05$ ,  $\hbar\omega = 0.003$ ,  $g = 0.02$ ,  $\bar{E}_d = 0$ . 100 trajectories have been used to calculate the momentum-momentum correlation function. Note that EF-LD agrees better with SH for large  $\Gamma$ .

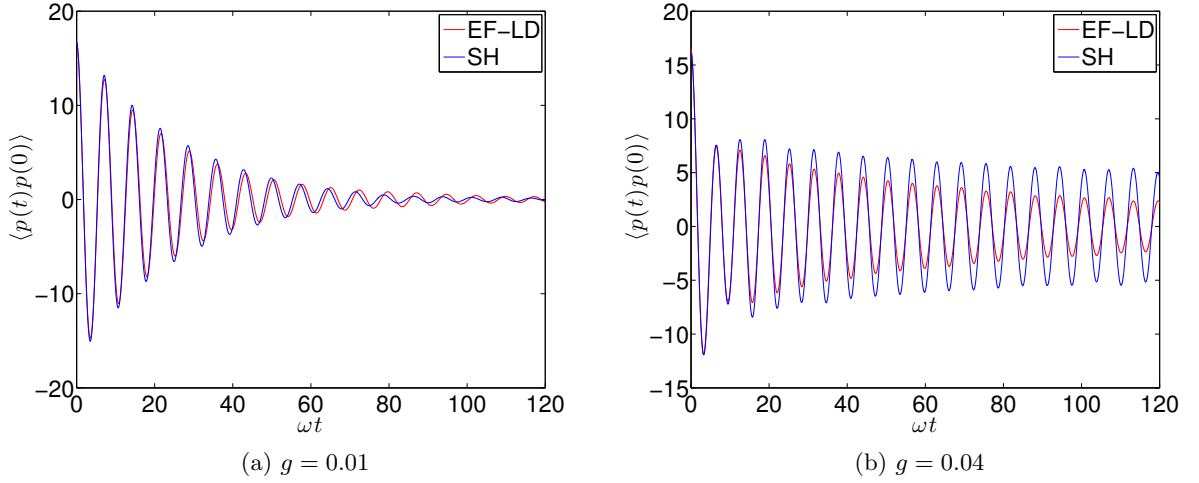


Figure 24: The effect of electronic friction on the momentum-momentum correlation function.  $kT = 0.05$ ,  $\Gamma = 0.01$ ,  $\hbar\omega = 0.003$ ,  $\bar{E}_d = 0$ . 100 trajectories have been used to calculate the momentum-momentum correlation function. Note that EF-LD agrees better with SH when  $g$  is smaller.

useful only for physical intuition.

#### 4.3.2. The effect of friction on barrier crossings

### Electronic Friction

The potential of mean force for the AH model is a double well with a barrier (Fig. 20), and the friction increases as  $\Gamma$  decreases (see Eq. 4.22). Thus, in the context of EF-LD, the electron transfer rate as a function of friction (or  $\Gamma$ ) should give a turnover effect just as in standard transition state theory.

In Fig. 25 we plot ET rates as a function of  $\Gamma$  for both EF-LD and SH. When calculating ET rates from SH dynamics, we fit the long time electronic population to an exponential function, which should yield total ET rates,

$$K_T = K_{1 \rightarrow 0} + K_{0 \rightarrow 1}. \quad (4.34)$$

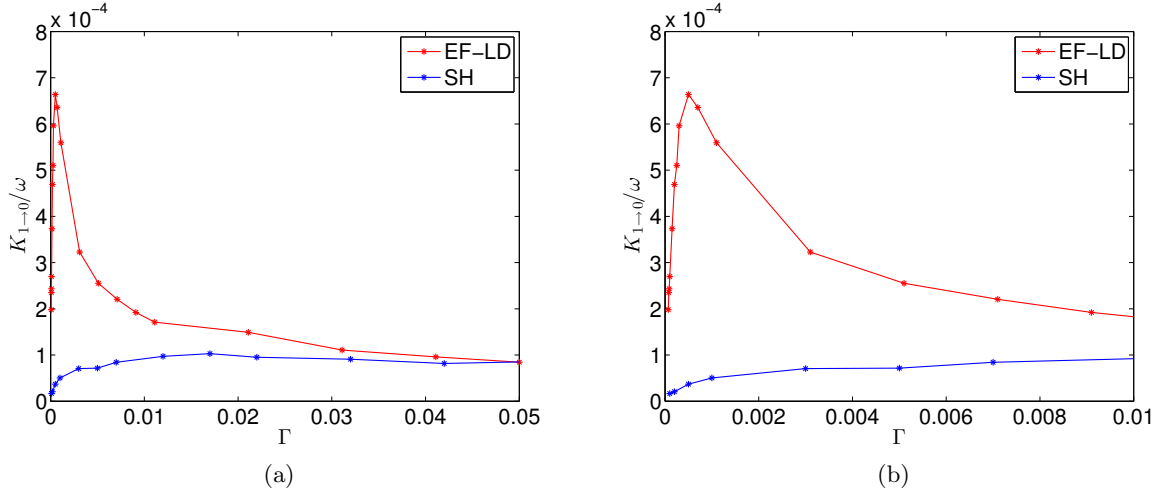


Figure 25: (a): Electron transfer rate as a function of  $\Gamma$ ; (b): A zoomed in picture of (a) in the range  $\Gamma \in [0, 0.01]$ .  $g = 0.02$ ,  $\hbar\omega = 0.003$ ,  $\bar{E}_d = 0$ ,  $kT = 0.01$ . The electronic friction varies as  $1/\Gamma$ , so that over damped dynamics occur as  $\Gamma \rightarrow 0$ .

To determine the forward rates ( $K_{1 \rightarrow 0}$ ), we invoke detailed balance<sup>[117]</sup>, so that

$$K_{1 \rightarrow 0} = K_{0 \rightarrow 1} \exp(\beta \bar{E}_d). \quad (4.35)$$

To determine the ET rates from EF-LD, we fit the average position  $\langle x \rangle$  as a function of time with an exponential. Again, by using the detailed balance in Eq. 4.35, we can determine the forward ET rates. This prescription allows us to extract ET rates without ever calculating the electronic population explicitly.

In Fig. 25, we see that, according to EF-LD, there is large turnover effect in the ET rate as function of  $\Gamma$ . This Kramer turnover is a well-known function of overdamping. For SH dynamics, we do not see such a large effect, but there is an optimal range of  $\Gamma$  that maximizes the ET rate (around  $\Gamma = 0.015$ ). Note that EF-LD should not (and does not) agree with SH dynamics for small  $\Gamma$  ( $\Gamma \leq \hbar\omega$ ). The rates in Fig. 25 are quite slow and SH and EF-LD are in near agreement for  $\Gamma \geq 0.01$ .

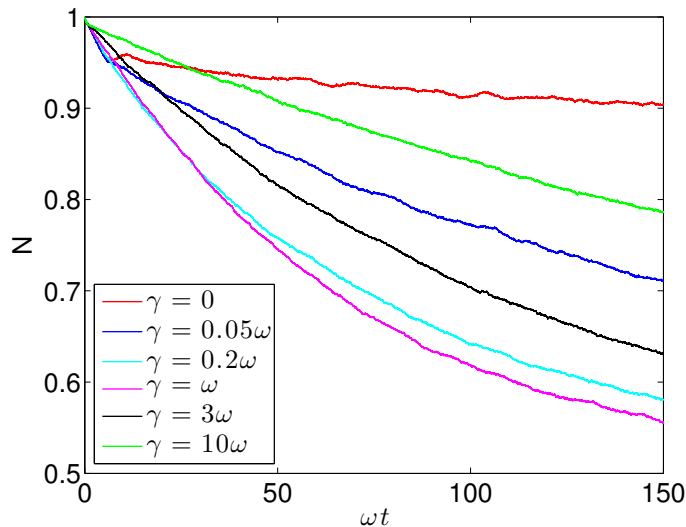


Figure 26: Electronic population in the impurity as a function of time with different phonon frictions.  $g = 0.02$ ,  $\hbar\omega = 0.003$ ,  $\Gamma = 0.01$ ,  $\bar{E}_d = 0$ ,  $kT = 0.01$ .

### Imposition of external (phonon) frictional bath

As seen in Fig. 25, we obtain a pronounced turnover in the rate as a function of  $\Gamma$  from the EF-LD dynamics when this dynamics fails to correctly describe system behavior ( $\Gamma \ll \hbar\omega$ ). For comparison with standard descriptions of environmental (phonon) effects on reaction rates, we next simulate the effect of a thermal environment (solvent motions) by adding standard (Markovian and position independent) frictional damping and the associated random force that together satisfy the fluctuation-dissipation theorem.

Fig. 26 shows electronic population in the impurity as a function of time with different phonon frictions from SH. Here we are operating in the limit  $E_r \gg kT$ . If we compare Fig. 21 against Fig. 26, we find that, except for an early time transient, there are no oscillations in the electronic population. When we increase the phonon friction from 0 to  $\omega$ , the ET rates increase. Thereafter, increasing the phonon friction reduces the ET rates. Thus again, we find a Kramer's turnover effect.<sup>[110,117]</sup>

In Fig. 27(a), we plot the forward ET rates ( $K_{1 \rightarrow 0}$ ) as function of phonon frictions from

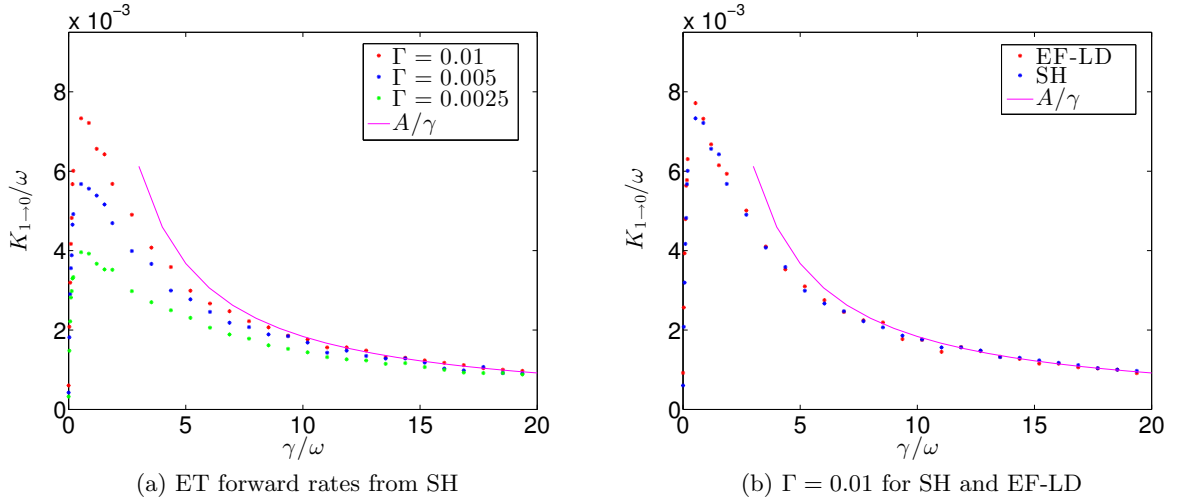


Figure 27: ET forward rates as function of phonon friction  $\gamma$  from SH and EF-LD.  $g = 0.02$ ,  $\hbar\omega = 0.003$ ,  $\bar{E}_d = 0$ ,  $kT = 0.01$ . Note the agreement between EF-LD and SH. For large  $\gamma$ , we fit the ET rates as  $A/\gamma$  (where  $A$  is a fitting parameter), which indicates that ET decays as  $1/\gamma$  for large friction.

SH, which shows the turnover phenomenon clearly. Moreover, the ET rates tend to agree for large phonon friction regardless of  $\Gamma$ . Note the relative scale of ET rates between Figs. 25 and 27. A simple fit shows that the ET rate scales as  $1/\gamma$ , as would be expected from Kramer’s theory. As Fig. 27(b) shows, ET rates from EF-LD agree well with results from SH.

#### 4.4. Conclusions

In this paper, we have found a Fokker-Planck (FP) equation to characterize a classical master equation (CME) for an impurity subsystem coupled to an electronic continuum and a nuclear DoF. (If the nuclear DoF is harmonic, we assume that we are in the limit of  $\Gamma \gg \hbar\omega$ .) We have found an explicit form for the electronic friction and random force. For the case of one bath, the FP equation satisfies the fluctuation-dissipation theorem automatically. In equilibrium, we have shown that the FP equation gives the same solution as the CME. For the transient dynamics, electronic friction-Langevin dynamics (EF-LD) agrees well with surface hopping (SH) for large  $\Gamma$  if we focus on nuclear properties and

we assume that the system begins close enough to equilibrium (i.e. not photoexcitation). Finally, we also have investigated the effect of friction on ET rates, where we have found an analog to the Kramer’s turnover effect.

Looking forward, several questions arise. First, recent experiments<sup>[24,25]</sup> have suggested that electronic friction cannot treat electron-molecule scattering at a metal surface. However, Wodtke *et al* have used the Head-Gordon/Tully prescription for frictional dynamics (which we cannot fully recover in our theory). It will be interesting to see how the electronic frictional model described here in Eq. 4.22 performs (compared to both the more robust SH calculation and to experiments).

Second, there are many other exciting questions to address in the regime of nonequilibrium dynamics, including the instability as induced by current<sup>[32,33]</sup>. This work is ongoing.

#### 4.5. Appendix

In contrast with the body of this paper, we now work in standard units, where  $X$  and  $P$  have units of position and momentum.

##### *4.5.1. A rough sketch relating our model of electronic friction to the Head-Gordon/Tully model*

In this paper, we have derived the von Oppen model of electronic friction (Eq. 4.22) starting from a SH picture of nuclear-electronic dynamics (i.e. the classical master equation). Now in the literature, there is a different model of electronic friction, due to Head-Gordon and Tully (HGT). As presented in Ref. [82], in practice, the HGT model has been used for ab initio calculations of clusters where there is at least a small band gap. In such a case, the HGT frictional damping parameter can be written down as<sup>[71]</sup>:

$$\gamma = \pi \hbar d_{j,j+1}^2 \tag{4.36}$$

where  $j$  is the highest occupied adiabatic orbital and  $j+1$  is the lowest unoccupied adiabatic orbital.  $d_{j,j+1}$  is the derivative coupling between orbital  $j$  and  $j+1$ . In this Appendix, we would like to make a heuristic sketch for how one might try to reconcile Eq. 4.22 (which was derived at large temperature) and Eq. 4.36 (which was derived at zero temperatures). The argument goes as follows.

In the context of a true many-body calculation, with an infinite number of electronic DoFs, a natural extension of Eq. 4.36 would be to assume that the damping term varies as

$$\gamma = \pi \hbar \sum_{\alpha, \alpha'} d_{\alpha, \alpha'}^2, \quad (4.37)$$

where  $\alpha$  and  $\alpha'$  are the adiabatic orbitals below and above Fermi level. For a Hamiltonian of the form in Eqs. 4.1-4.4, we can then rewrite the electronic friction as

$$\gamma = \pi \hbar \sum_{\alpha, \alpha'} d_{\alpha, \alpha'}^2 = \pi \hbar \sum_{\alpha, \alpha'} \frac{|\langle \alpha | \frac{\partial H}{\partial X} | \alpha' \rangle|^2}{(\epsilon_\alpha - \epsilon_{\alpha'})^2} = \pi \hbar \left( \frac{dE}{dX} \right)^2 \sum_{\alpha, \alpha'} \frac{|\langle \alpha | d^+ d | \alpha' \rangle|^2}{(\epsilon_\alpha - \epsilon_{\alpha'})^2}, \quad (4.38)$$

where we have used Hellmann-Feynman theorem. Converting the sum to an integral in energy domain, and using a Green function formalism, we can represent  $d^+d$  explicitly in adiabatic basis<sup>[118]</sup>,

$$\begin{aligned} \sum_{\alpha, \alpha'} \frac{|\langle \alpha | d^+ d | \alpha' \rangle|^2}{(\epsilon_\alpha - \epsilon_{\alpha'})^2} &= \int_{-\infty}^{\epsilon_F} d\epsilon_1 \rho(\epsilon_1) \int_{\epsilon_F}^{\infty} d\epsilon_2 \rho(\epsilon_2) \frac{1}{2\pi\rho(\epsilon_1)} \frac{\Gamma}{(\epsilon_1 - E(X))^2 + (\Gamma/2)^2} \\ &\times \frac{1}{2\pi\rho(\epsilon_2)} \frac{\Gamma}{(\epsilon_2 - E(X))^2 + (\Gamma/2)^2} \frac{1}{(\epsilon_1 - \epsilon_2)^2}. \end{aligned} \quad (4.39)$$

$\rho(\epsilon_1)$  ( $\rho(\epsilon_2)$ ) is the density of states at  $\epsilon_1$  ( $\epsilon_2$ ).

At this point, noting that Eq. 4.37 (or Eq. 4.39) is a zero temperature result, one might propose incorporating finite temperature by including the Fermi-Dirac distribution and

adding a small number  $\xi$  in the denominator. Eq. 4.39 then becomes

$$\int d\epsilon_1 f(\epsilon_1) \int d\epsilon_2 (1 - f(\epsilon_2)) \left(\frac{1}{2\pi}\right)^2 \frac{\Gamma}{(\epsilon_1 - E(X))^2 + (\Gamma/2)^2} \times \frac{\Gamma}{(\epsilon_2 - E(X))^2 + (\Gamma/2)^2} \frac{1}{(\epsilon_1 - \epsilon_2)^2 + \xi^2}. \quad (4.40)$$

Assuming  $\xi$  is small, we can further approximate,

$$\frac{1}{(\epsilon_1 - \epsilon_2)^2 + \xi^2} = \frac{\xi}{(\epsilon_1 - \epsilon_2)^2 + \xi^2} \frac{1}{\xi} \approx \pi \delta(\epsilon_1 - \epsilon_2) \frac{1}{\xi}. \quad (4.41)$$

Then the electronic friction becomes,

$$\gamma \approx \pi \hbar \left(\frac{dE}{dX}\right)^2 \int \frac{d\epsilon_1}{\pi} f(\epsilon_1) (1 - f(\epsilon_1)) \left(\frac{\Gamma/2}{(\epsilon_1 - E(X))^2 + (\Gamma/2)^2}\right)^2 \frac{1}{\xi}. \quad (4.42)$$

Finally, if we make the ansatz that temperature is the relevant broadening parameter and set  $\xi$  to be order of temperature ( $\xi \sim kT$ ), we get the same expression for the friction as in Ref. [80] (up to a constant factor). In the limit  $\Gamma \ll kT$ , we can ignore the level broadening and we recover

$$\gamma \sim \frac{\hbar}{\Gamma} \frac{1}{kT} f(E) (1 - f(E)) \left(\frac{dE}{dX}\right)^2, \quad (4.43)$$

which is exactly the same as what we get from the CME (Eq. 4.22) but now in standard units. See Eq. 4.51 .

We must emphasize that this “derivation” is highly ad hoc. On the one hand, given the leaps of faith in this derivation, the reader might well decide that the HGT model is a very different model of friction than the von Oppen model. On the other hand, this derivation does show some relevant features in common—for instance, both frictional models scale as  $g^2$  and peak near the crossing region. Further research will be necessary to assess the connection derived here and the validity of the HGT model.

4.5.2. *Beyond the harmonic approximation for the motion of the nuclei*

We will now show that the model of friction in Eq. 4.22 does not rely on a harmonic potential energy surface for the nuclei. Consider the general potential  $U_0(X)$  for the nuclei,

$$H = H_s + H_b + H_c, \quad (4.44)$$

$$H_s = E(X)d^\dagger d + \frac{P^2}{2m} + U_0(X), \quad (4.45)$$

$$H_b = \sum_k (\epsilon_k - \mu) c_k^\dagger c_k, \quad (4.46)$$

$$H_c = \sum_k V_k (c_k^\dagger d + d^\dagger c_k), \quad (4.47)$$

In such a case, the CME is<sup>[83]</sup>

$$\begin{aligned} \frac{\partial P_0(X, P, t)}{\partial t} = & - \frac{P}{m} \frac{\partial P_0(X, P, t)}{\partial X} + \frac{dU_0}{dX} \frac{\partial P_0(X, P, t)}{\partial P} - \frac{\Gamma}{\hbar} f(E) P_0(X, P, t) \\ & + \frac{\Gamma}{\hbar} (1 - f(E)) P_1(X, P, t), \end{aligned} \quad (4.48)$$

$$\begin{aligned} \frac{\partial P_1(X, P, t)}{\partial t} = & - \frac{P}{m} \frac{\partial P_1(X, P, t)}{\partial X} + \left( \frac{dU_0}{dX} + \frac{dE}{dX} \right) \frac{\partial P_1(X, P, t)}{\partial P} + \frac{\Gamma}{\hbar} f(E) P_0(X, P, t) \\ & - \frac{\Gamma}{\hbar} (1 - f(E)) P_1(X, P, t). \end{aligned} \quad (4.49)$$

Following the exact procedure as above in Eqs. 4.16-4.21, we can write the FP equation for the general case,

$$\begin{aligned} \frac{\partial A(X, P, t)}{\partial t} = & - \frac{P}{m} \frac{\partial A(X, P, t)}{\partial X} + \frac{\partial U(X)}{\partial X} \frac{\partial A(X, P, t)}{\partial P} \\ & + \frac{\gamma_e}{m} \frac{\partial}{\partial P} (PA(X, P, t)) + \gamma_e kT \frac{\partial^2 A(X, P, t)}{\partial P^2}, \end{aligned} \quad (4.50)$$

where  $\gamma_e$  is the electronic friction

$$\gamma_e = \frac{\hbar}{\Gamma} \frac{1}{kT} f(E)(1 - f(E)) \left( \frac{dE}{dX} \right)^2, \quad (4.51)$$

and  $U(X)$  is the potential of mean force,

$$U(X) = U_0(X) - \frac{1}{\beta} \log(1 + \exp(-\beta E(X))). \quad (4.52)$$

The equivalent Langevin dynamics is

$$m\ddot{X} = -\frac{\partial U(X)}{\partial X} - \gamma_e \dot{X} + \xi(t), \quad (4.53)$$

where  $\xi(t)$  is the random force that satisfies

$$\langle \xi(t)\xi(t') \rangle = 2kT\gamma_e\delta(t - t'). \quad (4.54)$$

Eq. 4.51 is a general form of electronic friction that does not depend on any harmonic approximation.

## CHAPTER 5 : A broadened classical master equation approach for nonadiabatic dynamics at metal surfaces: beyond the weak molecule-metal coupling limit

This chapter was adapted from Ref. [119]

### 5.1. Introduction

The dynamics of molecules near metal surfaces are often nonadiabatic, i.e. the dynamics do not obey the Born-Oppenheimer approximation<sup>[82]</sup>. In such a case, just as for problems in photochemistry, there are several energy scales that are relevant. Consider, for example, the Anderson-Holstein (AH) model (Eqs. 5.1-5.4), which is the simplest model Hamiltonian for describing such dynamics. The Anderson-Holstein model (and generalizations thereof) has been broadly used to describe molecular junctions<sup>[78,79,120]</sup>, quantum dots<sup>[121–123]</sup>, gas scattering from metals<sup>[24,71,72]</sup>, and electrochemical systems.<sup>[124]</sup> For the AH model, we consider an impurity energy level coupled both to a manifold of electronic states representing the metal and also to a single nuclear degree of freedom<sup>[76,77]</sup>. There are at least three important energy scales for the AH Hamiltonian: the inverse time scale for nuclear motion  $\omega$ , the strength of the molecule-metal coupling  $\Gamma$ , and the temperature of the metal  $T$ .<sup>1</sup> In general, propagating dynamics for the simple AH model with an arbitrary set of parameter values to convergence can be difficult for numerically exact methods, such as Numerical Renormalization Group<sup>[4,88,98]</sup>, Multi-Configuration Time-Dependent Hartree<sup>[99]</sup>, and Path Integral Monte Carlo<sup>[1]</sup>. Thus, if we seek an algorithm to describe more complicated, realistic systems beyond the AH model, appropriate approximations must be made.

For this paper, we restrict ourselves to the case  $kT > \hbar\omega$ , where a classical description of the nuclear motion should be feasible. Even for this regime, however, no simple solution is available. For example, in the literature, we find two different approaches for further

---

<sup>1</sup>In fact, for this model problem, we can list three more energy scales: the reorganization energy for the nuclear degree of freedom ( $E_r$ , which is proportional to the electron-phonon coupling  $g$ ,  $E_r = g^2/(\hbar\omega)$ ), the energy difference between the occupied and unoccupied level ( $E_d$ ), and the bandwidth of the metal  $W$ .

simplifying the AH model, each based on the strength of electron-metal coupling ( $\Gamma$ ). (See Fig. 28.) On the one hand, for small  $\Gamma$ , a perturbative treatment leads to a variety of master equations<sup>[31,33,38,83,86,95]</sup>, where usually the level broadening is disregarded; for the most part, these approaches are valid only when the electron-metal coupling is small compared to temperature ( $\Gamma < kT$ ). On the other hand, in the limit of large  $\Gamma$ , an adiabatic approach yields a broadened Fokker-Planck (BFP) equation, or equivalently Langevin dynamics on a broadened potential of mean force<sup>[80,81,115,116]</sup>. As usual, the adiabatic approximation requires that the nuclear dynamics be slow compared to electron-metal coupling, roughly  $\Gamma > \hbar\omega$ ; the adiabatic approximation also cannot be used in a straightforward formalism for short times if the system begins out of equilibrium.

In a series of recent papers<sup>[6,38,95]</sup>, we have now started to analyze both of the approaches above. Almost a year ago, in Refs. [38] and [95], we followed the first approach above and studied a classical master equation (CME) to model nonadiabatic dynamics near metal surfaces in the limit  $\Gamma < kT$ . This CME did not include broadening. More recently, in Ref. [6], we considered our CME in the further limit that  $\Gamma > \hbar\omega$ , and we showed that our CME can be mapped to a Fokker-Planck (FP) equation (where the nuclei move on the potential of mean force with random force and experience frictional damping from the electronic degrees of freedom). Most importantly, in Ref. [6], we also showed that our FP equation is equivalent to the broadened Fokker-Planck (BFP) equation derived by von Oppen and co-workers in the limit of high temperature<sup>[80]</sup>. It must be emphasized that von Oppen and co-workers derived their BFP equation using the second approach listed above, i.e. assuming only that  $\Gamma > \hbar\omega$  (and not requiring that  $\Gamma < kT$ ). Thus, for low temperature, the von Oppen BFP equation includes broadening whereas our FP equation does not.

With this background in mind, in the present paper, we will argue that it is possible to bridge the small and large  $\Gamma$  cases above by extrapolation. While a rigorous approach for connecting these two limits was recently proposed by Galperin and Nitzan<sup>[125]</sup>, we will

propose a practical approach by ansatz. To make this connection, we will modify our CME to incorporate level broadening, and we will refer to the resulting equation (see below) as a “broadened classical master equation (BCME).” In the limit that  $\Gamma < kT$ , our BCME reduces to the unbroadened CME; in the limit that  $\Gamma > \hbar\omega$ , our BCME can be mapped to von Oppen’s BFP equation. Therefore, we would hope that our BCME valid for all  $\Gamma$  (see Fig. 28), so long as the nuclei are classical,  $kT > \hbar\omega$ . Note that such an approach would be key for two important applications. First, with such an approach, we would be able to study the photoinduced dynamics of molecules near strongly coupled metal surfaces; recall that von Oppen’s BFP equation assumes that the nuclei must begin and remain in quasi-equilibrium with the electronic degrees of freedom so that out of equilibrium initial conditions are not permitted). Second, for many reactions on surfaces, the molecule-metal coupling changes strongly with position ( $x$ ), where  $x$  might be the distance to the metal surface. In such a case, if  $\Gamma$  is not a constant, one cannot assume that  $\Gamma(x) < kT$  or  $\Gamma(x) > \hbar\omega$ . With an accurately BCME, however, one should be able to treat both cases so that one can model inner sphere electrochemical reactions occurring at surfaces.

Before concluding this introduction, we note that the BCME presented below can be solved numerically with a simple, stable surface hopping (SH) procedure. Compared with our previous SH algorithm<sup>[38]</sup> without broadening, there is now one difference: whereas all jumps between potential energy surfaces are local in phase space for the standard CME, momentum adjustments become necessary for the BCME. Of course, momentum jumps also occur in Tully’s fewest-switches surface hopping algorithm<sup>[16]</sup>. Thus, one must wonder whether in the future we will find additional connections between our BCME and Tully style surface hopping; this theme will be explored in a future article.

An outline of this article is as follows. In Sec. 5.2 we present a BCME that incorporates level broadening. In Sec. 5.3 we describe the surface hopping algorithm to solve the BCME. In Sec. 5.4, we show results. We conclude in Sec. 5.5.

Methods	Eqs.	Refs.
Fokker-Planck (FP)	14, 17, 18	Dou <i>et al</i> <sup>30</sup>
broadened Fokker-Planck (BFP)	21, 22, A1	von Oppen <i>et al</i> <sup>26</sup>
classical master equation (CME)	6-7	Dou <i>et al</i> <sup>20</sup> von Oppen <i>et al</i> <sup>21</sup>
broadened classical master equation (BCME)	23-24	

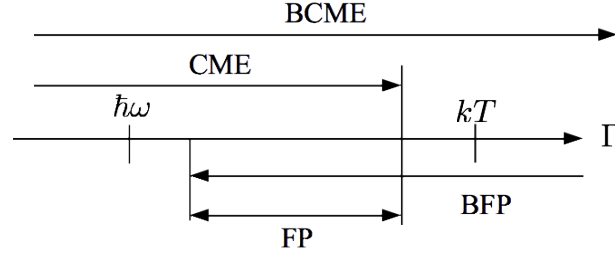


Figure 28: The energy regimes for different theoretical approaches. All methods treat the nuclei classically, hence  $kT > \hbar\omega$ . Depending on how strong the electron-metal coupling ( $\Gamma$ ) is, different methods will be applicable. A broadened CME (BCME) will have the largest range of applicability, connecting the domains of the standard CME and broadened FP (BFP) equation.

## 5.2. Theory

For simplicity, we now discuss the Anderson-Holstein (AH) model, which is the simplest possible model for describing coupled nuclear electronic motion near a metal surface. (A more general discussion of our algorithm is given in Appendix 5.6.2, where we consider the case of arbitrary potential energy surfaces and many nuclear degrees of freedom.) The AH Hamiltonian is:

$$H = H_s + H_b + H_c, \quad (5.1)$$

$$H_s = E(x)d^+d + \frac{1}{2}\hbar\omega(x^2 + p^2), \quad (5.2)$$

$$H_b = \sum_k (\epsilon_k - \mu) c_k^+ c_k, \quad (5.3)$$

$$H_c = \sum_k V_k (c_k^+ d + d^+ c_k). \quad (5.4)$$

where the energy difference between diabats is defined as

$$E(x) \equiv \sqrt{2}gx + E_d. \quad (5.5)$$

Here, we find an impurity electronic energy level (with creation operator  $d^+$  and annihilation operator  $d$ ) coupled both to a manifold of electrons ( $c_k^+$ ,  $c_k$  labeled by Bloch state  $k$ ) and a nuclear degree of freedom ( $x$ ,  $p$ ). We use dimensionless  $x$  and  $p$  coordinates. In Eq. 5.5,  $g$  describes the strength of electron-phonon coupling ( $\sqrt{2}$  is a factor used by convention).

### 5.2.1. Standard Classical Master Equation

In a classical master equation (CME) approach, we use probability density  $P_0(x, p, t)$  ( $P_1(x, p, t)$ ) to describe a state with the impurity being unoccupied (occupied), and the oscillator being at position  $x$  with momentum  $p$ . When  $\Gamma \ll kT$ , the time evolution of the probability density is given by<sup>[38,83]</sup>

$$\begin{aligned} \hbar \frac{\partial P_0(x, p, t)}{\partial t} = & -\hbar\omega p \frac{\partial P_0(x, p, t)}{\partial x} + \hbar\omega x \frac{\partial P_0(x, p, t)}{\partial p} \\ & -\Gamma f(E(x))P_0(x, p, t) + \Gamma(1 - f(E(x)))P_1(x, p, t), \end{aligned} \quad (5.6)$$

$$\begin{aligned} \hbar \frac{\partial P_1(x, p, t)}{\partial t} = & -\hbar\omega p \frac{\partial P_1(x, p, t)}{\partial x} + (\hbar\omega x + \sqrt{2}g) \frac{\partial P_1(x, p, t)}{\partial p} \\ & +\Gamma f(E(x))P_0(x, p, t) - \Gamma(1 - f(E(x)))P_1(x, p, t). \end{aligned} \quad (5.7)$$

Here,  $\Gamma$  is the hybridization function that describes the strength of electron-metal coupling, and we assume  $\Gamma$  is a constant (i.e. the wide band approximation),  $\Gamma(\epsilon) = 2\pi \sum_k |V_k|^2 \delta(\epsilon - \epsilon_k) \equiv \Gamma$ .  $f(E(x)) = \frac{1}{e^{E(x)/kT} + 1}$  is a Fermi function.

Eqs. 5.6-5.7 have a simple physical picture: motion along two diabatic potential surfaces (with a timescale of  $1/\omega$ ), plus hopping (with a timescale of  $\hbar/\Gamma$ ) between  $P_0(x, p, t)$  and

$P_1(x, p, t)$ . The two diabatic potential surfaces are:

$$V_{diab}^0 = \frac{1}{2}\hbar\omega x^2, \quad (5.8)$$

$$V_{diab}^1 = \frac{1}{2}\hbar\omega x^2 + \sqrt{2}gx + E_d. \quad (5.9)$$

Following Ref. [6], we can define new densities  $A(x, p, t)$  and  $B(x, p, t)$  according to

$$P_0(x, p, t) = (1 - f(E(x)))A(x, p, t) + B(x, p, t), \quad (5.10)$$

$$P_1(x, p, t) = f(E(x))A(x, p, t) - B(x, p, t). \quad (5.11)$$

Plugging Eqs. 5.10-5.11 into Eqs. 5.6-5.7, we arrive at

$$\hbar \frac{\partial A(x, p, t)}{\partial t} = -\hbar\omega p \frac{\partial A(x, p, t)}{\partial x} + (\hbar\omega x + \sqrt{2}gf(E(x))) \frac{\partial A(x, p, t)}{\partial p} - \sqrt{2}g \frac{\partial B(x, p, t)}{\partial p} \quad (5.12)$$

$$\begin{aligned} \hbar \frac{\partial B(x, p, t)}{\partial t} = & -\hbar\omega p \frac{\partial B(x, p, t)}{\partial x} + (\hbar\omega x + \sqrt{2}g - \sqrt{2}gf(E(x))) \frac{\partial B(x, p, t)}{\partial p} - \Gamma B(x, p, t) \\ & - \sqrt{2}gf(E(x))(1 - f(E(x))) \frac{\partial A(x, p, t)}{\partial p} + \hbar\omega \frac{\partial f(E(x))}{\partial x} p A(x, p, t) \end{aligned} \quad (5.13)$$

Now we see  $A(x, p, t)$  and  $B(x, p, t)$  are moving on two different potential surfaces, which we will refer to as adiabatic potential surfaces:

$$V_{adiab}^0 = \frac{1}{2}\hbar\omega x^2 + \sqrt{2}g \int_{x_0}^x f(E(x')) dx', \quad (5.14)$$

$$V_{adiab}^1 = \frac{1}{2}\hbar\omega x^2 + \sqrt{2}g \int_{x_0}^x (1 - f(E(x'))) dx'. \quad (5.15)$$

As explained in Ref. [6], if  $\Gamma > \hbar\omega$  – such that  $B(x, p, t)$  is small compared with  $A(x, p, t)$  and such that  $B(x, p, t)$  changes slowly with respect to  $x, p, t$  – we can approximate Eq.

5.13 by

$$\Gamma B(x, p, t) = -\sqrt{2}gf(E(x))(1 - f(E(x)))\frac{\partial A(x, p, t)}{\partial p} + \hbar\omega\frac{\partial f(E(x))}{\partial x}pA(x, p, t) \quad (5.16)$$

If we plug Eq. 5.16 back into Eq. 5.12, we get a Fokker-Planck (FP) equation (we have used  $\frac{\partial f(E(x))}{\partial x} = -\sqrt{2}gf(E(x))(1 - f(E(x)))\frac{1}{kT}$ ),

$$\begin{aligned} \hbar\frac{\partial A(x, p, t)}{\partial t} = & - \hbar\omega p\frac{\partial A(x, p, t)}{\partial x} + \frac{\partial V_{adiab}^0}{\partial x}\frac{\partial A(x, p, t)}{\partial p} \\ & + \hbar\gamma_e(x)\frac{\partial}{\partial p}(pA(x, p, t)) + \hbar\gamma_e(x)\frac{kT}{\hbar\omega}\frac{\partial^2 A(x, p, t)}{\partial p^2}, \end{aligned} \quad (5.17)$$

where  $\gamma_e(x)$  is the electronic friction,

$$\gamma_e(x) = \frac{2g^2}{\Gamma}\frac{\omega}{kT}f(E(x))(1 - f(E(x))). \quad (5.18)$$

### 5.2.2. The Incorporation of Broadening

To incorporate level broadening, we propose replacing  $f(E(x))$  in Eq. 5.12 by  $n(E(x))$ ,

$$\hbar\frac{\partial A(x, p, t)}{\partial t} = -\hbar\omega p\frac{\partial A(x, p, t)}{\partial x} + (\hbar\omega x + \sqrt{2}gn(E(x)))\frac{\partial A(x, p, t)}{\partial p} - \sqrt{2}g\frac{\partial B(x, p, t)}{\partial p} \quad (5.19)$$

where  $n(Z)$  is defined as

$$n(Z) = \int \frac{d\epsilon}{2\pi} \frac{\Gamma}{(\epsilon - Z)^2 + (\Gamma/2)^2} f(\epsilon) \quad (5.20)$$

If we plug Eq. 5.16 back into Eq. 5.19, we get

$$\begin{aligned} \hbar\frac{\partial A(x, p, t)}{\partial t} = & - \hbar\omega p\frac{\partial A(x, p, t)}{\partial x} + \frac{\partial \tilde{V}_{adia}^0}{\partial x}\frac{\partial A(x, p, t)}{\partial p} \\ & + \hbar\gamma_e(x)\frac{\partial}{\partial p}(pA(x, p, t)) + \hbar\gamma_e(x)\frac{kT}{\hbar\omega}\frac{\partial^2 A(x, p, t)}{\partial p^2}, \end{aligned} \quad (5.21)$$

Here  $\tilde{V}_{adia}^0$  is the (broadened) potential of mean force, which we also refer to as the broadened adiabatic potential surface 0 compared with the unbroadened adiabatic potential surface 0 in Eq. 5.14:

$$\frac{\partial \tilde{V}_{adia}^0}{\partial x} = \hbar\omega x + \sqrt{2}gn(E(x)). \quad (5.22)$$

Finally, if we use Eqs. 5.10-5.11 to calculate  $P_0$  and  $P_1$  from Eqs. 5.13 and 5.19, we find

$$\begin{aligned} \hbar \frac{\partial P_0(x, p, t)}{\partial t} &= -\hbar\omega p \frac{\partial P_0(x, p, t)}{\partial x} + \hbar\omega x \frac{\partial P_0(x, p, t)}{\partial p} \\ &- \Gamma f(E(x))P_0(x, p, t) + \Gamma(1 - f(E(x)))P_1(x, p, t) \\ &+ \sqrt{2}g(n(E(x)) - f(E(x)))(1 - f(E(x))) \frac{\partial (P_0(x, p, t) + P_1(x, p, t))}{\partial p} \end{aligned} \quad (5.23)$$

$$\begin{aligned} \hbar \frac{\partial P_1(x, p, t)}{\partial t} &= -\hbar\omega p \frac{\partial P_1(x, p, t)}{\partial x} + (\hbar\omega x + \sqrt{2}g) \frac{\partial P_1(x, p, t)}{\partial p} \\ &+ \Gamma f(E(x))P_0(x, p, t) - \Gamma(1 - f(E(x)))P_1(x, p, t) \\ &+ \sqrt{2}g(n(E(x)) - f(E(x)))f(E(x)) \frac{\partial (P_0(x, p, t) + P_1(x, p, t))}{\partial p} \end{aligned} \quad (5.24)$$

Henceforward, we will refer to set of Equations 5.23-5.24 as one broadened CME (BCME). Several comments must now be made.

- Compared with the original CME (Eqs. 5.6-5.7), one finds new terms in the BCME proportional to  $\frac{\partial (P_0(x, p, t) + P_1(x, p, t))}{\partial p}$ . Interestingly, these new terms correspond not only to modified forces, but also to dynamical momentum jumps (which are also present in the usual, Tully style surface hopping algorithm<sup>[16]</sup> for molecular photochemistry).
- In the limit of small  $\Gamma$ , i.e.  $\Gamma \ll kT$ , level broadening can be disregarded and  $n(E(x)) \approx f(E(x))$ . Thus, in this case, the BCME obviously reduces to the original CME (Eqs. 5.6-5.7).

- In the limit of large  $\Gamma$ , where we can make an adiabatic approximation if  $\Gamma \gg \hbar\omega$ , the potential of mean force in Eq. 5.22 agrees exactly with the work of von Oppen et al: the potential of mean force is broadened (i.e.  $f(E(x))$  is replaced by  $n(E(x))$ ).
- Regarding the definition of electronic friction  $\gamma_e(x)$ , Eq. 5.18 agrees only partially with the work von Oppen *et al*<sup>[80]</sup>. Whereas we invoke a frictional damping value without broadening (i.e. the raw Fermi function appears in Eq. 5.18), von Oppen et al derive a damping term with broadening. See Eq. 5.37. Both frictional terms will be identical in the limit of large temperature,  $\Gamma \ll kT$ .

In practice, our BCME (Eqs. 5.23-5.24) can be further corrected to account for a broadened frictional damping term; see Appendix 5.6.1. For most problems, such a broadened correction for the friction is small (Eq. 5.37 versus Eq. 5.18) relative to the broadened correction for potential of mean force (Eq. 5.22 versus Eq. 5.14). Below, we do not include such corrections in our discussion of a surface hopping algorithm.

### 5.3. Modified surface hopping procedure

We use a modified surface hopping (SH) procedure to solve the BCME (Eqs. 5.23-5.24). As in any Monte Carlo algorithm, we use a swarm of trajectories to sample the probability densities<sup>[16,38]</sup>. The modified SH algorithm is as simple as the following:

1. We initialize the positions, momenta and active surface for each trajectory. In this paper, we will usually prepare our initial state in the following distribution (unless stated otherwise):

$$P_1(x, p, 0) = C \exp\left(-\frac{1}{2}\hbar\omega(x - x_1)^2/kT_i - \frac{1}{2}\hbar\omega p^2/kT_i\right), \quad (5.25)$$

$$P_0(x, p, 0) = 0, \quad (5.26)$$

such that  $N \equiv \int dx dp P_1(x, p, 0) = 1$ . The constant  $x_1 \equiv -\sqrt{2}g/\hbar\omega$  is the center of potential surface 1.  $T_i$  is some initial temperature that can be different from the

temperature of the electronic bath.  $C$  is a normalization factor.

2. For each trajectory, suppose the active potential surface is 1 [or 0]. At each time step, we generate a random number  $\xi$  from 0 to 1. If  $\xi > \Gamma(1-f(E(x)))dt$  [ $\xi > \Gamma f(E(x))dt$ ], the oscillator continues to move along potential surface 1 [surface 0] for a time step  $dt$ . The force felt by the oscillator on surface 1 is

$$F_1 \equiv \frac{d\tilde{V}_{diab}^1}{dx} = -\hbar\omega(x - x_1) - \sqrt{2}g(n(E(x)) - f(E(x)))f(E(x)), \quad (5.27)$$

and the force felt on surface 0 is

$$F_0 \equiv \frac{d\tilde{V}_{diab}^0}{dx} = -\hbar\omega x - \sqrt{2}g(n(E(x)) - f(E(x)))(1 - f(E(x))). \quad (5.28)$$

We refer to the corresponding potentials as broadened diabatic potential surfaces

$$\tilde{V}_{diab}^\alpha = \int_{x_0}^x F_\alpha dx', \quad \alpha = 0, 1.$$

3. if  $\xi < \Gamma(1 - f(E(x)))dt$  [ $\xi < \Gamma f(E(x))dt$ ], the oscillator hops to the potential surface 0 [surface 1]. When the oscillator hops, the momentum changes by

$$\Delta p = -\sqrt{2}g(n(E(x)) - f(E(x)))/\Gamma, \quad (5.29)$$

while the position remains unchanged. This momentum adjustment always pushes the particle in the direction of the crossing. Thereafter, the trajectory moves along its new surface for the next time step  $dt$ .

4. We repeat steps 2-3 for all trajectories until we reach the desired time slice.

Now, to calculate observables, we will define new densities,

$$\begin{aligned}\tilde{P}_0(x, p, t) &= (1 - n(E(x)))A(x, p, t) + B(x, p, t) \\ &+ (n(E(x)) - f(E(x)))A(x, p, t) \exp\left(-\int_0^t dt \Gamma(x(t))\right),\end{aligned}\quad (5.30)$$

$$\begin{aligned}\tilde{P}_1(x, p, t) &= n(E(x))A(x, p, t) - B(x, p, t) \\ &- (n(E(x)) - f(E(x)))A(x, p, t) \exp\left(-\int_0^t dt \Gamma(x(t))\right).\end{aligned}\quad (5.31)$$

Initially, at time zero, by construction we have  $\tilde{P}_\alpha = P_\alpha$  ( $\alpha = 0, 1$ ). Afterwards, at longer times, both the second and third term (in the above equations) will decay, so that

$$\tilde{P}_0(x, p, t) \rightarrow (1 - n(E(x)))A(x, p, t),\quad (5.32)$$

$$\tilde{P}_1(x, p, t) \rightarrow n(E(x))A(x, p, t).\quad (5.33)$$

Thus, it is obviously true that our algorithm will find the correct long time electronic population<sup>[126]</sup>,

$$N = \int dx dp \tilde{P}_1(x, p, t) \xrightarrow{\Gamma t \gg 1} \int dx dp n(E(x))A(x, p, t).\quad (5.34)$$

## 5.4. Results

### 5.4.1. Potential Energy Surfaces

Before considering dynamics, we study the different potential surfaces (broadened and unbroadened). Because broadened diabatic potentials are defined only up to a constant, we fix the minimum of each potential to have value  $V(x)_{min} = 0$ .

From Fig. 29, we notice that, by incorporating level broadening, the barrier between wells along the the potential of mean force is lowered significantly, and the the crossing point between diabats is similarly lowered. Furthermore, even though the broadened diabatic potential surfaces can be shifted from the unbroadened diabatic surfaces asymptotically,

the two quantities will predict identical forces far from the crossing region. Finally, to convince the reader that our SH solution to the BCME with momentum jumps is accurate, in Fig. 29, we also plot minus the log of the position distribution of the oscillator (times  $kT$ ) from SH trajectories,  $-kT \ln(A)$ . This quantity agrees with the broadened potential of mean force very well, indicating that our SH procedure does capture the correct equilibrium distribution.

#### 5.4.2. *Electronic Dynamics*

We now turn to dynamics, and we begin with electronic properties. In Fig. 30, we plot the electronic population ( $N$ ) as a function of time for the different theoretical approaches. Here,  $\Gamma$  is larger than  $kT$ ,  $\Gamma = 2kT \approx 6\hbar\omega$ . To estimate an electronic population with an unbroadened FP equation, we average the Fermi function  $f(E(x(t)))$  over simulation trajectories  $x(t)$ <sup>[6]</sup>; for a broadened BFP equation, we average the function  $n(E(x(t)))$  where  $n$  is defined in Eq. 5.20.

From Fig. 30, we find that, on the one hand, at long times, the BCME/SH results agree with BFP results. Thus, our BCME approach does recover the correct long time equilibrium population (on a broadened surface). Note that, at long times, our broadened results do not agree with the unbroadened results. Thus, for such a large  $\Gamma$ , broadening the potential energy surface will clearly be important for dynamics. At short times, on the other hand, we note that BCME/SH results agree with unbroadened CME/SH results and disagree with BFP results. As discussed earlier and in Ref. [6], all FP equations (broadened or unbroadened) cannot be trusted at very early times if the simulation does not start from near equilibrium. In this case, because of the inevitable mixing of surfaces, the FP approaches cannot even recover the correct initial electronic population at time zero ( $N = 1$ )<sup>[6]</sup>.

In the end, only a BCME approach is reliable in the short and long time limits.

### 5.4.3. Nuclear Dynamics

Finally, we consider nuclear dynamics and begin by plotting the kinetic energy of the oscillator in Fig. 31. As should be expected, when  $\Gamma$  is less than or nearly equal to  $kT$ ,  $\Gamma \leq kT$ , Fig. 31(a) shows that the level broadening does not affect the real time dynamics. That being said, Fig. 31(a) does show that when  $\Gamma < \hbar\omega$ , the CME and FP methods do not agree with each other. As shown in Fig. 31(b), the CME and FP methods agree only for large  $\Gamma$ ,  $\Gamma \gg \hbar\omega$ , where the adiabatic approximation is valid.

Next, consider the case where  $\Gamma \gg kT$ . Here, one might expect to find large signature of broadening. However, even for very large  $\Gamma$ , the average kinetic energy does not seem to be very different with or without broadening, as shown in Fig. 31(c). Thus, the average kinetic energy would not appear to be the most useful reporter on the effect of broadening.

2

Lastly, in Fig. 32, we plot the average position of the oscillator as a function of time for different  $\Gamma$  according to CME/SH and FP. We take the symmetric case,  $\bar{E}_d = 0$  ( $\bar{E}_d \equiv E_d - g^2/\hbar\omega$  is the renormalized energy level), so that at long times, all positions should relax to  $0.5x_1$  (where  $x_1$  is the minimum of diabat 1 and 0 is the minimum of diabat 0). We consider two separate cases:

- The nuclei are initialized to be in equilibrium with the donor diabat 1 as in Eqs. 5.25-5.26, so that the nuclei start off in the left well and the molecular level is occupied.

See Fig. 29. This configuration is denoted “quasi equilibrium initial states” in Fig.

32.

---

<sup>2</sup>There is one important nuance, here, however. We find that, for large electron phonon couplings, the effect of broadening the frictional parameter can be very important and easily measured by plotting the average kinetic energy (or many other observables as well). For the present BCME algorithm, however, our SH protocol does not broaden the friction; in general, we presume that there will usually be other sources of friction that might swamp out such effects. Nevertheless, see the Appendix A for a detailed approach regarding how such broadening may be implemented.

- The nuclei are initialized in a photo-excited initial state, for which we prepare

$$P_0(x, p, 0) = C \exp \left( -\frac{1}{2} \hbar \omega (x - x_1)^2 / kT_i - \frac{1}{2} \hbar \omega p^2 / kT_i \right), \quad (5.35)$$

$$P_1(x, p, 0) = 0. \quad (5.36)$$

In other words, nuclei are positioned initially in the left well (corresponding to diabatic 1), even though the molecular level is unoccupied (which corresponds to diabatic 0 and is minimized in the right well).

Note that, with a FP equation, one cannot distinguish these two different cases because FP equations depend only on the total nuclear density  $A(x, p) = P_0(x, p) + P_1(x, p)$ , and these densities are identical above.

Fig. 32 succinctly summarizes the results of this manuscript. When  $\Gamma$  is small, broadening does not affect the dynamics (see subplots (a), (b)). That being said, CME and FP approaches will disagree here because  $\Gamma < \hbar \omega$ . Furthermore, for photo-excited initial conditions, CME trajectories reflect the dramatic effects of electronic relaxation over a long time scale while FP results cannot treat this electronic relaxation correctly.

As  $\Gamma$  increases, the BFP data agrees more and more with BCME/SH (see subplots (c), (d)), since now  $\Gamma$  is slightly larger than  $\omega$  and an adiabatic approximation is reasonable. Moreover, as  $\Gamma$  increases, the differences between the quasi equilibrium initial conditions and photo excited initial conditions become smaller. This convergence can be explained by recognizing that, for large  $\Gamma$ , electronic relaxation is swift and the remaining (slow) nuclear dynamics will occur along the unique potential of mean force.

Finally, we consider very large  $\Gamma$  in subplots (e), (f). Here, as before, the effects of initial conditions are, of course, minimal and the FP and SH approaches agree. The interesting new feature is that, because broadening lowers the barrier between left and right wells, the dynamics on the broadened surfaces undergo large oscillations and relax rather quickly. By contrast, the unbroadened trajectories relax very, very slowly. Note that the reorganization

energy here is  $E_r = g^2/\hbar\omega = 7.5kT$ , so that the diabatic crossing point is  $7.5kT/4 \approx 1.88kT$ ; with broadening the crossing point becomes  $0.6kT$ .

Lastly, there is one quirk to point out regarding the speed of relaxation. Consider the unbroadened CME/SH algorithm in subplot (b). Note that, for small  $\Gamma$  and photo-excited initial conditions, relaxation occurs much faster than it does for larger  $\Gamma$  in subplots (e), (f). This inversion, whereby smaller  $\Gamma$  leads to faster relaxation, comes about because there is no direct barrier to relaxation with photo-excited initial conditions; moreover, a photo-excited electronic state will live longer with smaller  $\Gamma$  so that nuclei can explore more of phase space before relaxation. This realization will perhaps have fruitful consequences for modeling photo-induced electron transfer at metal surfaces.

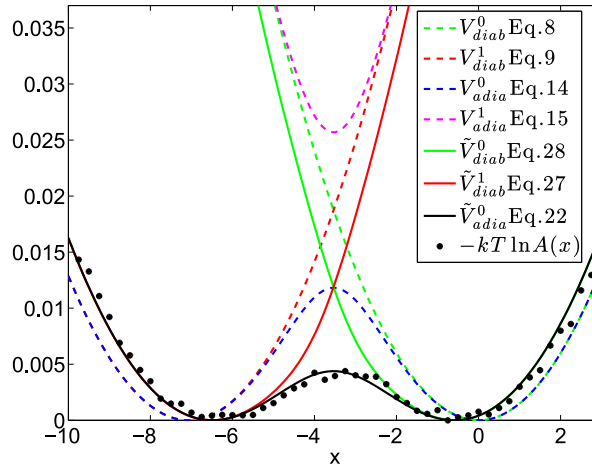
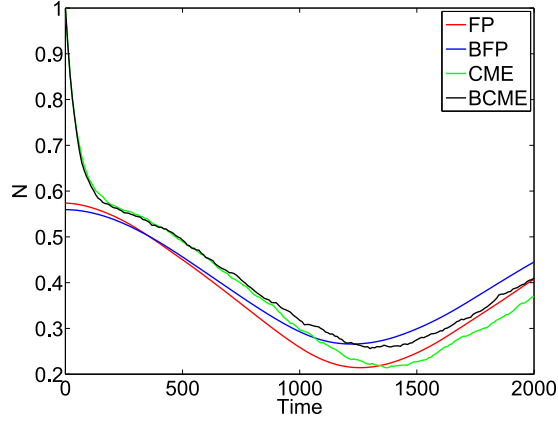


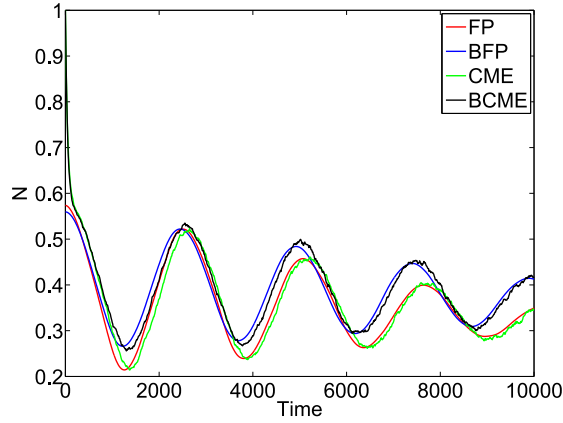
Figure 29: Potential surfaces (diabatic and adiabatic, with and without broadening) for the AH model.  $\hbar\omega = 0.003$ ,  $g = 0.015$ ,  $\Gamma = 0.03$ ,  $kT = 0.01$ ,  $\bar{E}_d = 0$  ( $\bar{E}_d \equiv E_d - g^2/\hbar\omega$  is the renormalized energy level). We also plot minus the log of equilibrium total density,  $-kT \ln(A)$ ,  $A(x) = \int dp (P_0(x, p) + P_1(x, p))$  from surface hopping simulation (black dots); the latter quantity agrees with the broadened potential of mean force  $\tilde{V}_{adia}^0$  very well. Diabat 1 corresponds to the molecular level being occupied. Diabat 0 corresponds to the molecular level being unoccupied.

## 5.5. Conclusions

In this paper, we have used a broadened classical master equation (BCME) to model nonadiabatic dynamics for the cases of both strong and weak molecule-metal couplings. On the

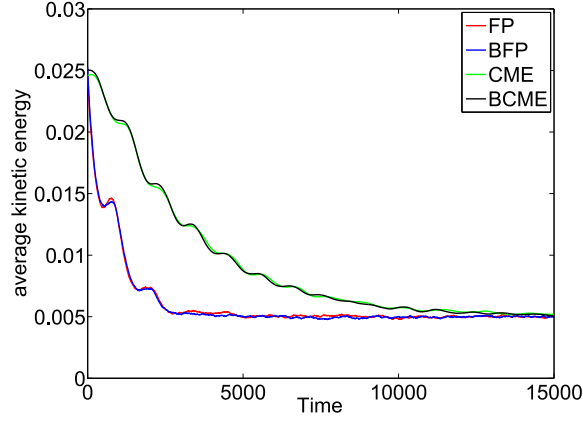


(a)

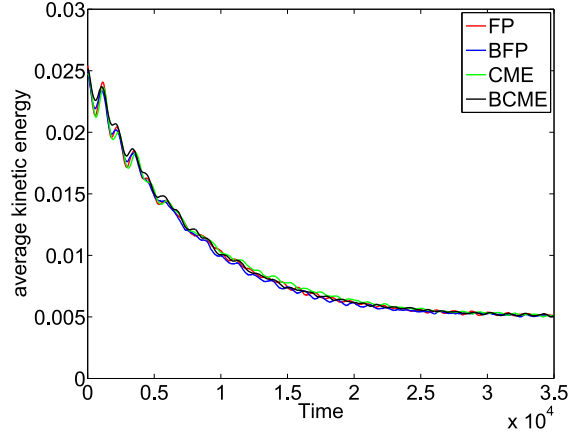


(b)

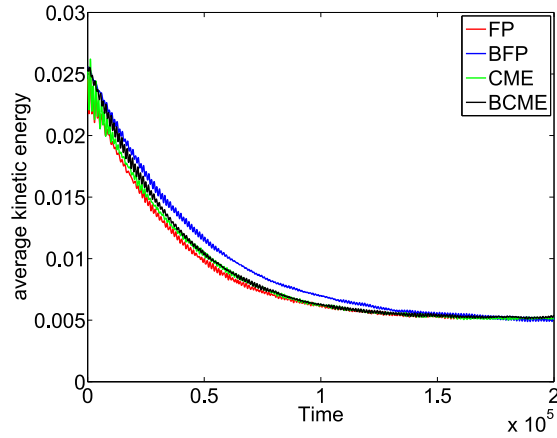
Figure 30: Electronic population as a function of (a) shorter time (b) longer time:  $\Gamma = 0.02$ ,  $\omega = 0.003$ ,  $g = 0.0075$ ,  $kT = 0.01$ ,  $\bar{E}_d = 0.01$  ( $\bar{E}_d \equiv E_d - g^2/\hbar\omega$  is the renormalized energy level). We set  $\hbar = 1$ . We prepare the initial temperature as  $T_i = 5T$  for symmetry with Fig. 31. For notation, FP=Fokker-Planck (unbroadened), BFP=broadened Fokker-Planck, CME=classical master equation (unbroadened), BCME=broadened classical master equation. See Fig. 28. Note that the BCME results agree with CME at short time and BFP at long time; as one would hope.



(a)  $\Gamma = 0.002$



(b)  $\Gamma = 0.02$



(c)  $\Gamma = 0.1$

Figure 31: Average kinetic energy as a function of real time:  $\omega = 0.003$ ,  $g = 0.0075$ ,  $kT = 0.01$ ,  $\bar{E}_d = 0.01$  ( $\bar{E}_d \equiv E_d - g^2/\hbar\omega$  is the renormalized energy level). We set  $\hbar = 1$ . We prepare the initial temperature as  $T_i = 5T$ . Note that the BCME agrees with the CME for small  $\Gamma$ . Same notation as in Fig. 28.

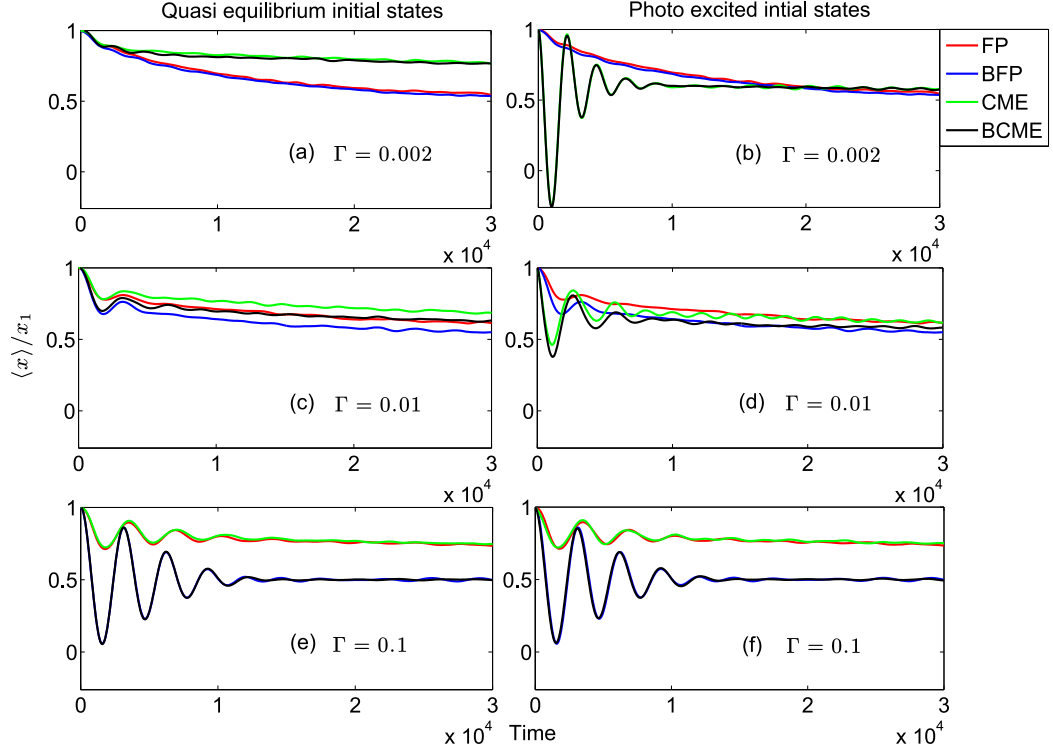


Figure 32: Average position of the oscillator as a function of time.  $\omega = 0.003$ ,  $g = 0.015$ ,  $kT = 0.01$ ,  $\bar{E}_d = 0$  ( $\bar{E}_d \equiv E_d - g^2/\hbar\omega$  is the renormalized energy level). We have set  $\hbar = 1$ . We prepare the initial temperature as  $T_i = T$ .  $x_1$  corresponds to the position that minimizes the energy of the occupied diabat,  $x_1 = -\sqrt{2}g/\hbar\omega$ . The nuclei are initialized either to be in quasi-equilibrium with the electron (Eqs. 5.25-5.26) or to be photoexcited and out of equilibrium with the electron (Eq. 5.35-5.36). Note that the BCME correctly agrees with the CME for small  $\Gamma$  ( $\Gamma \ll kT$ ) and with the BFP for large  $\Gamma$  ( $\Gamma \gg \hbar\omega$ ). Same notation as in Fig. 28.

one hand, in the limit of strong molecule-metal coupling, the BCME can be mapped to a broadened Fokker-Planck (BFP) equation and captures level broadening correctly. On the other hand, in the limit of weak molecule-metal coupling, the BCME can be reduced to the (unbroadened) classical master equation (CME). Numerically, the BCME (in Eqs. 5.23-5.24) can be solved easily with a surface hopping (SH) procedure. Using such a procedure, we have shown that level broadening can affect electronic and nuclear dynamics dramatically by lowering the barrier between wells along the lower adiabatic surface. In the future, it will be crucial to benchmark this result against rigorous quantum dynamics; this research is now in progress. Furthermore, because we have introduced broadening in an ad hoc manner, by extrapolation, there may well be other efficient approaches that can compete with this BCME. Numerical tests will be needed. If this BCME proves as accurate and efficient as we would like, looking forward, this algorithm should be a very important tool for modeling nonadiabatic dynamics for realistic systems, e.g. scattering of gas molecules from metal surfaces<sup>[24,71,72]</sup> and hopefully electrochemical catalysis<sup>[124]</sup>.

## 5.6. Appendix

### 5.6.1. How to Account for Broadening the Electronic Friction Damping Parameter

According to Ref. [80], the correctly broadened friction is of the form

$$\gamma_e^B = \frac{2g^2}{\Gamma} \frac{\omega}{kT} \mathcal{D}(E(x)) \quad (5.37)$$

where we have defined

$$\mathcal{D}(Z) \equiv \Gamma \int \frac{d\epsilon}{\pi} \left( \frac{\Gamma/2}{(\epsilon - Z)^2 + (\Gamma/2)^2} \right)^2 f(\epsilon)(1 - f(\epsilon)) \quad (5.38)$$

This damping parameter should be contrasted with Eq. 5.18.

Let us now show how we can alter our BCME in Eqs. 5.23-5.24 such that we match the correctly broadened electronic friction. To do so, it is important to consider two cases.

First, there is the case that  $\mathcal{D}(E(x)) > f(E(x))(1 - f(E(x)))$ . (Below, for the sake of brevity, we do not include the inner variables  $E(x)$  explicitly for  $\mathcal{D}$  or  $f$ .) In such a case, one can simply include extra frictional damping (with corresponding random force) on top of our BCME.

Second, however, is the opposite case, whereby  $\mathcal{D} < f(1 - f)$ . In such a case, our BCME includes too much friction already. To correct this deficiency, we propose replacing the term  $-\sqrt{2}gf(1 - f)\frac{\partial A(x,p,t)}{\partial p}$  in Eq. 5.13 by  $-\sqrt{2}g\mathcal{D}\frac{\partial A(x,p,t)}{\partial p}$ , and  $\hbar\omega\frac{\partial f}{\partial x}pA(x,p,t)$  by  $-\sqrt{2}g\frac{\hbar\omega}{kT}\mathcal{D}pA(x,p,t)$ . Such a replacement will give us the correctly broadened friction from a BFP equation. Then, if we transform back from  $A$  and  $B$  to  $P_0$  and  $P_1$  using the definitions in Eqs. 5.10-5.11, we find:

$$\begin{aligned}
\hbar\frac{\partial P_0(x,p,t)}{\partial t} &= -\hbar\omega p\frac{\partial P_0(x,p,t)}{\partial x} + \hbar\omega x\frac{\partial P_0(x,p,t)}{\partial p} - \Gamma f P_0(x,p,t) \\
&+ \Gamma(1 - f)P_1(x,p,t) + \sqrt{2}g(n - f)(1 - f)\frac{\partial(P_0(x,p,t) + P_1(x,p,t))}{\partial p} \\
&- \sqrt{2}g\frac{\hbar\omega}{kT}(\mathcal{D} - f(1 - f))p(P_0(x,p,t) + P_1(x,p,t)) \\
&- \sqrt{2}g(\mathcal{D} - f(1 - f))\frac{\partial(P_0(x,p,t) + P_1(x,p,t))}{\partial p} \tag{5.39}
\end{aligned}$$

$$\begin{aligned}
\hbar\frac{\partial P_1(x,p,t)}{\partial t} &= -\hbar\omega p\frac{\partial P_1(x,p,t)}{\partial x} + (\hbar\omega x + \sqrt{2}g)\frac{\partial P_1(x,p,t)}{\partial p} + \Gamma f P_0(x,p,t) \\
&- \Gamma(1 - f)P_1(x,p,t) + \sqrt{2}g(n - f)f\frac{\partial(P_0(x,p,t) + P_1(x,p,t))}{\partial p} \\
&+ \sqrt{2}g\frac{\hbar\omega}{kT}(\mathcal{D} - f(1 - f))p(P_0(x,p,t) + P_1(x,p,t)) \\
&+ \sqrt{2}g(\mathcal{D} - f(1 - f))\frac{\partial(P_0(x,p,t) + P_1(x,p,t))}{\partial p} \tag{5.40}
\end{aligned}$$

Equations 5.39-5.40 can be solved via a surface hopping procedure as well. As compared with the surface hopping procedure described in Sec. 5.3, the hopping rates now depend on both position and momentum, and we also find additional force and momentum jumps.

Of course, one might wonder: why not apply Eqs.5.39-5.40 more generally, instead of Eqs.5.23-5.24, if one wants to correctly extrapolate between the small and large  $\Gamma$  limits? To answer this question, we note that the new momentum jump terms are proportional to  $(\mathcal{D} - (1 - f)f)/f$  (or  $(\mathcal{D} - (1 - f)f)/(1 - f)$ ). These factors will be unstable in practice when  $(\mathcal{D} - (1 - f)f) > 0$ . Because of this practical limitation, if one requires the correctly broadened electronic friction, we propose switching between Eqs. 5.39-5.40 and Eqs. 5.23-5.24. We have found empirically that such a combination works very well.

We may now sum up this final SH algorithm:

1. Initialize all positions, momenta and active potential surfaces for all trajectories.
2. For each trajectory, if we suppose the active potential surface is 0 [or 1], we compare  $\mathcal{D}$  with  $(1 - f)f$ .
3. If  $(\mathcal{D} - (1 - f)f) > 0$ , we compare  $\Gamma f dt$  [ $\Gamma(1 - f)dt$ ] with a random number  $\xi$  in the range  $[0, 1]$ .
  - If  $\xi > \Gamma f dt$  [ $\xi > \Gamma(1 - f)dt$ ], the oscillator continues to move along potential surface 0 [surface 1] for a time step  $dt$ . In addition to the mean force  $F_0$  [ $F_1$ ], the oscillator feels an extra frictional damping  $\frac{2g^2}{\Gamma} \frac{\omega}{kT} (\mathcal{D} - (1 - f)f)$  and an extra random force. The mean force  $F_0$  and  $F_1$  are defined as,

$$F_0 = -\hbar\omega x - \sqrt{2}g(n - f)f, \quad (5.41)$$

$$F_1 = -\hbar\omega(x - x_1) - \sqrt{2}g(n - f)f. \quad (5.42)$$

And the random force is chosen from a Gaussian distribution with variance  $\sigma^2 = \frac{2g^2}{\Gamma} (\mathcal{D} - (1 - f)f)/dt$ .

- Otherwise, the oscillator jumps to potential surface 1 [surface 0], with the same position, and the momentum is adjusted by  $-\sqrt{2}g(n - f)/\Gamma$ . Thereafter, the oscillator moves for a time step  $dt$  with the mean force  $F_1$  [ $F_0$ ], extra frictional

damping  $\frac{2g^2}{\Gamma} \frac{\omega}{kT} (\mathcal{D} - (1-f)f)$  and an extra random force. Again, the random force is chosen from a Gaussian distribution with variance  $\sigma^2 = \frac{2g^2}{\Gamma} (\mathcal{D} - (1-f)f)/dt$ .

4. If  $(\mathcal{D} - (1-f)f) < 0$ , we compare  $\bar{\gamma}_{0 \rightarrow 1} dt$  [ $\bar{\gamma}_{1 \rightarrow 0} dt$ ] with a random number  $\xi$  in the range  $[0, 1]$ , where

$$\bar{\gamma}_{0 \rightarrow 1} = \Gamma f + \sqrt{2}g \frac{\hbar\omega}{kT} (\mathcal{D} - f(1-f))p, \quad (5.43)$$

$$\bar{\gamma}_{1 \rightarrow 0} = \Gamma(1-f) - \sqrt{2}g \frac{\hbar\omega}{kT} (\mathcal{D} - f(1-f))p. \quad (5.44)$$

- If  $\xi > \bar{\gamma}_{0 \rightarrow 1} dt$  [ $\xi > \bar{\gamma}_{1 \rightarrow 0} dt$ ], the oscillator continues moving along potential surface 0 [surface 1] for a time step  $dt$  with the force  $\bar{F}_0$  [ $\bar{F}_1$ ], where

$$\bar{F}_0 = -\hbar\omega x - \sqrt{2}g(n-f)(1-f) + \sqrt{2}g(\mathcal{D} - f(1-f)), \quad (5.45)$$

$$\bar{F}_1 = -\hbar\omega(x - x_1) - \sqrt{2}g(n-f)f - \sqrt{2}g(\mathcal{D} - f(1-f)). \quad (5.46)$$

- Otherwise, the oscillator jumps to surface 1 [surface 0] with the same position but the momentum is adjusted by  $\Delta p_{0 \rightarrow 1}$  [ $\Delta p_{1 \rightarrow 0}$ ], where

$$\Delta p_{0 \rightarrow 1} = -\frac{\sqrt{2}g}{\Gamma} ((n-f)f - \mathcal{D} + f(1-f))/f, \quad (5.47)$$

$$\Delta p_{1 \rightarrow 0} = -\frac{\sqrt{2}g}{\Gamma} ((n-f)(1-f) + \mathcal{D} - f(1-f))/(1-f). \quad (5.48)$$

Thereafter, the oscillator moves for a time step  $dt$  with the force  $\bar{F}_1$  [ $\bar{F}_0$ ].

5. Repeat steps 2-4 for all trajectories until one reaches the desired final time.

### 5.6.2. Multiple Nuclear Degrees of Freedom, Beyond the Harmonic Approximation

The Hamiltonian for the case of multiple, arbitrary nuclear degrees of freedom is:

$$H = H_s + H_b + H_c, \quad (5.49)$$

$$H_s = E(\mathbf{X})d^\dagger d + \sum_i \frac{P_i^2}{2m_i} + U_0(\mathbf{X}), \quad (5.50)$$

$$H_b = \sum_k (\epsilon_k - \mu) c_k^\dagger c_k, \quad (5.51)$$

$$H_c = \sum_k V_k (c_k^\dagger d + d^\dagger c_k). \quad (5.52)$$

For such a Hamiltonian, the CME is

$$\begin{aligned} \frac{\partial P_0(\mathbf{X}, \mathbf{P}, t)}{\partial t} &= - \sum_i \frac{P_i}{m_i} \frac{\partial P_0(\mathbf{X}, \mathbf{P}, t)}{\partial X_i} + \sum_i \frac{\partial U_0(\mathbf{X})}{\partial X_i} \frac{\partial P_0(\mathbf{X}, \mathbf{P}, t)}{\partial P_i} \\ &\quad - \frac{\Gamma}{\hbar} f(E) P_0(\mathbf{X}, \mathbf{P}, t) + \frac{\Gamma}{\hbar} (1 - f(E)) P_1(\mathbf{X}, \mathbf{P}, t), \end{aligned} \quad (5.53)$$

$$\begin{aligned} \frac{\partial P_1(\mathbf{X}, \mathbf{P}, t)}{\partial t} &= - \sum_i \frac{P_i}{m_i} \frac{\partial P_1(\mathbf{X}, \mathbf{P}, t)}{\partial X_i} + \sum_i \left( \frac{\partial E(\mathbf{X})}{\partial X_i} + \frac{\partial U_0(\mathbf{X})}{\partial X_i} \right) \frac{\partial P_1(\mathbf{X}, \mathbf{P}, t)}{\partial P_i} \\ &\quad + \frac{\Gamma}{\hbar} f(E) P_0(\mathbf{X}, \mathbf{P}, t) - \frac{\Gamma}{\hbar} (1 - f(E)) P_1(\mathbf{X}, \mathbf{P}, t) \end{aligned} \quad (5.54)$$

where  $f(E)$  is the Fermi function  $f(E) = \frac{1}{e^{E(\mathbf{X})/kT} + 1}$ . As above, we define new densities  $A(\mathbf{X}, \mathbf{P}, t)$  and  $B(\mathbf{X}, \mathbf{P}, t)$ ,

$$P_0(\mathbf{X}, \mathbf{P}, t) = (1 - f(E))A(\mathbf{X}, \mathbf{P}, t) + B(\mathbf{X}, \mathbf{P}, t) \quad (5.55)$$

$$P_1(\mathbf{X}, \mathbf{P}, t) = f(E)A(\mathbf{X}, \mathbf{P}, t) - B(\mathbf{X}, \mathbf{P}, t) \quad (5.56)$$

Following the same procedures as we described in Sec. 5.2, after incorporating level broadening for the the potential of mean force, we arrive at a BFP equation:

$$\begin{aligned} \frac{\partial A(\mathbf{X}, \mathbf{P}, t)}{\partial t} &= - \sum_i \frac{P_i}{m_i} \frac{\partial A(\mathbf{X}, \mathbf{P}, t)}{\partial X_i} + \sum_i \frac{\partial U(\mathbf{X})}{\partial X_i} \frac{\partial A(\mathbf{X}, \mathbf{P}, t)}{\partial P_i} \\ &\quad + \sum_{ij} \frac{\gamma_{ij}}{m_j} \frac{\partial}{\partial P_i} (P_j A(\mathbf{X}, \mathbf{P}, t)) + kT \sum_{ij} \gamma_{ij} \frac{\partial^2 A(\mathbf{X}, \mathbf{P}, t)}{\partial P_i \partial P_j}, \end{aligned} \quad (5.57)$$

Here  $U(\mathbf{X})$  is the potential of mean force,

$$\frac{\partial U(\mathbf{X})}{\partial X_i} = \frac{\partial U_0(\mathbf{X})}{\partial X_i} + n(E) \frac{\partial E(\mathbf{X})}{\partial X_i} \quad (5.58)$$

where  $n(Z)$  is defined as

$$n(Z) = \int \frac{d\epsilon}{2\pi} \frac{\Gamma}{(\epsilon - Z)^2 + (\Gamma/2)^2} f(\epsilon) \quad (5.59)$$

$\gamma_{ij}$  is the frictional damping coefficient

$$\gamma_{ij} = \frac{\hbar}{\Gamma} \frac{1}{kT} f(E)(1 - f(E)) \frac{dE(\mathbf{X})}{dX_j} \frac{dE(\mathbf{X})}{dX_i} \quad (5.60)$$

Finally, we transform back to the original variables  $P_0$  and  $P_1$  and we find:

$$\begin{aligned} \frac{\partial P_0(\mathbf{X}, \mathbf{P}, t)}{\partial t} = & - \sum_i \frac{P_i}{m_i} \frac{\partial P_0(\mathbf{X}, \mathbf{P}, t)}{\partial X_i} + \sum_i \frac{\partial U_0(\mathbf{X})}{\partial X_i} \frac{\partial P_0(\mathbf{X}, \mathbf{P}, t)}{\partial P_i} \\ & - \frac{\Gamma}{\hbar} f(E) P_0(\mathbf{X}, \mathbf{P}, t) + \frac{\Gamma}{\hbar} (1 - f(E)) P_1(\mathbf{X}, \mathbf{P}, t), \\ & + (n(E) - f(E))(1 - f(E)) \sum_i \frac{\partial E(\mathbf{X})}{\partial X_i} \frac{\partial (P_0(\mathbf{X}, \mathbf{P}, t) + P_1(\mathbf{X}, \mathbf{P}, t))}{\partial P_i} \end{aligned} \quad (5.61)$$

$$\begin{aligned} \frac{\partial P_1(\mathbf{X}, \mathbf{P}, t)}{\partial t} = & - \sum_i \frac{P_i}{m_i} \frac{\partial P_1(\mathbf{X}, \mathbf{P}, t)}{\partial X_i} + \sum_i \left( \frac{\partial E(\mathbf{X})}{\partial X_i} + \frac{\partial U_0(\mathbf{X})}{\partial X_i} \right) \frac{\partial P_1(\mathbf{X}, \mathbf{P}, t)}{\partial P_i} \\ & + \frac{\Gamma}{\hbar} f(E) P_0(\mathbf{X}, \mathbf{P}, t) - \frac{\Gamma}{\hbar} (1 - f(E)) P_1(\mathbf{X}, \mathbf{P}, t) \\ & + (n(E) - f(E)) f(E) \sum_i \frac{\partial E(\mathbf{X})}{\partial X_i} \frac{\partial (P_0(\mathbf{X}, \mathbf{P}, t) + P_1(\mathbf{X}, \mathbf{P}, t))}{\partial P_i} \end{aligned} \quad (5.62)$$

### 5.6.3. A Correction for Electronic Friction

At this point, we remind the reader that Eq. 5.60 does not incorporate broadening correctly.

The correct friction should read:

$$\gamma_{ij} = \frac{\hbar}{\Gamma} \frac{1}{kT} \mathcal{D}(E) \frac{dE(\mathbf{X})}{dX_i} \frac{dE(\mathbf{X})}{dX_j} \quad (5.63)$$

where  $\mathcal{D}(Z)$  is

$$\mathcal{D}(Z) \equiv \Gamma \int \frac{d\epsilon}{\pi} \left( \frac{\Gamma/2}{(\epsilon - Z)^2 + (\Gamma/2)^2} \right)^2 f(\epsilon)(1 - f(\epsilon)) \quad (5.64)$$

If we want to use the prescription discussed above in Appendix 5.6.1 to correctly broaden the electronic friction, the corresponding CME becomes:

$$\begin{aligned} \frac{\partial P_0(\mathbf{X}, \mathbf{P}, t)}{\partial t} = & - \sum_i \frac{P_i}{m_i} \frac{\partial P_0(\mathbf{X}, \mathbf{P}, t)}{\partial X_i} + \sum_i \frac{\partial U_0(\mathbf{X})}{\partial X_i} \frac{\partial P_0(\mathbf{X}, \mathbf{P}, t)}{\partial P_i} \\ & - \frac{\Gamma}{\hbar} f(E) P_0(\mathbf{X}, \mathbf{P}, t) + \frac{\Gamma}{\hbar} (1 - f(E)) P_1(\mathbf{X}, \mathbf{P}, t), \\ & + (n(E) - f(E))(1 - f(E)) \sum_i \frac{\partial E(\mathbf{X})}{\partial X_i} \frac{\partial (P_0(\mathbf{X}, \mathbf{P}, t) + P_1(\mathbf{X}, \mathbf{P}, t))}{\partial P_i} \\ - \sum_i \frac{1}{kT} (\mathcal{D}(E) - f(E)(1 - f(E))) & \frac{\partial E(\mathbf{X})}{\partial X_i} \frac{P_i}{m_i} (P_0(\mathbf{X}, \mathbf{P}, t) + P_1(\mathbf{X}, \mathbf{P}, t)) \\ - \sum_i (\mathcal{D}(E) - f(E)(1 - f(E))) & \frac{\partial E(\mathbf{X})}{\partial X_i} \frac{\partial (P_0(\mathbf{X}, \mathbf{P}, t) + P_1(\mathbf{X}, \mathbf{P}, t))}{\partial P_i} \end{aligned} \quad (5.65)$$

$$\begin{aligned}
\frac{\partial P_1(\mathbf{X}, \mathbf{P}, t)}{\partial t} = & - \sum_i \frac{P_i}{m_i} \frac{\partial P_1(\mathbf{X}, \mathbf{P}, t)}{\partial X_i} + \sum_i \left( \frac{\partial E(\mathbf{X})}{\partial X_i} + \frac{\partial U_0(\mathbf{X})}{\partial X_i} \right) \frac{\partial P_1(\mathbf{X}, \mathbf{P}, t)}{\partial P_i} \\
& + \frac{\Gamma}{\hbar} f(E) P_0(\mathbf{X}, \mathbf{P}, t) - \frac{\Gamma}{\hbar} (1 - f(E)) P_1(\mathbf{X}, \mathbf{P}, t) \\
& + (n(E) - f(E)) f(E) \sum_i \frac{\partial E(\mathbf{X})}{\partial X_i} \frac{\partial (P_0(\mathbf{X}, \mathbf{P}, t) + P_1(\mathbf{X}, \mathbf{P}, t))}{\partial P_i} \\
& + \sum_i \frac{1}{kT} (\mathcal{D}(E) - f(E)(1 - f(E))) \frac{\partial E(\mathbf{X})}{\partial X_i} \frac{P_i}{m_i} (P_0(\mathbf{X}, \mathbf{P}, t) + P_1(\mathbf{X}, \mathbf{P}, t)) \\
& + \sum_i (\mathcal{D}(E) - f(E)(1 - f(E))) \frac{\partial E(\mathbf{X})}{\partial X_i} \frac{\partial (P_0(\mathbf{X}, \mathbf{P}, t) + P_1(\mathbf{X}, \mathbf{P}, t))}{\partial P_i} \quad (5.66)
\end{aligned}$$

The surface hopping procedure for solving Eqs. 5.61-5.62 or Eqs. 5.65-5.66 are effectively the same as the one phonon case described in Sec. 5.3 and Appendix 5.6.1. For brevity, we do not repeat the algorithm here.

## CHAPTER 6 : A broadened classical master equation approach for treating electron-nuclear coupling in non-equilibrium transport

This chapter was adapted from Ref. [127]

### 6.1. Introduction

Single-molecule junctions have gained a lot of interest over the past few decades<sup>[120,128,129]</sup> where many interesting phenomena have been found, such as Coulomb blockades<sup>[130–133]</sup>, Kondo effects<sup>[97,134–137]</sup>, and Franck-Condon blockades<sup>[27–29,138]</sup>. It is now well known that electron-nuclear couplings can play an important role in many molecular junction transport processes<sup>[139,140]</sup>, leading to heating<sup>[30,31,33,141,142]</sup>, nonadiabatic effects<sup>[143–146]</sup>, enhanced current fluctuations<sup>[147–149]</sup>, hysteresis or switching<sup>[150–153]</sup>, negative differential resistance<sup>[79,154–157]</sup>, and current induced chemistry<sup>[158–162]</sup>. To understand these phenomena, theoretical insight can be gained from a non-equilibrium Green’s function (NEGF)<sup>[78,80,141,163–170]</sup> formalism, the quantum master equation (QME)<sup>[32,157,163,171,172]</sup>, and semiclassical methods<sup>[81,173,174]</sup>. At the same time, numerically exact methods including numerical renormalization group (NRG) theory<sup>[175]</sup>, quantum Monte Carlo (QMC)<sup>[1,111,176,177]</sup>, the multilayer multiconfiguration time-dependent Hartree (ML-MCTDH) approach<sup>[178,179]</sup> and the hierarchical quantum master equation (HQME)<sup>[180–182]</sup> allow one to benchmark the former approximate tools.

For the most part, in order to model a realistic molecule present in a junction or near metal surfaces, many nuclear degrees of freedom (DoFs) are involved, such that a quantum treatment of all of the nuclear motion is challenging. That being said, a semiclassical treatment is possible for a large number of low frequency modes at relatively high temperature. Motivated by such a consideration, over the past two years, two of us have investigated a classical master equation (CME) approach to describe the semiclassical dynamics of coupled electron-nuclear motion for molecules near metal surfaces.<sup>[38,95,183]</sup> Because it is based on perturbation theory, a straightforward, undressed CME works well only for weak molecule-

metal couplings. However, this CME can successfully be then mapped onto a Fokker-Planck (FP) equation through an adiabatic transformation<sup>[6]</sup>. By comparing the resulting FP equation against the standard form of Langevin dynamics produced by a non-equilibrium Green's function (NEGF) expansion (which is based on the idea of small nuclear velocities)<sup>[80]</sup>, it has been previously demonstrated that, for the case of a single metal surface, one can modify the potential energy surfaces to incorporate broadening effects in an ad hoc manner. The resulting broadened CME successfully extrapolates between both weak and strong molecule-metal couplings.<sup>[119]</sup>

In the present paper, we now extend the previous results to the case of two electrodes so that we may calculate non-equilibrium transport properties. Following a similar procedure as for the case of one electrode, a Fokker-Planck equation will be obtained via an adiabatic approximation. The corresponding friction and random force agree with previously published results,<sup>[80]</sup> provided broadening can be disregarded. Note that, in the non-equilibrium case, i.e. the case of two different Fermi levels on the different metals, the friction and random force will not obey the second fluctuation-dissipation theorem, resulting in heating of the nuclear modes. A simple broadening scheme is introduced to calculate transport properties. Finally and most importantly, we will benchmark our results against numerically exact results from HQME, and demonstrate strong agreement across nonadiabatic and adiabatic regimes (as long as the nuclei are classical).

Lastly, to address the low temperature (quantum) limit, a similar (and simple) broadening scheme for the QME is introduced (which we will denote as a bQME). The results from the bQME recover bCME results at relatively high temperature and agree well with numerically exact HQME solutions at fairly low temperature. That being said, however, in the case of very low temperature, both the bCME and the bQME show deviations from the exact HQME results.

We organize our paper as follows. In Sec. 6.2, we review our CME and introduce the bCME. In Sec. 6.3, we briefly review the QME and introduce the bQME. In Sec. 6.4, we

discuss the numerical exact solutions from HQME. We plot results in Sec. 6.5 and conclude in Sec. 6.6.

## 6.2. Broadened classical master equation (BCME)

### 6.2.1. The Anderson-Holstein (AH) model

The model we study in this paper is the generalized spinless Anderson-Holstein (AH) model, where one level  $d$  (with creation/annihilation operator  $\hat{d}^\dagger/\hat{d}$ ) couples both to a manifold of electronic levels indexed by  $k$  (with creation/annihilation operator  $\hat{c}_k^\dagger/\hat{c}_k$ ) and to a nuclear degree of freedom (DoF, with position/momentum operator  $\hat{x}/\hat{p}$ ),

$$\hat{H} = h(\hat{x})\hat{d}^\dagger\hat{d} + U_0(\hat{x}) + \frac{\hat{p}^2}{2m} + \sum_{k \in \text{L,R}} V_k(\hat{c}_k^\dagger\hat{d} + \hat{d}^\dagger\hat{c}_k) + \sum_{k \in \text{L,R}} \epsilon_k \hat{c}_k^\dagger\hat{c}_k \quad (6.1)$$

For such a model, we can define the hybridization function due to coupling to the left and right lead,

$$\Gamma^K(\epsilon) \equiv 2\pi \sum_{k \in K} V_k^2 \delta(\epsilon - \epsilon_k) \quad (6.2)$$

We have introduced the lead index  $K = \text{L, R}$  (i.e. left and right). Below, we will assume the wide band approximation, such that  $\Gamma^K$  is independent of energy. For convenience, we will further define

$$\Gamma \equiv \Gamma^{\text{L}} + \Gamma^{\text{R}} \quad (6.3)$$

### 6.2.2. Classical master equation

In the high temperature limit, i.e.  $k_B T > \hbar\omega$  ( $\omega$  is the typical frequency of the nuclear motion) and  $k_B T > \Gamma$ , as shown in Refs. [38] and [83], we can use a classical master

equation (CME) to describe the dynamics

$$\frac{\partial}{\partial t}\rho_0(x,p,t) = -\frac{p}{m}\frac{\partial\rho_0}{\partial x} + \frac{\partial U_0}{\partial x}\frac{\partial\rho_0}{\partial p} - \frac{\Gamma}{\hbar}\bar{f}(h)\rho_0 + \frac{\Gamma}{\hbar}(1-\bar{f}(h))\rho_1 \quad (6.4a)$$

$$\frac{\partial}{\partial t}\rho_1(x,p,t) = -\frac{p}{m}\frac{\partial\rho_1}{\partial x} + \frac{\partial U_1}{\partial x}\frac{\partial\rho_1}{\partial p} + \frac{\Gamma}{\hbar}\bar{f}(h)\rho_0 - \frac{\Gamma}{\hbar}(1-\bar{f}(h))\rho_1 \quad (6.4b)$$

where  $\rho_0(x,p)$  ( $\rho_1(x,p)$ ) is the probability density for the nuclei to be located in phase space at  $(x,p)$  with energy level  $d$  being unoccupied (occupied). In the above equations, we have defined

$$U_1(x) = U_0(x) + h(x), \quad (6.5a)$$

$$\bar{f}(h) = \frac{1}{\Gamma}(\Gamma^L f^L(h) + \Gamma^R f^R(h)) \quad (6.5b)$$

where  $f^K(h) = (e^{(h(x)-\mu_K)/k_B T} + 1)^{-1}$  is the Fermi function of lead  $K$  ( $\mu_K$  is the corresponding chemical potential). Below, for brevity, we will abbreviate  $\bar{f}(h)$  as  $\bar{f}$ . Physically, if there is no nuclear motion,  $\bar{f}(h)$  would be the equilibrium population of the level at position  $x$ .

Note that the CME (Eq. 6.4) is valid in the high temperature limit: 1)  $k_B T > \hbar\omega$ , such that a classical treatment of the nuclei with the CME is feasible; 2)  $k_B T > \Gamma$ , such that all broadening effects can be disregarded. Below, similar to Ref. [119, 184], we will modify our CME to partially incorporate broadening effects. To achieve such a modification, we require an adiabatic transformation.

### 6.2.3. Adiabatic transformation and Fokker-Planck equation

We start our adiabatic transformation by defining new density probabilities  $A(x, p, t)$  and  $B(x, p, t)$ :

$$\rho_0(x, p, t) \equiv (1 - \bar{f})A(x, p, t) + B(x, p, t) \quad (6.6a)$$

$$\rho_1(x, p, t) \equiv \bar{f}A(x, p, t) - B(x, p, t) \quad (6.6b)$$

These new definitions imply that  $A(x, p) \equiv \rho_0(x, p) + \rho_1(x, p)$  is the total probability density at  $(x, p)$  and  $B \equiv \bar{f}\rho_0 - (1 - \bar{f})\rho_1$  are the fluctuations from equilibrium. Together with the CME (Eq. 6.4), we can easily recover the EOM for  $A$  and  $B$ ,

$$\frac{\partial}{\partial t}A(x, p, t) = -\frac{p}{m}\frac{\partial A}{\partial x} + \left(\frac{\partial U_0}{\partial x} + \bar{f}\frac{\partial h}{\partial x}\right)\frac{\partial A}{\partial p} - \frac{\partial h}{\partial x}\frac{\partial B}{\partial p} \quad (6.7a)$$

$$\begin{aligned} \frac{\partial}{\partial t}B(x, p, t) = & -\frac{p}{m}\frac{\partial B}{\partial x} + \left(\frac{\partial U_0}{\partial x} + (1 - \bar{f})\frac{\partial h}{\partial x}\right)\frac{\partial B}{\partial p} + \frac{p}{m}A\frac{\partial \bar{f}}{\partial x} \\ & - \bar{f}(1 - \bar{f})\frac{\partial h}{\partial x}\frac{\partial A}{\partial p} - \frac{\Gamma}{\hbar}B \end{aligned} \quad (6.7b)$$

As argued in Refs. [6, 119, 185], in the adiabatic limit, i.e., when the nuclear motion is slow compared with electronic transition ( $\Gamma > \hbar\omega$ ), we approximate Eq. 6.7b as

$$\frac{\Gamma}{\hbar}B \approx \frac{p}{m}A\frac{\partial \bar{f}}{\partial x} - \bar{f}(1 - \bar{f})\frac{\partial h}{\partial x}\frac{\partial A}{\partial p} \quad (6.8)$$

When plugging the above equation into Eq. 6.7a, we get a closed EOM for  $A$ ,

$$\frac{\partial}{\partial t}A(x, p, t) = -\frac{p}{m}\frac{\partial A}{\partial x} - F_{pmf}(x)\frac{\partial A}{\partial p} + \gamma_e(x)\frac{\partial}{\partial p}\left(\frac{p}{m}A\right) + D_e(x)\frac{\partial^2 A}{\partial p^2} \quad (6.9)$$

We remind the reader that Eq. 6.9 is a Fokker-Planck equation for the total density probability  $A$  (i.e.,  $A \equiv \rho_0 + \rho_1$  is the density for both electronic states combined). The corresponding mean force  $F_{pmf}$ , electronic friction  $\gamma_e$  and correlation of the random force  $D_e$

are given by

$$F_{pmf}(x) = -\frac{\partial U_0}{\partial x} - \frac{\partial h}{\partial x} \bar{f} \quad (6.10a)$$

$$\gamma_e(x) = -\frac{\hbar}{\Gamma} \frac{\partial \bar{f}}{\partial x} \frac{\partial h}{\partial x} \quad (6.10b)$$

$$D_e(x) = \frac{\hbar}{\Gamma} \bar{f}(1 - \bar{f}) \left( \frac{\partial h}{\partial x} \right)^2 \quad (6.10c)$$

We note that, if  $\mu_L = \mu_R$ , then we have  $\frac{\partial \bar{f}}{\partial x} = -\beta \bar{f}(1 - \bar{f}) \frac{\partial h}{\partial x}$ , such that  $D_e = k_B T \gamma_e$ , i.e. the second fluctuation-dissipation theorem is satisfied. By contrast, when a voltage is applied to the leads, such that  $\mu_L \neq \mu_R$ ,  $D_e = k_B T \gamma_e$  does not hold any longer. Note also that Eqs. 6.10 agree with other previously published results (for example, Ref. [80]), when level broadening can be disregarded (i.e.  $k_B T > \Gamma$ ).

#### 6.2.4. Incorporating broadening effects

In Ref. [80], using a velocity expansion, the NEGF formalism gives a slightly different mean force (versus Eq. 6.10a):

$$\tilde{F}_{pmf}(x) = -\frac{\partial U_0}{\partial x} - \frac{\partial h}{\partial x} \bar{n}(h) \quad (6.11)$$

where we have defined

$$\bar{n}(h) = \int \frac{d\epsilon}{2\pi} \frac{\Gamma}{(\Gamma/2)^2 + (\epsilon - h(x))^2} \bar{f}(\epsilon) \quad (6.12)$$

(Again, we will abbreviate  $\bar{n}(h)$  as  $\bar{n}$ .)

We emphasize that Eq. 6.11 includes broadening effects. To incorporate such effects into our EOM, we must replace the mean force  $F_{pmf}$  (in Eq. 6.10a) by the broadened mean force  $\tilde{F}_{pmf}$ ,

$$\frac{\partial}{\partial t} A(x, p, t) = -\frac{p}{m} \frac{\partial A}{\partial x} + \left( \frac{\partial U_0}{\partial x} + \bar{n} \frac{\partial h}{\partial x} \right) \frac{\partial A}{\partial p} - \frac{\partial h}{\partial x} \frac{\partial B}{\partial p} \quad (6.13)$$

Now, the key issue becomes if and how to modify the mean force for  $B$ . In Ref. [119], the mean force for  $B$  was not altered. In Ref. [184], in order to make the final bcME simpler (as shown below), we modify the mean force for  $B$  as follows:

$$\begin{aligned} \frac{\partial}{\partial t} B(x, p, t) = & -\frac{p}{m} \frac{\partial B}{\partial x} + \left( \frac{\partial U_0}{\partial x} + (1 + \bar{n} - 2\bar{f}) \frac{\partial h}{\partial x} \right) \frac{\partial B}{\partial p} + \frac{p}{m} A \frac{\partial \bar{f}}{\partial x} \\ & - \bar{f}(1 - \bar{f}) \frac{\partial h}{\partial x} \frac{\partial A}{\partial p} - \frac{\Gamma}{\hbar} B \end{aligned} \quad (6.14)$$

Empirically, Eq. 6.7b and Eq. 6.14 (together with Eq. 6.13) give almost identical results for a large regime of parameters.<sup>[184]</sup> Hence, for simplicity, we will use Eq. 6.14 instead of Eq. 6.7b.

Finally, using the modified EOM for  $A$  and  $B$  (Eqs. 6.13-6.14), together with the definitions in Eq. 6.6, we arrive at a broadened CME (bcME) for  $\rho_0$  and  $\rho_1$

$$\frac{\partial}{\partial t} \rho_0(x, p, t) = -\frac{p}{m} \frac{\partial \rho_0}{\partial x} + \frac{\partial \tilde{U}_0}{\partial x} \frac{\partial \rho_0}{\partial p} - \frac{\Gamma}{\hbar} \bar{f} \rho_0 + \frac{\Gamma}{\hbar} (1 - \bar{f}) \rho_1 \quad (6.15a)$$

$$\frac{\partial}{\partial t} \rho_1(x, p, t) = -\frac{p}{m} \frac{\partial \rho_1}{\partial x} + \frac{\partial \tilde{U}_1}{\partial x} \frac{\partial \rho_1}{\partial p} + \frac{\Gamma}{\hbar} \bar{f} \rho_0 - \frac{\Gamma}{\hbar} (1 - \bar{f}) \rho_1 \quad (6.15b)$$

where  $\tilde{U}_0$  and  $\tilde{U}_1$  are broadened diabatic surfaces defined as

$$\frac{\partial \tilde{U}_0}{\partial x} = \frac{\partial U_0}{\partial x} + (\bar{n} - \bar{f}) \frac{\partial h}{\partial x} \quad (6.16a)$$

$$\frac{\partial \tilde{U}_1}{\partial x} = \frac{\partial U_1}{\partial x} + (\bar{n} - \bar{f}) \frac{\partial h}{\partial x} \quad (6.16b)$$

In this paper, our goal is to benchmark Eq. 6.15. Note the simplicity of these equations: Such simple equations would not have resulted if our extrapolation had joined Eq. 6.13 and Eq. 6.7b together.

The bcME (Eq. 6.15) or the CME (Eq. 6.4) can be easily solved using surface hopping procedures: a swarm of trajectories running on the two potential energy surface with stochastic hopping between the two surfaces. Details of the surface hopping algorithm can be found

in Ref. [38].

### 6.2.5. Observables

Below, we will compare steady state current-voltage characteristics (I-V curves) and phonon excitation for the bCME/CME against exact HQME results. A few words are appropriate regarding how we extract observables.

#### I-V Curves

For the CME, in the spirit of a master equation,<sup>[38]</sup> the current is given by

$$I = \frac{e}{\hbar} \int dx dp (\Gamma^L f^L(h) \rho_0(x, p) - \Gamma^L (1 - f^L(h)) \rho_1(x, p)) \quad (6.17)$$

For the bCME, to incorporate broadening effects into the current, we first define the local Landauer current,

$$I_{loc}(x) \equiv \frac{e}{\hbar} \int \frac{d\epsilon}{2\pi} \frac{\Gamma^L \Gamma^R}{(\epsilon - h(x))^2 + (\Gamma/2)^2} (f^L(\epsilon) - f^R(\epsilon)) \quad (6.18)$$

The final current is then given by averaging over the phase space distribution,

$$I = \int dx dp I_{loc}(x) A(x, p) \quad (6.19)$$

Again,  $A(x, p) \equiv \rho_0(x, p) + \rho_1(x, p)$ .

#### Phonon Excitation

Below, we will assume the nuclear motion is harmonic, i.e.  $U_0(x) = \frac{1}{2}m\omega^2 x^2$ , such that we can compare the average phonon excitation  $\langle \hat{a}^\dagger \hat{a} \rangle$ . By definition,  $\hbar\omega(\hat{a}^\dagger \hat{a} + \frac{1}{2}) = \frac{1}{2}m\omega^2 \hat{x}^2 +$

$\frac{\hat{p}^2}{2m}$ , so that we may calculate average phonon excitations in the classical regime as follows:

$$\langle \hat{a}^\dagger \hat{a} \rangle = \frac{m\omega}{2\hbar} \langle x^2 \rangle + \frac{\langle p^2 \rangle}{2m\omega\hbar} - \frac{1}{2} \quad (6.20)$$

In the CME or bCME,  $\langle x^2 \rangle$  and  $\langle p^2 \rangle$  are given by averaging phase space distribution,

$$\langle x^2 \rangle = \int dx dp x^2 A(x, p) \quad (6.21a)$$

$$\langle p^2 \rangle = \int dx dp p^2 A(x, p) \quad (6.21b)$$

### 6.3. QME and bQME

For the bCME or CME, the nuclear potential  $U_0(x)$  and electron-nuclear coupling  $h(x)$  are general, but results hold only at reasonably large temperature. To be able to push our results into the quantum (low temperature) limit, we will restrict ourselves to the case of harmonic oscillator and linear coupling, such that  $U_0 = \frac{1}{2}m\omega^2 x^2$  and  $h(x) = E_d + g\sqrt{\frac{2m\omega}{\hbar}}x$ . Now we rewrite the Hamiltonian (in Eq. 6.1) in terms of raising and lowering operators ( $\hat{a}^\dagger$  and  $\hat{a}$ ) instead of position and momentum operators ( $\hat{x}$  and  $\hat{p}$ ) and perform a system bath partitioning,

$$\hat{H} = \hat{H}_S + \hat{H}_B + \hat{H}_{SB} \quad (6.22)$$

with

$$\hat{H}_S = \hat{d}\hat{d}^\dagger \hat{H}_0 + \hat{d}^\dagger \hat{d} \hat{H}_1, \quad (6.23a)$$

$$\hat{H}_B = \sum_{k \in L, R} \epsilon_k \hat{c}_k^\dagger \hat{c}_k, \quad (6.23b)$$

$$\hat{H}_{SB} = \sum_{k \in L, R} (V_k \hat{c}_k^\dagger \hat{d} + \text{h.c.}), \quad (6.23c)$$

where

$$\hat{H}_0 = \hbar\omega(\hat{a}^\dagger\hat{a} + \frac{1}{2}), \quad (6.24a)$$

$$\hat{H}_1 = \hbar\omega(\hat{a}^\dagger\hat{a} + \frac{1}{2}) + g(\hat{a}^\dagger + \hat{a}) + E_d. \quad (6.24b)$$

In such a case, assuming  $\Gamma < k_B T$ , it is straightforward to derive a quantum master equation for the reduced density matrix  $\hat{\rho}_0$  and  $\hat{\rho}_1$ ,<sup>[83,95]</sup>

$$\begin{aligned} \frac{\partial \hat{\rho}_0}{\partial t} = & -\frac{i}{\hbar}[\hat{H}_0, \hat{\rho}_0] - \sum_K \sum_{k \in K} \frac{|V_k|^2}{\hbar^2} \int_0^\infty d\tau e^{i\epsilon_k \tau/\hbar} f^K(\epsilon_k) e^{-i\hat{H}_1 \tau/\hbar} e^{i\hat{H}_0 \tau/\hbar} \hat{\rho}_0 \\ & - e^{i\epsilon_k \tau/\hbar} (1 - f^K(\epsilon_k)) \hat{\rho}_1 e^{-i\hat{H}_1 \tau/\hbar} e^{i\hat{H}_0 \tau/\hbar} + h.c. \end{aligned} \quad (6.25a)$$

$$\begin{aligned} \frac{\partial \hat{\rho}_1}{\partial t} = & -\frac{i}{\hbar}[\hat{H}_1, \hat{\rho}_1] - \sum_K \sum_{k \in K} \frac{|V_k|^2}{\hbar^2} \int_0^\infty d\tau e^{-i\epsilon_k \tau/\hbar} (1 - f^K(\epsilon_k)) e^{-i\hat{H}_0 \tau/\hbar} e^{i\hat{H}_1 \tau/\hbar} \hat{\rho}_1 \\ & - e^{-i\epsilon_k \tau/\hbar} f^K(\epsilon_k) \hat{\rho}_0 e^{-i\hat{H}_0 \tau/\hbar} e^{i\hat{H}_1 \tau/\hbar} + h.c. \end{aligned} \quad (6.25b)$$

To include broadening within the QME, similar to the bCME, we replace  $\hat{H}_0/\hat{H}_1$  by the corresponding broadened  $\hat{\hat{H}}_0/\hat{\hat{H}}_1$  in Eq. 6.25

$$\begin{aligned} \frac{\partial \hat{\rho}_0}{\partial t} = & -\frac{i}{\hbar}[\hat{\hat{H}}_0, \hat{\rho}_0] - \sum_K \sum_{k \in K} \frac{|V_k|^2}{\hbar^2} \int_0^\infty d\tau e^{i\epsilon_k \tau/\hbar} f^K(\epsilon_k) e^{-i\hat{\hat{H}}_1 \tau/\hbar} e^{i\hat{\hat{H}}_0 \tau/\hbar} \hat{\rho}_0 \\ & - e^{i\epsilon_k \tau/\hbar} (1 - f^K(\epsilon_k)) \hat{\rho}_1 e^{-i\hat{\hat{H}}_1 \tau/\hbar} e^{i\hat{\hat{H}}_0 \tau/\hbar} + h.c. \end{aligned} \quad (6.26a)$$

$$\begin{aligned} \frac{\partial \hat{\rho}_1}{\partial t} = & -\frac{i}{\hbar}[\hat{\hat{H}}_1, \hat{\rho}_1] - \sum_K \sum_{k \in K} \frac{|V_k|^2}{\hbar^2} \int_0^\infty d\tau e^{-i\epsilon_k \tau/\hbar} (1 - f^K(\epsilon_k)) e^{-i\hat{\hat{H}}_0 \tau/\hbar} e^{i\hat{\hat{H}}_1 \tau/\hbar} \hat{\rho}_1 \\ & - e^{-i\epsilon_k \tau/\hbar} f^K(\epsilon_k) \hat{\rho}_0 e^{-i\hat{\hat{H}}_0 \tau/\hbar} e^{i\hat{\hat{H}}_1 \tau/\hbar} + h.c. \end{aligned} \quad (6.26b)$$

Here  $\hat{\hat{H}}_0 = \hat{H}_0 + \Delta U(x)$  and  $\hat{\hat{H}}_1 = \hat{H}_1 + \Delta U(x)$ , where  $\Delta U(x)$  is the shift of the two PESs,

$$\Delta U(x) = \int_{x_0}^x dx' (\bar{n}(h(x')) - \bar{f}(h(x'))) \frac{\partial}{\partial x'} h(x') \quad (6.27)$$

where  $x_0$  is some reference point.

Both the bQME and QME can be further simplified using the eigenbasis of the vibrational states. In Appendix 6.7.1, we show how to solve these equations and calculate the observables in practice.

#### 6.4. Hierarchical Quantum Master Equation (HQME)

In the following, we provide some details regarding the numerically exact HQME approach which will be used to benchmark the results of our newly developed methods. The HQME approach (also known as hierarchical equation of motion (HEOM) approach) was originally proposed in the context of relaxation dynamics<sup>[186,187]</sup> and later on applied to charge transport.<sup>[180–182]</sup> We closely follow Ref. [182], where the HQME approach for a numerically exact treatment of vibrationally coupled transport was introduced.

Based on the system-bath partitioning in Eq. (6.22), it is numerically expedient (see supplementary material of Ref. [182] for details) to diagonalize the Hamiltonian of the reduced system  $\hat{H}_S$  by employing a small polaron transformation,  $\hat{\tilde{H}} = \hat{S}\hat{H}\hat{S}^\dagger$  with  $\hat{S} = \exp\left((g/\hbar\omega)(\hat{a}^\dagger - \hat{a})\hat{d}^\dagger\hat{d}\right)$ . The resulting Hamiltonian is given by

$$\hat{\tilde{H}} = \hat{\tilde{H}}_S + \hat{H}_B + \hat{H}_{SB} \quad (6.28)$$

with

$$\hat{\tilde{H}}_S = \tilde{E}_d \hat{d}^\dagger \hat{d} + \hbar\omega \left( \hat{a}^\dagger \hat{a} + \frac{1}{2} \right), \quad (6.29a)$$

$$\hat{H}_{SB} = \sum_{k \in \text{L,R}} (V_k \hat{X} \hat{c}_k^\dagger \hat{d} + \text{h.c.}). \quad (6.29b)$$

The small polaron transformation leads to a renormalization of the energy of the electronic state  $\tilde{E}_d = E_d - g^2/(\hbar\omega)$  and the molecule-lead coupling term is dressed by the shift operator  $\hat{X} = \exp\{(g/\hbar\omega)(\hat{a} - \hat{a}^\dagger)\}$ .

Employing a bath interaction picture, the bath coupling operators are defined by

$$\hat{b}_K^\sigma(t) = \exp\left(i\hat{H}_B t/\hbar\right) \left(\sum_{k \in K} V_k \hat{c}_k^\sigma\right) \exp\left(-i\hat{H}_B t/\hbar\right) \quad (6.30)$$

with  $\sigma = \pm$ ,  $\hat{c}_k^- \equiv \hat{c}_k$  and  $\hat{c}_k^+ \equiv \hat{c}_k^\dagger$ . As these operators obey Gaussian statistics, all information about system-bath coupling is encoded in the two-time correlation function of the free bath  $C_K^\sigma(t - \tau) = \langle \hat{b}_K^\sigma(t) \hat{b}_K^{\bar{\sigma}}(\tau) \rangle_B$  where  $\bar{\sigma} \equiv -\sigma$ . Via Fourier transformation

$$C_K^\sigma(t) = \frac{1}{2\pi} \int_{-\infty}^{\infty} d\epsilon e^{i\epsilon t/\hbar} \Gamma^K(\epsilon) f[\sigma(\epsilon - \mu_K)], \quad (6.31)$$

$C_K^\sigma(t)$  is related to the spectral density in the leads  $\Gamma^K(\epsilon)$  and the Fermi-Dirac distribution  $f(\epsilon) = (\exp(\epsilon/k_B T) + 1)^{-1}$ . To derive a closed set of EOMs within the HQME method,  $C_K^\sigma(t)$  is expressed by a sum over exponentials,<sup>[180]</sup>  $C_K^\sigma(t) = \sum_{l=0}^{l_{\max}} \eta_{K,l} e^{-\gamma_{K,\sigma,l} t}$ . To this end, the Fermi distribution is represented by a sum-over-poles scheme employing a Pade decomposition<sup>[188–190]</sup> and the spectral density of the leads is assumed to be a single Lorentzian  $\Gamma^K(\epsilon) = \frac{1}{2} \frac{\Gamma W^2}{(\epsilon - \mu_K)^2 + W^2}$ . The band width  $W$  is set to be  $10^6$  times larger than  $\Gamma$  to effectively describe the leads in the wide-band limit, which implies that the overall molecule-lead coupling strength is independent of energy and symmetric,  $\Gamma^L = \Gamma^R = \frac{1}{2}\Gamma$ .

The HQMEs for vibrationally coupled transport are given by

$$\begin{aligned} \frac{\partial}{\partial t} \hat{\rho}_{j_n \dots j_1}^{(n)} = & - \left( \frac{i}{\hbar} \hat{\mathcal{L}}_S + \sum_{m=1}^n \gamma_{j_m} \right) \hat{\rho}_{j_n \dots j_1}^{(n)} - \frac{i}{\hbar^2} \sum_j \hat{\mathcal{A}}^{\bar{\sigma}} \hat{\rho}_{j j_n \dots j_1}^{(n+1)} \\ & - i \sum_{m=1}^n (-)^{n-m} \hat{\mathcal{C}}_{j_m} \hat{\rho}_{j_n \dots j_{m+1} j_{m-1} \dots j_1}^{(n-1)}, \end{aligned} \quad (6.32)$$

with the multi-index  $j = (K, \sigma, l)$  and  $\hat{\mathcal{L}}_S \hat{O} = [\hat{H}_S, \hat{O}]$ . Here,  $\hat{\rho}^{(0)} \equiv \hat{\rho}$  stands for the reduced density matrix and  $\hat{\rho}_{j_n \dots j_1}^{(n)}$  ( $n > 0$ ) denote auxiliary density operators, which describe bath-

related observables such as, e.g., the current

$$\langle \hat{I}_K(t) \rangle = i \frac{e}{\hbar} \sum_l \text{Tr}_S \left\{ \hat{d} \hat{X} \hat{\rho}_{K,+l}^{(1)}(t) - \text{h.c.} \right\}. \quad (6.33)$$

The superoperators  $\hat{\mathcal{A}}$  and  $\hat{\mathcal{C}}$  read

$$\hat{\mathcal{A}}^{\bar{\sigma}} \hat{\rho}^{(n)} = \hat{d}^{\bar{\sigma}} \hat{X}^{\bar{\sigma}} \hat{\rho}^{(n)} + (-)^n \hat{\rho}^{(n)} \hat{d}^{\bar{\sigma}} \hat{X}^{\bar{\sigma}}, \quad (6.34a)$$

$$\hat{\mathcal{C}}_{K,\sigma,l} \hat{\rho}^{(n)} = \eta_{K,l} \hat{d}^{\sigma} \hat{X}^{\sigma} \hat{\rho}^{(n)} - (-)^n \eta_{K,l}^* \hat{\rho}^{(n)} \hat{d}^{\sigma} \hat{X}^{\sigma}. \quad (6.34b)$$

Note that, above,  $\hat{d}^- \equiv \hat{d}$  (and  $\hat{d}^+ \equiv \hat{d}^\dagger$ ) are dressed by  $\hat{X}^- \equiv \hat{X}$  (and  $\hat{X}^+ \equiv \hat{X}^\dagger$ ) due to the small polaron transformation. According to system-bath interaction, the superoperator  $\hat{\mathcal{A}}$  ( $\hat{\mathcal{C}}$ ) couples the  $n$ th-level of the hierarchy to the  $(n+1)$ th ( $(n-1)$ th) level. The coupled set of equations is solved directly for the steady state by setting  $\dot{\hat{\rho}}_{j_n \dots j_1}^{(n)}(t = \infty) = 0$  ( $n \geq 0$ ). In the calculations presented below, the results are quantitatively converged for a truncation of the hierarchy at level  $n = 3$ .

The coupled set of HQMEs in Eq. (6.32) is evaluated in the electronic-vibrational product basis,  $\langle b | \langle i_0 | \hat{\rho}_{j_n \dots j_1}^{(n)} | i'_0 \rangle | b' \rangle$ , where  $|b\rangle \in \{|0\rangle, |1\rangle\}$  and  $|i_0\rangle$  denote eigenstates of  $\hat{d}^\dagger \hat{d}$  and  $\hat{H}_0$  (defined in Eq. 6.24a), respectively, with  $b \in \{0, 1\}$  and  $i_0 \in \{0, \dots, i_0^{\max}\}$ . Without performing the small polaron transformation, an identical set of EOMs can be obtained if the HQMEs are evaluated in the eigenstate-basis of  $\hat{H}_S$ . This basis set is given by the product states  $|0\rangle |i_0\rangle$  and  $|1\rangle |i_1\rangle$  where  $|i_1\rangle$  with  $i_1 \in \{0, \dots, i_1^{\max}\}$  denotes the eigenstates of  $\hat{H}_1$  (cf. Eq. 6.24b).

The results presented in Figs. 35 and 36 are obtained by the HQME approach outlined above. For the results shown in Figs. 33 and 34 an alternative HQME approach is applied where the vibration is treated as part of the bath subspace. Due to the high average vibrational excitation in the systems considered in Figs. 33 and 34, a treatment of the vibrational mode as part of the reduced system would require a huge vibrational basis set  $\{0, \dots, i_0^{\max}\}$  which is computationally not feasible.

## 6.5. Results

Below, we will restrict ourselves to the symmetric case with voltage  $\mu_L = -\mu_R = \Phi/2$ ,  $\Gamma_L = \Gamma_R = \frac{1}{2}\Gamma$  and reorganized energy level  $\tilde{E}_d \equiv E_d - g^2/(\hbar\omega) = 0$ .

### 6.5.1. Classical regime

In this subsection, we look at the classical regime, where  $k_B T > \hbar\omega$ , such that a classical treatment of the nuclear motion is feasible.

For the I-V curves, as shown in Fig. 33, the bCME agrees almost perfectly with numerically exact results from HQME, regardless of whether we look at the adiabatic limit  $\Gamma > \hbar\omega$  or the nonadiabatic limit  $\Gamma < \hbar\omega$ . Not surprisingly, if we do not incorporate broadening, in the limit that  $\Gamma > k_B T$ , both the CME and the QME fail to recover the correct I-V results. In this limit ( $k_B T > \hbar\omega$ ), the quantum treatment (the QME) completely agrees with a classical treatment (i.e. the CME).

In Fig. 34, we show the results for phonon excitation, which is a property of the nuclear distribution. The agreement between the bCME and HQME indicates that, in the limit of large  $\Gamma$ , the potential surface has to be broadened in order to recover the correct phonon distribution. Again, the (b)QME and (b)CME are completely identical.

To understand why the bCME can capture broadening effects correctly in the classical limit ( $k_B T > \hbar\omega$ ), we note that broadening is important only when  $\Gamma > k_B T$ , which automatically implies that we are in the adiabatic regime  $\Gamma > \hbar\omega$ . Furthermore, in such an adiabatic regime, the bCME reduces to a Fokker-Planck equation with the correct potential of mean force (Eq. 6.11) and a roughly correct friction tensor.<sup>[80]</sup> Thus, the bCME should be quite valid. That being said, as shown below, such a broadening scheme will not work perfectly in the quantum and nonadiabatic regimes, where  $\hbar\omega > \Gamma > k_B T$ , especially when  $k_B T$  is very low.

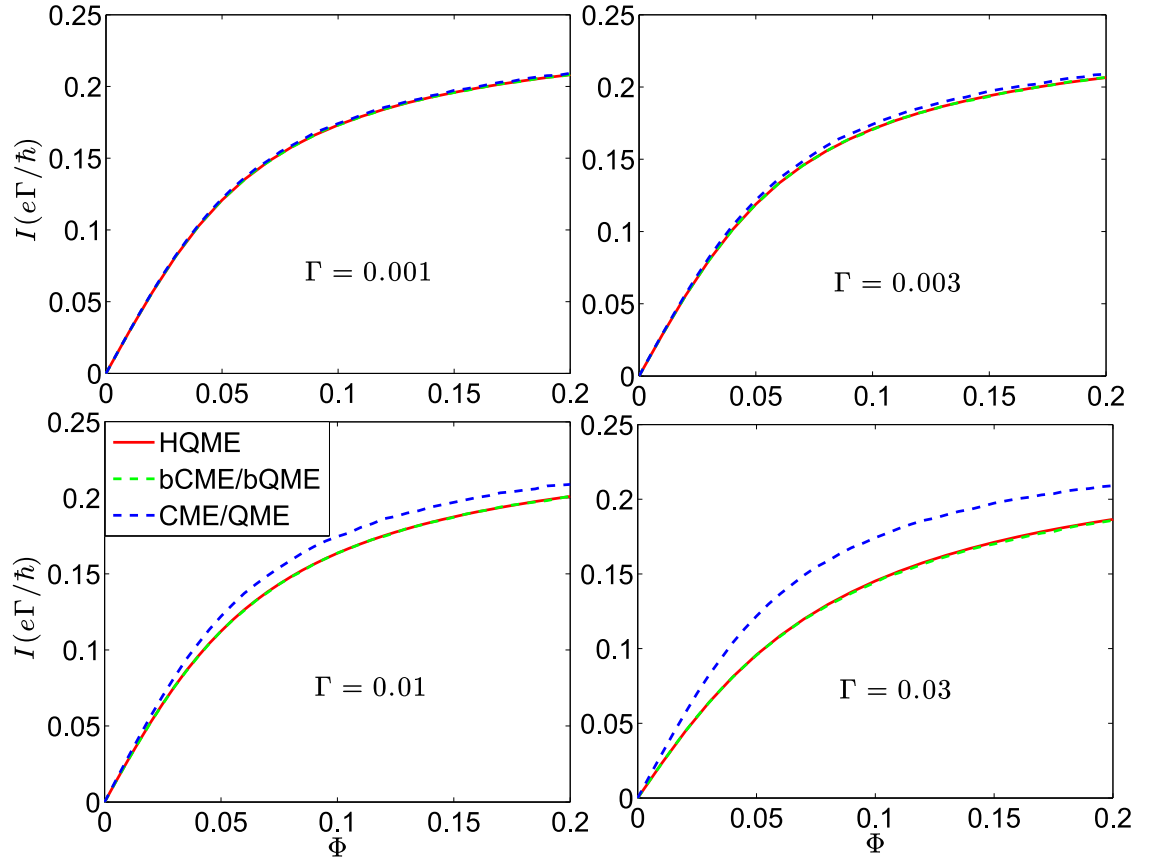


Figure 33: I-V curves in the classical limit:  $k_B T = 0.01$ ,  $\hbar\omega = 0.003$ . The bQME and bCME agree with HQME almost exactly, whereas the QME and CME fail in the limit of large  $\Gamma$ . Other parameters:  $g = 0.0075$ ,  $\tilde{E}_d = 0$ .  $\mu_L = -\mu_R = \Phi/2$ ,  $\Gamma_L = \Gamma_R = \Gamma/2$ .

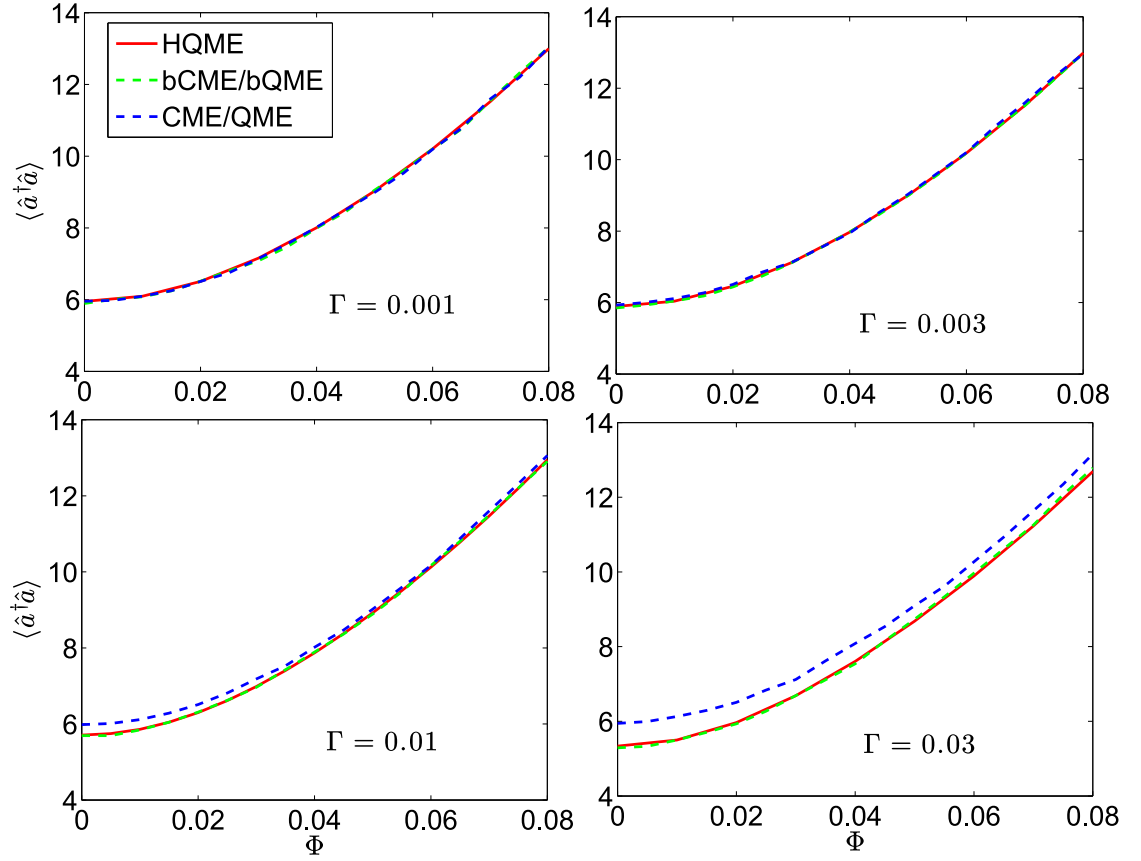


Figure 34: Phonon excitation-voltage curves in the classical limit:  $k_B T = 0.01$ ,  $\hbar\omega = 0.003$ . bQME and bCME agree with HQME almost exactly, whereas QME and CME fail in the limit of large  $\Gamma$ . Other parameters:  $g = 0.0075$ ,  $\vec{E}_d = 0$ .  $\mu_L = -\mu_R = \Phi/2$ ,  $\Gamma_L = \Gamma_R = \Gamma/2$ .

### 6.5.2. Quantum regime

In the highly quantum regime, where  $\hbar\omega > k_B T$ , Fig. 35 starts to show differences between the (b)QME with (b)CME. A classical treatment fails in this limit, whereas the bQME agrees with the numerically exact solution very well. Straightforward QME shows deviations from the HQME in the limit of larger  $\Gamma$ .

Overall, the results in Fig. 35 give us a great deal of confidence that the bQME should work well both in the high temperature ( $k_B T \gg \hbar\omega$ ) and intermediate temperature regimes ( $k_B T = \hbar\omega$ ); by contrast, the bCME can be valid only in the high temperature limit. As discussed above, for broadening to be important,  $\Gamma$  must be larger than  $k_B T$  ( $\Gamma > k_B T$ ), which agains brings us back to the adiabatic regime ( $\Gamma > \hbar\omega$ ), where the bQME should be valid. As shown in Fig. 35, the bQME works well even for the nonadiabatic and quantum regime,  $\hbar\omega > \Gamma > k_B T$ , provided that  $k_B T$  is not very small compared to  $\hbar\omega$ .

Finally, in the nonadiabatic and quantum regime ( $\hbar\omega > \Gamma > k_B T$ ), provided  $\hbar\omega \gg k_B T$ , in Fig. 36, the I-V curves show step-like features. Compared with numerically exact results, the QME shows very sharp step features, which is a signature of the fact that the QME lacks broadening. By contrast, the bQME shows a less obvious step feature, though the results are not perfect. Looking forward, we cannot be sure our techniques to incorporate broadening are optimal at very low temperatures, and the data in Fig. 36 provide one set of benchmarks for further improvement of semiclassical methods. That being said, we are also not sure whether such an improved broadening technique exists given the ad hoc nature of our correction. For the moment, however, we are reasonably confident that the bCME/bQME are reliable at reasonable large temperatures. The next step will be to benchmark these techniques with more than one orbital in the system, so that these techniques can be applied to realistic molecules near surfaces. This work is ongoing.

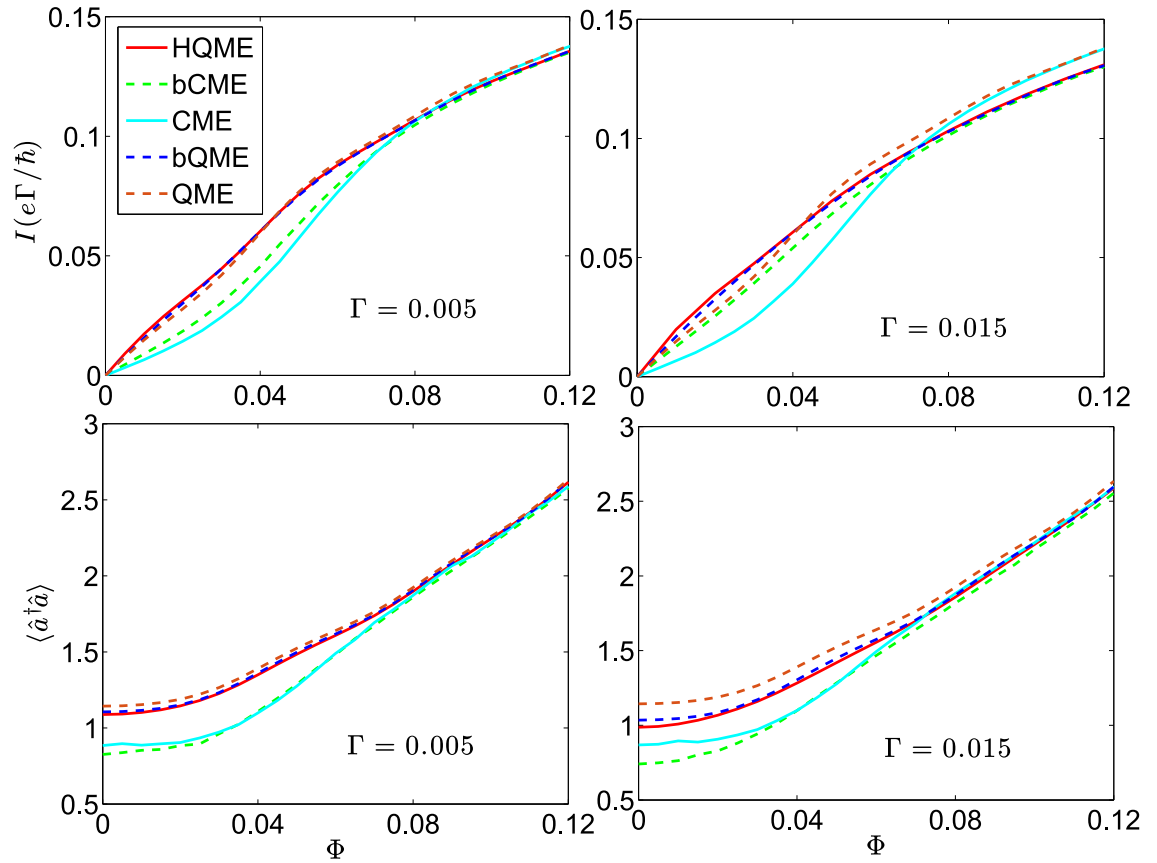


Figure 35: Quantum regime:  $k_B T = 0.005$ ,  $\hbar\omega = 0.02$ . In this limit, a classical treatment fails. Overall the bQME performs well. Other parameters:  $g = 0.03$ ,  $\tilde{E}_d = 0$ .  $\mu_L = -\mu_R = \Phi/2$ ,  $\Gamma_L = \Gamma_R = \Gamma/2$ .

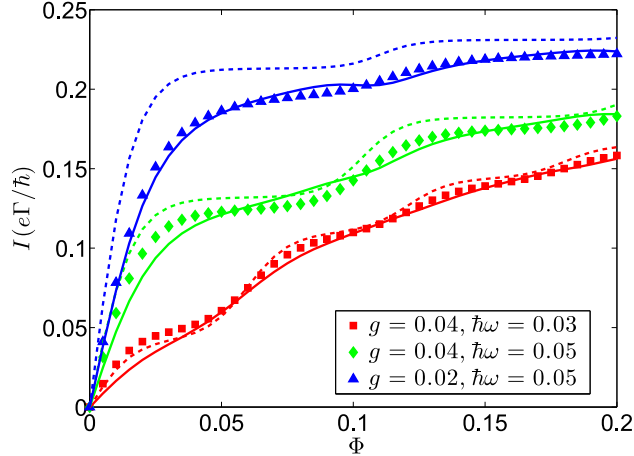


Figure 36: Low temperature:  $\Gamma = 0.01$ ,  $k_B T = 0.004$ . Data from the QME (dashed lines) and bQME (solid lines) is benchmarked against HQME (squares, diamonds, triangles). The QME data shows very sharp step-like features. By contrast, the bQME data shows step-like features that are much less sharp. The current from the bQME data is in closer overall agreement with the HQME, but neither the bQME or the QME is quantitatively accurate here.  $\tilde{E}_d = 0$ ,  $\mu_L = -\mu_R = \Phi/2$ ,  $\Gamma_L = \Gamma_R = \Gamma/2$ .

## 6.6. Conclusions

In this paper, the broadened classical master equation (bCME) introduced previously<sup>[119]</sup> to treat coupled electron-nuclear motions at molecule-metal interfaces has been extended to the non-equilibrium case, whereby two electrodes surround the molecule and a bias voltage is applied. The bCME algorithm agrees with the numerical exact solution almost perfectly in the limit of  $k_B T > \hbar\omega$ . In the quantum limit,  $k_B T < \hbar\omega$ , an analogous broadening strategy is suggested for the QME, and the resulting bQME strategy works fairly well. That being said, at very low temperature, the I-V curves produced by the bQME yield step features that are too soft compared with exact HQME data, reminding us that there are clear limits to the validity of semiclassical approaches. Looking forward, we hope soon to test both the bCME and bQME for larger Hamiltonians with anharmonic surfaces and multiple system orbitals (beyond the limit of wide-band coupling), and thus learn much more about when semiclassical dynamics can or cannot be used safely for realistic systems.

## 6.7. Appendix

### 6.7.1. The QME and bQME

Here we provide details for solving the bQME set of equations. We first express the operators  $\hat{H}_0, \hat{H}_1$

$$\hat{H}_0 = \hbar\omega(\hat{a}^\dagger\hat{a} + \frac{1}{2}) \quad (6.35a)$$

$$\hat{H}_1 = \hbar\omega(\hat{a}^\dagger\hat{a} + \frac{1}{2}) + g(\hat{a}^\dagger + \hat{a}) + E_d \quad (6.35b)$$

in the basis of eigenstates of  $\hat{a}^\dagger\hat{a}$  (referred to as boson basis), where

$$\hat{a}^\dagger\hat{a} = \begin{bmatrix} 0 & & & \\ & 1 & & \\ & & 2 & \\ & & & \dots \end{bmatrix}, \hat{a} + \hat{a}^\dagger = \begin{bmatrix} 0 & 1 & & \\ 1 & 0 & \sqrt{2} & \\ & \sqrt{2} & 0 & \sqrt{3} \\ & & \dots & \dots \dots \end{bmatrix} \quad (6.36)$$

To build matrices for  $\hat{\hat{H}}_0$  and  $\hat{\hat{H}}_1$ , we need to express  $\Delta U(\hat{x})$  (Eq. 6.27) in the boson basis (since  $\hat{\hat{H}}_0 = \hat{H}_0 + \Delta U(\hat{x})$  and  $\hat{\hat{H}}_1 = \hat{H}_1 + \Delta U(\hat{x})$ ). To do so, we diagonalize the position operator  $\hat{x} = \sqrt{\frac{\hbar}{2m\omega}}(\hat{a} + \hat{a}^\dagger)$ , such that  $\hat{x}|x_i\rangle = x_i|x_i\rangle$ , where in such a basis,  $\langle x_i|U(\hat{x})|x_j\rangle = U(x_i)\delta_{ij}$ . We then transform  $U(\hat{x})$  back to the boson basis.

We next express the bQME (Eq. 6.26) in the respective eigenbases of  $\hat{\hat{H}}_0$  and  $\hat{\hat{H}}_1$

$$\hat{\hat{H}}_0|i_0\rangle = E_{i_0}|i_0\rangle \quad (6.37a)$$

$$\hat{\hat{H}}_1|i_1\rangle = E_{i_1}|i_1\rangle \quad (6.37b)$$

After a secular approximation, the bQME reads

$$\dot{\rho}_0(i_0) = - \sum_{i_1, K} W_{i_0 \rightarrow i_1}^{0 \rightarrow 1, K} \rho_0(i_0) + \sum_{i_1, K} W_{i_1 \rightarrow i_0}^{1 \rightarrow 0, K} \rho_1(i_1) \quad (6.38a)$$

$$\dot{\rho}_1(i_1) = \sum_{i_0, K} W_{i_0 \rightarrow i_1}^{0 \rightarrow 1, K} \rho_0(i_0) - \sum_{i_0, K} W_{i_1 \rightarrow i_0}^{1 \rightarrow 0, K} \rho_1(i_1) \quad (6.38b)$$

where

$$W_{i_0 \rightarrow i_1}^{0 \rightarrow 1, K} = |\langle i_1 | i_0 \rangle|^2 \frac{\Gamma^K}{\hbar} f^K(E_{i_1} - E_{i_0}) \quad (6.39a)$$

$$W_{i_1 \rightarrow i_0}^{1 \rightarrow 0, K} = |\langle i_1 | i_0 \rangle|^2 \frac{\Gamma^K}{\hbar} (1 - f^K(E_{i_1} - E_{i_0})) \quad (6.39b)$$

The steady state solution of the above equation is the nontrivial solution that satisfies  $\dot{\rho}_0 = 0, \dot{\rho}_1 = 0$  When calculating the current, we use the expression

$$I = \frac{e}{\hbar} \sum_{i_0, i_1} |\langle i_1 | i_0 \rangle|^2 \int d\epsilon \frac{\Gamma^L \Gamma^R}{(\epsilon - (E_{i_1} - E_{i_0}))^2 + \Gamma^2} (f^L(\epsilon) - f^R(\epsilon)) (\rho_0(i_0) + \rho_1(i_1)) \quad (6.40)$$

For the unbroadened QME, we calculate the current by

$$I = e \sum_{i_0, i_1} W_{i_0 \rightarrow i_1}^{0 \rightarrow 1, L} \rho_0(i_0) - W_{i_1 \rightarrow i_0}^{1 \rightarrow 0, L} \rho_1(i_1) \quad (6.41)$$

Finally, for calculating phonon excitations  $\langle \hat{a}^\dagger \hat{a} \rangle$  within both QME and bQME, we set

$$\langle \hat{a}^\dagger \hat{a} \rangle = \sum_{i_0} \langle i_0 | \hat{a}^\dagger \hat{a} | i_0 \rangle \rho_0(i_0) + \sum_{i_1} \langle i_1 | \hat{a}^\dagger \hat{a} | i_1 \rangle \rho_1(i_1) \quad (6.42)$$

The number of phonon basis states is truncated once the final results have converged.

## CHAPTER 7 : A generalized surface hopping algorithm to model non-adiabatic dynamics near metal surfaces: The case of multiple electronic orbitals

This chapter was adapted from Ref. [183]

### 7.1. Introduction

Non-adiabatic dynamics near metal surfaces has gained wide interest across the areas of electrochemistry<sup>[25,34,120,191]</sup>, molecular junctions<sup>[78,128,139]</sup> and surface scattering<sup>[12,24,72,192]</sup>. For example, in the area of molecular junctions, coupled electron-nuclear motion has been found to account for a variety of phenomena, including heating or cooling<sup>[30,86,193]</sup>, hysteresis<sup>[79,151,152]</sup>, instability or bistability<sup>[31,33,194]</sup>. Numerically exact solutions do exist, including numerical renormalization group (NRG) techniques<sup>[4,93]</sup>, multi-configuration time dependent Hartree (MC-TDH)<sup>[99]</sup>, quantum Monte Carlo (QMC)<sup>[1,97]</sup>, and the hierarchical quantum master equation (HQME)<sup>[182]</sup>. However, due to the large number of degrees of freedom (DoFs) needed to model a metal, exact methods are limited to relatively small systems. New, inexpensive tools are needed.

To motivate the approach below, on the one hand, consider a molecule (or molecules) which is out of equilibrium in the absence of a metal. For such a problem, a lot of semiclassical methods have been developed to model the non-adiabatic dynamics in the gas phase or solution, including multiple spawning<sup>[195]</sup>, frozen gaussian dynamics<sup>[196,197]</sup>, mean-field dynamics<sup>[44,198]</sup>, and semiclassical initial value dynamics<sup>[199–201]</sup>, partially linearized density matrix dynamics<sup>[22]</sup>, generalized quantum master equations<sup>[202,203]</sup>, and exact factorization dynamics<sup>[204]</sup>. Tully’s fewest switch surface hopping (FSSH)<sup>[16]</sup> is one other important tool for propagating such dynamics, and has been successfully applied to many systems, including electron transfer<sup>[23]</sup>, photochemistry<sup>[60,63]</sup>, and proton transfer<sup>[44]</sup>. FSSH was introduced originally by ansatz alone, and recent work has shown a connection between FSSH and the quantum-classical Liouville equation (QCLE)<sup>[17,18,21]</sup>. Meanwhile, a lot of work has been done over the years to improve decoherence within FSSH.<sup>[40,42,56,205,206]</sup>

Now on the other hand, consider the simplest molecule possible, a one-level system, near a metal surface. Recently, for such a case, a classical master equation (CME) was derived to model the coupled electron-nuclear motion<sup>[38,83]</sup>. Just as above, this CME can be solved with a surface hopping (SH) algorithm, i.e. classical motion on two different PESs with stochastic hops between the PESs.<sup>[38,95]</sup> The main differences between CME-SH and Tully’s FSSH are that: 1) our CME-SH does not propagate a density matrix, hence we do not have any coherence/decoherence problems; 2) no momentum adjustment has been introduced for CME-SH because there are open electronic boundary conditions; 3) our CME-SH results recover the correct detailed balance, with the fluctuation-dissipation theorem satisfied exactly, whereas Tully’s FSSH recovers detailed balance approximately<sup>[84,85]</sup>. For completeness, note that Ref. [6] shows that the CME can be mapped onto a Fokker-Planck equation with explicit forms for the friction and random force, and the resulting friction agrees with the Head-Gordon/Tully result as well as other previously published results.<sup>[6,80,82,184]</sup> In Ref. [119], we also suggested a simple way to incorporate the effects of level broadening, such that we could extrapolate from the limits of small to large metal-molecule couplings.

Finally, let us return to the case of a realistic molecule on a metal surface. With more than one orbital on the molecule, we can embed the quantum-classical Liouville equation (QCLE) inside a CME (QCLE-CME) to account for both intramolecular and metal-molecule interactions. In Ref. [185], we previously analyzed the natural friction from this QCLE-CME in the adiabatic limit. In this paper, we will now go beyond the adiabatic limit and propose a surface hopping algorithm to approximately solve the full QCLE-CME over a broad range of parameter space, that includes the adiabatic and diabatic limits. We will not address broadening in this paper; that topic will be treated in a forthcoming publication. This surface hopping scheme extends FSSH naturally to the case of a dissipative electronic bath, by connecting FSSH with CME-SH dynamics. As described below, to address decoherence, we will further propose an augmented surface hopping (A-SH) algorithm, which works well across a large range of parameter regimes. We expect this final algorithm (A-SH) will be very useful for modeling realistic systems.

We organize the paper as follows: in Sec. 7.2, we briefly introduce the QCLE-CME. In Sec. 7.3, we propose a couple of different surface hopping algorithms to solve the QCLE-CME. We discuss our results in Sec. 7.4, and conclude in Sec. 7.5.

**Notation.** Below we will use a “hat”, e.g.  $\hat{O}$ , to denote an operator, either for nuclei and electrons (or both). The subscript “el”, e.g.  $\hat{\rho}_{el}(\mathbf{R}, \mathbf{P})$ , indicates that the nuclear DoFs are classical (i.e. parameters instead of operators).  $\alpha, \beta$  index nuclear vectors (e.g.  $R^\alpha$ ). Small Roman letters (n, m, k) exclusively index electronic orbitals. Capital Roman letters ( $I, J, K, L$ ) index electronic states.

## 7.2. Equation of motion

To be self-consistent, we briefly introduce the QCLE-CME for the coupled electron-nuclear dynamics near metal surfaces. For more details, see Ref. [185]. We divide the total Hamiltonian  $\hat{H}$  into three parts: the system  $\hat{H}_s$ , the bath  $\hat{H}_b$ , and the system-bath coupling  $\hat{H}_c$ ,

$$\hat{H} = \hat{H}_s + \hat{H}_b + \hat{H}_c. \quad (7.1)$$

$\hat{H}_s$  describes a molecule with electronic orbitals with corresponding creation (annihilation)  $\hat{d}_n^+$  ( $\hat{d}_m$ ) operators plus nuclear degrees of freedom (DoFs, with position operator  $\hat{R}^\alpha$  and momentum operators  $\hat{P}^\alpha$ ):

$$\hat{H}_s = \sum_{mn} h_{mn}(\hat{\mathbf{R}}) \hat{d}_m^+ \hat{d}_n + U(\hat{\mathbf{R}}) + \sum_{\alpha} \frac{\hat{P}_{\alpha}^2}{2M^{\alpha}}. \quad (7.2)$$

$\hat{H}_b$  describes a metal consisting of a manifold of non-interacting electrons  $\hat{c}_k^+$  ( $\hat{c}_k$ ):

$$\hat{H}_b = \sum_k \epsilon_k \hat{c}_k^+ \hat{c}_k. \quad (7.3)$$

The coupling between the system and bath  $\hat{H}_c$  is bilinear

$$\hat{H}_c = \sum_{nk} V_{nk} (\hat{d}_n^\dagger \hat{c}_k + \hat{c}_k^\dagger \hat{d}_n). \quad (7.4)$$

For the system-bath coupling, we will assume the wide band approximation, i.e. the hybridization function  $\Gamma_{mn}(\epsilon)$  is independent of  $\epsilon$ ,

$$\Gamma_{mn}(\epsilon) = 2\pi \sum_k V_{mk} V_{nk} \delta(\epsilon - \epsilon_k) = \Gamma_{mn}. \quad (7.5)$$

Following Ref. [185], assuming weak system-bath coupling, we apply Redfield theory to describe the equation of motion (EOM) for the density matrix of the molecule  $\hat{\rho}$ ,

$$\frac{\partial}{\partial t} \hat{\rho} = -\frac{i}{\hbar} [\hat{H}_s, \hat{\rho}] - \hat{\mathcal{L}}_{bs} \hat{\rho} \quad (7.6)$$

Here,  $[\cdot, \cdot]$  is the canonical commutator, and the superoperator  $\hat{\mathcal{L}}_{bs}$  is

$$\begin{aligned} & \hat{\mathcal{L}}_{bs} \hat{\rho} \\ = & \frac{1}{\hbar^2} \int_0^\infty d\tau e^{-i\hat{H}_s t/\hbar} \text{Tr}_b \left( [\hat{H}_{Ic}(t), [\hat{H}_{Ic}(t-\tau), e^{i\hat{H}_s t/\hbar} \hat{\rho}(t) e^{-i\hat{H}_s t/\hbar} \otimes \hat{\rho}_b^{eq}]] \right) e^{i\hat{H}_s t/\hbar}. \end{aligned} \quad (7.7)$$

In the above equation,  $\hat{\rho}_b^{eq}$  is the equilibrium density of states for the electronic bath,  $\text{Tr}_b$  means treating the DoFs in the bath.  $\hat{H}_{Ic}(t)$  in Eq. 7.7 is written in the interaction picture  $\hat{H}_{Ic}(t) = e^{i(\hat{H}_b + \hat{H}_s)t} \hat{H}_c e^{-i(\hat{H}_b + \hat{H}_s)t}$ . We refer to Eq. 7.6 as a quantum master equation (QME).

We then proceed to perform a partial Wigner transformation for the density operator  $\hat{\rho}$  ( $N_\alpha$  is the total number of nuclear DoFs),

$$\hat{\rho}_{el}(\mathbf{R}, \mathbf{P}) \equiv (2\pi\hbar)^{-N_\alpha} \int d\mathbf{X} \langle \mathbf{R} - \mathbf{X}/2 | \hat{\rho} | \mathbf{R} + \mathbf{X}/2 \rangle e^{i\mathbf{P} \cdot \mathbf{X}/\hbar}. \quad (7.8)$$

In the above equation,  $\mathbf{R}$  and  $\mathbf{P}$  in  $\hat{\rho}_{el}(\mathbf{R}, \mathbf{P})$  are now interpreted as position and momentum vectors instead of operators.

After performing a partial Wigner transformation for Eq. 7.6 and making the approximation for the classical nuclei (details can be found in Ref. [185]), we arrive at a quantum-classical Liouville equation-classical master equation (QCLE-CME),

$$\begin{aligned} \frac{\partial}{\partial t} \hat{\rho}_{el}(\mathbf{R}, \mathbf{P}, t) = & \frac{1}{2} \{ \hat{H}_s^{el}(\mathbf{R}, \mathbf{P}), \hat{\rho}_{el} \} - \frac{1}{2} \{ \hat{\rho}_{el}, \hat{H}_s^{el}(\mathbf{R}, \mathbf{P}) \} \\ & - \frac{i}{\hbar} [ \hat{H}_s^{el}, \hat{\rho}_{el} ] - \hat{\mathcal{L}}_{bs}^{el}(\mathbf{R}) \hat{\rho}_{el}(t). \end{aligned} \quad (7.9)$$

Here,  $\{\cdot, \cdot\}$  is Poisson bracket,

$$\{A, B\} = \sum_{\alpha} \left( \frac{\partial A}{\partial R^{\alpha}} \frac{\partial B}{\partial P^{\alpha}} - \frac{\partial A}{\partial P^{\alpha}} \frac{\partial B}{\partial R^{\alpha}} \right). \quad (7.10)$$

and  $\hat{H}_s^{el}$  is the partial Wigner transformation of  $\hat{H}_s$

$$\begin{aligned} \hat{H}_s^{el}(\mathbf{R}, \mathbf{P}) &= \sum_{mn} h_{mn}(\mathbf{R}) \hat{d}_m^{\dagger} \hat{d}_n + U(\mathbf{R}) + \sum_{\alpha} \frac{P_{\alpha}^2}{2M^{\alpha}} \\ &\equiv \hat{V}(\mathbf{R}) + \sum_{\alpha} \frac{P_{\alpha}^2}{2M^{\alpha}} \end{aligned} \quad (7.11)$$

The superoperator  $\hat{\mathcal{L}}_{bs}^{el}(\mathbf{R})$  in Eq. 7.9 is now,

$$\begin{aligned} & \hat{\mathcal{L}}_{bs}^{el}(\mathbf{R}) \hat{\rho}_{el}(\mathbf{R}, \mathbf{P}, t) \\ = & \frac{1}{\hbar^2} \int_0^{\infty} d\tau e^{-i\hat{H}_s^{el}t/\hbar} \text{tr}_b \left( [ \hat{H}_{Ic}^{el}(t), [ \hat{H}_{Ic}^{el}(t-\tau), e^{i\hat{H}_s^{el}t/\hbar} \hat{\rho}_{el}(t) e^{-i\hat{H}_s^{el}t/\hbar} \otimes \hat{\rho}_b^{eq} ] ] \right) e^{i\hat{H}_s^{el}t/\hbar}, \end{aligned} \quad (7.12)$$

In the above equation,  $\hat{H}_{Ic}^{el}(t) = e^{i(\hat{H}_b + \hat{H}_s^{el})t} \hat{H}_c e^{-i(\hat{H}_b + \hat{H}_s^{el})t}$ . We give a simplified form for the Redfield operator  $\hat{\mathcal{L}}_{bs}^{el}(\mathbf{R})$  in Appendix 7.6.1.<sup>[207]</sup>

Eq. 7.9 reads naturally in a diabatic basis. For surface hopping, however, it is useful to

express the QCLE-CME in an adiabatic basis  $|\Psi_I^{ad}(\mathbf{R})\rangle$ , where

$$\hat{V}(\mathbf{R})|\Psi_I^{ad}(\mathbf{R})\rangle = E_I^{ad}(\mathbf{R})|\Psi_I^{ad}(\mathbf{R})\rangle \quad (7.13)$$

In such an adiabatic basis, the QCLE-CME (Eq. 7.9) can be written as

$$\begin{aligned} \frac{\partial}{\partial t}\rho_{IJ}^{ad,el}(\mathbf{R}, \mathbf{P}, t) = & -\frac{i}{\hbar}(E_I^{ad}(\mathbf{R}) - E_J^{ad}(\mathbf{R}))\rho_{IJ}^{ad,el} \\ & - \sum_{\alpha K} \frac{P^\alpha}{M^\alpha} (d_{IK}^\alpha(\mathbf{R})\rho_{KJ}^{ad,el} - \rho_{IK}^{ad,el} d_{KJ}^\alpha(\mathbf{R})) \\ & - \frac{1}{2} \sum_{\alpha K} \left( F_{IK}^\alpha(\mathbf{R}) \frac{\partial \rho_{KJ}^{ad,el}}{\partial P^\alpha} + \frac{\partial \rho_{IK}^{ad,el}}{\partial P^\alpha} F_{KJ}^\alpha(\mathbf{R}) \right) \\ & - \sum_{\alpha} \frac{P^\alpha}{M^\alpha} \frac{\partial \rho_{IJ}^{el}}{\partial R^\alpha} - \sum_{KL} \mathcal{L}_{IJ,KL}^{ad,el,bs}(\mathbf{R})\rho_{KL}^{ad,el}(t). \end{aligned} \quad (7.14)$$

Here we have defined the force  $F_{IJ}^\alpha \equiv -\langle \Psi_I^{ad} | \frac{\partial \hat{H}_s^{el}}{\partial R^\alpha} | \Psi_J^{ad} \rangle$ , and the derivative coupling  $d_{IJ}^\alpha \equiv F_{IJ}^\alpha / (E_I^{ad} - E_J^{ad})$ . In Appendix 7.6.1, we give an explicit form for the Redfield operator  $\hat{\mathcal{L}}_{bs}^{ad,el}$  in an adiabatic basis.

Notice that the only difference between the QCLE-CME and the usual QCLE is the Redfield operator ( $\hat{\mathcal{L}}_{bs}^{el}$ ) in the latter which exchanges electrons between the molecule and the metal. Because the electron number in the molecule is not conserved, the QCLE-CME must be solved in a many-body (Fock) basis. Below we will use trajectory-based algorithms to solve the QCLE-CME approximately.

### 7.3. Surface hopping algorithms

Here we propose a surface hopping algorithm to solve the QCLE-CME approximately. This surface hopping algorithm is a natural extension of Tully's FSSH such that we now incorporate the exchange of electrons between molecule and metal. Just as FSSH represents a very approximate solutions to the QCLE<sup>[17]</sup>, this surface hopping algorithm represents a very approximate solution to the QCLE-CME.

Similar to FSSH, for each trajectory, we propagate the density matrix  $\hat{\sigma}$  according to

$$\begin{aligned} \dot{\sigma}_{IJ}^{ad} = & - \sum_{\alpha K} \frac{P^\alpha}{M^\alpha} (d_{IK}^\alpha(\mathbf{R})\sigma_{KJ}^{ad} - \sigma_{IK}^{ad}d_{KJ}^\alpha(\mathbf{R})) \\ & - \frac{i}{\hbar} (E_I^{ad}(\mathbf{R}) - E_J^{ad}(\mathbf{R}))\sigma_{IJ}^{ad} - \sum_{KL} \mathcal{L}_{IJ,KL}^{ad,el,bs}(\mathbf{R})\sigma_{KL}^{ad} \end{aligned} \quad (7.15)$$

as well as position and momentum ( $\mathbf{R}$  and  $\mathbf{P}$ ) on the active potential surface (denoted as  $\lambda$ ),

$$\dot{R}^\alpha = \frac{P^\alpha}{M^\alpha}, \quad (7.16)$$

$$\dot{P}^\alpha = F_{\lambda\lambda}^\alpha. \quad (7.17)$$

Now we have to decide the hopping rates between PES's. In the spirit of Tully's surface hopping, the nuclei hop from population to population. The total change of the population on state  $J$  is

$$\dot{\sigma}_{JJ}^{ad} = - \sum_{\alpha I} \frac{P^\alpha}{M^\alpha} (d_{JI}^\alpha(\mathbf{R})\sigma_{IJ}^{ad} - \sigma_{JI}^{ad}d_{IJ}^\alpha(\mathbf{R})) - \sum_{KL} \mathcal{L}_{JJ,KL}^{ad,el,bs}(\mathbf{R})\sigma_{KL}^{ad} \quad (7.18)$$

The first term on the right hand side (RHS) of the above equation indicates hopping due to derivative coupling  $d_{IJ}^\alpha$ . Following FSSH, we define the hopping rate from  $I$  to  $J$  to be

$$k_{I \rightarrow J}^d = \Theta \left( -2\text{Re} \left\{ \sum_{\alpha} \frac{P^\alpha}{M^\alpha} \frac{d_{JI}^\alpha \sigma_{IJ}^{ad}}{\sigma_{II}^{ad}} \right\} \right). \quad (7.19)$$

Here the  $\Theta$  function is defined as

$$\Theta(x) = \begin{cases} x, & \text{if } x \geq 0 \\ 0, & \text{if } x < 0 \end{cases} \quad (7.20)$$

The second term on the RHS of Eq. 7.18 gives an extra hopping due to molecule-metal

interaction. This term can be divided into diagonal and off-diagonal contributions:

$$-\sum_{KL} \mathcal{L}_{JJ,KL}^{ad,el,bs} \sigma_{KL}^{ad} = -\sum_I \mathcal{L}_{JJ,II}^{ad,el,bs} \sigma_{II}^{ad} - \sum_{K \neq L} \mathcal{L}_{JJ,KL}^{ad,el,bs} \sigma_{KL}^{ad} \quad (7.21)$$

Just as in any master equation, the diagonal contribution implies a hopping rate from population  $I$  to  $J$  of the form

$$k_{I \rightarrow J}^{on} = -\mathcal{L}_{JJ,II}^{ad,el,bs} \quad (7.22)$$

To deal with the off-diagonal contribution in Eq. 7.21, we will apply a global flux surface hopping (GFSH) scheme,<sup>[208]</sup> where we denote

$$b_{JJ} = -\sum_{K \neq L} \mathcal{L}_{JJ,KL}^{ad,el,bs} \sigma_{KL}^{ad} \quad (7.23)$$

such that the hopping rate from  $I$  to  $J$  is given by

$$k_{I \rightarrow J}^{off} = \begin{cases} \frac{-b_{II} b_{JJ}}{\sigma_{II}^{ad} \sum_K \Theta(b_{KK})}, & \text{if } b_{JJ} > 0 \text{ and } b_{II} < 0 \\ 0, & \text{otherwise} \end{cases} \quad (7.24)$$

Again, the definition of  $\Theta$  function is given in Eq. 7.20. The need for a GFSH hopping rate might well appear superfluous and unjustified here. To that end, we emphasize that there are many other possible rates for the hopping rate here beyond GFSH. In other words, since  $\sum_J b_{JJ} = 0$ , the best approach would really be to investigate the functional form of  $\mathcal{L}_{JJ,KL}^{ad,el,bs}$  and pair up all hopping terms so that final sum vanishes. With such a pairing in hand, one could construct more natural hopping rates accordingly. However, constructing such positive and negative pairs is tedious; see, e.g. Eqs. 7.54-7.57 in Appendix 7.6.2, and now imagine we had  $N \gg 4$  possible charge states and  $M \gg 2$  orbitals! Furthermore, in model problems studied thus far, we find that implementing a more rigorous hopping rate yields nearly identical results as the GFSH rates. Thus, for now, we simply use the GFSH

rates to hop between surfaces.

Finally, combining the diagonal and off-diagonal contributions, we find the hopping rate induced by  $\hat{\mathcal{L}}_{bs}^{el}$  is then

$$k_{I \rightarrow J}^{\mathcal{L}} = k_{I \rightarrow J}^{on} + k_{I \rightarrow J}^{off} \quad (7.25)$$

For convenience, we define the total hopping rate

$$k_{I \rightarrow J}^{total} = k_{I \rightarrow J}^d + k_{I \rightarrow J}^{\mathcal{L}}. \quad (7.26)$$

In Eq. 7.26, we add up hopping rates as induced by the derivate coupling operator ( $k^d$ ) and the Redfield operator ( $k^{\mathcal{L}}$ ). Just as in the CME<sup>[38]</sup>, when hop occurs due to  $k^{\mathcal{L}}$ , we postulate that there should be no momentum adjustment. However, if hop occurs due to  $k^d$ , we rescale momenta on the direction of the derivative coupling to conserve energy, just as in FSSH<sup>[17]</sup>. As such, one has constructed a SH scheme that reduces correctly to both FSSH and CME-SH respectively.

Now we can formalize our protocol explicitly:

1. Prepare the initial  $\hat{\sigma}$ ,  $\mathbf{R}$ , and  $\mathbf{P}$ . Choose the active PES (say  $\lambda = I$ ).
2. Evolve  $\hat{\sigma}$ ,  $\mathbf{R}$  and  $\mathbf{P}$  according to Eqs. 7.15-7.17 for a time interval  $\Delta t$  on the active PES ( $\lambda = I$ ).
3. Calculate the hopping rate  $k_{I \rightarrow K}^d$  and  $k_{I \rightarrow K}^{\mathcal{L}}$  for all  $K$ , according to Eq. 7.19, Eq. 7.25 (Eq. 7.22 plus Eq. 7.24). Generate a random number  $\xi \in [0, 1]$ . We now define  $S_I^J = \sum_{K=1}^J k_{I \rightarrow K}^{total}$

- If  $\xi > S_I^N \Delta t$  (here  $N$  is the total number of PESs), the nuclei remain on surface  $I$ .
- Else if  $S_I^{J-1} \Delta t < \xi < (S_I^{J-1} + k_{I \rightarrow J}^{\mathcal{L}}) \Delta t$ , the nuclei hop to surface  $J$  ( $\lambda = J$ ),

without momentum rescaling.

- Else if  $(S_I^{J-1} + k_{I \rightarrow J}^{\mathcal{L}})\Delta t < \xi < S_I^J \Delta t$ , the nuclei hops to PES  $J$  ( $\lambda = J$ ), with momentum rescaling along the direction of the derivative coupling:

$$\mathbf{P}^{new} = \mathbf{P} + \kappa \mathbf{d}_{IJ} / |\mathbf{d}_{IJ}| \quad (7.27)$$

which satisfies

$$\sum_{\alpha} \frac{(P^{\alpha, new})^2}{2M^{\alpha}} + E_J^{ad}(\mathbf{R}) = \sum_{\alpha} \frac{(P^{\alpha})^2}{2M^{\alpha}} + E_I^{ad}(\mathbf{R}) \quad (7.28)$$

Among the two roots satisfying Eq. 7.28, the root with smaller  $|\kappa|$  is chosen.

4. Repeat step 2 and 3 for the desired number of time steps.

### 7.3.1. Secular surface hopping (sec-SH)

The scheme above can be simplified through a secular approximation. In a sec-SH, the GFSH is turned off, i.e.  $k^{off} = 0$  in Eq. 7.24. Otherwise, the SH algorithm above is unchanged. To motivate why a secular approximation is appealing, consider the long time dynamics of a master equation. Without any nuclear motion, it is well known that secular master equations must recover the correct equilibrium long time populations<sup>[110]</sup>. To understand this unique long-time equilibrium feature of secular master equations, note secular master equations set all coherences to zero (in an adiabatic basis) and thus can be written down in a Lindblad form<sup>[209]</sup>. By contrast, for a nonsecular master equation, again in the adiabatic basis, the correct equilibrium distribution can be achieved only if the coherence vanishes naturally at long times; in other words, a non-secular master equation can behave correctly at long times only if decoherence is treated properly. Thus, there is a natural tradeoff. On the one hand, the secular approximation can recover the correct equilibrium, but gives the wrong short time dynamics. On the other hand, the non secular approximation gives the correct short time dynamics, but achieving the correct equilibrium

is not guaranteed.

Now, we have shown previously that, for the specific Hamiltonian in Eqs. 7.1-7.4, without any nuclear motion, both the nonsecular and secular approximation recover the correct equilibrium populations.<sup>[185]</sup> Unfortunately, as will be shown below, this feature disappears when nuclear motion is introduced, and only the secular approximation succeeds for long time populations. In particular, with nuclear motion, we will show that the off-diagonal matrix elements do not always decohere to zero according to nonsecular trajectories, and hence the latter can destroy the long-time equilibrium density matrix.

### 7.3.2. Augmented surface hopping (A-SH)

Because nuclear motion can destroy the long time population of an electronic master equation, below, it will be useful to introduce an augmented surface hopping (A-SH) scheme that interpolates between the usual SH and sec-SH approach. That is, at short times, A-SH should recover SH, while at longer times, A-SH should reduce to sec-SH. To connect these two limits, we will hypothesize that the timescale for turning off GFSH is the decoherence rate, i.e. the rate of coherence loss lifetime of electronic states as dictated by nuclear motion. Thus, for A-SH, similar to the A-FSSH algorithm in Ref. [210], we propagate moments  $\delta\hat{\mathbf{R}}$  and  $\delta\hat{\mathbf{P}}$ ,

$$\begin{aligned} \frac{\partial}{\partial t}\delta R_{IJ}^\alpha = & \frac{\delta P_{IJ}^\alpha}{M^\alpha} - \sum_{\alpha K} \frac{P^\alpha}{M^\alpha} (d_{IK}^\alpha(\mathbf{R})\delta R_{KJ}^\alpha - \delta R_{IK}^\alpha d_{KJ}^\alpha(\mathbf{R})) \\ & - \frac{i}{\hbar}(E_I^{ad}(\mathbf{R}) - E_J^{ad}(\mathbf{R}))\delta R_{IJ}^\alpha \end{aligned} \quad (7.29)$$

$$\begin{aligned} \frac{\partial}{\partial t}\delta P_{IJ}^\alpha = & \frac{1}{2} \sum_K (\delta F_{IK}^\alpha \sigma_{KJ}^{ad} + \sigma_{IK}^{ad} \delta F_{KJ}^\alpha) - \frac{i}{\hbar}(E_I^{ad}(\mathbf{R}) - E_J^{ad}(\mathbf{R}))\delta P_{IJ}^\alpha \\ & - \sum_{\alpha K} \frac{P^\alpha}{M^\alpha} (d_{IK}^\alpha(\mathbf{R})\delta P_{KJ}^\alpha - \delta P_{IK}^\alpha d_{KJ}^\alpha(\mathbf{R})) \end{aligned} \quad (7.30)$$

We have defined  $\delta F_{KJ}^\alpha = F_{KJ}^\alpha - F_{\lambda,\lambda}^\alpha \delta_{KJ}$ . Then, the final decoherence rate is defined as (just as in Ref. [17]),

$$\frac{1}{\tau^{(K,L)}} = \frac{1}{2} \sum_{\alpha} (F_{K,K}^\alpha - F_{L,L}^\alpha) (\delta R_{K,K}^\alpha - \delta R_{L,L}^\alpha) \quad (7.31)$$

In A-SH, Eq. 7.31 is used to turn off the GFSH hopping contributed from off-diagonal matrix element of  $K, L$ . To be explicit, we define

$$\tilde{b}_{JJ} = - \sum_{K \neq L} \mathcal{L}_{JJ,KL}^{ad,el,bs} \sigma_{KL}^{ad} \zeta^{K,L} \quad (7.32)$$

Here  $\zeta^{K,L}$  is either 0 or 1. The hopping rate from off-diagonal matrix elements is

$$\tilde{k}_{I \rightarrow J}^{off} = \begin{cases} \frac{-\tilde{b}_{II} \tilde{b}_{JJ}}{\sigma_{II}^{ad} \sum_K \Theta(b_{KK})}, & \text{if } \tilde{b}_{JJ} > 0 \text{ and } \tilde{b}_{II} < 0 \\ 0, & \text{otherwise} \end{cases} \quad (7.33)$$

If  $\zeta^{K,L} = 1$  for all  $K \neq L$ ,  $\tilde{k}_{I \rightarrow J}^{off} = k_{I \rightarrow J}^{off}$  (Eq. 7.24), such that A-SH recovers SH. If  $\zeta^{K,L} = 0$  for all  $K \neq L$ ,  $\tilde{k}_{I \rightarrow J}^{off} = 0$ , A-SH reduces to the sec-SH.

For convenience, we denote

$$\tilde{k}_{I \rightarrow J}^{\mathcal{L}} = k_{I \rightarrow J}^{on} + \tilde{k}_{I \rightarrow J}^{off} \quad (7.34)$$

$$\tilde{k}_{I \rightarrow J}^{total} = k_{I \rightarrow J}^d + \tilde{k}_{I \rightarrow J}^{\mathcal{L}}. \quad (7.35)$$

We are now prepared to formalize the A-SH protocol. Note that the interpolation in Eqs. 7.31-7.33 is rather ad hoc for now. Our rationale for invoking a A-SH decoherence rate will be partially explained below. Our A-SH algorithm is as follows.

1. Prepare initial  $\hat{\sigma}$ ,  $\mathbf{R}$ ,  $\mathbf{P}$ . Choose active potential surface (say  $\lambda = I$ ). Set  $\delta \hat{\mathbf{R}} = 0$ ,  $\delta \hat{\mathbf{P}} = 0$ ,  $\zeta^{K,L} = 1$  (for all  $K \neq L$ )

2. Evolve  $\hat{\sigma}$ ,  $\mathbf{R}$  and  $\mathbf{P}$  according to Eqs.7.15-7.17 for a time interval  $\Delta t$  on the active potential surface. For any  $K \neq L$ , if  $\zeta^{K,L} = 1$ , propagate  $\delta\hat{\mathbf{R}}$  and  $\delta\hat{\mathbf{P}}$  according to Eq. 7.29 and Eq. 7.30.
3. Calculate the hopping rate  $k_{I \rightarrow K}^d$  and  $\tilde{k}_{I \rightarrow K}^{\mathcal{L}}$  according to Eq. 7.19 and Eq. 7.34 (Eq. 7.22 plus Eq. 7.33). Generate a random number  $\xi \in [0, 1]$ . Define  $\tilde{S}_I^J = \sum_{K=1}^J \tilde{k}_{I \rightarrow K}^{total}$ 
  - If  $\xi > \tilde{S}_I^N \Delta t$  (here  $N$  is the total number of PESs), the nuclei remain on surface  $I$ .
  - Else if  $\tilde{S}_I^{J-1} \Delta t < \xi < (\tilde{S}_I^{J-1} + \tilde{k}_{I \rightarrow J}^{\mathcal{L}}) \Delta t$ , the nuclei hops to surface  $J$ , without momentum rescaling. Set  $\delta\hat{\mathbf{P}} = 0$ .
  - Else if  $(\tilde{S}_I^{J-1} + \tilde{k}_{I \rightarrow J}^{\mathcal{L}}) \Delta t < \xi < \tilde{S}_I^J \Delta t$ , the nuclei hops to PES  $J$ , with momentum rescaling along the direction of the derivative coupling.

$$\mathbf{P}^{new} = \mathbf{P} + \kappa \mathbf{d}_{IJ} / |\mathbf{d}_{IJ}| \quad (7.36)$$

$$\sum_{\alpha} \frac{(P^{\alpha, new})^2}{2M^{\alpha}} + E_J^{ad}(\mathbf{R}) = \sum_{\alpha} \frac{(P^{\alpha})^2}{2M^{\alpha}} + E_I^{ad}(\mathbf{R}) \quad (7.37)$$

Among the two roots satisfying Eq. 7.37, the root with smaller  $|\kappa|$  is chosen. Set  $\delta\hat{\mathbf{P}} = 0$ ,  $\delta\hat{\mathbf{R}} = 0$ .

4. For all  $K \neq L$ , if  $\zeta^{K,L} = 1$ , calculate the decoherence rates  $\frac{1}{\tau^{(K,L)}}$ , and generate a new random number  $\xi \in [0, 1]$ . If  $\frac{\Delta t}{\tau^{(K,L)}} > \xi$ , set  $\zeta^{K,L} = 0$ , and set (for all  $J = 1, \dots, N$ )

$$\delta\hat{\mathbf{R}}_{K,J} = \delta\hat{\mathbf{P}}_{K,J} = 0, \quad (7.38)$$

$$\delta\hat{\mathbf{R}}_{J,K} = \delta\hat{\mathbf{P}}_{J,K} = 0, \quad (7.39)$$

$$\delta\hat{\mathbf{R}}_{L,J} = \delta\hat{\mathbf{P}}_{L,J} = 0, \quad (7.40)$$

$$\delta\hat{\mathbf{R}}_{J,L} = \delta\hat{\mathbf{P}}_{J,L} = 0. \quad (7.41)$$

5. Repeat step 2 through 5 for the desired number of time steps.

### 7.3.3. Electronic friction-Langevin dynamics (EF-LD)

In the adiabatic limit, which nuclear motion is slow relative to electron transfer, the QCLE-CME can be mapped onto an electronic friction-Langevin dynamics (EF-LD)<sup>[185]</sup>,

$$M^\alpha \ddot{R}^\alpha = \mathcal{F}^\alpha(\mathbf{R}) - \sum_{\beta} \gamma^{\alpha\beta}(\mathbf{R}) \dot{R}^\beta + \delta\mathcal{F}^\alpha(t). \quad (7.42)$$

Here the the mean force and electronic friction are given by

$$\mathcal{F}^\alpha(\mathbf{R}) = -tr_e \left( \frac{\partial \hat{H}_s^{el}}{\partial R^\alpha} \hat{\sigma}_{eq} \right) \quad (7.43)$$

$$\gamma^{\alpha\beta}(\mathbf{R}) = -tr_e \left( \frac{\partial \hat{H}_s^{el}}{\partial R^\alpha} \hat{\mathcal{L}}_{el}^{-1} \frac{\partial \hat{\sigma}_{eq}}{\partial R^\beta} \right) \quad (7.44)$$

In the above equations,  $tr_e$  implies a trace over the electronic DoFs in the molecule, and  $\hat{\sigma}_{eq} = \frac{1}{Z} e^{-\hat{H}_s^{el}/kT}$  ( $Z = tr_e e^{-\hat{H}_s^{el}/kT}$ ).  $\hat{\mathcal{L}}_{el}^{-1}$  is inverse of  $\hat{\mathcal{L}}_{el}$ , which is defined as  $\hat{\mathcal{L}}_{el}(\cdot) \equiv \hat{\mathcal{L}}_{bs}^{el}(\cdot) + \frac{i}{\hbar} [\hat{H}_s^{el}, \cdot]$ .  $\delta\mathcal{F}^\alpha$  is a random force with a correlation function that is Markovian:

$$\langle \delta\mathcal{F}^\alpha(t) \delta\mathcal{F}^\beta(t') \rangle = 2D^{\alpha\beta}(\mathbf{R}) \delta(t - t'). \quad (7.45)$$

where the correlation function is

$$D^{\alpha\beta}(\mathbf{R}) = \frac{1}{2} tr_e \left( \frac{\partial \hat{H}_s^{el}}{\partial R^\alpha} \hat{\mathcal{L}}_{el}^{-1} \left( \frac{\partial \hat{H}_s^{el}}{\partial R^\beta} \hat{\sigma}_{eq} + \hat{\sigma}_{eq} \frac{\partial \hat{H}_s^{el}}{\partial R^\beta} - 2tr_e \left( \frac{\partial \hat{H}_s^{el}}{\partial R^\beta} \hat{\sigma}_{eq} \right) \hat{\sigma}_{eq} \right) \right) \quad (7.46)$$

Note that the friction (plus random force) given in Eq. 7.44 (plus Eq.7.46) is not exactly equal to the standard form of electronic friction by von Oppen et al.<sup>[80]</sup> The difference between our friction here and the results from von Oppen<sup>[80]</sup> is that we do not take level broadening into account in Eq. 7.44, due to our approach based on a perturbative treatment of the system-bath coupling. That being said, we have shown previously,<sup>[185]</sup> the difference between the QCLE-CME friction (in Eq. 7.44) and the friction in Ref. [80] is small for the

case of not very strong system-bath coupling and high temperature, such that the two sets of Langevin dynamics should be very similar. For very large system-bath couplings, one must invoke the von Oppen results<sup>[80]</sup> which are accurate to infinite order in the system-bath coupling parameter. See also Appendix 7.6.4.

#### 7.4. Results and Discussion

To test our SH algorithms above, we use a donor-acceptor-metal model. The system Hamiltonian is,

$$\hat{H}_s^{el}(x) = E_D(x)\hat{d}_D^+\hat{d}_D + E_A(x)\hat{d}_A^+\hat{d}_A + W(\hat{d}_D^+\hat{d}_A + \hat{d}_A^+\hat{d}_D) + \frac{1}{2}m\omega^2x^2 + \frac{p^2}{2m} \quad (7.47)$$

In the donor-acceptor-metal model, we have

$$\Gamma_{AA} = \Gamma, \Gamma_{DD} = \Gamma_{DA} = \Gamma_{AD} = 0 \quad (7.48)$$

We will further set  $E_D(x) = \sqrt{2}gx + \epsilon_D$ ,  $E_A(x) = 0$ .

In Appendix 7.6.2, we express the Redfield operator explicitly in the adiabatic basis for this two-level model. We prepare the nuclei with a Boltzmann distribution on the donor (i.e. the acceptor is empty). We use the scheme in Ref. [211] to convert between the diabatic and adiabatic states. In Appendix 7.6.3, we show how to calculate the diabatic population  $\langle \hat{d}_D^+\hat{d}_D \rangle$  for SHs and EF-LD. We will compare our results against the QME (see Appendix 7.6.4).

In Fig. 37, we work in the regime where  $W$  is relatively large than  $\Gamma$ . We see good agreement between the QME and all SH algorithms (SH, sec-SH and A-SH), for both diabatic population and kinetic energy. When  $W$  and  $\Gamma$  are both large (which is the adiabatic limit,  $W = 0.04$ ,  $\Gamma = 0.01$ ), EF-LD works well for longer dynamics, yet fails to recover the correct initial conditions for diabatic population. This failure arises because, according to EF-LD, we assume local equilibrium for electronic states; the transformation for calculating diabatic

populations is provided in Appendix 7.6.3. In the non-adiabatic limit (smaller  $\Gamma$ ), EF-LD fails completely.

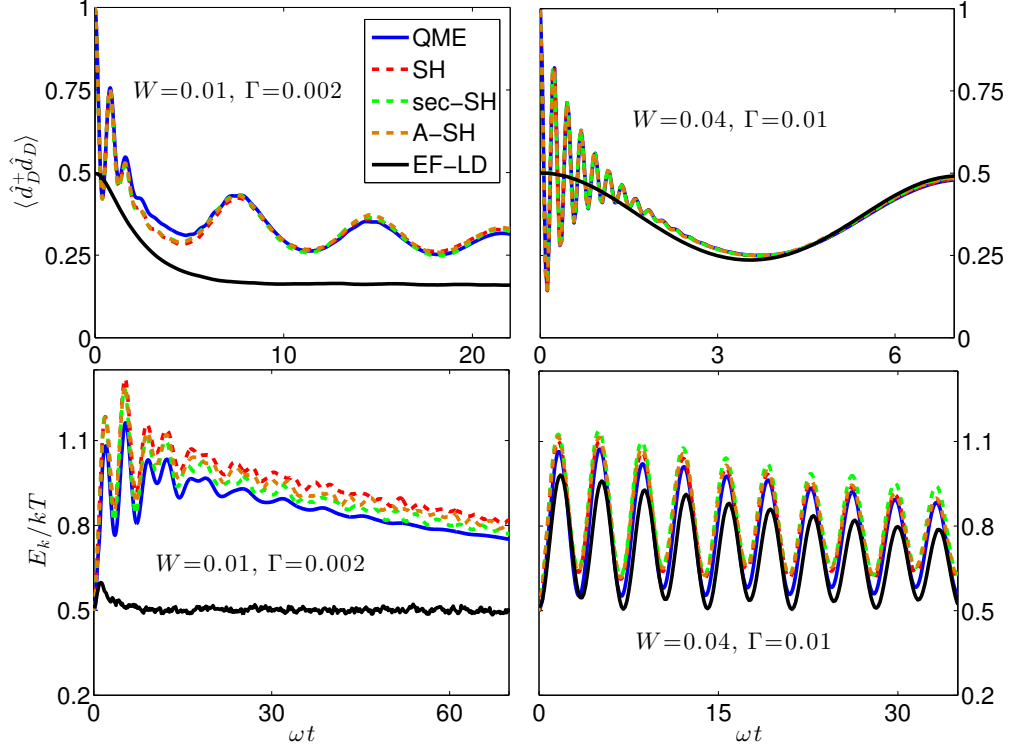


Figure 37: Diabatic electronic population on the donor ( $\langle \hat{d}_D^+ \hat{d}_D \rangle$ ) and the kinetic energy ( $E_k$ ) as a function of time. The QME results can be considered nearly exact (see Appendix 7.6.4). All the SH algorithms (SH, sec-SH, A-SH) agree well with the QME. In the adiabatic limit (large  $W$  and  $\Gamma$ ), EF-LD works for long-time dynamics.  $kT = 0.01$ ,  $\hbar\omega = 0.003$ ,  $g = 0.0075$ ,  $\epsilon_D = 2E_r$ ,  $E_r = g^2/\hbar\omega$ .

Now we turn to the decoherence issue as implemented in A-SH, and to which we alluded above in Sec. 7.3.2. In Fig. 38, we plot results for the case that  $W$  is relatively small compared with  $\Gamma$ . Now we see differences in the performances of the different SH protocols. Standard SH works well for short time dynamics, yet fails to recover the correct equilibrium (either for the diabatic population or the kinetic energy). In fact, the system reaches a different temperature from the bath (as shown by the kinetic energy in Fig. 38). Vice versa, sec-SH fails at short times but does recover the correct equilibrium at long times. Overall, A-SH agrees best with the QME. Again, EF-LD works best in the adiabatic limit (when  $W$  and  $\Gamma$  are both large).

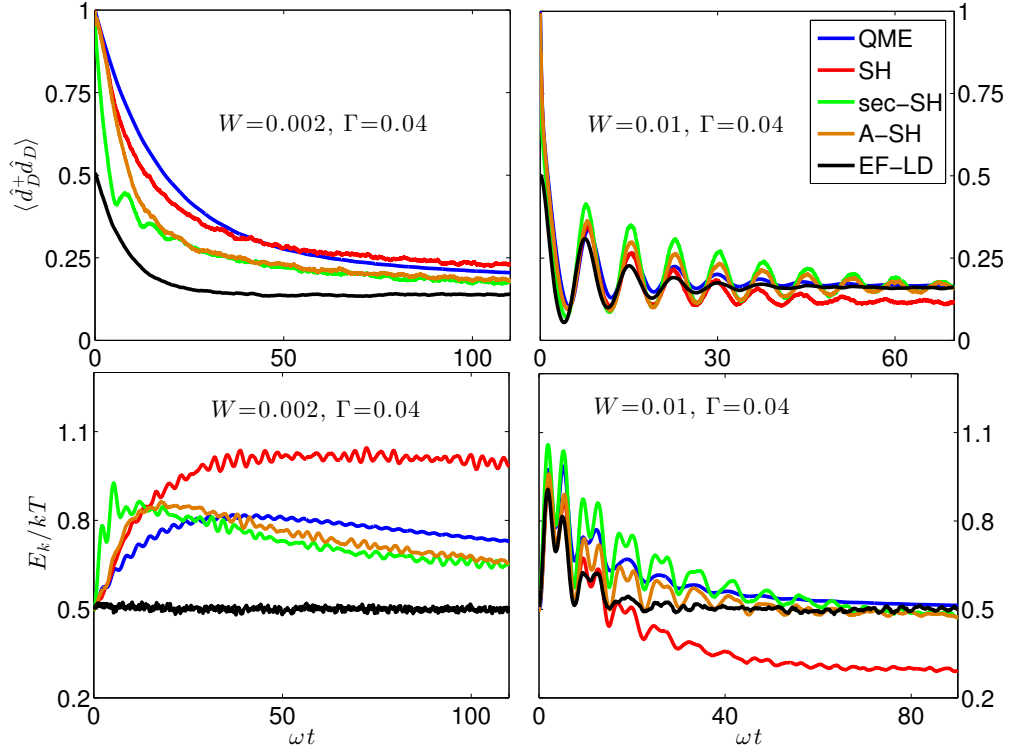


Figure 38: Diabatic electronic population on the donor ( $\langle \hat{d}_D^+ \hat{d}_D \rangle$ ) and the kinetic energy ( $E_k$ ) as a function of time. SH fails to recover the correct equilibrium. Sec-SH does recover the correct equilibrium but fails for early dynamics. Overall, A-SH performs the best among different SH methods.  $kT = 0.01$ ,  $\hbar\omega = 0.003$ ,  $g = 0.0075$ ,  $\epsilon_D = 2E_r$ ,  $E_r = g^2/\hbar\omega$ .

To understand the origin of this behavior (especially for surface hopping), note that in this parameter regime, the GFSH hopping rate (which accounts for the off-diagonal elements of the electronic density matrix  $\hat{\sigma}$ ) is rather large. Now, according to Eq. 7.59, if all matrix elements of  $\Gamma_{pq}$  and if all of the Fermi functions do not fluctuate, it follows at long times that,  $\sigma_{KL} \rightarrow 0$  ( $K \neq L$ ). See the discussion below Eq. 7.59. That being said, however, these matrix elements *will* fluctuate because of nuclear motion, and thus, in practice, we may not find that  $\sigma_{KL} \rightarrow 0$ . And thus, the large GFSH rate can destroy long time detailed balance because of an inexact treatment of the coherence in  $\hat{\sigma}$ .

To address this deficiency, we have hypothesized in this paper that, just as the FSSH algorithm lacks decoherence and cannot properly follow the QCLE without a decoherence correction, so too the FSSH-CME-SH algorithm lacks some decoherence and cannot follow the QCLE-CME. Because this decoherence is necessarily tied to the effect of nuclear motion on electronic dynamics, we therefore propagate nuclear moments (just as in A-FSSH) and turn off GFSH accordingly. Empirically, in Figs. 37-38, we find that the resulting A-SH algorithm yields very strong results, as A-SH recovers relatively accurate short time dynamics and finds the correct detailed balance at longer times.

That being said, the A-SH algorithm we introduced in Sec. 7.3.2 is only a preliminary algorithm, and it is very possible that further improvements can and will be made; in particular, our understanding of decoherence at a metal surface is not yet fully clear or complete (unlike the case in solution). Future work is required to test and improve the A-SH algorithm across many model problems, especially for the case of more than two molecular orbitals in the molecule (where electronic coherence terms can be coupled with each other).

Finally, in the future, it will also be very interesting to test the SH algorithms in an environment where extra phonon friction appears and the correct temperature is maintained: how will A-SH, SH and sec-SH compare with each other?

## 7.5. Conclusions

We have proposed several efficient algorithms to solve the QCLE-CME, which models the non-adiabatic dynamics for a molecule near a metal surface. These algorithms (i) generalize Tully's FSSH to incorporate the exchange of electrons between molecule and metal, and also (ii) generalize the CME-SH to the case of multiple levels in the molecule. Among all the surface hopping algorithms tested here, an augmented surface hopping (A-SH) thus far performs best in most regimes. Further research must strenuously test the algorithms in the condensed phase, especially when extra friction is presented from phonons. The role of decoherence also requires further investigation in the QCLE-CME. Overall, we expect this surface hopping algorithm or variants thereof to be very useful for modeling realistic electrochemical systems and non-adiabatic scattering of molecules off metal surfaces.

## 7.6. Appendix

### 7.6.1. The Redfield Operator

In the Appendix of Ref. [185], we have written the Redfield operator in the diabatic basis,

$$\begin{aligned} \hat{\mathcal{L}}_{bs}^{el} \hat{\rho}_{el} &= \sum_{mn} \frac{\Gamma_{mn}}{2\hbar} \hat{d}_m^+ \hat{S} \tilde{\mathbb{D}}_n \hat{S}^+ \hat{\rho}_{el}(t) + \sum_{mn} \frac{\Gamma_{mn}}{2\hbar} \hat{d}_m \hat{S} \mathbb{D}_n^+ \hat{S}^+ \hat{\rho}_{el}(t) \\ &- \sum_{mn} \frac{\Gamma_{mn}}{2\hbar} \hat{d}_m^+ \hat{\rho}_{el}(t) \hat{S} \mathbb{D}_n \hat{S}^+ - \sum_{mn} \frac{\Gamma_{mn}}{2\hbar} \hat{d}_m \hat{\rho}_{el}(t) \hat{S} \tilde{\mathbb{D}}_n^+ \hat{S}^+ + h.c. \end{aligned} \quad (7.49)$$

Here  $\hat{S}$  is the matrix that diagonalizes the system Hamiltonian  $\hat{H}_s^{el}$ , with adiabatic PESs  $E_I^{ad}$ ,  $I = 1, \dots, N$  ( $N$  is total number of PESs). We have defined  $(\tilde{\mathbb{D}}_n)_{IJ} \equiv (\hat{S}^+ \hat{d}_n \hat{S})_{IJ} (1 - f(E_J^{ad} - E_I^{ad}))$ ,  $(\mathbb{D}_n)_{IJ} \equiv (\hat{S}^+ \hat{d}_n \hat{S})_{IJ} f(E_J^{ad} - E_I^{ad})$ .  $f(E) = 1/(e^{E/kT} + 1)$  is a Fermi function.  $\tilde{\mathbb{D}}_n^+ / \mathbb{D}_n^+$  is the Hermitian conjugate of  $\tilde{\mathbb{D}}_n / \mathbb{D}_n$ .

The above equation can be rewritten in an adiabatic basis (noting  $\hat{\rho}_{el}^{ad} = \hat{S}^+ \hat{\rho}_{el} \hat{S}$ ),

$$\begin{aligned} \hat{\mathcal{L}}_{bs}^{ad,el} \hat{\rho}_{el}^{ad} &= \sum_{mn} \frac{\Gamma_{mn}}{2\hbar} \hat{S}^+ \hat{d}_m^+ \hat{S} \tilde{\mathbb{D}}_n \hat{\rho}_{el}^{ad}(t) + \sum_{mn} \frac{\Gamma_{mn}}{2\hbar} \hat{S}^+ \hat{d}_m \hat{S} \mathbb{D}_n^+ \hat{\rho}_{el}^{ad}(t) \\ &- \sum_{mn} \frac{\Gamma_{mn}}{2\hbar} \hat{S}^+ \hat{d}_m^+ \hat{S} \hat{\rho}_{el}^{ad}(t) \mathbb{D}_n - \sum_{mn} \frac{\Gamma_{mn}}{2\hbar} \hat{S}^+ \hat{d}_m \hat{S} \hat{\rho}_{el}^{ad}(t) \tilde{\mathbb{D}}_n^+ + h.c. \end{aligned} \quad (7.50)$$

### 7.6.2. The Redfield Operator for donor-acceptor metal model

Now we apply the results above to the two-level model in Sec. 7.4. We write the diabatic system Hamiltonian in a Fock space,

$$\hat{H}_s^{el} = \begin{pmatrix} 0 & & & & \\ & E_D & W & & \\ & W & E_A & & \\ & & & & \\ & & & & E_D + E_A \end{pmatrix} + \left( \frac{1}{2} m \omega^2 x^2 + \frac{p^2}{2m} \right) \hat{I}_{el} \quad (7.51)$$

Here  $\hat{I}_{el}$  is an (electronic) identity matrix. The annihilation operators  $\hat{d}_D$  and  $\hat{d}_A$  are,

$$\hat{d}_D = \begin{pmatrix} 0 & 1 & 0 & 0 \\ 0 & 0 & 0 & 0 \\ 0 & 0 & 0 & -1 \\ 0 & 0 & 0 & 0 \end{pmatrix}, \hat{d}_A = \begin{pmatrix} 0 & 0 & 1 & 0 \\ 0 & 0 & 0 & 1 \\ 0 & 0 & 0 & 0 \\ 0 & 0 & 0 & 0 \end{pmatrix}. \quad (7.52)$$

The  $\hat{S}$  matrix that diagonalizes  $\hat{H}_s^{el}$  takes the form

$$\hat{S} = \begin{pmatrix} 1 & & & & \\ & \cos \theta & \sin \theta & & \\ & -\sin \theta & \cos \theta & & \\ & & & & \\ & & & & 1 \end{pmatrix}. \quad (7.53)$$

For simplicity, below we denote  $f(E_I^{ad} - E_J^{ad}) = f_{IJ}$  ( $I, J=1, \dots, 4$ ). We further denote  $\Gamma_{aa} = \Gamma \sin^2 \theta$ ,  $\Gamma_{bb} = \Gamma \cos^2 \theta$ ,  $\Gamma_{ab} = -\Gamma \cos \theta \sin \theta$ . Now we can write the Redfield operator explicitly for the two-level system in the adiabatic basis,

$$\begin{aligned}
-(\mathcal{L}_{bs}^{ad,el} \rho_{el}^{ad})_{11} = & -\left(\frac{\Gamma_{aa}}{\hbar} f_{21} + \frac{\Gamma_{bb}}{\hbar} f_{31}\right) \rho_{11}^{ad,el} + \frac{\Gamma_{aa}}{\hbar} f_{12} \rho_{22}^{ad,el} + \frac{\Gamma_{bb}}{\hbar} f_{13} \rho_{33}^{ad,el} \\
& + \frac{\Gamma_{ab}}{2\hbar} (f_{12} + f_{13}) (\rho_{32}^{ad,el} + \rho_{23}^{ad,el}), \tag{7.54}
\end{aligned}$$

$$\begin{aligned}
-(\mathcal{L}_{bs}^{ad,el} \rho_{el}^{ad})_{22} = & -\left(\frac{\Gamma_{aa}}{\hbar} f_{12} + \frac{\Gamma_{bb}}{\hbar} f_{42}\right) \rho_{22}^{ad,el} + \frac{\Gamma_{aa}}{\hbar} f_{21} \rho_{11}^{ad,el} + \frac{\Gamma_{bb}}{\hbar} f_{24} \rho_{44}^{ad,el} \\
& - \frac{\Gamma_{ab}}{2\hbar} (f_{13} - f_{43}) (\rho_{ad,32}^{el} + \rho_{ad,23}^{el}), \tag{7.55}
\end{aligned}$$

$$\begin{aligned}
-(\mathcal{L}_{bs}^{ad,el} \rho_{el}^{ad})_{33} = & -\left(\frac{\Gamma_{aa}}{\hbar} f_{43} + \frac{\Gamma_{bb}}{\hbar} f_{13}\right) \rho_{33}^{ad,el} + \frac{\Gamma_{aa}}{\hbar} f_{34} \rho_{44}^{ad,el} + \frac{\Gamma_{bb}}{\hbar} f_{31} \rho_{11}^{ad,el} \\
& - \frac{\Gamma_{ab}}{2\hbar} (f_{12} - f_{42}) (\rho_{32}^{ad,el} + \rho_{23}^{ad,el}), \tag{7.56}
\end{aligned}$$

$$\begin{aligned}
-(\mathcal{L}_{bs}^{ad,el} \rho_{el}^{ad})_{44} = & -\left(\frac{\Gamma_{aa}}{\hbar} f_{34} + \frac{\Gamma_{bb}}{\hbar} f_{24}\right) \rho_{44}^{ad,el} + \frac{\Gamma_{aa}}{\hbar} f_{43} \rho_{33}^{ad,el} + \frac{\Gamma_{bb}}{\hbar} f_{42} \rho_{22}^{ad,el} \\
& - \frac{\Gamma_{ab}}{2\hbar} (f_{42} + f_{43}) (\rho_{32}^{ad,el} + \rho_{23}^{ad,el}). \tag{7.57}
\end{aligned}$$

The coherence term is:

$$-(\mathcal{L}_{bs}^{ad,el} \rho_{el}^{ad})_{23} = \chi(\varrho) - \frac{1}{2\hbar} \left( \Gamma_{aa} f_{12} + \Gamma_{bb} f_{13} + \Gamma_{bb} f_{42} + \Gamma_{aa} f_{43} \right) \rho_{23}^{ad,el}. \tag{7.58}$$

with the complex conjugate  $(\mathcal{L}_{bs}^{ad,el} \rho_{el}^{ad})_{32} = (\mathcal{L}_{bs}^{ad,el} \rho_{el}^{ad})_{23}^*$ . The second term on the RHS of Eq. 7.58 is a natural decoherence term. We have defined  $\chi(\varrho)$  in Eq. 7.58 as

$$\begin{aligned}
\chi(\varrho) = & \frac{\Gamma_{ab}}{2\hbar} \left( (f_{31} + f_{21}) \rho_{11}^{ad,el} - (f_{12} - f_{42}) \rho_{22}^{ad,el} \right. \\
& \left. - (f_{13} - f_{43}) \rho_{33}^{ad,el} - (f_{24} + f_{34}) \rho_{44}^{ad,el} \right) \tag{7.59}
\end{aligned}$$

If  $\Gamma_{pq}$  ( $p, q = a, b$ ) and the Fermi function  $f_{IJ}$  do not fluctuate, Eqs. 7.54 to 7.58 have a simple steady states solution,  $\rho_{IJ}^{ad,el} = \frac{1}{Z} \delta_{IJ} e^{-E_I^{ad}/kT}$  ( $Z$  is the normalization factor). We note that, at steady states,  $\chi(\varrho) = 0$  as well as  $\rho_{23}^{ad,el} = 0$ .

### 7.6.3. Diabatic population

In a surface hopping scheme, when calculating the diabatic population, we must transform from the adiabatic basis to a diabatic basis. Following Ref. [211], the diabatic population  $\langle \hat{d}_D^+ \hat{d}_D \rangle$  is given

$$\langle \hat{d}_D^+ \hat{d}_D \rangle = \frac{1}{N_{tra}} \sum_{l=1}^{N_{tra}} \left( \cos^2 \theta_l \delta_{2,\lambda^l} + \sin^2 \theta_l \delta_{3,\lambda^l} + 2 \sin \theta_l \cos \theta_l \text{Re} \{ \sigma_{l,23}^{ad,el} \} + \delta_{4,\lambda^l} \right) \quad (7.60)$$

Here,  $l$  is an index for trajectories,  $N_{tra}$  is total number of trajectories, and  $\lambda$  is the active potential energy surface. The only difference between Eq. 7.60 and Eq. 11 in Ref. [211] is that, whereas Ref. [211] treats a two-state system, formally we are now treating a four-state system in Fock space. Furthermore, note that for state 4, both donor and acceptor are occupied (see the system Hamiltonian, Eq. 7.51). As a result, we include the term  $\delta_{4,\lambda^l}$  on the right-hand side of Eq. 7.60.

In a EF-LD,  $\langle \hat{d}_D^+ \hat{d}_D \rangle$  is given by averaging local equilibrium population:

$$\langle \hat{d}_D^+ \hat{d}_D \rangle = \frac{1}{N_{tra}} \sum_{l=1}^{N_{tra}} \text{tr}_e(\hat{\sigma}_{eq}(\mathbf{R}^l) \hat{d}_D^+ \hat{d}_D) \quad (7.61)$$

### 7.6.4. Details for the QME calculations

We write the QME again,

$$\frac{\partial}{\partial t} \hat{\rho} = -\frac{i}{\hbar} [\hat{H}_s, \hat{\rho}] - \hat{\mathcal{L}}_{bs} \hat{\rho} \quad (7.62)$$

For the model we chose in Sec. 7.4 (Eq. 7.47), the corresponding system Hamiltonian with

quantum nuclear DoFs is

$$\hat{H}_s = \epsilon_D \hat{d}_D^\dagger \hat{d}_D + \epsilon_A \hat{d}_A^\dagger \hat{d}_A + W(\hat{d}_D^\dagger \hat{d}_A + \hat{d}_A^\dagger \hat{d}_D) \quad (7.63)$$

$$+ \hbar\omega(\hat{a}^\dagger \hat{a} + \frac{1}{2}) + g(\hat{a}^\dagger + \hat{a}) \hat{d}_D^\dagger \hat{d}_D \quad (7.64)$$

In the exciton basis, we can express the system Hamiltonian as

$$\hat{H}_s = \begin{bmatrix} \hat{H}_{11} & & & \\ & \hat{H}_{22} & \hat{H}_{23} & \\ & \hat{H}_{32} & \hat{H}_{33} & \\ & & & \hat{H}_{44} \end{bmatrix} \quad (7.65)$$

where

$$\hat{H}_{11} = \hbar\omega(\hat{a}^\dagger \hat{a} + \frac{1}{2}) \quad (7.66)$$

$$\hat{H}_{22} = \hbar\omega(\hat{a}^\dagger \hat{a} + \frac{1}{2}) + g(\hat{a}^\dagger + \hat{a}) + \epsilon_D \quad (7.67)$$

$$\hat{H}_{33} = \hbar\omega(\hat{a}^\dagger \hat{a} + \frac{1}{2}) + \epsilon_A \quad (7.68)$$

$$\hat{H}_{44} = \hbar\omega(\hat{a}^\dagger \hat{a} + \frac{1}{2}) + g(\hat{a}^\dagger + \hat{a}) + \epsilon_D + \epsilon_A \quad (7.69)$$

and

$$\hat{H}_{23} = \hat{H}_{32} = W \hat{I}_n \quad (7.70)$$

$\hat{I}_n$  is the nuclear identity operator. The phonon operator is given by

$$\hat{a}^\dagger \hat{a} = \begin{bmatrix} 0 & & & \\ & 1 & & \\ & & 2 & \\ & & & \dots \end{bmatrix}, \hat{a} + \hat{a}^\dagger = \begin{bmatrix} 0 & 1 & & \\ 1 & 0 & \sqrt{2} & \\ & \sqrt{2} & 0 & \sqrt{3} \\ & & \dots & \dots & \dots \end{bmatrix} \quad (7.71)$$

We will truncate the number of the dimension to  $N_{ph}$ . For the parameters we used in the main body of the text, we found good converges with  $N_{ph} = 40$ .

The superoperator in Eq. 7.62 can be simplified after we diagonalize the system Hamiltonian  $\hat{H}_s$ .

$$\begin{aligned}\hat{\mathcal{L}}_{bs}\hat{\rho} &= \sum_{mn} \frac{\Gamma_{mn}}{2\hbar} \hat{d}_m^+ \hat{U} \tilde{\mathbb{T}}_n \hat{U}^+ \hat{\rho} + \sum_{mn} \frac{\Gamma_{mn}}{2\hbar} \hat{d}_m \hat{U} \mathbb{T}_n^+ \hat{U}^+ \hat{\rho} \\ &- \sum_{mn} \frac{\Gamma_{mn}}{2\hbar} \hat{d}_m^+ \hat{\rho} \hat{U} \mathbb{T}_n \hat{U}^+ - \sum_{mn} \frac{\Gamma_{mn}}{2\hbar} \hat{d}_m \hat{\rho} \hat{U} \tilde{\mathbb{T}}_n^+ \hat{U}^+ + h.c.\end{aligned}\quad (7.72)$$

where

$$\hat{d}_D = \begin{bmatrix} 0 & \hat{I}_n & 0 & 0 \\ 0 & 0 & 0 & 0 \\ 0 & 0 & 0 & -\hat{I}_n \\ 0 & 0 & 0 & 0 \end{bmatrix}, \quad \hat{d}_A = \begin{bmatrix} 0 & 0 & \hat{I}_n & 0 \\ 0 & 0 & 0 & \hat{I}_n \\ 0 & 0 & 0 & 0 \\ 0 & 0 & 0 & 0 \end{bmatrix}\quad (7.73)$$

Here  $\hat{U}$  is the matrix that diagonalizes the system Hamiltonian  $\hat{H}_s$ , with energy levels  $\bar{\epsilon}_i$  ( $i = 1, \dots, 4N_{ph}$ ). We have defined  $(\tilde{\mathbb{T}}_n)_{ij} \equiv (\hat{U}^+ \hat{d}_n \hat{U})_{ij} (1 - f(\bar{\epsilon}_j - \bar{\epsilon}_i))$ ,  $(\mathbb{T}_n)_{ij} \equiv (\hat{U}^+ \hat{d}_n \hat{U})_{ij} f(\bar{\epsilon}_j - \bar{\epsilon}_i)$ .

A few more words are appropriate regarding the validity of the QME. In the regime where the temperature is fairly large, QME dynamics should be relatively reliable, except for broadening effects. For the Donor-Acceptor-Metal model in Sec. 7.4 (Eqs. 7.47-7.48), we see that nuclear motion is coupled only to the donor, whereas any broadening effects on the donor should be relatively small (because the donor is coupled only indirectly to the continuum through the acceptor). Thus, overall, we expect the QME should be quantitatively accurate. Furthermore, in the same vein, the electronic friction in Eq. 7.44 should also be accurate here, in complete agreement with the von Oppen friction.

## CHAPTER 8 : Born-Oppenheimer Dynamics, Electronic Friction, and the Inclusion of Electron-Electron Interactions

This chapter was adapted from Ref. [212]

### 8.1. Introduction

The Born-Oppenheimer (BO) approximation is probably the most important framework underlying modern physics and chemistry. According to the BO approximation, for a system of nuclei and electrons, we split up the total Hamiltonian into the nuclear kinetic energy ( $\hat{T}_{nuc}$ ) and the electronic Hamiltonian  $\hat{H}$ :

$$\hat{H}_{tot} = \hat{T}_{nuc} + \hat{H} \quad (8.1)$$

$$\hat{H} = \hat{T}_e + \hat{V}_{ee} + \hat{V}_{nn} + \hat{V}_{en} \quad (8.2)$$

The electronic Hamiltonian  $\hat{H}$  includes the electronic kinetic energy  $\hat{T}_e$ , electron-electron repulsion ( $\hat{V}_{ee}$ ), nucleus-nucleus repulsion ( $\hat{V}_{nn}$ ), and nucleus-electron attraction ( $\hat{V}_{en}$ ). According to the BO approximation, we diagonalize  $\hat{H}$  and propagate all nuclear motion along a single eigenvalue of  $\hat{H}$ , which is called an adiabatic state; for a large system in the condensed phase, that special state is usually chosen to be the ground state.

When applying the BO approximation, one must use caution because BO approximation is strictly valid only when nuclear motion is infinitesimally slow, and there are very well known instances where BO approximation breaks down: see, e.g., the recent work of Wodtke on vibrational relaxation and electron transfer at metal surfaces<sup>[24,26]</sup>. Furthermore, nonadiabatic effects in molecular electronics are known to account for a huge number of interesting phenomena including heating<sup>[30,86]</sup>, instability<sup>[31,33]</sup>, and inelastic scattering effects<sup>[78,139]</sup>. Thus, for many experiments, theory must go beyond the BO approximation.

The goal of the present paper is to show that, each and every time one invokes the BO approximation in the condensed phase – provided there is a continuous manifold of elec-

tronic states that relax quickly – there is a single, unique Fokker-Planck equation guiding the nuclear dynamics<sup>[213]</sup>. In other words, if one is considering a system with a manifold of electronic states and one wishes to treat the nuclei classically, BO dynamics should always be propagated with a well-defined frictional damping term and corresponding random force. The universal expressions for such friction and random force are presented below and should be applicable to many dynamical scenarios: e.g., nuclei scattering off metal surfaces<sup>[12]</sup>, atoms vibrating within metal surfaces<sup>[214]</sup>, molecules relaxing when tethered to photo-excited metals<sup>[215]</sup>, and molecules stretching and contracting when experiencing a current (and sitting between two metal contacts)<sup>[129,216]</sup>.

*Previous Results.*— The notion that the BO approximation can sometimes lead to friction is not new. In particular, such a friction was identified long ago in the context of molecular motion at metal surfaces, where a manifold of electronic states is clearly present and can lead to so-called “electronic friction.”

One early derivation of electronic friction is due to Head-Gordon and Tully (HGT)<sup>[82,217]</sup>, who followed the dynamics of electrons and nuclei with Ehrenfest dynamics. At zero temperature, and without any electron-electron interactions in the Hamiltonian, they derived the following functional form for the electronic friction:

$$\begin{aligned} \gamma_{\alpha\nu} = & \pi\hbar \sum_{pq} \langle \phi_p | \partial_\alpha \hat{V}_{SCF} | \phi_q \rangle \langle \phi_q | \partial_\nu \hat{V}_{SCF} | \phi_p \rangle \\ & \times \delta(\epsilon_F - \epsilon_q) \delta(\epsilon_F - \epsilon_p) \end{aligned} \quad (8.3)$$

Here  $\epsilon_p$  and  $\phi_p$  are, respectively, the energies and orbitals that diagonalize  $\hat{V}_{SCF}$ , the one-electron self-consistent potential.  $\epsilon_F$  is the Fermi level, and  $\alpha$  (or  $\nu$ ) indices nuclear DoF’s. To date, this mean-field form of electronic friction has been applied to many systems using ab initio electronic structure theory (e.g., DFT)<sup>[71,218–223]</sup>, and Langevin dynamics on a metal surface with DFT potentials has become a standard tool.

We emphasize, however, that Eq. 8.3 is based on the assumption of independent (either free

or mean-field) electrons at equilibrium (i.e. with only one metallic lead). That being said, this form for electronic friction is consistent with the one-dimensional rates for vibrational relaxation previously published by Persson and Hellsing<sup>[224,225]</sup> and others<sup>[226,227]</sup>. Several other research groups have also identified the same effective friction tensor<sup>[6]</sup> using different methodologies, some using influence functionals<sup>[81]</sup> and some using non-equilibrium Green's functions (NEGF)<sup>[116,173]</sup>. The effects of non-Condon terms have also been considered<sup>[184,228,229]</sup> at finite temperature.

More recently, von Oppen and co-workers have provided an explicit form for the electronic friction using a non-equilibrium Green's function and scattering matrix approach<sup>[80]</sup> plus an explicit adiabatic expansion in terms of nuclear velocity. The resulting expression is valid both in and out of equilibrium, e.g. for a molecule sitting between two metals with a current running through it. However, again one must assume either a quadratic Hamiltonian without electron-electron repulsion<sup>[80]</sup> or a mean-field electronic Hamiltonian<sup>[7]</sup>. (In a forthcoming article, we will show that the von Oppen and HGT expressions are identical at equilibrium<sup>[230]</sup>.)

In the end, many distinct approaches for electronic friction can be found in the literature, most assuming electrons at equilibrium and almost all assuming non-interacting electrons. However, for a realistic description of molecular electronic structure, even if we ignore the effects of an external voltage, it is well-known that one cannot waive away electron-electron interactions<sup>[231]</sup>. Despite decades of work on electronic friction, we believe the most general expression for electronic friction (that includes electron-electron correlation) arguably still belongs to Suhl and co-workers<sup>[232]</sup>. In Ref.<sup>[232]</sup>, the authors conjectured (without proof) a form for electronic friction that does actually include electron-electron correlation (see below). A few years ago, Daligault and Mozyrsky<sup>[233]</sup> successfully derived Suhl's conjecture at equilibrium with a proper random force for the first time, although they did not investigate electron-electron interactions explicitly. Most importantly, we emphasize that Refs.<sup>[232,233]</sup> are limited to an electronic system in equilibrium.

*Outline.*— Given (i) how many important effects break the BO approximation, (ii) how little attention has been paid to the effects of electron-electron correlation on the friction tensor<sup>[9,234,235]</sup>, and (iii) how many experiments routinely apply voltages to metals with molecules nearby, *the goal of the present letter is to derive one universal expression for electronic friction (with a random force) that is valid both with and without electron-electron interactions and in and out of equilibrium.* We will also show that this universal friction reduces to the HGT model for the case of a quadratic Hamiltonian (i.e. free electrons) at equilibrium. At equilibrium, our final expression matches Suhl’s expression<sup>[232,233]</sup> and can be understood easily through the lens of linear response and correlation functions. However, we emphasize that, in contrast with Refs.<sup>[232,233]</sup>, our derived Fokker-Planck equation is valid out of equilibrium so that the effects of non-equilibrium initial conditions can be analyzed. We will show that the second fluctuation-dissipation theorem is satisfied only at equilibrium.

Lastly, to demonstrate just why electron-electron interactions are so important for nonadiabatic effects, we will study the electronic friction tensor for the Anderson-Holstein model in the limit of reasonably large  $U$ . Here, we will show that a mean-field treatment of electron-electron interactions (as in Eq. 8.3) can yield a qualitatively incorrect picture of electronic friction. Given the current push to extend correlated electronic structure methods (beyond mean-field theory) to extended systems<sup>[236,237]</sup>, the present letter should be immediately useful for describing coupled nuclear-electron motion in the condensed phase.

## 8.2. Theory

Consider the very general Hamiltonian in Eqs. 8.1-8.2 and let us make a temperature-dependent BO approximation, whereby we assume that the nuclei are propagated along a Boltzmann average of the Born-Oppenheimer adiabatic surfaces:

$$F_\alpha = -tr_e(\partial_\alpha \hat{H} \hat{\rho}_{ss}) \tag{8.4}$$

Here,  $\hat{\rho}_{ss}$  is a steady-state electronic density matrix. At equilibrium and in the limit of zero temperature,  $\hat{\rho}_{ss} = |g\rangle\langle g|$  and the force  $F_\alpha$  is simply the ground-state force, which is the more standard BO approximation.  $tr_e$  implies tracing over all electronic DoF's.

As shown in the Supplemental Material (SM, Sec. I) of Ref. [212], starting with the quantum-classical Liouville equation (QCLE)<sup>[18,19]</sup> and assuming that electronic motion is much faster than nuclear motion, we derive a Fokker-Planck equation for the nuclear motion in the same spirit as a Mori-Zwanzig projection<sup>[238-243]</sup>. We denote the nuclear phase space density as  $\mathcal{A}(\mathbf{R}, \mathbf{P})$ . The explicit Fokker-Planck equation reads:

$$\begin{aligned} \partial_t \mathcal{A} = & - \sum_{\alpha} \frac{P_{\alpha}}{m_{\alpha}} \partial_{\alpha} \mathcal{A} - \sum_{\alpha} F_{\alpha} \frac{\partial \mathcal{A}}{\partial P_{\alpha}} \\ & + \sum_{\alpha\nu} \gamma_{\alpha\nu} \frac{\partial}{\partial P_{\alpha}} \left( \frac{P_{\nu}}{m_{\nu}} \mathcal{A} \right) + \sum_{\alpha\nu} \bar{D}_{\alpha\nu}^S \frac{\partial^2 \mathcal{A}}{\partial P_{\alpha} \partial P_{\nu}} \end{aligned} \quad (8.5)$$

Thus, all BO trajectories should be Langevin dynamics with an electronic friction and a random force:

$$-m_{\alpha} \ddot{R}_{\alpha} = -F_{\alpha} + \sum_{\nu} \gamma_{\alpha\nu} \dot{R}_{\nu} - \zeta_{\alpha} \quad (8.6)$$

The electronic friction has the following simple form in the time domain (expressed in terms of correlation functions)

$$\gamma_{\alpha\nu} = - \int_0^{\infty} dt \, tr_e \left( \partial_{\alpha} \hat{H} e^{-i\hat{H}t/\hbar} \partial_{\nu} \hat{\rho}_{ss} e^{i\hat{H}t/\hbar} \right) \quad (8.7)$$

or the following form in the energy domain (expressed in terms of Greens functions)

$$\gamma_{\alpha\nu} = -\hbar \int_{-\infty}^{\infty} \frac{d\epsilon}{2\pi} tr_e \left( \partial_{\alpha} \hat{H} \hat{G}^R(\epsilon) \partial_{\nu} \hat{\rho}_{ss} \hat{G}^A(\epsilon) \right) \quad (8.8)$$

Here we have defined the many-body (as opposed to one-body) retarded and advanced Green's functions  $\hat{G}^{R/A}(\epsilon) = (\epsilon - \hat{H} \pm i\eta)^{-1}$ . These expressions prove that the friction must

always be real,  $\gamma_{\alpha\nu} = \gamma_{\alpha\nu}^\dagger$ .

For the random force, at steady state and in the Markovian limit, we find:

$$\begin{aligned}\bar{D}_{\alpha\nu}^S &= \frac{1}{2} \int_0^\infty dt \operatorname{tr}_e (e^{i\hat{H}t/\hbar} \delta\hat{F}_\alpha e^{-i\hat{H}t/\hbar} (\delta\hat{F}_\nu \hat{\rho}_{ss} + \hat{\rho}_{ss} \delta\hat{F}_\nu)) \\ \delta\hat{F}_\alpha &\equiv -\partial_\alpha \hat{H} + \operatorname{tr}_e (\partial_\alpha \hat{H} \hat{\rho}_{ss})\end{aligned}\quad (8.9)$$

so that

$$\frac{1}{2} (\langle \zeta_\alpha(t) \zeta_\nu(t') \rangle + \langle \zeta_\nu(t) \zeta_\alpha(t') \rangle) \equiv \bar{D}_{\alpha\nu}^S \delta(t - t') \quad (8.10)$$

Note  $\bar{D}_{\alpha\nu}^S$  is always real and symmetric. Here, we assume that the electronic Hamiltonian  $\hat{H}$  is real-valued.

Eqs. 8.7-8.10 are completely general: they express the friction and random force that correspond to the BO approximation, in or out of equilibrium. Note that Eqs. 8.7-8.9 require taking a full electronic trace, whereas Eq. 8.3 is expressed in terms of single electronic orbitals. In the SM of Ref. [212], we prove that Eq. 8.7 in fact reduces to Tully's expression (Eq. 8.3) at equilibrium if there are no electron-electron interactions. At this point, there is no simple relationship between  $\gamma_{\alpha\nu}$  and  $\bar{D}_{\alpha\nu}^S$ .

*Equilibrium, the second fluctuation-dissipation theorem and the symmetry of the friction.—*

At equilibrium, the steady state electronic density matrix is  $\hat{\rho}_{ss} = e^{-\hat{H}/k_B T} / Z$ , where  $Z$  is the corresponding normalization factor or partition function:  $Z = \operatorname{tr}_e (e^{-\hat{H}/k_B T})$ . In the SM (Sec. II) of Ref. [212], we show that:

$$\gamma_{\alpha\nu} = \frac{1}{k_B T} \bar{D}_{\alpha\nu}^S \quad (8.11)$$

Thus, the second fluctuation-dissipation theorem is satisfied at equilibrium. Since  $\bar{D}_{\alpha\nu}^S$  is symmetric,  $\gamma_{\alpha\nu}$  is also symmetric along  $\alpha$  and  $\nu$  at equilibrium.

### 8.3. Anderson-Holstein model

To establish the importance of electron-electron interactions, we will now calculate the electronic friction for the Anderson-Holstein (AH) model,

$$\hat{H}_{AH} = \hat{H}_A + \hat{H}_{osc} \quad (8.12)$$

$$\begin{aligned} \hat{H}_A = & E(x) \sum_{\sigma} \hat{d}_{\sigma}^{\dagger} \hat{d}_{\sigma} + U \hat{n}_{\uparrow} \hat{n}_{\downarrow} + \sum_{k\sigma} \epsilon_k \hat{c}_{k\sigma}^{\dagger} \hat{c}_{k\sigma} \\ & + \sum_{k\sigma} V_k (\hat{d}_{\sigma}^{\dagger} \hat{c}_{k\sigma} + \hat{c}_{k\sigma}^{\dagger} \hat{d}_{\sigma}) \end{aligned} \quad (8.13)$$

$$\hat{H}_{osc} = \frac{1}{2} \hbar \omega (x^2 + p^2) \quad (8.14)$$

Physically, the AH model represents an electronic impurity  $d$  sitting near a metal surface and coupled to a vibrating oscillator ( $x$ ). The impurity can be filled with an electron of up or down spin, and so  $\sigma = \uparrow, \downarrow$  indicates spin. The oscillator is a vibrational degree of freedom and feels a different force depending on the occupation of the impurity,  $E(x) \equiv E_d + \sqrt{2}gx$ . Note we have defined  $x$  and  $p$  to be in dimensionless units.

To understand how the motion of the oscillator is perturbed by the fluctuating charge of the impurity, we will calculate the electronic friction. Of course, to apply Eq. 8.7, we must diagonalize  $\hat{H}_A$ , which will be done via a numerical renormalization group (NRG) calculation<sup>[4]</sup>. We take the wide band approximation, such that the hybridization function  $\Gamma \equiv 2\pi \sum_k V_k^2 \delta(\epsilon - \epsilon_k)$  is assumed to be independent of energy. We leave all details of the calculation to the SM (Sec. III and IV) of Ref. [212], and show results below.

In Fig. 39(a), we compare the electronic friction as calculated from NRG versus the electronic friction as calculated with mean-field theory (MFT), Eq. 8.3, which is commonly used to treat the Anderson model<sup>[7]</sup>. We study the case of a large repulsion  $U$ . Whereas NRG predicts two peaks in the electronic friction – where there is a resonance of electron attachment/detachment with the Fermi level of the metal  $\epsilon_F$  (i.e.  $E_d + \sqrt{2}gx = 0$  and  $E_d + \sqrt{2}gx + U = 0$ , where we have set  $\epsilon_F = 0$ ) – MFT predicts only a very broad plateau in

friction. We have attempted to reconstruct these two peaks by manipulating the multiple (broken-symmetry) mean-field solutions of the Anderson-Holstein model, but we have so far been unable to qualitatively match the correct answer.

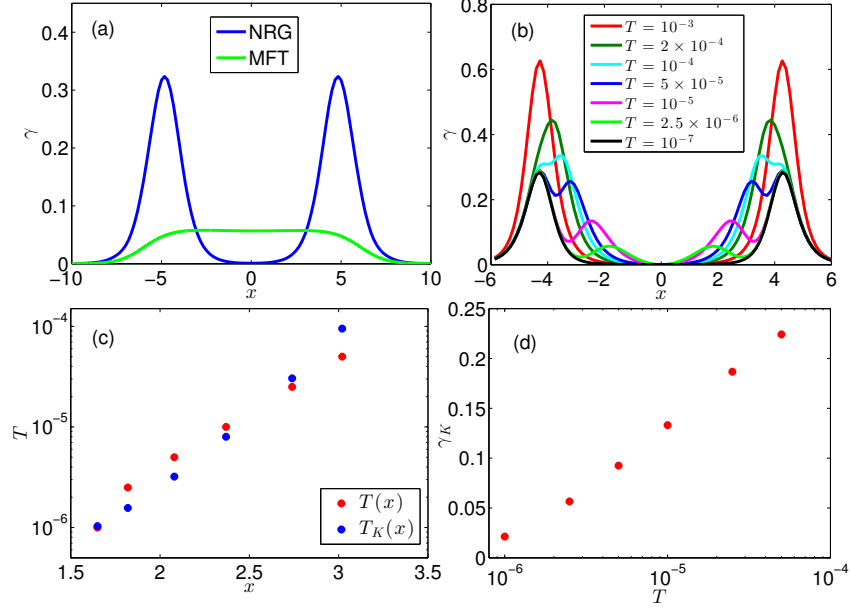


Figure 39: (a) Electronic friction as function of position  $x$  according to both NRG and MFT<sup>[7,8]</sup> calculations at temperature  $T=0.005$ . Note that MFT fails to recover two peaks in the friction. (b) Electronic friction according to NRG at low temperature; note that the two peaks in friction become four peaks in friction at low temperature. (c) The Kondo temperature  $T_K(x)$  as a function of position and the physical temperature  $T(x)$  for which find a peak in friction at position  $x$ . Note that these two temperatures are in rough agreement, as predicted by Langreth<sup>[9]</sup>. (d) The height of the Kondo peak  $\gamma_K$  as a function of temperature; note that these peaks decrease exponentially and vanish at zero Kelvin, in disagreement with Ref.<sup>[9]</sup>. Other parameters  $U = 0.1$ ,  $\Gamma = 0.01$ ,  $E_d = -0.05$ ,  $g = 0.0075$ , bandwidth  $D = 1$ . We have set  $k_B = \hbar = 1$ .

Beyond the formation of two peaks, even more interesting feature arises from NRG at still lower temperatures, where Kondo physics now shows a signature. In Fig. 39(b), we now show that, below  $T = 1 \times 10^{-4}$ , the electronic friction exhibits two additional peaks for a total of **four** peaks. Previously, in Ref.<sup>[9]</sup>, Plihal and Langreth argued that such new peaks might arise from Kondo resonances. In other words, we might expect to find peaks in electronic friction at those positions in space for which the Kondo temperature is equal to the system temperature. Here, we define the Kondo temperature to be:  $T_K(x) =$

$D \exp(-2\pi|E(x)||E(x)+U|/U/\Gamma)$ , where  $D$  is the bandwidth. Thus, for Fig. 39(c), we plot both  $T_K(x)$  and the actual  $T(x)$ , i.e. the temperature at which one finds (with NRG) a peak in friction at position  $x$ . Note that, as the data shows, the relevant Kondo temperature  $T_K$  is close to the physical temperature  $T$ , though the agreement is not perfect.

Let us now establish, however, that Ref.<sup>[9]</sup> (which is based on the non-crossing approximation (NCA) and the case of infinite  $U$ ) may not be entirely applicable for our data. First, in contrast with Ref.<sup>[9]</sup>, we observe that the width of the frictional Kondo peak does not decrease with the temperature. Second, again in contrast with Ref.<sup>[9]</sup>, we find that the frictional peaks associated with a Kondo resonance disappear as the temperature decreases to zero (rather than increase). The height of these peaks is plotted in Fig. 39(d) and appears to decrease exponentially with temperature. Future pencil and paper work will be required to understand these features.

#### 8.4. Conclusions

We have derived a universal expression for the electronic friction as experienced by a set of classical nuclear particles coupled to a manifold of quantum mechanical electronic DoF's. The key equations are Eqs. 8.7, 8.8 and 8.9. The derivation is simple and, in the same spirit as a Mori-Zwanzig projection: Assuming all dynamics follow the quantum-classical Liouville equation, we simply make an adiabatic approximation and isolate fluctuations around a slow variable. Our final expression is quite general, insofar as it applies in/out of equilibrium and with an arbitrary electronic Hamiltonian; at equilibrium, our work validates the Suhl's "bootstrap" conjecture<sup>[232]</sup>.

Looking forward, Eq. 8.7 is demanding to apply because, without any further approximations, these equations require the full diagonalization the electronic Hamiltonian in terms of the many-body electronic states (much like the Meir-Wingreen formula<sup>[244]</sup>). However, using numerical renormalization group (NRG) theory, we have now shown how to calculate electronic friction tensors exactly for small model problems. Thus, extending the work of

von Oppen *et al*<sup>[80]</sup>, one can now study model Hamiltonians and learn how nuclear motion near metal surfaces will be effected by electron-electron correlation, either with or without a current through the molecule. For example, in the present letter, we have studied the Anderson-Holstein model and shown that the usual electronic friction expression (with mean-field theory) yields qualitatively wrong features; when we account for electronic friction, we find multiple peaks, including two associated with Kondo physics. Beyond model problems, even if we cannot use NRG to diagonalize the Hamiltonian, there are currently several research groups that are seeking to calculate approximate energies for extended systems beyond mean-field theory (MFT). For instance, within the condensed matter world, there is currently a big push to calculate correlated electron attachment/detachment energies with GW<sup>[245]</sup> and optical excitations with the Bethe-Salper Equation, all for periodic systems<sup>[237,246]</sup>. Furthermore, within the chemistry world, there has been recent work to calculate ground state coupled-cluster (CC) and excited state equation of motion CC energies for periodic systems<sup>[236,247]</sup>. All of these methods can be used to calculate electronic friction through Eq. 8.8 going beyond MFT and thus improve our understanding of nuclear motion in the condensed phase.

Finally, one pressing question remains regarding the validity of electronic friction: just like the BO approximation, the adiabatic approximation that we make (in the SM of Ref. [212]) to move from Eq. 38 to Eq. 39 is uncontrolled and without a unique small parameter. On the one hand, Tully has argued that electronic friction fails for NO scattering off of gold<sup>[72]</sup>. On the other hand, while one would certainly expect electronic friction to fail in the nonadiabatic Marcus electron transfer regime, in fact we recently showed<sup>[248]</sup> that, with just a little bit of external nuclear friction, electronic friction recovers Marcus theory. From Ref.<sup>[248]</sup>, the only lesson we have so far learned is that Langevin dynamics with electronic friction will fail if truly excited state dynamics appear. In this case, one possible path forward is to include memory effects with a non-Markovian Fokker-Planck equation<sup>[213]</sup> (see the SM of Ref. [212]); another approach is to employ surface hopping techniques that can include frictional effects<sup>[38,183,185]</sup>. In the future, it will be essential to further

investigate when and how such excited state dynamics occurs, and given how important are electronic-electronic interactions for identifying curve crossings, the present paper takes an important step forward by unambiguously identifying the correct, universal electronic friction tensor accompanying all Born-Oppenheimer dynamics.

## CHAPTER 9 : Universality of electronic friction I: the equivalence of von Oppen’s nonequilibrium Green’s function approach and the Head-Gordon–Tully model at equilibrium

This chapter was adapted from Ref. [230]

### 9.1. Introduction

The dynamics of molecules near metal surfaces underlie many interesting phenomena in the area of electrochemistry<sup>[35,36,124,191,192,249]</sup> and molecular electronics<sup>[1,30,31,78,128,129,151]</sup>. While these dynamics can be directly related to straightforward gas-molecule/metal scattering processes<sup>[24,218,221,250]</sup> and chemisorption/dissociation<sup>[26,251,252]</sup>, one must always remember that these dynamics can also display surprising behavior.<sup>[27,152,194,235,253–255]</sup> Due to electron transfer processes between molecule and metal, the charge state of the molecule need not be static and thus the Born-Oppenheimer approximation can break down<sup>[11,12]</sup>. Compared with more conventional nonadiabatic effects for molecules in the gas phase or solution<sup>[16,19,22,40,195,197,203,204,206]</sup>, such non-adiabaticity at a metal surface is extremely challenging because the metal presents a continuous manifold of electron states (rather than a handful)<sup>[38,71,99,125,182,256]</sup>.

The simplest way to model the non-adiabaticity at a metal surface is the electronic friction model. In the limit of fast electronic dynamics, where electron transfer occurs very quickly, the nuclei move effectively on an average PES while also experiencing friction and a fluctuating force. In the literature, quite a variety of friction models have been derived using different methods, some systematic and some ad hoc. Techniques for deriving friction include path integrals<sup>[233]</sup>, non-equilibrium Green’s functions (NEGF) and scattering approaches<sup>[80,116,229]</sup>, influence functionals<sup>[81,173]</sup>, Meyer-Miller (MM) mappings<sup>[82,213]</sup>, quantum-classical Liouville equation projections<sup>[212]</sup>, as well as simple Fermi-Golden rule arguments<sup>[114,220]</sup>. The final expression for electronic friction can also be expressed in a variety of different forms, i.e. in the time or energy domains<sup>[184,213]</sup>, in terms of greens

functions or scattering matrices<sup>[80,116]</sup>, in diabatic or adiabatic basis representations (e.g. Kohn-Sham orbitals)<sup>[82,173,222,225]</sup>, or in the form of response/correlation functions or derivative couplings<sup>[82,217,232,233]</sup>, etc.

Among these different forms for electronic friction, probably the mostly common used expression was given by Head-Gordon and Tully (HGT) in 1995<sup>[82]</sup>. The HGT friction model has been successfully used to calculate the time scale for vibrational relaxation, and has been implemented in ab initio electronic structure theory<sup>[8]</sup>. The original HGT model is based on a MM mapping in the adiabatic basis combined with Ehrenfest dynamics. While the original article was restricted to zero temperature, very recently, as argued in Ref.<sup>[220]</sup> and confirmed in Ref.<sup>[212]</sup>, the fluctuating force and other finite temperature effects can also be included<sup>[114]</sup>.

Apart from the HGT expression, another important (and very different) type of electronic friction has been given by von Oppen *et al*, using a NEGF and scattering matrix formalism<sup>[80]</sup>. This approach has certain advantages relative to the HGT approach. In particular, through this approach Langevin dynamics are more rigorously derived with the proper random force; the approximation can also be systematically verified. Moreover, the friction can be applied to the non-equilibrium case, resulting in, for instance, current induced friction. However, the derivation is rather complicated for those without expertise in nonequilibrium field theory, especially when non-Condon effects are incorporated<sup>[184]</sup>. Furthermore, both the HGT and von Oppen NEGF models effectively assume non-interacting electrons, where electron-electron (el-el) correlation is missing; el-el interactions can give very new and interesting physics at low temperature<sup>[9,212,235]</sup>.

Finally, a third form for electronic friction can also be found in the literature: the friction can be expressed in terms of response/correlation functions<sup>[212,232,233]</sup>. Indeed, the HGT form for electronic friction can be rewritten in the form of Fermi's Golden rule rate, i.e. second order perturbation theory<sup>[220]</sup>, which is equivalent to a correlation function expression. More generally, el-el interactions can also be incorporated into the friction tensor when expressed

with correlation functions (as was argued by Suhl *et al* long ago<sup>[232]</sup>).

Now, despite the presence of so many different approaches to electronic friction, to date, unfortunately, there have been very few studies comparing the different formal expressions. Furthermore, there has been no conclusion in the literature as to the differences between these friction tensors. For instance, on the one hand, are there perhaps different forms for electronic friction, just as there are many slightly different master equations<sup>[6,212,241–243,257]</sup>? When studying rate crossings near a metal surface, Hynes *et al* derived a non-Markovian friction tensor and argued that this friction tensor was “quite distinct [from the HGT] Markovian electronic friction, acting on a particle impinging from the gas phase on a metallic surface.”<sup>[213]</sup> Or perhaps, on the other hand, are the different forms for electronic friction just a matter of notation?

In a recent letter, we have argued that there is a unique, universal electronic friction tensor<sup>[212]</sup> that is valid in and out of equilibrium, with or without el-el interactions:

$$\gamma_{\alpha\nu}(\mathbf{R}) = \int_0^\infty dt \operatorname{tr}_e \left( \delta \hat{f}_\alpha(\mathbf{R}) e^{-i\hat{H}(\mathbf{R})t/\hbar} \partial_\nu \hat{\rho}_{ss}(\mathbf{R}) e^{i\hat{H}(\mathbf{R})t/\hbar} \right) \quad (9.1)$$

Here  $\delta \hat{f}_\alpha = -\partial_\alpha \hat{H} + \operatorname{tr}_e(\partial_\alpha \hat{H} \hat{\rho}_{ss})$  is the random force,  $\hat{H}$  is the electronic Hamiltonian, and  $\hat{\rho}_{ss}$  is the steady state electronic density matrix (all parameterized at position  $\mathbf{R}$ ).  $\operatorname{tr}_e$  implies tracing over the many-body electronic eigenstate states. At equilibrium, where  $\hat{\rho}_{ss}$  is a Boltzmann average ( $\hat{\rho}_{ss}(\mathbf{R}) = e^{-\beta \hat{H}(\mathbf{R})}/Z$ ), Ref.<sup>[212]</sup> proves that the friction tensor can be recast into the form of a correlation function of the random force:

$$\gamma_{\alpha\nu} = \frac{\beta}{2} \int_0^\infty dt \operatorname{tr}_e \left( \delta \hat{f}_\alpha e^{-i\hat{H}t/\hbar} (\delta \hat{f}_\nu \hat{\rho}_{ss} + \hat{\rho}_{ss} \delta \hat{f}_\nu) e^{i\hat{H}t/\hbar} \right) \quad (9.2)$$

Eq. 9.2 agrees with the results of Suhl<sup>[232]</sup> and mozyrsky<sup>[233]</sup> and co-workers. Furthermore, without el-el interaction, Ref.<sup>[212]</sup> also demonstrates that Eq. 9.2 can be further reduced to the HGT model (Eq. 9.25).

With this background in mind, in the present article, our goal is to take one more step

forward towards consolidating electronic friction models. In particular, our goal is to prove that the electronic friction as calculated with NEGFs (following von Oppen *et al*<sup>[80]</sup>) is in complete agreement with the HGT model<sup>[82]</sup> *at equilibrium* (which in turn agrees with the universal friction tensor in Ref.<sup>[212]</sup>). Note that we do not consider electron-electron interactions in this paper (because von Oppen’s NEGF treatment assumes independent electrons). While we have previously shown agreement between von Oppen and HGT for a one-level problem<sup>[184]</sup>, our earlier approach was not direct and could not be easily extended to the case of many system (molecular) orbitals with or without non-Condon effects. In the current paper, however, we claim that this agreement can be proven quite generally.

We organize this paper as follows. In Sec. 9.2, using a NEGF approach in order to connect with von Oppen’s formalism, we derive a Langevin equation for a non-interacting electronic system. In Sec. 9.3, we apply our results to a model of a molecule (system) with many orbitals in contact with a bath of metallic electrons at equilibrium. Here, we demonstrate that the NEGF formalism is entirely equivalent to the HGT model, even when we include non-Condon effects, whereby metal-molecule couplings may fluctuate with nuclear motion. In Sec. 9.4, we discuss a key nuance which must be properly addressed when performing an NEGF gradient expansion with non-Condon effects. We conclude in Sec. 9.5.

**Notations:** Below we use a hat to denote electronic operators.  $\alpha$  and  $\nu$  index nuclear degrees of freedom (DoFs) with position and momentum vectors  $\mathbf{R}$  and  $\mathbf{P}$ .  $p$  and  $q$  index electronic orbitals in general.  $m$  and  $n$  index the electronic orbitals in the system (molecule), whereas  $k$  and  $k'$  index the orbitals in the bath (metal).  $\hat{H}$  denotes the electronic Hamiltonian, including the pure nuclear potential  $U_0(\mathbf{R})$ . The total Hamiltonian is represented by  $\hat{H}_{tot}$ , i.e. the electronic Hamiltonian plus the nuclear kinetic energy.

## 9.2. Non-Equilibrium Green's Function

### 9.2.1. Equation of motion

We consider coupled electron-nuclear motion, where the total Hamiltonian  $\hat{H}_{tot}$  can be divided into the electronic Hamiltonian  $\hat{H}$ , and nuclear kinetic energy,

$$\hat{H}_{tot} = \hat{H} + \sum_{\alpha} \frac{P_{\alpha}^2}{2m^{\alpha}} \quad (9.3)$$

The electronic Hamiltonian  $\hat{H}$  consists of a manifold of electrons that is quadratic (in electronic orbitals  $p, q$ ) plus a nuclear potential energy  $U_0(\mathbf{R})$ :

$$\hat{H} = \sum_{pq} \mathcal{H}_{pq}(\mathbf{R}) \hat{d}_p^{\dagger} \hat{d}_q + U_0(\mathbf{R}) \quad (9.4)$$

Without loss of generality, we restrict ourselves to the case of a real-valued  $\mathcal{H}$  matrix below. Here, we re-emphasize that we are treating a non-interacting electronic (or Hartree-Fock or mean-field) Hamiltonian. (For a very general treatment that includes electron-electron interactions, see Ref.<sup>[212]</sup>.)

We consider the classical dynamics of the nuclei, such that the equation of motion (EOM) for the nuclei is given by the Newtonian equation,

$$m^{\alpha} \ddot{R}^{\alpha} = -\partial_{\alpha} \hat{H} = -\partial_{\alpha} U_0 - \sum_{pq} \partial_{\alpha} \mathcal{H}_{pq} \langle \hat{d}_p^{\dagger} \hat{d}_q \rangle + \delta f_{\alpha} \quad (9.5)$$

where we have defined the random force  $\delta f_{\alpha}$

$$\delta f_{\alpha} = - \sum_{pq} \partial_{\alpha} \mathcal{H}_{pq} \left( \hat{d}_p^{\dagger} \hat{d}_q - \langle \hat{d}_p^{\dagger} \hat{d}_q \rangle \right) \quad (9.6)$$

Our goal is to transform Eq. 9.5 into a Langevin equation. To achieve this purpose, we

define the lesser and retarded Green's functions (GFs) respectively,

$$\tilde{G}_{qp}^<(t_1, t_2) = \frac{i}{\hbar} \langle \hat{d}_p^\dagger(t_2) \hat{d}_q(t_1) \rangle_{\mathbf{R}(t_1)} \quad (9.7)$$

$$\tilde{G}_{qp}^R(t_1, t_2) = -\frac{i}{\hbar} \theta(t_1 - t_2) \langle \{ \hat{d}_q(t_1), \hat{d}_p^\dagger(t_2) \} \rangle_{\mathbf{R}(t_1)} \quad (9.8)$$

Since the electronic Hamiltonian  $\hat{H}$  is quadratic, and the nuclei are prescribed by  $\mathbf{R}(t_1)$  and not  $\mathbf{R}(t_2)$ , the equation of motion (EOM) for  $\tilde{G}^R$  is given by

$$-i\hbar\partial_{t_2}\tilde{G}^R(t_1, t_2) = \delta(t_1 - t_2) + \tilde{G}^R(t_1, t_2)\mathcal{H}. \quad (9.9)$$

### 9.2.2. Gradient Expansion: mean force and friction

To proceed, it will be convenient to work in the Wigner representation, where the Wigner transformation is defined as,

$$\tilde{G}^R(t, \epsilon) = \int d\tau e^{i\epsilon\tau/\hbar} \tilde{G}^R(t + \tau/2, t - \tau/2). \quad (9.10)$$

For a convolution,  $D(t_1, t_2) = \int dt_3 B(t_1, t_3)C(t_3, t_2)$ , the Wigner transformation can be expressed with a ‘‘Moyal operator’’ as:

$$\begin{aligned} D^W(t, \epsilon) &= \exp \left[ \frac{i\hbar}{2} (\partial_\epsilon^A \partial_t^B - \partial_\epsilon^B \partial_t^A) \right] B^W C^W \\ &\approx B^W C^W + \frac{i\hbar}{2} \partial_\epsilon B^W \partial_t C^W - \frac{i\hbar}{2} \partial_\epsilon C^W \partial_t B^W. \end{aligned} \quad (9.11)$$

The approximation made in the above equation is known as a gradient expansion in some fields of physics (and an  $\hbar$  expansion in others).

After applying the Wigner transform and the gradient expansion to the EOM of  $\tilde{G}^R(t_1, t_2)$  (Eq. 9.9), we find

$$\tilde{G}^R_\epsilon - \tilde{G}^R\mathcal{H} = 1 + \frac{i\hbar}{2} \partial_\epsilon \tilde{G}^R \partial_t \mathcal{H} + \frac{i\hbar}{2} \partial_t \tilde{G}^R. \quad (9.12)$$

At this point, we note that we are looking for a general friction tensor, i.e. a tensor that multiplies the velocity  $\dot{\mathbf{R}}$ . Because we will eventually replace  $\partial_t = \sum_\nu \dot{R}^\nu \partial_\nu$ , it is clear that, for all terms where there is already one factor of  $\partial_t$ , we may safely replace  $\tilde{G}^R$  with the frozen  $G^R$ . We define the frozen GF,

$$G^R(\mathbf{R}, \epsilon) = (\epsilon - \mathcal{H}(\mathbf{R}) + i\eta)^{-1} \quad (9.13)$$

Here  $G^R$  represents the responses of an electron achieving instantaneous equilibration with the electronic Hamiltonian  $\mathcal{H}$  (which will eventually be modulated by some nuclear motion). Substitution of the frozen Green's function for the full Green's function leads to

$$\tilde{G}^R(G^R)^{-1} \approx 1 + \frac{i\hbar}{2} \partial_\epsilon G^R \partial_t \mathcal{H} + \frac{i\hbar}{2} \partial_t G^R. \quad (9.14)$$

Note that  $\partial_\epsilon G^R = -G^R G^R$ ,  $\partial_t G^R = G^R \partial_t \mathcal{H} G^R$ , as well as  $\partial_t \mathcal{H} = \sum_\nu \dot{R}^\nu \partial_\nu \mathcal{H}$ . Therefore, Eq. 9.14 can be solved as

$$\tilde{G}^R \approx G^R + \frac{i\hbar}{2} \sum_\nu \dot{R}^\nu (\partial_\epsilon G^R \partial_\nu \mathcal{H} G^R - G^R \partial_\nu \mathcal{H} \partial_\epsilon G^R) \quad (9.15)$$

At this point, we have a straightforward adiabatic first order correction to the frozen retarded GF. This correction can be transformed back into the time domain as follows:

$$\begin{aligned} \tilde{G}^R(t_1, t_2) &\approx G^R(t_1, t_2) \\ &+ \frac{i\hbar}{2} \sum_\nu \dot{R}^\nu \int dt_3 \partial_\epsilon G^R(t_1, t_3) \partial_\nu \mathcal{H} G^R(t_3, t_2) \\ &- \frac{i\hbar}{2} \sum_\nu \dot{R}^\nu \int dt_3 G^R(t_1, t_3) \partial_\nu \mathcal{H} \partial_\epsilon G^R(t_3, t_2) \end{aligned} \quad (9.16)$$

Here we have used the backwards Wigner transformation. For instance,  $\partial_\epsilon G^R(t_1, t_2)$  is defined as

$$\partial_\epsilon G^R(t_1, t_2) \equiv \int \frac{d\epsilon}{2\pi\hbar} e^{-i\epsilon(t_1-t_2)/\hbar} \partial_\epsilon G^R\left(\frac{t_1+t_2}{2}, \epsilon\right) \quad (9.17)$$

Note that the correction of the full Green's function takes the form of a time convolution in real time. If this convolution is extended to a convolution on the Keldysh contour, we may now reproject onto the real time domain for the lesser GF. Using the standard projection rules for NEGF<sup>[258]</sup>, we find

$$\begin{aligned}
\tilde{G}^<(t_1, t_2) &\approx G^<(t_1, t_2) \\
&+ \frac{i\hbar}{2} \sum_{\nu} \dot{R}^{\nu} \int dt_3 \partial_{\epsilon} G^<(t_1, t_3) \partial_{\nu} \mathcal{H} G^A(t_3, t_2) \\
&+ \frac{i\hbar}{2} \sum_{\nu} \dot{R}^{\nu} \int dt_3 \partial_{\epsilon} G^R(t_1, t_3) \partial_{\nu} \mathcal{H} G^<(t_3, t_2) \\
&- \frac{i\hbar}{2} \sum_{\nu} \dot{R}^{\nu} \int dt_3 G^<(t_1, t_3) \partial_{\nu} \mathcal{H} \partial_{\epsilon} G^A(t_3, t_2) \\
&- \frac{i\hbar}{2} \sum_{\nu} \dot{R}^{\nu} \int dt_3 G^R(t_1, t_3) \partial_{\nu} \mathcal{H} \partial_{\epsilon} G^<(t_3, t_2)
\end{aligned} \tag{9.18}$$

Finally, if we again perform a Wigner transformation, we recover,

$$\tilde{G}^< \approx G^< + \frac{i\hbar}{2} \sum_{\nu} \dot{R}^{\nu} (\partial_{\epsilon} G^< \partial_{\nu} \mathcal{H} G^A - G^R \partial_{\nu} \mathcal{H} \partial_{\epsilon} G^< + \partial_{\epsilon} G^R \partial_{\nu} \mathcal{H} G^< - G^< \partial_{\nu} \mathcal{H} \partial_{\epsilon} G^A) \tag{9.19}$$

Using Eq. 9.5, we can now identify the correct friction coefficient

$$\gamma_{\alpha\nu} = \hbar \int \frac{d\epsilon}{2\pi} \text{tr}(\partial_{\alpha} \mathcal{H} \partial_{\epsilon} G^< \partial_{\nu} \mathcal{H} G^A - \partial_{\alpha} \mathcal{H} G^R \partial_{\nu} \mathcal{H} \partial_{\epsilon} G^<) \tag{9.20}$$

as well as a mean force,

$$F_{\alpha} = i \int \frac{d\epsilon}{2\pi} \text{tr}(\partial_{\alpha} \mathcal{H} G^<) \tag{9.21}$$

Thus, we have derived several terms in the desired Langevin equation,

$$m^{\alpha} \ddot{R}^{\alpha} = -\partial_{\alpha} U_0 + F_{\alpha} - \sum_{\nu} \gamma_{\alpha\nu} \dot{R}^{\nu} + \delta f_{\alpha} \tag{9.22}$$

### 9.2.3. Equilibrium

Eq. 9.20 is a general form for friction valid in or out of equilibrium. At equilibrium, this expression can be simplified further using the following relationships:

$$G^< = i2\pi\mathcal{P}f \quad (9.23)$$

$$\mathcal{P} = -\frac{1}{\pi}\text{Im}G^R = \delta(\epsilon - \mathcal{H}) \quad (9.24)$$

Here  $f$  is the Fermi function,  $f(\epsilon) = (e^{\beta\epsilon} + 1)^{-1}$  ( $1/\beta \equiv k_B T$ ). We also have the universal relationship,  $G^A = (G^R)^\dagger$ . Using these relationships and integration by parts, Eq. 9.20 can be further rewritten as:

$$\gamma_{\alpha\nu} = -\pi\hbar \int d\epsilon \text{tr}(\partial_\alpha \mathcal{H} \mathcal{P} \partial_\nu \mathcal{H} \mathcal{P}) \partial_\epsilon f \quad (9.25)$$

The exact form of Eq. 9.25 was not derived by von Oppen *et al*, but this result does agree with the HGT model.<sup>[82]</sup> Similarly, the mean force at equilibrium reads:

$$F_\alpha = - \int d\epsilon \text{tr}(\partial_\alpha \mathcal{H} \mathcal{P}) f \quad (9.26)$$

To make the Langevin equation (Eq. 9.22) closed, we must now evaluate the correlation function of the random force  $\delta\hat{f}_\alpha$ .

### 9.2.4. Correlation of the Random Force

We now evaluate the correlation of the random force. While Ref.<sup>[212]</sup> provides a complete non-Markovian correlation function, here we consider only the Markovian correlation function:

$$\langle \delta\hat{f}_\alpha(t) \delta\hat{f}_\nu(t') \rangle = D_{\alpha\nu} \delta(t - t') \quad (9.27)$$

This Markovian assumption is consistent with an adiabatic approximation (where electrons move much faster than nuclei).

Since the electronic Hamiltonian  $\hat{H}$  is quadratic, Wick's theorem can be applied,

$$\langle \delta \hat{f}_\alpha(t) \delta \hat{f}_\nu(t') \rangle = \hbar^2 \sum_{p'q'pq} \partial_\alpha \mathcal{H}_{p'q'} \tilde{G}_{q'p}^>(t, t') \partial_\nu \mathcal{H}_{pq} \tilde{G}_{qp'}^<(t', t), \quad (9.28)$$

In the limit of fast electronic motion and relaxation, we replace the adiabatic GF ( $\tilde{G}$ ) by the corresponding frozen GF ( $G$ ), such that

$$\begin{aligned} D_{\alpha\nu} &= \hbar^2 \int d\tau \text{tr}(\partial_\alpha \mathcal{H} G^>(\tau) \partial_\nu \mathcal{H} G^<(-\tau)) \\ &= \hbar \int \frac{d\epsilon}{2\pi} \text{tr}(\partial_\alpha \mathcal{H} G^>(\epsilon) \partial_\nu \mathcal{H} G^<(\epsilon)) \end{aligned} \quad (9.29)$$

Eq. 9.29 is valid in or out of equilibrium. At equilibrium, similar to Eq. 9.23, we have

$$G^> = -i2\pi(1-f)\mathcal{P} \quad (9.30)$$

Now the correlation function of the random force reads

$$D_{\alpha\nu} = 2\pi\hbar \int d\epsilon \text{tr}(\partial_\alpha \mathcal{H} P \partial_\nu \mathcal{H} P) f(1-f). \quad (9.31)$$

If we compare Eq. 9.31 with the friction in Eq. 9.25, and note that, at equilibrium  $\partial_\epsilon f = -\beta f(1-f)$ , we see that the second fluctuation-dissipation theorem is satisfied ( $D_{\alpha\nu} = 2k_B T \gamma_{\alpha\nu}$ ) at equilibrium. Therefore, after equilibration, the nuclei will always reach the same temperature as the (electronic) metal surface.

### 9.3. A model with system-bath separation

Eq. 9.25 and Eq. 9.31 are very general expressions which make no distinction between a system and bath, and thus might appear nonintuitive. To connect with more traditional

views of electronic friction, as in Ref. [80], we now separate the total system into a molecule with orbitals (index  $m$  and  $n$ ), and a metal with a manifold of electronic orbitals (index  $k$ ). The system-bath (molecule-metal) coupling is taken to be linear:

$$\hat{H} = \hat{H}_s + \hat{H}_b + \hat{H}_c, \quad (9.32)$$

$$\hat{H}_s = \sum_{mn} h_{mn}(\mathbf{R}) \hat{b}_m^\dagger \hat{b}_n + U_0(\mathbf{R}), \quad (9.33)$$

$$\hat{H}_b = \sum_k \epsilon_k \hat{c}_k^\dagger \hat{c}_k, \quad (9.34)$$

$$\hat{H}_c = \sum_{km} V_{km}(\mathbf{R}) (\hat{b}_m^\dagger \hat{c}_k + \hat{c}_k^\dagger \hat{b}_m). \quad (9.35)$$

Notice that, aside from the bare nuclear potential  $U_0(\mathbf{R})$ , the energy of the system  $h_{mn}(\mathbf{R})$  and the system-bath coupling  $V_{km}(\mathbf{R})$  also depend on nuclear position  $\mathbf{R}$ .

Now, because all of the electronic terms are quadratic, we can apply Eq. 9.25 to evaluate

$$tr(\partial_\alpha \mathcal{H} \mathcal{P} \partial_\beta \mathcal{H} \mathcal{P}) \quad (9.36)$$

$$= \frac{1}{\pi^2} \sum_{mnm'n'} \partial_\alpha h_{mn} \text{Im} G_{nn'}^R \partial_\nu h_{n'm'} \text{Im} G_{m'm}^R \quad (9.37)$$

$$+ \frac{2}{\pi^2} \sum_{mnkm'} \partial_\alpha h_{mn} \text{Im} G_{nk}^R \partial_\nu V_{km'} \text{Im} G_{m'm}^R \quad (9.38)$$

$$+ \frac{2}{\pi^2} \sum_{mknm'} \partial_\alpha V_{km} \text{Im} G_{mn}^R \partial_\nu h_{nm'} \text{Im} G_{m'k}^R \quad (9.39)$$

$$+ \frac{2}{\pi^2} \sum_{mnkk'} \partial_\alpha V_{km} \text{Im} G_{mk'}^R \partial_\nu V_{k'n} \text{Im} G_{nk}^R \quad (9.40)$$

$$+ \frac{2}{\pi^2} \sum_{mnkk'} \partial_\alpha V_{km} \text{Im} G_{mn}^R \partial_\nu V_{nk'} \text{Im} G_{k'k}^R \quad (9.41)$$

Here, we have used the imaginary part of the retarded frozen GF to replace  $\mathcal{P}$ , since  $\mathcal{P}(\epsilon) = -\frac{1}{\pi} \text{Im} G^R(\epsilon)$ .

To proceed, for the non-interacting electrons, the following relationship can be applied

(because of the Dyson equation)

$$G_{nk}^R = \sum_{n'} G_{nn'}^R V_{n'k} g_k^R \quad (9.42)$$

$g_k^R$  is the retarded GF for the electron in the metal

$$g_k^R = (\epsilon - \epsilon_k + i\eta)^{-1} \quad (9.43)$$

so that

$$\text{Im} \sum_k G_{nk}^R \partial_\alpha V_{km'} = \text{Im} \sum_{kn'} G_{nn'}^R V_{n'k} g_k^R \partial_\alpha V_{km'} \quad (9.44)$$

We denote

$$2 \sum_k V_{n'k} g_k^R \partial_\alpha V_{km'} = \bar{\Sigma}_{n'm'}^\alpha \quad (9.45)$$

For  $G_{k'k}^R$ , again from the Dyson equation,

$$G_{k'k}^R = g_k^R \delta_{k'k} + \sum_{m'n'} g_{k'}^R V_{k'm'} G_{m'n'}^R V_{n'k} g_k^R \quad (9.46)$$

We denote,

$$\sum_k \partial_\nu V_{nk} g_k^R \partial_\alpha V_{km} = \frac{1}{4} \bar{\Sigma}_{nm}^{\nu,\alpha} \quad (9.47)$$

From Eq. 9.45 and Eq. 9.47, we now have,

$$\text{Im} \sum_{kk'} \partial_\nu V_{nk'} G_{k'k}^R \partial_\alpha V_{km} = \frac{1}{4} \text{Im} \bar{\Sigma}_{nm}^{\nu,\alpha} + \frac{1}{4} \text{Im} ((\bar{\Sigma}^\nu)^T G_s^R \bar{\Sigma}^\alpha)_{nm} \quad (9.48)$$

Thus, we find

$$\begin{aligned}
& tr(\partial_\alpha \mathcal{H} \mathcal{P} \partial_\beta \mathcal{H} \mathcal{P}) \\
&= \frac{1}{\pi^2} tr_s \left( (\text{Im} G_s^R \partial_\alpha h + \text{Im}(G_s^R \bar{\Sigma}^\alpha)) (\text{Im} G_s^R \partial_\nu h + \text{Im}(G_s^R \bar{\Sigma}^\nu)) \right) \\
&+ \frac{1}{2\pi^2} tr_s (\text{Im} G_s^R \text{Im} \bar{\Sigma}^{\nu, \alpha} + \text{Im} G_s^R \text{Im}((\bar{\Sigma}^\nu)^T G_s^R \bar{\Sigma}^\alpha) - \text{Im}(G_s^R \bar{\Sigma}^\alpha) \text{Im}(G_s^R \bar{\Sigma}^\nu)) \quad (9.49)
\end{aligned}$$

Here the trace  $tr_s$  implies a summation over only the system orbitals (m, n), and  $G_s^R$  is the retarded GF for the system,

$$G_s^R = (\epsilon - h - \Sigma)^{-1} \quad (9.50)$$

$$\Sigma_{mn} = \sum_k V_{mk} g_k^R V_{kn} \quad (9.51)$$

We note that, from the definitions in Eq. 9.45 and Eq. 9.51,  $\partial_\alpha \Sigma_{mn} = \frac{1}{2}(\bar{\Sigma}_{mn}^\alpha + \bar{\Sigma}_{nm}^\alpha)$ . The final friction is then

$$\begin{aligned}
\gamma_{\alpha\nu} &= -\hbar \int \frac{d\epsilon}{\pi} tr_s \left( (\text{Im} G_s^R \partial_\alpha h + \text{Im}(G_s^R \bar{\Sigma}^\alpha)) (\text{Im} G_s^R \partial_\nu h + \text{Im}(G_s^R \bar{\Sigma}^\nu)) \right) \partial_\epsilon f \\
&- \hbar \int \frac{d\epsilon}{2\pi} tr_s (\text{Im} G_s^R \text{Im} \bar{\Sigma}^{\nu, \alpha} + \text{Im} G_s^R \text{Im}((\bar{\Sigma}^\nu)^T G_s^R \bar{\Sigma}^\alpha) - \text{Im}(G_s^R \bar{\Sigma}^\alpha) \text{Im}(G_s^R \bar{\Sigma}^\nu)) \partial_\epsilon f \quad (9.52)
\end{aligned}$$

For the case that  $\partial_\alpha V_{km} = 0$  (which is known as the Condon approximation), Eq. 9.52 was derived previously by von Oppen *et al.* Here, however, we have shown that the von Oppen friction results are identical to the HGT friction results (Eq. 9.25). Furthermore, in the present manuscript, we have now extended von Oppen's results to account for non-Condon effects, i.e. the fact that  $V_{km}$  should generally depend on  $\mathbf{R}$ .

### 9.3.1. Wide-band limit

To better understand the implication of the non-Condon effects, we note that in the literature the wide-band approximation is often used, such that the following purely imaginary

quantities can be defined,

$$\sum_k V_{n'k} g_k^R V_{km'} = -i\Gamma_{n'm'}/2 \quad (9.53)$$

$$2 \sum_k V_{n'k} g_k^R \partial_\alpha V_{km'} = -i\bar{\Gamma}_{n'm'}^\alpha/2 \quad (9.54)$$

Here  $\Gamma_{mm}$  is the lifetime or hybridization of molecular orbital  $m$  on the metal surface. By definition, we have  $\partial_\alpha \Gamma_{mn} = \frac{1}{2}(\bar{\Gamma}_{nm}^\alpha + \bar{\Gamma}_{mn}^\alpha)$ , and  $G_s^R = (\epsilon - h + i\Gamma/2)^{-1}$ .

If we further assume that  $V_{km}$  does not depend on  $k$  ( $V_{km} = V_m$ ), the last term of the friction (Eq. 9.52) vanishes (see the Supplemental Material of Ref. [230]). Thus, the friction becomes:

$$\gamma_{\alpha\nu} = -\hbar \int \frac{d\epsilon}{\pi} \text{tr}_s \left( (\text{Im} G_s^R \partial_\alpha h - \frac{1}{2} \text{Re} G_s^R \bar{\Gamma}^\alpha) (\text{Im} G_s^R \partial_\nu h - \frac{1}{2} \text{Re} G_s^R \bar{\Gamma}^\nu) \right) \partial_\epsilon f \quad (9.55)$$

Thus, we see that non-Condon effects restructure the wide-band approximation so that the electronic friction will now depend on both the imaginary and real parts of the system Green's function. In general, non-Condon effects can increase or decrease friction, depending on the relative signs of the two components in Eq. 9.55.

#### 9.4. Discussion

The results above are fairly straightforward. We have shown (i) that an NEGF formalism recovers the exact same electronic friction as the Head-Gordon/Tully approach; this agreement confirms our earlier claim<sup>[212]</sup> there is only a single, universal electronic friction tensor that is relevant to semi-classical dynamics. We have also shown (ii) that non-Condon effects can be incorporated into the relevant electronic friction. In a previous paper, with only a single electronic orbital, we demonstrated that non-Condon contributions to the electronic friction can sometimes be significant<sup>[184]</sup>.

At this point, before concluding, there is one key feature that ought to be addressed regarding formalisms. In the present article, our approach was to (i) perform a gradient

expansion of the full Green’s function (Sec. 9.2), and then (ii) project the full GF onto the system and system-bath coupling to learn about molecular motion on a surface. Through this procedure, we arrived at the relevant friction coefficient (Sec. 9.3) which satisfies the second fluctuation-dissipation theorem. Now, while the formalism just described might seem obvious enough, we must emphasize that the steps taken above are not standard at all. By contrast, the more typical approach would be the opposite: (i) first focus on the system coordinates and (ii) second apply a gradient expansion in the smaller space of (system) nuclear motion. For instance, in Ref.<sup>[80]</sup>, von Oppen *et al* take the latter (not former) approach.

In our experience, we have found that these two approaches usually agree, but can disagree when non-Condon effects are present. Here, there are two data points worth mentioning. First, in Ref.<sup>[184]</sup>, for the case of one system molecular orbital with non-Condon effects, we have previously performed a gradient expansion separately for the system and system-bath coupling GFs. In such a case, the resulting friction does agree with HGT model. However, second, although we do not reproduce the derivation here, for the case of multiple system orbitals in contact with a metal with non-Condon effects, one finds that the two approaches above do *not* agree. Instead, if one invokes a naive gradient expansion which separates the system and system-bath GFs, one will recover a different friction tensor that is clearly incorrect. This incorrect friction tensor does not agree with the HGT method and does not satisfy the second fluctuation-dissipation theorem. Furthermore, this incorrect friction tensor is not symmetric along nuclear DoFs at equilibrium (whereas the correct friction tensor in this manuscript [ Eq. 9.25 or Eq. 9.55] is symmetric). Hence, by studying non-Condon effects, the present manuscript has clearly discerned how to perform a proper gradient expansion when system-bath couplings become complicated and position-dependent.

## 9.5. Conclusions

In conclusion, we have extended the non-equilibrium Green Function (NEGF) approach to deal with a very general Hamiltonian with many molecular orbitals sitting near a metal sur-

face. We have derived a general form of electronic friction as felt by the system nuclei, and we have included the effects of non-Condon terms in the Hamiltonian. At equilibrium, we have shown the equivalence between a NEGF approach and the Head-Gordon/Tully (HGT) model, providing strong evidence to back up our recent claim of a single, universal friction tensor arising from the Born-Oppenheimer approach<sup>[212]</sup>. Future work will necessarily investigate the connection between Ref.<sup>[212]</sup>, the HGT model and the NEGF formalism under out of equilibrium conditions, i.e. for a molecule sitting between two leads with a current running through it.

## CHAPTER 10 : The universality of electronic friction II: Equivalence of the quantum-classical Liouville equation approach with von Oppen’s nonequilibrium Green’s function methods out of equilibrium

This chapter was adapted from Ref. [259]

### 10.1. Introduction

The dynamics of molecules at molecule-metal interfaces often go beyond the Born-Oppenheimer approximation, where the interplay of electron and nuclei can give rise to a host of nonadiabatic effects.<sup>[1,12,125,169,182,192,214,215,251,253,256,260–264]</sup> These nonadiabatic effects can be seen in many systems. For the case of a single metal surface at equilibrium, a simple scattering process can reveal unexpected vibrational or translational kinetic energy losses for the molecule due to electronic excitations in the metal as induced by nuclear movement.<sup>[24,26,72,250,250]</sup> For the case of two or more metal surfaces out of equilibrium, e.g., a molecular junction, under an applied voltage bias with an electronic current running through the molecule, non-Born-Oppenheimer forces can result in heating,<sup>[30,86,141,173]</sup> photo (or current) induced chemistry,<sup>[159,265–267]</sup> Franck-Condon blockades,<sup>[27,29,138]</sup> switching,<sup>[79,126,139,152,194]</sup> instability,<sup>[31–33]</sup> or pumping of the molecule.<sup>[80,268,269]</sup>

Over the past several decades, in order to describe such nonadiabatic effects at molecule-metal interface, many researchers have adopted the idea of “electronic friction”, such that the nuclei move on a single potential of mean force, while experiencing a frictional force and a random force induced by electronic motion.<sup>[6,82,226]</sup> In the literature, quite a few forms of electronic friction have been derived, using a variety of methodologies,<sup>[81,115,185]</sup> with or without electron-electron (el-el) interactions,<sup>[9,212,232]</sup> including or not including non-Condon effects,<sup>[81,184,228,229]</sup> invoking a Markovian or non-Markovian frictional kernel,<sup>[212,213,217,224]</sup> and addressing equilibrium or nonequilibrium scenarios (or both).<sup>[80,116,212,233]</sup> Electronic friction has been widely and successfully used to treat vibrational relaxation, chemisorption, and photo induced reaction *et al* at molecule-metal interfaces.<sup>[8,219,222,251,270]</sup>

Now, in the equilibrium scenario, probably the most commonly used electronic friction was given by Head-Gordon and Tully (HGT) in 1995.<sup>[82]</sup> Starting from Ehrenfest dynamics, the HGT friction was derived at zero temperature assuming no el-el interactions, and later extended to finite temperature by ansatz.<sup>[8,114]</sup> At finite temperature, the second fluctuation-dissipation theorem was assumed rather than derived, i.e. a fluctuating force was added by hand to guarantee the nuclear degrees of freedom (DoFs) reach the same temperature with the electronic temperature. Besides Head-Gordon and Tully, many other researchers have also derived similar electronic friction tensors, including, for example, Suhl (Eq. 27 in Ref. [232]), Galperin (Eq. 17 in Ref. [229]), Brandbyge (Eq. A49 in Ref. [81]), Persson (Eq. 32 in Ref. [228]), and Hynes (non-Markovian kernel, Eq. 3.18 in Ref. [213]). Of the list above, perhaps the most important contributions have been from Suhl (who first extrapolated that electronic friction should look like a force-force correlation function).<sup>[232]</sup> A further advance was made by Daligault and mozyrsky who derived the random force for the HGT model at equilibrium for finite temperature.<sup>[233]</sup>

As far as the nonequilibrium scenario is concerned, the situation becomes more complicated and there has been far less development. To our knowledge, the most general nonequilibrium, Markovian electronic friction tensor was given by von Oppen and coworkers, using a nonequilibrium Green's function (NEGF) and a scattering matrix formalism.<sup>[80]</sup> Quite different from the equilibrium case, where the electronic friction is a simple damping force, i.e. positive definite and symmetric along nuclear DoFs, the *nonequilibrium* electronic friction is no longer symmetric, and can be even negative. Furthermore, the second fluctuation-dissipation theorem breaks down, where the electronic current leads to the heating or pumping of the molecule. The von Oppen result should hold for small nuclear velocities assuming that there are no el-el interactions and that there are no non-Condon effects.

At this point in time, given the plethora of different results discussed above, one of our ongoing research goals has been to compare and connect different approaches for electronic friction and ascertain whether an unifying form exists. And in fact, recently, in Ref. [212],

we successfully derived a universal electronic friction from a quantum-classical Liouville equation (QCLE), that should be valid in and out of equilibrium, with or without el-el interactions:

$$\gamma_{\mu\nu}(\mathbf{R}) = - \int_0^\infty dt \operatorname{tr}_e \left( \partial_\mu \hat{H}(\mathbf{R}) e^{-i\hat{H}(\mathbf{R})t/\hbar} \partial_\nu \hat{\rho}_{ss}(\mathbf{R}) e^{i\hat{H}(\mathbf{R})t/\hbar} \right), \quad (10.1)$$

where  $\mu$  and  $\nu$  are nuclear DoFs, and  $\hat{H}(\mathbf{R})$  is the electronic Hamiltonian,  $\hat{\rho}_{ss}(\mathbf{R})$  is the steady states electronic density matrix.  $\operatorname{tr}_e$  implies tracing over many-body electronic states. Thus far, we have shown (i) that Eq. 10.1 reduces to Suhl’s results as well as the HGT model at equilibrium (without el-el interactions). Furthermore (ii), Ref. [184] shows that, at equilibrium, the HGT model is comparable with the results of Brandbyge and Galperin. Moreover (iii), Ref. [230] demonstrates that the generalized NEGF electronic friction agrees with HGT model at equilibrium. Thus, altogether, we have been able to connect the QCLE, NEGF, and HGT friction at equilibrium. Finally, we have also shown that the non-Markovian friction suggested by Hynes has a natural QCLE expression.<sup>[212,213]</sup>

In all of the comparative work above, however, one essential element has been missing. While we have proven that all of the Markovian results of mozyrsky, Suhl, Persson, Galperin, Hynes, Brandbyge, HGT, and von Oppen reduce to Eq. 10.1 at equilibrium, no further consideration has yet been established for the out of equilibrium scenario. Thus, in this article, we will take one step further, and prove that, without el-el interactions, indeed the QCLE friction (Eq. 10.1) reduces to von Oppen’s generalized NEGF friction in case of two metals *out of equilibrium*. This agreement greatly strengthens our claim that there is only one, unique electronic friction associated with the Born-Oppenheimer approximation. In what follows, we will also provide an explicit, very general formula for calculating that friction tensor in the limit of no el-el interactions; our work will include non-Condon effects and thus go beyond von Oppen’s results.

We organize the structure of the paper as follows. In Sec. 10.2, we explain our model and provide important relationships that will be used later on. In Sec. 10.3, we demonstrate the

agreement between QCLE friction and NEGF friction. In Sec. 10.4, we adopt the commonly used molecule-metal Hamiltonian and evaluate the nonequilibrium electronic friction tensor while accounting for non-Condon effects. We conclude in Sec. 10.5.

Regarding the notation, we use  $p$  and  $q$  to denote electronic orbitals in general,  $m$  and  $n$  for the electronic orbitals in a molecule (dots), and  $k$  and  $k'$  for the electronic orbitals in a metal (lead). We further use  $\alpha = L, R$  to signify the left or right metal.  $\mathcal{G}$  will denote the total system (dots plus leads) steady-state non-equilibrium Green's functions, and  $G$  will denote the dots' (i.e. molecules') steady-state non-equilibrium Green's functions. We use  $\mu$  (or  $\nu$ ) to denote nuclear degrees of freedom (DoFs), and we use  $\mu_L$  (and  $\mu_R$ ) to denote the Fermi level of the left (and right) metal.

## 10.2. Quadratic Hamiltonian

We consider a total Hamiltonian  $\hat{H}_{tot}$  which can be divided into an electronic Hamiltonian  $\hat{H}$  and a nuclear kinetic energy operator:

$$\hat{H}_{tot} = \hat{H} + \sum_{\mu} \frac{P_{\mu}^2}{2m^{\mu}}. \quad (10.2)$$

The electronic Hamiltonian  $\hat{H}$  consists of a manifold of electrons that is quadratic (in electronic orbitals  $p, q$ ) plus a pure nuclear potential energy  $U_0(\mathbf{R})$ :

$$\hat{H} = \sum_{pq} \mathcal{H}_{pq}(\mathbf{R}) \hat{d}_p^{\dagger} \hat{d}_q + U_0(\mathbf{R}). \quad (10.3)$$

For such an electronic Hamiltonian (Eq. 10.3, without el-el interaction), the general form of the electronic friction (Eq. 10.1) can be recast into the single particle basis (as shown in Appendix 10.6.1),

$$\gamma_{\mu\nu} = -\hbar \int \frac{d\epsilon}{2\pi} Tr_m (\partial_{\mu} \mathcal{H} \mathcal{G}^R(\epsilon) \partial_{\nu} \sigma_{ss} \mathcal{G}^A(\epsilon)). \quad (10.4)$$

Here

$$\mathcal{G}^{R/A}(\epsilon) = \frac{1}{\epsilon - \mathcal{H} \pm i\eta} \quad (10.5)$$

are retarded and advanced Green's function of the electrons respectively ( $\eta$  is an positive infinitesimal). Thus, for the NEGFs, one can easily establish the following identities,

$$\partial_\nu \mathcal{G}^R(\epsilon') = \mathcal{G}^R(\epsilon') \partial_\nu \mathcal{H} \mathcal{G}^R(\epsilon'), \quad \partial_{\epsilon'} \mathcal{G}^R(\epsilon') = -\mathcal{G}^R(\epsilon') \mathcal{G}^R(\epsilon'), \quad (10.6)$$

$$\partial_\nu \mathcal{G}^A(\epsilon') = \mathcal{G}^A(\epsilon') \partial_\nu \mathcal{H} \mathcal{G}^A(\epsilon'), \quad \partial_{\epsilon'} \mathcal{G}^A(\epsilon') = -\mathcal{G}^A(\epsilon') \mathcal{G}^A(\epsilon'). \quad (10.7)$$

Besides the retarded and advanced GFs, we also find in Eq. 10.4 the steady-state electronic population matrix  $\sigma_{qp}^{ss} = tr_e(\hat{\rho}_{ss} \hat{d}_p^\dagger \hat{d}_q)$ .  $\sigma_{ss}$  is usually expressed in terms of the lesser NEGF  $\mathcal{G}^<$ ,

$$\sigma_{ss} = \int \frac{d\epsilon'}{2\pi i} \mathcal{G}^<(\epsilon'), \quad (10.8)$$

where  $\mathcal{G}^<(\epsilon')$  is the Fourier transform of  $\mathcal{G}^<(t_1, t_2)$ . In turn, the lesser nonequilibrium Green's function (NEGF)  $\mathcal{G}^<(t_1, t_2)$  is defined as

$$\mathcal{G}_{qp}^<(t_1, t_2) = \frac{i}{\hbar} tr_e(\hat{\rho}_{ss} \hat{d}_p^\dagger(t_2) \hat{d}_q(t_1)), \quad (10.9)$$

where the electronic operators are written in the Heisenberg picture  $\hat{d}_p^\dagger(t) \equiv e^{i\hat{H}t/\hbar} \hat{d}_p^\dagger e^{-i\hat{H}t/\hbar}$  (and  $\hat{d}_q(t) \equiv e^{i\hat{H}t/\hbar} \hat{d}_q e^{-i\hat{H}t/\hbar}$ ). Note that, in the single particle basis,  $Tr_m$  implies summing over the electronic orbitals ( $p$  and  $q$ ); vice versa, in the many-particle basis,  $tr_e$  implies a trace of all many-body electronic states.

In order to evaluate  $\sigma_{ss}$  in Eq. 10.8, we must first evaluate the lesser NEGF  $\mathcal{G}^<$  and the derivative  $\partial_\nu \mathcal{G}^<$ . To do so, we invoke the Keldysh equation,

$$\mathcal{G}^<(\epsilon') = \mathcal{G}^R(\epsilon') \Pi^< \mathcal{G}^A(\epsilon'), \quad (10.10)$$

where  $\Pi^<$  is the total electronic lesser self-energy.

Below we will adopt a dot-lead (system-bath) separation (Eqs. 10.21-10.24), such that  $\Pi^<$  can be written explicitly (Eq. 10.52 in Appendix 10.6.2). That being said, we emphasize that all of the results below do not depend on the exact value of  $\Pi^<$ . We require only that  $\Pi^<$  does not depend on energy ( $\epsilon'$ ) or position ( $\mathbf{R}$ ). As outlined in Eq. 10.52, these assumptions about  $\Pi^<$  follow because the bath Hamiltonian does not depend on  $\mathbf{R}$ .

Since  $\Pi^<$  does not depend on position ( $\mathbf{R}$ ), together with the Keldysh equation (Eq. 10.10) and the identities in Eqs. 10.6-10.7, it is straightforward to show that

$$\begin{aligned}\partial_\nu \mathcal{G}^< &= \mathcal{G}^R \partial_\nu \mathcal{H} \mathcal{G}^R \Pi^< \mathcal{G}^A + \mathcal{G}^R \Pi^< \mathcal{G}^A \partial_\nu \mathcal{H} \mathcal{G}^A \\ &= \mathcal{G}^R \partial_\nu \mathcal{H} \mathcal{G}^< + \mathcal{G}^< \partial_\nu \mathcal{H} \mathcal{G}^A.\end{aligned}\quad (10.11)$$

With the above identities (Eqs. 10.10-10.11), below we will show that Eq. 10.4 reduces to the following NEGF result (derived in Ref. [230]),

$$\gamma_{\mu\nu} = \hbar \int \frac{d\epsilon}{2\pi} Tr_m (\partial_\mu \mathcal{H} \partial_\epsilon \mathcal{G}^R(\epsilon) \partial_\nu \mathcal{H} \mathcal{G}^<(\epsilon) - \partial_\mu \mathcal{H} \mathcal{G}^<(\epsilon) \partial_\nu \mathcal{H} \partial_\epsilon \mathcal{G}^A(\epsilon)). \quad (10.12)$$

### 10.3. Agreement of QCLE friction and NEGF friction

To prove the equivalence between Eq. 10.4 and Eq. 10.12, we use the eigenbasis of the electronic Hamiltonian  $\mathcal{H}$ ,  $\mathcal{H}|m\rangle = \epsilon_m|m\rangle$ , such that Eq. 10.4 can be expressed as

$$\begin{aligned}\gamma_{\mu\nu} &= -\hbar \sum_{mn} \int \frac{d\epsilon}{2\pi} \langle n | \partial_\mu \mathcal{H} | m \rangle \frac{1}{\epsilon - \epsilon_m + i\eta} \langle m | \partial_\nu \sigma_{ss} | n \rangle \frac{1}{\epsilon - \epsilon_n - i\eta} \\ &= -i\hbar \sum_{mn} \langle n | \partial_\mu \mathcal{H} | m \rangle \frac{1}{\epsilon_n - \epsilon_m + 2i\eta} \langle m | \partial_\nu \sigma_{ss} | n \rangle.\end{aligned}\quad (10.13)$$

In the above equation, we have used the residue theorem for contour integration. Using Eq. 10.8 and Eq. 10.11,  $\langle m | \partial_\nu \sigma_{ss} | n \rangle$  in Eq. 10.13 can be rewritten as

$$\begin{aligned} \langle m | \partial_\nu \sigma_{ss} | n \rangle &= \int \frac{d\epsilon'}{2\pi i} \langle m | \partial_\nu \mathcal{G}^<(\epsilon') | n \rangle \\ &= \int \frac{d\epsilon'}{2\pi i} \langle m | \mathcal{G}^R(\epsilon') \partial_\nu \mathcal{H} \mathcal{G}^<(\epsilon') + \mathcal{G}^<(\epsilon') \partial_\nu \mathcal{H} \mathcal{G}^A(\epsilon') | n \rangle. \end{aligned} \quad (10.14)$$

Note that the second term in Eq. 10.14 is the Hermitian conjugate of the first term. We now evaluate the first term of Eq. 10.14. In the eigenbasis of the electronic Hamiltonian, with the definition of  $\mathcal{G}^{R/A}$  and the Keldysh equation (Eq. 10.10), we have

$$\begin{aligned} &\int \frac{d\epsilon'}{2\pi i} \langle m | \mathcal{G}^R(\epsilon') \partial_\nu \mathcal{H} \mathcal{G}^<(\epsilon') | n \rangle \\ = &\int \frac{d\epsilon'}{2\pi i} \langle m | \mathcal{G}^R(\epsilon') \partial_\nu \mathcal{H} \mathcal{G}^R(\epsilon') \Pi^< \mathcal{G}^A(\epsilon') | n \rangle \\ = &\sum_{m'} \int \frac{d\epsilon'}{2\pi i} \frac{1}{\epsilon' - \epsilon_m + i\eta} \langle m | \partial_\nu \mathcal{H} | m' \rangle \frac{1}{\epsilon' - \epsilon_{m'} + i\eta} \langle m' | \Pi^< | n \rangle \frac{1}{\epsilon' - \epsilon_n - i\eta} \end{aligned} \quad (10.15)$$

As stated before,  $\Pi^<$  does not depend on energy ( $\epsilon'$ ), such that we can apply the residue theorem to the above equation,

$$\begin{aligned} &\int \frac{d\epsilon'}{2\pi i} \langle m | \mathcal{G}^R(\epsilon') \partial_\nu \mathcal{H} \mathcal{G}^<(\epsilon') | n \rangle \\ = &\sum_{m'} \frac{1}{\epsilon_n - \epsilon_m + 2i\eta} \langle m | \partial_\nu \mathcal{H} | m' \rangle \frac{1}{\epsilon_n - \epsilon_{m'} + 2i\eta} \langle m' | \Pi^< | n \rangle. \end{aligned} \quad (10.16)$$

A similar analysis applies to the second term of Eq. 10.14.

At this point, we consider the first term of Eq. 10.12. Again, using the definition of  $\mathcal{G}^{R/A}$

as well as the Keldysh equation, and applying the residue theorem, we find

$$\begin{aligned}
& - \int \frac{d\epsilon}{2\pi} \text{Tr}_m (\partial_\mu \mathcal{H} \partial_\epsilon \mathcal{G}^R(\epsilon) \partial_\nu \mathcal{H} \mathcal{G}^<(\epsilon)) \\
= & \int \frac{d\epsilon}{2\pi} \text{Tr}_m (\partial_\mu \mathcal{H} \mathcal{G}^R(\epsilon) \mathcal{G}^R(\epsilon) \partial_\nu \mathcal{H} \mathcal{G}^R(\epsilon) \Pi^< \mathcal{G}^A(\epsilon)) \\
= & \sum_{mnm'} \int \frac{d\epsilon}{2\pi} \langle n | \partial_\mu \mathcal{H} | m \rangle \frac{1}{(\epsilon - \epsilon_m + i\eta)^2} \langle m | \partial_\nu \mathcal{H} | m' \rangle \frac{1}{\epsilon - \epsilon_{m'} + i\eta} \langle m' | \Pi^< | n \rangle \frac{1}{\epsilon - \epsilon_n - i\eta} \\
= & i \sum_{mnm'} \langle n | \partial_\mu \mathcal{H} | m \rangle \frac{1}{(\epsilon_n - \epsilon_m + 2i\eta)^2} \langle m | \partial_\nu \mathcal{H} | m' \rangle \frac{1}{\epsilon_n - \epsilon_{m'} + 2i\eta} \langle m' | \Pi^< | n \rangle. \quad (10.17)
\end{aligned}$$

Comparing the above equation with Eq. 10.16, we have the following identity:

$$\begin{aligned}
& \int \frac{d\epsilon}{2\pi} \text{Tr}_m (\partial_\mu \mathcal{H} \partial_\epsilon \mathcal{G}^R(\epsilon) \partial_\nu \mathcal{H} \mathcal{G}^<(\epsilon)) \\
= & -i \sum_{mn} \langle n | \partial_\mu \mathcal{H} | m \rangle \frac{1}{\epsilon_n - \epsilon_m + 2i\eta} \int \frac{d\epsilon'}{2\pi i} \langle m | \mathcal{G}^R(\epsilon') \partial_\nu \mathcal{H} \mathcal{G}^<(\epsilon') | n \rangle. \quad (10.18)
\end{aligned}$$

Similarly, we can show

$$\begin{aligned}
& - \int \frac{d\epsilon}{2\pi} \text{Tr}_m (\partial_\mu \mathcal{H} \mathcal{G}^<(\epsilon) \partial_\nu \mathcal{H} \partial_\epsilon \mathcal{G}^A(\epsilon)) \\
= & -i \sum_{mn} \langle n | \partial_\mu \mathcal{H} | m \rangle \frac{1}{\epsilon_n - \epsilon_m + 2i\eta} \int \frac{d\epsilon'}{2\pi i} \langle m | \mathcal{G}^<(\epsilon') \partial_\nu \mathcal{H} \mathcal{G}^A(\epsilon') | n \rangle. \quad (10.19)
\end{aligned}$$

Note that Eq. 10.19 is the Hermitian conjugate of Eq. 10.18.

Finally, if we put Eq. 10.14 back into Eq. 10.13, together with the relationships shown in Eq. 10.18 and Eq. 10.19, we recover

$$\begin{aligned}
\gamma_{\mu\nu} = & -\hbar \int \frac{d\epsilon}{2\pi} \text{Tr}_m (\partial_\mu \mathcal{H} \mathcal{G}^R(\epsilon) \partial_\nu \sigma_{ss} \mathcal{G}^A(\epsilon)) \\
= & \hbar \int \frac{d\epsilon}{2\pi} \text{Tr}_m (\partial_\mu \mathcal{H} \partial_\epsilon \mathcal{G}^R(\epsilon) \partial_\nu \mathcal{H} \mathcal{G}^<(\epsilon) - \partial_\mu \mathcal{H} \mathcal{G}^<(\epsilon) \partial_\nu \mathcal{H} \partial_\epsilon \mathcal{G}^A(\epsilon)). \quad (10.20)
\end{aligned}$$

Thus, we have proven our claim that QCLE friction (Eq. 10.4) agrees with NEGF friction (Eq. 10.12). Note that Eq. 10.1 is much more general than any of these expressions since el-el interactions are allowed in Eq. 10.1, whereas el-el interactions are absent from Eq.

10.4 as well as Eq. 10.12.

#### 10.4. System-bath separation and Non-Condon effects

The results in Eq. 10.4 are very general and are applicable for any quadratic Hamiltonian without el-el interactions. To investigate non-Condon effects, we now adopt the standard dot-lead separation, such that the total electronic Hamiltonian  $\hat{H}$  can be divided into system  $\hat{H}_s$  and bath  $\hat{H}_b$ , as well as system-bath coupling  $\hat{H}_c$ ,

$$\hat{H} = \hat{H}_s + \hat{H}_b + \hat{H}_c, \quad (10.21)$$

$$\hat{H}_s = \sum_{mn} h_{mn}(\mathbf{R}) \hat{b}_m^\dagger \hat{b}_n + U_0(\mathbf{R}), \quad (10.22)$$

$$\hat{H}_b = \sum_{k\alpha} \epsilon_{k\alpha} \hat{c}_{k\alpha}^\dagger \hat{c}_{k\alpha}, \quad (10.23)$$

$$\hat{H}_c = \sum_{m,k\alpha} V_{m,k\alpha}(\mathbf{R}) \hat{b}_m^\dagger \hat{c}_{k\alpha} + V_{k\alpha,m}(\mathbf{R}) \hat{c}_{k\alpha}^\dagger \hat{b}_m. \quad (10.24)$$

Here  $m, n$  are orbitals in the molecule, and  $\alpha = L, R$  indicates left and right leads, which linearly couple to the molecule through  $\hat{H}_c$ . We remind the reader that the total Hamiltonian  $\hat{H}_{tot}$  still is a combination of the electronic Hamiltonian  $\hat{H}$  with the nuclear kinetic energy,  $\hat{H}_{tot} = \hat{H} + \sum_{\alpha} \frac{P_{\alpha}^2}{2m^{\alpha}}$ . Note also that the molecule-leads interactions  $V_{m,k\alpha}(\mathbf{R})$  also depend on nuclear position  $\mathbf{R}$ , which will give rise to non-Condon effects.

To evaluate the electronic friction (Eq. 10.12) and connect to the results in Ref. [80], we first consider the case where  $V_{m,k\alpha}(\mathbf{R})$  does not depend on  $\mathbf{R}$ . In such a case, only  $\hat{H}_s$  depends on  $\mathbf{R}$ , and therefore:

$$\begin{aligned} Tr_m (\partial_{\mu} \mathcal{H} \partial_{\epsilon} \mathcal{G}^R \partial_{\nu} \mathcal{H} \mathcal{G}^<) &= \sum_{mnm'n'} \partial_{\mu} h_{mn} \partial_{\epsilon} G_{nm'}^R \partial_{\nu} h_{m'n'} G_{n'm}^< \\ &= Tr_s (\partial_{\mu} h \partial_{\epsilon} G^R \partial_{\nu} h G^<). \end{aligned} \quad (10.25)$$

Here  $Tr_s$  implies summation over system orbitals ( $m$  and  $n$ ), and  $G^R = (\epsilon - h - \Sigma^R)^{-1}$  is the system retarded GF.  $\Sigma_{mn}^R = \sum_{k\alpha} V_{m,k\alpha} g_{k\alpha}^R V_{k\alpha,n}$  is the system retarded self-energy;  $G^<$  is

the system lesser GF (see Appendix 10.6.2). Thus, without any non-Condon contributions, the nonequilibrium electronic friction is

$$\gamma_{\mu\nu} = \hbar \int \frac{d\epsilon}{2\pi} \quad Tr_s (\partial_\mu h \partial_\epsilon G^R \partial_\nu h G^<) + \text{h.c.}, \quad (10.26)$$

which reduces to von Oppen's results in Ref. [80]. Here, h.c. denotes the Hermitian conjugate.

Second, for the case where  $V_{m,k\alpha}(\mathbf{R})$  does depend on  $\mathbf{R}$ , the results are much more complicated. However, in the wide-band approximation, as shown in the Supplemental Material of Ref. [259], the result can be simplified as

$$\begin{aligned} & Tr_m (\partial_\mu \mathcal{H} \partial_\epsilon \mathcal{G}^R \partial_\nu \mathcal{H} \mathcal{G}^<) \\ = & Tr_s \left( (\partial_\mu h \partial_\epsilon G^R + \bar{\Sigma}_\mu^R \partial_\epsilon G^R + \tilde{\Sigma}_\mu^A \partial_\epsilon G^R) (\partial_\nu h G^< + \partial_\nu \Sigma^R G^< + \bar{\Sigma}_\nu^< G^A) \right) \\ + & Tr_s (\tilde{\Sigma}_\mu^< \partial_\epsilon G^R (\partial_\nu h + \partial_\nu \Sigma^R) G^R + \partial_\epsilon G^R \Sigma_{\nu,\mu}^<). \end{aligned} \quad (10.27)$$

Again,  $Tr_s$  implies summation over system orbitals ( $m$  and  $n$ ). We have further defined the following quantities,

$$\bar{\Sigma}_{\mu,mn}^R = \sum_{k\alpha} \partial_\mu V_{m,k\alpha} g_{k\alpha}^r V_{k\alpha,n}, \quad (10.28)$$

$$\tilde{\Sigma}_{\mu,mn}^A = \sum_{k\alpha} V_{m,k\alpha} g_{k\alpha}^a \partial_\mu V_{k\alpha,n}, \quad (10.29)$$

$$\tilde{\Sigma}_{\mu,mn}^< = \sum_{k\alpha} V_{m,k\alpha} g_{k\alpha}^< \partial_\mu V_{k\alpha,n}, \quad (10.30)$$

$$\bar{\Sigma}_{\mu,mn}^< = \sum_{k\alpha} \partial_\mu V_{m,k\alpha} g_{k\alpha}^< V_{k\alpha,n}, \quad (10.31)$$

$$\Sigma_{\nu\mu,mn}^< = \sum_{k\alpha} \partial_\nu V_{m,k\alpha} g_{k\alpha}^< \partial_\mu V_{k\alpha,n}. \quad (10.32)$$

$g_{k\alpha}^r$ ,  $g_{k\alpha}^a$ , and  $g_{k\alpha}^<$  are the zero order retarded, advanced, and lesser Green's functions respectively for the non-interacting leads. The explicit forms are given in Appendix 10.6.2. With

these definitions, the nonequilibrium and non-Condon electronic friction can be written as

$$\begin{aligned} \gamma_{\mu\nu} = \hbar \int \frac{d\epsilon}{2\pi} & \quad Tr_s \left( (\partial_\mu h \partial_\epsilon G^R + \bar{\Sigma}_\mu^R \partial_\epsilon G^R + \tilde{\Sigma}_\mu^A \partial_\epsilon G^R) (\partial_\nu h G^< + \partial_\nu \Sigma^R G^< + \bar{\Sigma}_\nu^< G^A) \right) \\ & + Tr_s (\tilde{\Sigma}_\mu^< \partial_\epsilon G^R (\partial_\nu h + \partial_\nu \Sigma^R) G^R + \partial_\epsilon G^R \Sigma_{\nu\mu}^<) + h.c. \end{aligned} \quad (10.33)$$

Again, in the Condon approximation, Eqs. 10.28-10.32 vanish, such that the above equation (Eq. 10.33) reduces to von Oppen's result (Eq. 10.26).

#### 10.4.1. A single level with a harmonic oscillator

We will now apply the results above to the case of a single level (i.e. a dot) coupled to a harmonic oscillator (nuclear DoF) and two metallic baths. The corresponding system Hamiltonian is

$$\hat{H}_s = \epsilon_b(x) \hat{b}^\dagger \hat{b} + \frac{1}{2} m \omega^2 x^2, \quad (10.34)$$

where we assume  $\epsilon_b(x)$  depends linearly on  $x$ :

$$\epsilon_b(x) = \epsilon_0 + \lambda x \sqrt{m\omega/\hbar}. \quad (10.35)$$

The single level is coupled to the left and right leads through the following Hamiltonian:

$$\hat{H}_c = \sum_{k\alpha} V_{k\alpha}(x) (\hat{b}^\dagger \hat{c}_{k\alpha} + \hat{c}_{k\alpha}^\dagger \hat{b}). \quad (10.36)$$

Below we will apply the wide-band approximation, such that  $V_{k\alpha}(x)$  is independent of  $k$ .

We take  $V_{k\alpha}(x)$  to have the following form (as a function of  $x$ ):

$$V_{k\alpha}(x) = V_\alpha \sqrt{1 + z \exp(-m\omega x^2/\hbar)} \equiv V_\alpha Z(x). \quad (10.37)$$

Note that if we take  $z = 0$  in the above equation,  $V_{k\alpha}(x)$  will be independent of  $x$ , i.e.  $V_{k\alpha}(x)$  will satisfy the Condon approximation.

According to the wide-band approximation, the self-energy is purely imaginary and can be defined as

$$\sum_{k\alpha} V_{k\alpha}^2(x) g_{k\alpha}^r = \sum_{k\alpha} V_{\alpha}^2 g_{k\alpha}^r Z^2(x) = -\frac{i}{2}(\Gamma_0^L + \Gamma_0^R) Z^2(x), \quad (10.38)$$

$$\sum_{k\alpha} V_{k\alpha}^2(x) g_{k\alpha}^< = \sum_{k\alpha} V_{\alpha}^2 g_{k\alpha}^< Z^2(x) = i(\Gamma_0^L f^L + \Gamma_0^R f^R) Z^2(x). \quad (10.39)$$

Now we evaluate Eqs. 10.28-10.32, using the fact that all  $x$  dependence in Eqs. 10.28-10.32 is through the term  $Z(x)$  defined in Eq. 10.37. We sum up all of the relevant terms and calculate the electronic friction according to Eq. 10.33.

In Fig. 40, we plot the electronic friction as a function of  $x$ . For the equilibrium case (i.e. no bias,  $eV = 0$ ), when the Condon approximation holds ( $z = 0$ , such that  $V_{k\alpha}$  is independent of  $x$ ), the electronic friction exhibits a peak corresponding to the resonance of the dot level with the Fermi level of the leads:  $\epsilon_b(x) = \mu_L = \mu_R$ . With non-Condon effects ( $z = 1$ ), the electronic friction exhibits a dip at the position  $x = 0$ , where  $V_{k\alpha}(x)$  is maximum. This change from one peak to effectively two peaks was observed previously (in Ref. [184]) for the equilibrium case of one dot coupled to a single metal lead.

For the nonequilibrium case (i.e.  $eV \neq 0$ ), when the Condon approximation holds ( $z = 0$ ), again one peak becomes two peaks, but now for a different reason: two peaks arise from a resonance of the dot level with the each of the two different Fermi levels for the left and right leads:  $\epsilon_b(x) = \mu_L$  and  $\epsilon_b(x) = \mu_R$ . Interestingly, when non-Condon effects ( $z = 1$ ) are included, the electronic friction again exhibits a dip at the position where  $V_{k\alpha}(x)$  is maximum, which now effectively results in three peaks. Such results demonstrate that, when molecule-metal interactions depend strongly on nuclear geometry, non-Condon effects can strongly influence the relevant nonadiabatic dynamics at metal surfaces.

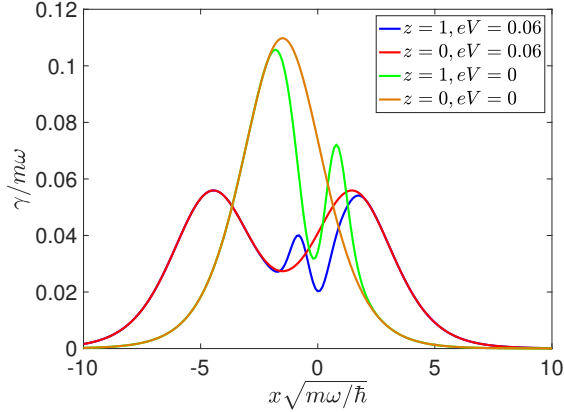


Figure 40: Electronic friction as a function of  $x$  for a single level coupled linearly to a harmonic oscillator. For the nonequilibrium case ( $eV \neq 0$ ), when the Condon approximation holds ( $z = 0$ ), the electronic friction exhibits two peaks corresponding to the resonance of the dot level with each of the two different Fermi levels for the leads:  $\epsilon_b(x) = \mu_L$  and  $\epsilon_b(x) = \mu_R$ . With non-Condon effects ( $z = 1$ ), the electronic friction exhibits a dip at the position  $x = 0$ , where  $V_{k\alpha}(x)$  is maximum. Thus, when we go out of equilibrium and break the Condon approximation, we effectively find three peaks.  $kT = 0.01$ ,  $\lambda = 0.01$ ,  $\Gamma_0^L = \Gamma_0^R = 0.01$ ,  $\hbar\omega = 0.003$ ,  $\epsilon_0 = 0.015$ ,  $\mu_L = -\mu_R = eV/2$ .

## 10.5. Conclusions

In summary, we have shown that, in the absence of electron-electron interactions, the electronic friction from a quantum-classical Liouville equation (QCLE) reduces to the results from von Oppen's nonequilibrium Green's function (NEGF) method. This agreement holds in general, in or out of equilibrium, for the case of quadratic Hamiltonian. Furthermore, we have shown that non-Condon effects can be easily included into a nonequilibrium electronic friction. Thus, given our previous work proving that, at equilibrium, the QCLE friction agrees with the Head-Gordon-Tully model as well as many other forms of electronic friction,<sup>[81,212,213,230,232]</sup> we believe there is now very strong proof that, in the limit of Markovian dynamics, there is only one, *universal* electronic friction associated with the Born-Oppenheimer approximation in the adiabatic limit. Future work must address how to incorporate non-Markovian effects efficiently; is there an optimal approach or many different approaches depending on the Hamiltonian?<sup>[125,173,212,213]</sup> We will address this question in a future study.<sup>[271]</sup>

## 10.6. Appendix

### 10.6.1. friction in the single particle basis

The friction tensor in the many-body representation is

$$\gamma_{\mu\nu} = - \int_0^\infty dt \operatorname{tr}_e \left( \partial_\mu \hat{H} e^{-i\hat{H}t/\hbar} \partial_\nu \hat{\rho}_{ss} e^{i\hat{H}t/\hbar} \right). \quad (10.40)$$

For the quadratic Hamiltonian in Eq. 10.3, we will recast the above equation into the single particle basis (Eq. 10.4).

We note first that  $U_0(\mathbf{R})$  does not contribute to the friction, because

$$\operatorname{tr}_e \left( \partial_\mu U_0 e^{-i\hat{H}t/\hbar} \partial_\nu \hat{\rho}_{ss} e^{i\hat{H}t/\hbar} \right) = \partial_\mu U_0 \operatorname{tr}_e (\partial_\nu \hat{\rho}_{ss}) = 0. \quad (10.41)$$

Here, we have used the fact that  $\operatorname{tr}_e (\hat{\rho}_{ss}) = 1$ . The friction can be rewritten as

$$\begin{aligned} \gamma_{\mu\nu} &= - \int_0^\infty dt \operatorname{tr}_e \left( e^{i\hat{H}t/\hbar} \partial_\mu \hat{H} e^{-i\hat{H}t/\hbar} \partial_\nu \hat{\rho}_{ss} \right) \\ &= - \int_0^\infty dt \sum_{pq} \partial_\mu \mathcal{H}_{pq} \operatorname{tr}_e \left( e^{i\hat{H}t/\hbar} \hat{d}_p^\dagger \hat{d}_q e^{-i\hat{H}t/\hbar} \partial_\nu \hat{\rho}_{ss} \right). \end{aligned} \quad (10.42)$$

We proceed to evaluate

$$\hat{d}_p^\dagger(t) = e^{i\hat{H}t/\hbar} \hat{d}_p^\dagger e^{-i\hat{H}t/\hbar}, \quad (10.43)$$

$$\hat{d}_q(t) = e^{i\hat{H}t/\hbar} \hat{d}_q e^{-i\hat{H}t/\hbar}. \quad (10.44)$$

The time derivatives of these operators are

$$\dot{\hat{d}}_p^\dagger(t) = e^{i\hat{H}t/\hbar} \frac{i}{\hbar} [\hat{H}, \hat{d}_p^\dagger] e^{-i\hat{H}t/\hbar} = \frac{i}{\hbar} \sum_a \hat{d}_a^\dagger(t) \mathcal{H}_{ap}, \quad (10.45)$$

$$\dot{\hat{d}}_q(t) = e^{i\hat{H}t/\hbar} \frac{i}{\hbar} [\hat{H}, \hat{d}_q] e^{-i\hat{H}t/\hbar} = -\frac{i}{\hbar} \sum_b \mathcal{H}_{qb} \hat{d}_b(t). \quad (10.46)$$

The above equations can be solved

$$e^{i\hat{H}t} \hat{d}_p^\dagger e^{-i\hat{H}t/\hbar} = \sum_a \hat{d}_a^\dagger (e^{i\mathcal{H}t/\hbar})_{ap}, \quad (10.47)$$

$$e^{i\hat{H}t} \hat{d}_q e^{-i\hat{H}t/\hbar} = \sum_b (e^{-i\mathcal{H}t/\hbar})_{qb} \hat{d}_b. \quad (10.48)$$

If we plug the above equations into Eq. 10.42, we arrive at

$$\begin{aligned} \gamma_{\mu\nu} &= - \int_0^\infty dt \sum_{pqab} \partial_\mu \mathcal{H}_{pq} (e^{i\mathcal{H}t/\hbar})_{ap} (e^{-i\mathcal{H}t/\hbar})_{qb} \text{tr}_e \left( \hat{d}_a^\dagger \hat{d}_b \partial_\nu \hat{\rho}_{ss} \right) \\ &= - \int_0^\infty dt \sum_{pqab} \partial_\mu \mathcal{H}_{pq} (e^{-i\mathcal{H}t/\hbar})_{qb} \partial_\nu \sigma_{ba}^{ss} (e^{i\mathcal{H}t/\hbar})_{ap} \\ &= - \int_0^\infty dt \text{Tr}_m (\partial_\mu \mathcal{H} e^{-i\mathcal{H}t/\hbar} \partial_\nu \sigma_{ss} e^{i\mathcal{H}t/\hbar}). \end{aligned} \quad (10.49)$$

Here, we have used the definition of  $\sigma_{ba}^{ss} = \text{tr}_e \left( \hat{d}_a^\dagger \hat{d}_b \hat{\rho}_{ss} \right)$ .

The above equation can be recast into the energy domain (with  $\eta$  being a positive infinitesimal),

$$\begin{aligned} \gamma_{\mu\nu} &= - \int_0^\infty dt \text{Tr}_m (\partial_\mu \mathcal{H} e^{-i(\mathcal{H}-i\eta)t/\hbar} \partial_\nu \sigma_{ss} e^{i(\mathcal{H}+i\eta)t/\hbar}) \\ &= - \int_0^\infty dt \int_0^\infty dt' \text{Tr}_m (\partial_\mu \mathcal{H} e^{-i(\mathcal{H}-i\eta)t/\hbar} \partial_\nu \sigma_{ss} e^{i(\mathcal{H}+i\eta)t'/\hbar}) \delta(t-t') \\ &= - \int_{-\infty}^\infty \frac{d\epsilon}{2\pi\hbar} \int_0^\infty dt \int_0^\infty dt' \text{Tr}_m (\partial_\mu \mathcal{H} e^{-i(\mathcal{H}-i\eta)t/\hbar} \partial_\nu \sigma_{ss} e^{i(\mathcal{H}+i\eta)t'/\hbar}) e^{i\epsilon(t-t')/\hbar} \\ &= -\hbar \int \frac{d\epsilon}{2\pi} \text{Tr}_m \left( \partial_\mu \mathcal{H} \frac{1}{\epsilon - \mathcal{H} + i\eta} \partial_\nu \sigma_{ss} \frac{1}{\epsilon - \mathcal{H} - i\eta} \right), \end{aligned} \quad (10.50)$$

which gives us Eq. 10.4.

### 10.6.2. The lesser self-energy of the total system, $\Pi^<$

For the quadratic Hamiltonian with dot-lead separation in Eqs. 10.21-10.24, we imagine embedding the total Hamiltonian (as in Eqs. 10.21-10.24) as the inner Hamiltonian inside

yet another, even larger outer bath <sup>1</sup>:

$$\hat{H} = \hat{H}_{inner} + \hat{H}_{outer} + \hat{V}_{inner-outer}. \quad (10.51)$$

Assuming small inner-outer coupling  $\hat{V}_{inner-outer}$ , as mediated only through the inner bath (leads), and assuming a completely quadratic Hamiltonian,  $\Pi^<$  of the inner Hamiltonian can be written as

$$\Pi_{k\alpha, k'\alpha'}^< = i2\eta f_\alpha(\epsilon_{k\alpha}) \delta_{k, k'} \delta_{\alpha, \alpha'}. \quad (10.52)$$

Here  $\eta$  is an positive infinitesimal, which implies that we have added a small dissipation ( $\eta$ ) to all of the non-interacting electrons in the leads (inner bath).  $f_\alpha(\epsilon_{k\alpha})$  is the Fermi function of the  $\alpha$  (left or right) lead. Clearly,  $\Pi^<$  does not depend on position or energy ( $\epsilon'$  as in Eq. 10.10) if we assume that the inner and outer baths do not depend on  $\mathbf{R}$ .

### 10.6.3. Evaluating $G_{mn}^<$

As an example of how the definition in the above equation works, we calculate  $G_{mn}^<$ . Starting from the Keldysh equation,  $\mathcal{G}^< = \mathcal{G}^R \Pi^< \mathcal{G}^A$ , we project the equation onto the dots,

$$G_{mn}^< = \sum_{k\alpha, k'\alpha'} \mathcal{G}_{m, k\alpha}^R \Pi_{k\alpha, k'\alpha'}^< \mathcal{G}_{k'\alpha', n}^A. \quad (10.53)$$

Using the Dyson equation,

$$\mathcal{G}_{m, k\alpha} = \sum_{n'} \mathcal{G}_{m, n'} V_{n', k\alpha} g_{k\alpha}, \quad (10.54)$$

$$\mathcal{G}_{k\alpha, m} = \sum_{n'} g_{k\alpha} V_{k\alpha, n'} \mathcal{G}_{n', m}, \quad (10.55)$$

---

<sup>1</sup>In general, this introduction of the outer bath with infinitesimal coupling will not affect any system dynamics. There are outstanding issues regarding the effect of the outer bath on entropy production and overall irreversibility, but these quantities will not be calculated here.

with the zero order retarded and advanced Green's functions for the leads,

$$g_{k\alpha}^r = \frac{1}{\epsilon - \epsilon_{k\alpha} + i\eta}, g_{k\alpha}^a = \frac{1}{\epsilon - \epsilon_{k\alpha} - i\eta}, \quad (10.56)$$

we can write Eq. 10.53 as

$$\begin{aligned} G_{mn}^< &= \sum_{k\alpha, k'\alpha', m', n'} G_{m, n'}^R V_{n', k\alpha} g_{k\alpha}^r 2i\eta f_\alpha(\epsilon_{k\alpha}) \delta_{k, k'} \delta_{\alpha, \alpha'} g_{k'\alpha'}^a V_{k'\alpha', m'} G_{m', n}^A \\ &= \sum_{k\alpha, m', n'} G_{m, n'}^R V_{n', k\alpha} g_{k\alpha}^r 2i\eta f_\alpha(\epsilon_{k\alpha}) g_{k\alpha}^a V_{k\alpha, m'} G_{m', n}^A. \end{aligned} \quad (10.57)$$

Note that

$$g_{k\alpha}^r 2i\eta f_\alpha(\epsilon_{k\alpha}) g_{k\alpha}^a = \frac{2i\eta}{(\epsilon - \epsilon_{k\alpha})^2 + \eta^2} f_\alpha(\epsilon_{k\alpha}) = i2\pi\delta(\epsilon - \epsilon_{k\alpha}) f_\alpha(\epsilon_{k\alpha}) = g_{k\alpha}^<, \quad (10.58)$$

$g_{k\alpha}^<$  is the zero order lesser Green's functions for the leads. Using the standard definition of  $\Sigma_{n', m'}^<$

$$\Sigma_{n', m'}^< = \sum_{k\alpha} V_{n', k\alpha} g_{k\alpha}^< V_{k\alpha, m'} = \sum_{k\alpha} V_{n', k\alpha} g_{k\alpha}^r 2i\eta f_\alpha(\epsilon_{k\alpha}) g_{k\alpha}^a V_{k\alpha, m'}, \quad (10.59)$$

we arrive at the standard NEGF Langreth equation for  $G^<$  for the dots<sup>[90,258]</sup>:

$$G_{mn}^< = \sum_{m', n'} G_{m, n'}^R \Sigma_{n', m'}^< G_{m', n}^A. \quad (10.60)$$

#### 10.6.4. Evaluating $\mathcal{G}_{k\alpha, k'\alpha'}^<$

As another example of how to apply the definition in Eq. 10.52, we calculate  $\mathcal{G}_{k\alpha, k'\alpha'}^<$  by projecting the Keldysh equation (Eq. 10.10) onto the leads,

$$\mathcal{G}_{k\alpha, k'\alpha'}^< = \sum_{k''\alpha''} \mathcal{G}_{k\alpha, k''\alpha''}^R \Pi_{k''\alpha'', k''\alpha''}^< \mathcal{G}_{k''\alpha'', k'\alpha'}^A. \quad (10.61)$$

Again, we have the Dyson equation for the leads:

$$\mathcal{G}_{k\alpha,k''\alpha''}^R = g_{k\alpha}^r \delta_{k\alpha,k''\alpha''} + \sum_{mn} g_{k\alpha}^r V_{k\alpha,m} G_{mn}^R V_{n,k''\alpha''} g_{k''\alpha''}^r, \quad (10.62)$$

$$\mathcal{G}_{k''\alpha'',k'\alpha'}^A = g_{k''\alpha''}^a \delta_{k''\alpha'',k'\alpha'} + \sum_{m'n'} g_{k''\alpha''}^a V_{k''\alpha'',m'} G_{m'n'}^A V_{n',k'\alpha'} g_{k'\alpha'}^a. \quad (10.63)$$

Using Eq. 10.58 ( $g_{k\alpha}^< = g_{k\alpha}^r \Pi_{k\alpha,k\alpha}^< g_{k\alpha}^a$ ), Eq. 10.59 and Eq. 10.60, we recast  $\mathcal{G}_{k\alpha,k'\alpha'}^<$  as

$$\begin{aligned} \mathcal{G}_{k\alpha,k'\alpha'}^< &= g_{k\alpha}^< \delta_{k\alpha,k'\alpha'} + \sum_{mn} g_{k\alpha}^r V_{k\alpha,m} G_{mn}^R V_{n,k'\alpha'} g_{k'\alpha'}^< \\ &+ \sum_{mn} g_{k\alpha}^< V_{k\alpha,m} G_{mn}^A V_{n,k'\alpha'} g_{k'\alpha'}^a \\ &+ \sum_{mn} g_{k\alpha}^r V_{k\alpha,m} G_{mn}^< V_{n,k'\alpha'} g_{k'\alpha'}^a \end{aligned} \quad (10.64)$$

Recall that  $G_{mn}^R = (\epsilon - h - \Sigma^R)_{mn}^{-1}$ . Thus we arrive at the standard NEGF result for  $\mathcal{G}_{k\alpha,k'\alpha'}^<$ . Eq. 10.64 can be derived equivalently by projecting the Dyson equation for the contour-ordered Green's function onto the two different branches of the Keldysh contour, i.e. projecting  $\mathcal{G}^c$  onto  $\mathcal{G}^<$ .<sup>[90,258]</sup>

Lastly, by projecting the Keldysh equation (Eq. 10.10) onto the appropriate contours in an analogous fashion, we can also derive similar expressions for the dot-lead coupling lesser GF,  $\mathcal{G}_{m,k\alpha}^<$ .

## CHAPTER 11 : Conclusions

This dissertation has focused on developing of new tools to study nonadiabatic dynamics at molecule-metal interfaces. Two methods have been implemented and explored extensively: surface hopping and electronic friction. To be specific,

- A simple surface hopping approach has been proposed to treat nonadiabatic electron transfer at molecule-metal interface. Such a surface hopping approach recovers detailed balance as well as the Marcus electron transfer rate.
- A electronic friction model has been used to deal with nonadiabatic effects and nuclear dissipation. We have further shown the connection between surface hopping and electronic friction.
- A broadened classical master equation (BCME) has been developed as a natural combination of the surface hopping scheme and the electronic friction model. Subsequently, the BCME was used to study nonequilibrium transport properties.
- The surface hopping approach has been further combined with Tully's fewest switches surface hopping (FSSH) scheme with the potential to study a large molecule near a metal surface, treating electron transfer within the molecule and electron transfer between the molecule and metal on equal footing.
- A very general form of electronic friction has been derived. We have explored this form of electronic friction in and out of equilibrium, with and without electron-electron interactions.

In the future, the effects of electron-electron interactions on nonadiabatic dynamics at molecule-metal interfaces should be further explored: How strong are the electron-electron interactions in realistic systems and how much do these electron-electron interactions affect the overall dynamics? In the meanwhile, to apply our dynamical approaches to realistic systems, effective and reliable excited states from electronic structure theory are required.

With so much interest in molecule-metal interfaces across the area of chemisorption, electrochemistry as well as molecular electronics, we believe these questions are both solvable and of crucial importance.

## BIBLIOGRAPHY

- [1] Mühlbacher, L.; Rabani, E. *Phys. Rev. Lett.* **2008**, *100*, 176403.
- [2] The data is tracked from Ref. [1] using Data Tracker. In the paper,  $E_d = 0$ , but it seems the renormalized impurity level should be 0, that is  $E_d - g^2/\hbar\omega = 0$ .
- [3] For the QME, the original statistics are quantum, whereas for the CME we choose initial conditions according to classical statistics (rather than the Wigner distribution).
- [4] Bulla, R.; Costi, T. A.; Pruschke, T. *Reviews of Modern Physics* **2008**, *80*, 395–450.
- [5] For NRG calculations, the band width is  $W = 1$ , the basis is initialized with 100 boson states, the maximum number of eigenstates kept is  $N_s = 1500$ , and the logarithmic discretizing parameter is  $\Lambda = 2$ .
- [6] Dou, W.; Nitzan, A.; Subotnik, J. E. *J. Chem. Phys.* **2015**, *143*, 054103.
- [7] Dzhioev, A. A.; Kosov, D. S.; von Oppen, F. *J. Chem. Phys.* **2013**, *138*, 134103.
- [8] Askerka, M.; Maurer, R. J.; Batista, V. S.; Tully, J. C. *Phys. Rev. Lett.* **2016**, *116*, 217601.
- [9] Plihal, M.; Langreth, D. C. *Phys. Rev. B* **1998**, *58*, 2191.
- [10] Born, M.; Oppenheimer, R. *Annalen der Physik* **1927**, *389*, 457.
- [11] Tully, J. C. *Theoretical Chemistry Accounts* **2000**, *103*, 173–176.
- [12] Wodtke, A. M.; Tully, J. C.; Auerbach, D. J. *International Reviews in Physical Chemistry* **2004**, *23*, 513.
- [13] Worth, G. A.; Cederbaum, L. S. *Annu. Rev. Phys. Chem.* **2004**, *55*, 127–158.
- [14] Yarkony, D. R. *Rev. Mod. Phys.* **1996**, *68*, 985–1013.
- [15] Levine, B. G.; Martínez, T. J. *Annu. Rev. Phys. Chem.* **2007**, *58*, 613–634.
- [16] Tully, J. C. *J. Chem. Phys.* **1990**, *93*, 1061–1071.
- [17] Subotnik, J. E.; Ouyang, W.; Landry, B. R. *J. Chem. Phys.* **2013**, *139*, 214107.
- [18] Kapral, R.; Ciccotti, G. *J. Chem. Phys.* **1999**, *110*, 8919.
- [19] Kapral, R. *Ann. Rev. Phys. Chem.* **2006**, *57*, 129–157.
- [20] Shi, Q.; Geva, E. *J. Chem. Phys.* **2004**, *121*, 3393.

- [21] Kapral, R. *Chemical Physics* **2016**, *481*, 77 – 83.
- [22] Huo, P.; Coker, D. F. *J. Chem. Phys.* **2012**, *137*, 22A535.
- [23] Landry, B. R.; Subotnik, J. E. *J. Chem. Phys.* **2012**, *137*, 22A513.
- [24] Huang, Y.; Rettner, C. T.; Auerbach, D. J.; Wodtke, A. M. *Science* **2000**, *290*, 111–114.
- [25] Bartels, C.; Cooper, R.; Auerbach, D. J.; Wodtke, A. M. *Chem. Sci.* **2011**, *2*, 1647–1655.
- [26] Bünermann, O.; Jiang, H.; Dorenkamp, Y.; Kandratsenka, A.; Janke, S. M.; Auerbach, D. J.; Wodtke, A. M. *Science* **2015**, *350*, 1346–1349.
- [27] Koch, J.; von Oppen, F. *Phys. Rev. Lett.* **2005**, *94*, 206804.
- [28] Leturcq, R.; Stampfer, C.; Inderbitzin, K.; Durrer, L.; Hierold, C.; Mariani, E.; Schultz, M. G.; von Oppen, F.; Ensslin, K. *Nat. Phys.* **2009**, *5*, 327.
- [29] Burzurí, E.; Yamamoto, Y.; Warnock, M.; Zhong, X.; Park, K.; Cornia, A.; van der Zant, H. S. *Nano Lett.* **2014**, *14*, 3191–3196.
- [30] Kaasbjerg, K.; Novotný, T.; Nitzan, A. *Phys. Rev. B* **2013**, *88*, 201405.
- [31] Siddiqui, L.; Ghosh, A. W.; Datta, S. *Phys. Rev. B* **2007**, *76*, 085433.
- [32] Koch, J.; Semmelhack, M.; von Oppen, F.; Nitzan, A. *Phys. Rev. B* **2006**, *73*, 155306.
- [33] Härtle, R.; Thoss, M. *Phys. Rev. B* **2011**, *83*, 125419.
- [34] Mishra, A. K.; Waldeck, D. H. *J. Phys. Chem. C* **2009**, *113*, 17904.
- [35] Gosavi, S.; Marcus, R. *J. Phys. Chem. B* **2000**, *104*, 2067–2072.
- [36] Willard, A. P.; Reed, S. K.; Madden, P. A.; Chandler, D. *Farad. Discuss* **2009**, *141*, 423–441.
- [37] White, J. D.; Chen, J.; Matsiev, D.; Auerbach, D. J.; Wodtke, A. M. *Nature* **2005**, *433*, 503.
- [38] Dou, W.; Nitzan, A.; Subotnik, J. E. *J. Chem. Phys.* **2015**, *142*, 084110.
- [39] Tully, J. C.; Preston, R. K. *J. Chem. Phys.* **1971**, *55*, 562.
- [40] Prezhdo, O. V.; Rossky, P. J. *J. Chem. Phys.* **1997**, *107*, 825.
- [41] Bedard-Hearn, M. J.; Larsen, R. E.; Schwartz, B. J. *J. Chem. Phys.* **2005**, *123*, 234106.

- [42] Larsen, R. E.; Bedard-Hearn, M. J.; Schwartz, B. J. *J. Phys. Chem. B* **2006**, *110*, 20055.
- [43] Fang, J. Y.; Hammes-Schiffer, S. *J. Phys. Chem. A* **1999**, *103*, 9399–9407.
- [44] Fang, J.-Y.; Hammes-Schiffer, S. *J. Chem. Phys.* **1999**, *110*, 11166.
- [45] Volobuev, Y. L.; Hack, M. D.; Topaler, M. S.; Truhlar, D. G. *J. Chem. Phys.* **2000**, *112*, 9716.
- [46] Hack, M. D.; Truhlar, D. G. *J. Chem. Phys.* **2001**, *114*, 2894–3002.
- [47] Jasper, A. W.; Hack, M. D.; Truhlar, D. G. *J. Chem. Phys.* **2001**, *115*, 1804–1816.
- [48] Zhu, C.; Jasper, A. W.; Truhlar, D. G. *J. Chem. Phys.* **2004**, *120*, 5543–5547.
- [49] Zhu, C.; Nangia, S.; Jasper, A. W.; Truhlar, D. G. *J. Chem. Phys.* **2004**, *121*, 7658–7670.
- [50] Jasper, A. W.; Truhlar, D. G. *J. Chem. Phys.* **2005**, *123*, 064103.
- [51] Webster, F.; Rossky, P. J.; Friesner, R. A. *Computational Physics Communications* **1991**, *63*, 494–522.
- [52] Webster, F.; Wang, E. T.; Rossky, P. J.; Friesner, R. A. *J. Chem. Phys.* **1994**, *100*, 4835–4847.
- [53] Wong, K. F.; Rossky, P. J. *J. Chem. Phys.* **2002**, *116*, 8418–8428.
- [54] Wong, K. F.; Rossky, P. J. *J. Chem. Phys.* **2002**, *116*, 8429–8438.
- [55] Schwartz, B. J.; Bittner, E. R.; Prezhdo, O. V.; Rossky, P. J. *J. Chem. Phys.* **1996**, *104*, 5942.
- [56] Subotnik, J. E.; Shenvi, N. *J. Chem. Phys.* **2011**, *134*, 024105.
- [57] Subotnik, J. E.; Shenvi, N. *J. Chem. Phys.* **2011**, *134*, 244114.
- [58] Shenvi, N.; Subotnik, J. E.; Yang, W. *J. Chem. Phys.* **2011**, *134*, 144102.
- [59] Schwartz, B. J.; Rossky, P. J. *J. Chem. Phys.* **1994**, *101*, 6917–6926.
- [60] Petit, A. S.; Subotnik, J. E. *J. Chem. Phys.* **2014**, *141*, 014107.
- [61] Zimmermann, T.; Vanicek, J. *J. Chem. Phys.* **2014**, *141*, 134102.
- [62] Petit, A. S.; Subotnik, J. E. *J. Chem. Phys.* **2014**, *141*, 154108.

- [63] Tempelaar, R.; van der Vegte, C. P.; Knoester, J.; Jansen, T. L. C. *J. Chem. Phys.* **2013**, *138*, 164106.
- [64] Martens, C. C.; Fang, J. Y. *J. Chem. Phys.* **1997**, *106*, 4918–4930.
- [65] Sterpone, F.; Bedard-Hearn, M. J.; Rossky, P. J. *J. Phys. Chem. A* **2009**, *113*, 3427–3430.
- [66] Hazra, A.; Soudakov, A. V.; Hammes-Schiffer, S. *J. Phys. Chem. B* **2010**, *114*, 12319–12332.
- [67] Nachtigallova, D.; Aquino, A. J. A.; Szymczak, J. J.; Barbatti, M.; Hobza, P.; Lischka, H. *J. Phys. Chem. A* **2011**, *115*, 5247–5255.
- [68] Nelson, T.; Fernandez-Alberti, S.; Roitberg, A. E.; Tretiak, S. *Accounts of Chemical Research* **2014**, *47*, 1155–1164.
- [69] Long, R.; Prezhdo, O. V. *J. Am. Chem. Soc.* **2014**, *136*, 4343–4354.
- [70] Fischer, S. A.; Chapman, C. T.; Li, X. *J. Chem. Phys.* **2011**, *135*, 144102.
- [71] Shenvi, N.; Roy, S.; Tully, J. C. *J. Chem. Phys.* **2009**, *130*, 174107.
- [72] Shenvi, N.; Roy, S.; Tully, J. C. *Science* **2009**, *326*, 829–832.
- [73] Shenvi, N.; Schmidt, J. R.; Edwards, S. T.; Tully, J. C. *Phys. Rev. A* **2008**, *78*, 022502.
- [74] Preston, R. K.; Cohen, J. S. *J. Chem. Phys.* **1976**, *65*, 1589.
- [75] Sisourat, N. *J. Chem. Phys.* **2013**, *139*, 074111.
- [76] Anderson, P. W. *Physical Review* **1961**, *124*, 41.
- [77] Holstein, T. *Ann. Phys.* **1959**, *8*, 325.
- [78] Galperin, M.; Ratner, M. A.; Nitzan, A. *J. Phys: Condens. Matter* **2007**, *19*, 103201.
- [79] Galperin, M.; Ratner, M. A.; Nitzan, A. *Nano Lett.* **2005**, *5*, 125.
- [80] Bode, N.; Kusminskiy, S. V.; Egger, R.; von Oppen, F. *Beilstein J. Nanotechnol* **2012**, *3*, 144.
- [81] Brandbyge, M.; Hedegård, P.; Heinz, T. F.; Misewich, J. A.; Newns, D. M. *Phys. Rev. B* **1995**, *52*, 6042–6056.
- [82] Head-Gordon, M.; Tully, J. C. *J. Chem. Phys.* **1995**, *103*, 10137.
- [83] Elste, F.; Weick, G.; Timm, C.; von Oppen, F. *Appl. Phys. A* **2008**, *93*, 345–354.

- [84] Schmidt, J. R.; Parandekar, P. V.; Tully, J. C. *J. Chem. Phys.* **2008**, *129*, 044104.
- [85] Parandekar, P. V.; Tully, J. C. *J. Chem. Phys.* **2005**, *122*, 094102.
- [86] Koch, J.; von Oppen, F.; Oreg, Y.; Sela, E. *Phys. Rev. B* **2004**, *70*, 195107.
- [87] Bruus, H.; Flensberg, K. *Many-Body Quantum Theory in Condensed Matter Physics: An Introduction*; Oxford University Press, 2004.
- [88] Wilson, K. G. *Rev. Mod. Phys.* **1975**, *47*, 773–840.
- [89] Another option would be to compare our results against MCTDH (multi-configuration time-dependent Hartree) calculations<sup>[99]</sup>.
- [90] Haug, H.; Jauho, A. *Quantum Kinetics in Transport and Optics of Semiconductors.*; Springer: New York, 2007.
- [91] Subotnik, J. E.; Hansen, T.; Ratner, M. A.; Nitzan, A. *J. Chem. Phys.* **2009**, *130*, 144105.
- [92] Segal, D.; Nitzan, A. *Chemical Physics* **2001**, *268*, 315 – 335.
- [93] Anders, F. B.; Schiller, A. *Phys. Rev. Lett.* **2005**, *95*, 196801.
- [94] Floß, G.; Granucci, G.; Saalfrank, P. *J. Chem. Phys.* **2012**, *137*, 234701.
- [95] Dou, W.; Nitzan, A.; Subotnik, J. E. *J. Chem. Phys.* **2015**, *142*, 234106.
- [96] Dou, W.; Nitzan, A.; Subotnik, J. E. *The Journal of chemical physics* **2015**, *143*, 189902.
- [97] Cohen, G.; Gull, E.; Reichman, D. R.; Millis, A. J. *Phys. Rev. Lett.* **2014**, *112*, 146802.
- [98] Hewson, A. C.; Meyer, D. *J. Phys. Condens. Matter* **2002**, *14*, 427–445.
- [99] Thoss, M.; Kondov, I.; Wang, H. *Phys. Rev. B* **2007**, *76*, 153313.
- [100] Ding, W.; Negre, C. F. A.; Vogt, L.; Batista, V. S. *J. Phys. Chem. C* **2014**, *118*, 8316.
- [101] Mujica, V.; Kemp, M.; Ratner, M. A. *J. Chem. Phys.* **1994**, *101*, 6849.
- [102] Reimers, J. R.; Solomon, G. C.; A. Gagliardi, A. B.; Hush, N. S.; Frauenheim, T.; Carlo, A. D.; Pecchia, A. *J. Phys. Chem. A* **2007**, *111*, 5692.
- [103] Ouyang, W.; Dou, W.; Subotnik, J. E. *J. Chem. Phys.* **2015**, *142*, 084109.
- [104] Chen, L.; Hansen, T.; Franco, I. *J. Phys. Chem. C* **2014**, *118*, 20009.

- [105] Zelovich, T.; Kronik, L.; Hod, O. *J. Chem. Theory Comp.* **2014**, *10*, 2927.
- [106] Ajisaka, S.; Barra, F.; Mejía-Monasterio, C.; Prosen, T. *Phys. Scripta* **2012**, *86*, 058501.
- [107] Sánchez, C. G.; Stamenova, M.; Sanvito, S.; Bowler, D. R.; Horsfield, A. P.; Todorov, T. N. *J. Chem. Phys.* **2006**, *124*, 214708.
- [108] McEniry, E. J.; Bowler, D. R.; Dundas, D.; Horsfield, A. P.; Sánchez, C. G.; Todorov, T. N. *J. Phys: Condens. Matter* **2007**, *19*, 196201.
- [109] Gata, M. A.; Antoniewicz, P. R. *Phys. Rev. B* **1993**, *47*, 13797.
- [110] Nitzan, A. *Chemical dynamics in condensed phases: relaxation, transfer and reactions in condensed molecular systems*; Oxford university press, 2006.
- [111] Cohen, G.; Gull, E.; Reichman, D. R.; Millis, A. J.; Rabani, E. *Phys. Rev. B* **2013**, *87*, 195108.
- [112] Tully, J. C. *J. Chem. Phys.* **1980**, *73*, 1975.
- [113] Adelman, S. A.; Doll, J. D. *J. Chem. Phys.* **1976**, *64*, 2375.
- [114] Head-Gordon, M.; Tully, J. C. *J. Chem. Phys.* **1992**, *96*, 3939–3949.
- [115] Thomas, M.; Karzig, T.; Kusminskiy, S. V.; Zaránd, G.; von Oppen, F. *Phys. Rev. B* **2012**, *86*, 195419.
- [116] Mozyrsky, D.; Hastings, M. B.; Martin, I. *Phys. Rev. B* **2006**, *73*, 035104.
- [117] Hänggi, P.; Talkner, P.; Borkovec, M. *Reviews of Modern Physics* **1988**, *89*, 6736.
- [118] Mahan, G. D. *Many-Particle Physics*; Plenum: New York, 2000.
- [119] Dou, W.; Subotnik, J. E. *J. Chem. Phys.* **2016**, *144*, 024116.
- [120] Nitzan, A. *Ann. Rev. Phys. Chem.* **2001**, *52*, 681–750.
- [121] Delbecq, M. R.; Schmitt, V.; Parmentier, F. D.; Roch, N.; Viennot, J. J.; Féve, G.; Huard, B.; C. Mora, A. C.; Kontos, T. *Phys. Rev. Lett.* **2011**, *107*, 256804.
- [122] Cavaliere, F.; Mariani, E.; Leturcq, R.; Stampfer, C.; Sasseti, M. *Phys. Rev. B* **2010**, *81*, 201303(R).
- [123] Albrecht, K. F.; Martin-Rodero, A.; Monreal, R. C.; Mühlbacher, L.; Yeyati, A. L. *Phys. Rev. B* **2013**, *87*, 085127.
- [124] Ouyang, W.; Saven, J. G.; Subotnik, J. E. *J. Phys. Chem. C* **2015**, *119*, 20833–20844.

- [125] Galperin, M.; Nitzan, A. *J. Phys. Chem. Lett.* **2015**, *6*, 4898.
- [126] Dou, W.; Nitzan, A.; Subotnik, J. E. *J. Chem. Phys.* **2016**, *144*, 074109.
- [127] Dou, W.; Schinabeck, C.; Thoss, M.; Subotnik, J. E. *J. Chem. Phys.* **2018**, *148*, 102317.
- [128] Nitzan, A.; Ratner, M. A. *Science* **2003**, *300*, 1384.
- [129] Tao, N. *Nat. Nanotechnol.* **2006**, *1*, 173–181.
- [130] Park, J.; Pasupathy, A. N.; Goldsmith, J. I.; Chang, C.; Yaish, Y.; Petta, J. R.; Rinkoski, M.; Sethna, J. P.; Abruña, H. D.; McEuen, P. L.; Ralph, D. C. *Nature* **2002**, *417*, 722.
- [131] Beenakker, C. W. J. *Phys. Rev. B* **1991**, *44*, 1646.
- [132] Dorogi, M.; Gomez, J.; Osifchin, R.; Andres, R. P.; Reifenberger, R. *Phys. Rev. B* **1995**, *52*, 9071.
- [133] Bogani, L.; Wernsdorfer, W. *Nat. Mater.* **2008**, *7*, 179.
- [134] Yu, L. H.; Natelson, D. *Nano Lett.* **2004**, *4*, 79.
- [135] Zhao, A.; Li, Q.; Chen, L.; Xiang, H.; Wang, W.; Pan, S.; Wang, B.; Xiao, X.; Yang, J.; Hou, J. G.; Zhu, Q. *Science* **2005**, *309*, 1542.
- [136] Liang, W.; Shores, M. P.; Bockrath, M.; Long, J. R.; Park, H. *Nature* **2002**, *417*, 725.
- [137] Romeike, C.; Wegewijs, M. R.; Hofstetter, W.; Schoeller, H. *Phys. Rev. Lett.* **2006**, *96*, 196601.
- [138] Hsu, L.-Y.; Tsai, T.-W.; Jin, B.-Y. *J. Chem. Phys.* **2010**, *133*, 144705.
- [139] Galperin, M.; Ratner, M. A.; Nitzan, A.; Troisi, A. *Science* **2008**, *319*, 1056.
- [140] Härtle, R.; Thoss, M. In *Molecular electronics: An experimental and theoretical approach*; Baldea, I., Ed.; Pan Stanford: Singapore, 2015; Chapter 5, p 155.
- [141] Volkovich, R.; Härtle, R.; Thoss, M.; Peskin, U. *Phys. Chem. Chem. Phys.* **2011**, *13*, 14333–14349.
- [142] Härtle, R.; Kulkarni, M. *Phys. Rev. B* **2015**, *91*, 245429.
- [143] Reckermann, F.; Leijnse, M.; Wegewijs, M.; Schoeller, H. *Europhys. Lett.* **2008**, *83*, 58001.
- [144] Frederiksen, T.; Franke, K.; A. Arnau; Schulze, G.; Pascual, J.; Lorente, N. *Phys. Rev. B* **2008**, *78*, 233401.

- [145] Repp, J.; Meyer, G. *Nat. Phys.* **2010**, *6*, 975.
- [146] Erpenbeck, A.; Härtle, R.; Thoss, M. *Phys. Rev. B* **2015**, *91*, 195418.
- [147] Koch, J.; von Oppen, F.; Andreev, A. V. *Phys. Rev. B* **2006**, *74*, 205438.
- [148] Secker, D.; Wagner, S.; Ballmann, S.; Härtle, R.; Thoss, M.; Weber, H. B. *Phys. Rev. Lett.* **2011**, *106*, 136807.
- [149] Schinabeck, C.; Härtle, R.; Weber, H.; Thoss, M. *Phys. Rev. B* **2014**, *90*, 075409.
- [150] Li, C.; Zhang, D.; Liu, X.; Han, S.; Tang, T.; Zhou, C.; Wendy Fan, J. K.; Han, J.; Meyyappan, M.; Rawlett, A. M.; Price, D. W.; Tour, J. M. *Appl. Phys. Lett.* **2003**, *82*, 645.
- [151] Wu, S. W.; Ogawa, N.; Nazin, G. V.; Ho, W. *J. Phys. Chem. C* **2008**, *112*, 5241.
- [152] Lörtscher, E.; Ciszek, J. W.; Tour, J.; Riel, H. *Small* **2006**, *2*, 973–977.
- [153] Wilner, E.; Wang, H.; Thoss, M.; Rabani, E. *Phys. Rev. B* **2014**, *89*, 205129.
- [154] Chen, J.; Reed, M. A.; Rawlett, A. M.; Tour, J. M. *Science* **1999**, *286*, 1550.
- [155] Walzer, K.; Marx, E.; Greenham, N. C.; Less, R. J.; Raithby, P. R.; Stokbro, K. *J. Am. Chem. Soc.* **2004**, *126*, 1229.
- [156] Amlani, I.; Rawlett, A. M.; Nagahara, L. A.; Tsui, R. K. *Appl. Phys. Lett.* **2002**, *80*, 2761.
- [157] Härtle, R.; Thoss, M. *Phys. Rev. B* **2011**, *83*, 115414.
- [158] Seideman, T. *J. Phys: Condens. Matter* **2003**, *15*, R521.
- [159] Mohn, F.; Repp, J.; Gross, L.; Meyer, G.; Dyer, M. S.; Persson, M. *Phys. Rev. Lett.* **2010**, *105*, 266102.
- [160] Hofmeister, C.; Coto, P.; Thoss, M. *J. Chem. Phys.* **2017**, *146*, 092317.
- [161] Weckbecker, D.; Coto, P. B.; Thoss, M. *Nano Lett.* **2017**, *17*, 3341–3346.
- [162] Pozner, R.; Lifshitz, E.; Peskin, U. *Nano Lett.* **2014**, *14*, 6244–6249.
- [163] Mitra, A.; Aleiner, I.; Millis, A. J. *Phys. Rev. B* **2004**, *69*, 245302.
- [164] Frederiksen, T.; Paulsson, M.; Brandbyge, M.; Jauho, A.-P. *Phys. Rev. B* **2007**, *75*, 205413.
- [165] Härtle, R.; Benesch, C.; Thoss, M. *Phys. Rev. B* **2008**, *77*, 205314.

- [166] Novotný, T. c. v.; Haupt, F.; Belzig, W. *Phys. Rev. B* **2011**, *84*, 113107.
- [167] Dash, L. K.; Ness, H.; Godby, R. W. *Phys. Rev. B* **2011**, *84*, 085433.
- [168] Utsumi, Y.; Entin-Wohlman, O.; Ueda, A.; Aharony, A. *Phys. Rev. B* **2013**, *87*, 115407.
- [169] Agarwalla, B. K.; Jiang, J.-H.; Segal, D. *Phys. Rev. B* **2015**, *92*, 245418.
- [170] Leijnse, M.; Wegewijs, M. R. *Phys. Rev. B* **2008**, *78*, 235424.
- [171] Erpenbeck, A.; Härtle, R.; Bockstedte, M.; Thoss, M. *Phys. Rev. B* **2016**, *93*, 115421.
- [172] Leijnse, M.; Wegewijs, M. R.; Flensberg, K. *Phys. Rev. B* **2010**, *82*, 045412.
- [173] Lü, J.-T.; Brandbyge, M.; Hedegård, P.; Todorov, T. N.; Dundas, D. *Phys. Rev. B* **2012**, *85*, 245444.
- [174] Li, B.; Wilner, E.; Thoss, M.; Rabani, E.; Miller, W. *J. Chem. Phys.* **2013**, *140*, 104110.
- [175] Jovchev, A.; Anders, F. B. *Phys. Rev. B* **2013**, *87*, 195112.
- [176] Segal, D.; Millis, A. J.; Reichman, D. R. *Phys. Rev. B* **2010**, *82*, 205323.
- [177] Simine, L.; Segal, D. *J. Chem. Phys.* **2013**, *138*, 214111.
- [178] Wang, H.; Pshenichnyuk, I.; Härtle, R.; Thoss, M. *The Journal of Chemical Physics* **2011**, *135*, 244506.
- [179] Wang, H.; Thoss, M. *The Journal of Chemical Physics* **2016**, *145*, 164105.
- [180] Jin, J.; Zheng, X.; Yan, Y. *J. Chem. Phys.* **2008**, *128*, 234703.
- [181] Härtle, R.; Cohen, G.; Reichman, D. R.; Millis, A. J. *Phys. Rev. B* **2013**, *88*, 235426.
- [182] Schinabeck, C.; Erpenbeck, A.; Härtle, R.; Thoss, M. *Phys. Rev. B* **2016**, *94*, 201407.
- [183] Dou, W.; Subotnik, J. E. *J. Chem. Theory Comp.* **2017**, *13*, 2430–2439.
- [184] Dou, W.; Subotnik, J. E. *J. Chem. Phys.* **2017**, *146*, 092304.
- [185] Dou, W.; Subotnik, J. E. *J. Chem. Phys.* **2016**, *145*, 054102.
- [186] Tanimura, Y.; Kubo, R. *J. Phys. Soc. Jpn.* **1989**, *58*, 101–114.
- [187] Tanimura, Y. *J. Phys. Soc. Jpn.* **2006**, *75*, 082001.
- [188] Ozaki, T. *Phys. Rev. B* **2007**, *75*, 035123.

- [189] Hu, J.; Xu, R.-X.; Yan, Y. *J. Chem. Phys.* **2010**, *133*, 101106.
- [190] Hu, J.; Luo, M.; Jiang, F.; Xu, R.-X.; Yan, Y. *J. Chem. Phys.* **2011**, *134*, 244106.
- [191] Mohr, J.-H.; Schmickler, W. *Phys. Rev. Lett.* **2000**, *84*, 1051.
- [192] Saalfrank, P.; Füchsel, G.; Monturet, S.; Tremblay, J. C.; Klamroth, T. In *Dynamics of Gas-Surface Interactions: Atomic-level Understanding of Scattering Processes at Surfaces*; Díez Muiño, R., Busnengo, H. F., Eds.; Springer Berlin Heidelberg: Berlin, Heidelberg, 2013; pp 323–348.
- [193] Arrachea, L.; Bode, N.; von Oppen, F. *Phys. Rev. B* **2014**, *90*, 125450.
- [194] Wilner, E.; Wang, H.; Cohen, G.; Thoss, M.; Rabani, E. *Phys. Rev. B* **2013**, *88*, 045137.
- [195] Ben-Nun, M.; Martinez, T. J. *J. Chem. Phys.* **1998**, *108*, 7244.
- [196] Heller, E. *J. Chem. Phys.* **1981**, *75*, 2923.
- [197] White, A.; Tretiak, S.; Mozyrsky, D. *Chem. Sci.* **2016**, *7*, 4905.
- [198] Bellonzi, N.; Jain, A.; Subotnik, J. E. *J. Chem. Phys.* **2016**, *144*, 154110.
- [199] Meyer, H.-D.; Miller, W. H. *J. Chem. Phys.* **1979**, *70*, 3214.
- [200] Sun, X.; Miller, W. H. *J. Chem. Phys.* **1997**, *106*, 6346.
- [201] Stock, G.; Thoss, M. *Phys. Rev. Lett.* **1997**, *78*, 578.
- [202] Shi, Q.; Geva, E. *J. Chem. Phys.* **2003**, *119*, 12063.
- [203] Kelly, A.; Brackbill, N.; Markland, T. E. *J. Chem. Phys.* **2015**, *142*, 094110.
- [204] Min, S. K.; Agostini, F.; Gross, E. *Phys. Rev. Lett.* **2015**, *115*, 073001.
- [205] Neria, E.; Nitzan, A. *J. Chem. Phys.* **1993**, *99*, 1109.
- [206] Subotnik, J. E.; Jain, A.; Landry, B.; Petit, A.; Ouyang, W.; Bellonzi, N. *Ann. Rev. Phys. Chem.* **2016**, *67*, 387.
- [207] Note that in Eq. 7.9, we have kept only the zeroth-order gradient expansion of the term  $\hat{\mathcal{L}}_{bs}\hat{\rho}$  in Eq. 7.6. As such, one might argue that Eq. 7.9 is not balanced: after all, in Eq. 7.9, we have included all first-order gradient corrections to the other term in Eq. 7.6,  $\left(-\frac{i}{\hbar}[\hat{H}_s, \hat{\rho}]\right)$ . To justify this apparent contradiction, let us consider an alternative route to the QCLE-CME (Eq. 7.9). Namely, consider the Liouville equation for the total density matrix (system nuclei plus system electrons plus electronic bath),

$\partial_t \hat{\rho}_{tot} = -i/\hbar [\hat{H}, \hat{\rho}_{tot}]$ . If we now take the Wigner transform, we find:

$$\begin{aligned} \partial_t \hat{\rho}_{tot}^{el} &= \frac{1}{2} \{ \hat{H}_{el}, \hat{\rho}_{tot}^{el} \} - \frac{1}{2} \{ \hat{\rho}_{tot}^{el}, \hat{H}_{el} \} - i/\hbar [\hat{H}_{el}, \hat{\rho}_{tot}^{el}] \\ &= \frac{1}{2} \{ \hat{H}_s^{el}, \hat{\rho}_{tot}^{el} \} - \frac{1}{2} \{ \hat{\rho}_{tot}^{el}, \hat{H}_s^{el} \} - i/\hbar [\hat{H}_s^{el}, \hat{\rho}_{tot}^{el}] - i/\hbar [\hat{H}_c, \hat{\rho}_{tot}^{el}] - i/\hbar [\hat{H}_b, \hat{\rho}_{tot}^{el}] \end{aligned}$$

Here, we have invoked the Condon approximation, i.e. the fact that  $\hat{H}_c$  does not depend on position in Eq. 7.4. At this point, we apply perturbation theory and trace over the bath, defining  $\hat{\rho}_{el} \equiv tr_b(\hat{\rho}_{tot}^{el})$ . Doing so, we find that the latter term  $(i/\hbar [\hat{H}_c, \hat{\rho}_{tot}^{el}])$  yields the term  $\hat{\mathcal{L}}_{bs}^{el}(\mathbf{R}) \hat{\rho}_{el}(t)$  in Eq. 7.9. Thus, the original zeroth order gradient expansion can be justified by assuming the Condon approximation and taking the limit of slow classical nuclei and fast electrons, such that electronic relaxation occurs at one instantaneous nuclear configuration.

- [208] Sifain, A. E.; Wang, L.; Prezhdo, O. V. *J. Chem. Phys.* **2016**, *142*, 224102.
- [209] Lindblad, G. *Commun. Math. Phys.* **1976**, *48*, 119–130.
- [210] Jain, A.; Alguire, E.; Subotnik, J. E. *J. Chem. Theory Comp.* **2016**, *12*, 5256.
- [211] Landry, B. R.; Falk, M. J.; Subotnik, J. E. *J. Chem. Phys.* **2013**, *139*, 211101.
- [212] Dou, W.; Miao, G.; Subotnik, J. E. *Phys. Rev. Lett.* **2017**, *119*, 046001.
- [213] Smith, B. B.; Hynes, J. T. *J. Chem. Phys.* **1993**, *99*, 6517–6530.
- [214] Ibach, H.; Mills, D. L. *Electron energy loss spectroscopy and surface vibrations*; Academic press, 2013.
- [215] Zhu, X.-Y. *Ann. Rev. Phys. Chem.* **2002**, *53*, 221–247.
- [216] Bruot, C.; Hihath, J.; Tao, N. *Nat. Nanotechnol.* **2012**, *7*, 35–40.
- [217] Ryabinkin, I. G.; Izmaylov, A. F. *J. Phys. Chem. Lett.* **2017**, *8*, 440–444.
- [218] Füchsel, G.; Klamroth, T.; Montureta, S.; Saalfrank, P. *Phys. Chem. Chem. Phys.* **2011**, *13*, 8659.
- [219] Struck, L. M.; Richter, L. J.; Buntin, S. A.; Cavanagh, R. R.; Stephenson, J. C. *Phys. Rev. Lett.* **1996**, *77*, 4576.
- [220] Maurer, R. J.; Askerka, M.; Batista, V. S.; Tully, J. C. *Phys. Rev. B* **2016**, *94*, 115432.
- [221] Luntz, A. In *Chemical Bonding at Surfaces and Interfaces*; Nilsson, A., Pettersson, L. G., Norskov, J. K., Eds.; Elsevier: Amsterdam, 2008; pp 143 – 254.

- [222] Luntz, A.; Persson, M.; Wagner, S.; Frischkorn, C.; Wolf, M. *J. Chem. Phys.* **2006**, *124*, 244702.
- [223] Luntz, A. C.; Persson, M. *J. Chem. Phys.* **2005**, *123*, 074704.
- [224] Persson, M.; Hellsing, B. *Phys. Rev. Lett.* **1982**, *49*, 662–665.
- [225] Hellsing, B.; Persson, M. *Phys. Scripta* **1984**, *29*, 360.
- [226] Persson, B.; Persson, M. *Solid State Commun.* **1980**, *36*, 175 – 179.
- [227] Allen, P. B. *Phys. Rev. B* **1972**, *6*, 2577–2579.
- [228] Mizielinski, M. S.; Bird, D. M.; Persson, M.; Holloway, S. *J. Chem. Phys.* **2005**, *122*, 084710.
- [229] Esposito, M.; Ochoa, M. A.; Galperin, M. *Phys. Rev. B* **2015**, *92*, 235440.
- [230] Dou, W.; Subotnik, J. E. *Phys. Rev. B* **2017**, *96*, 104305.
- [231] Martin, R. M.; Reining, L.; Ceperley, D. M. *Interacting Electrons: Theory and Computational Approaches*; Cambridge University Press, 2016.
- [232] d’Agliano, E. G.; Kumar, P.; Schaich, W.; Suhl, H. *Phys. Rev. B* **1975**, *11*, 2122–2143.
- [233] Daligault, J.; Mozyrsky, D. *Phys. Rev. E* **2007**, *75*, 026402.
- [234] Yoshimori, A.; Motchane, J.-L. *Jpn., and J. Phys. Soc.* **1982**, *51*, 1826–1833.
- [235] Plihal, M.; Langreth, D. C. *Phys. Rev. B* **1999**, *60*, 5969.
- [236] McClain, J.; Sun, Q.; Chan, G. K.; Berkelbach, T. C. *arXiv:1701.04832* **2017**,
- [237] Deslippe, J.; Samsonidze, G.; Strubbe, D. A.; Jain, M.; Cohen, M. L.; Louie, S. G. *Comput. Phys. Comm.* **2012**, *183*, 1269–1289.
- [238] Mori, H. *Progr. Theoret. Phys.* **1965**, *33*, 423–455.
- [239] Zwanzig, R. *Phys. Rev.* **1961**, *124*, 983–992.
- [240] Berne, B. J.; Pecora, R. *Dynamic light scattering: with applications to chemistry, biology, and physics*; Courier Corporation, 2000.
- [241] Romero-Rochin, V.; Oppenheim, I. *Physica A* **1989**, *155*, 52–72.
- [242] Romero-Rochin, V.; Orsky, A.; Oppenheim, I. *Physica A* **1989**, *156*, 244–259.
- [243] Toutounji, M.; Kapral, R. *Chem. Phys.* **2001**, *268*, 79–89.
- [244] Meir, Y.; Wingreen, N. S. *Phys. Rev. Lett.* **1992**, *68*, 2512–2515.

- [245] Hybertsen, M. S.; Louie, S. G. *Phys. Rev. B* **1986**, *34*, 5390–5413.
- [246] Rohlfing, M.; Louie, S. G. *Phys. Rev. B* **2000**, *62*, 4927–4944.
- [247] McClain, J.; Lischner, J.; Watson, T.; Matthews, D. A.; Ronca, E.; Louie, S. G.; Berkelbach, T. C.; Chan, G. K.-L. *Phys. Rev. B* **2016**, *93*, 235139.
- [248] Ouyang, W.; Dou, W.; Jain, A.; Subotnik, J. E. *J. Chem. Theory Comp.* **2016**, *12*, 4178–4183.
- [249] Hammes-Schiffer, S.; Soudackov, A. V. *J. Phys. Chem. B* **2008**, *112*, 14108–14123.
- [250] Krüger, B. C.; Meyer, S.; Kandratsenka, A.; Wodtke, A. M.; Schäfer, T. *J. Phys. Chem. Lett.* **2016**, *7*, 441–446.
- [251] Maurer, R. J.; Jiang, B.; Guo, H.; Tully, J. C. *Phys. Rev. Lett.* **2017**, *118*, 256001.
- [252] Rittmeyer, S. P.; Ward, D. J.; Gütlein, P.; Ellis, J.; Allison, W.; Reuter, K. *Phys. Rev. Lett.* **2016**, *117*, 196001.
- [253] Kisiel, M.; Gnecco, E.; Gysin, U.; Marot, L.; Rast, S.; Meyer, E. *Nat. Mater.* **2011**, *10*, 119–122.
- [254] Langer, M.; Kisiel, M.; Pawlak, R.; Pellegrini, F.; Santoro, G. E.; Buzio, R.; Gerbi, A.; Balakrishnan, G.; Baratoff, A.; Tosatti, E.; Meyer, E. *Nat. Mater.* **2014**, *13*, 173–177.
- [255] Kennes, D. M.; Wilner, E. Y.; Reichman, D. R.; Millis, A. J. *Nat. Phys.* **2017**, *13*, 479–483.
- [256] Chen, H.-T.; Cohen, G.; Millis, A. J.; Reichman, D. R. *Phys. Rev. B* **2016**, *93*, 174309.
- [257] Zwanzig, R. *Physica* **1964**, *30*, 1109–1123.
- [258] Jauho, A. P. Introduction to the Keldysh Nonequilibrium Green Function Technique. 2016; <https://nanohub.org/resources/1877>.
- [259] Dou, W.; Subotnik, J. E. *Phys. Rev. B* **2018**, *97*, 064303.
- [260] Liu, Z.-F.; Egger, D. A.; Refaely-Abramson, S.; Kronik, L.; Neaton, J. B. *J. Chem. Phys.* **2017**, *146*, 092326.
- [261] Flynn, G. W.; Parmenter, C. S.; Wodtke, A. M. *J. Phys. Chem.* **1996**, *100*, 12817–12838.
- [262] Li, S.; Guo, H. *J. Chem. Phys.* **2002**, *117*, 4499–4508.
- [263] Rittmeyer, S. P.; Bukas, V. J.; Reuter, K. *Advances in Physics: X* **2018**, *3*, 1381574.

- [264] Juaristi, J. I.; Alducin, M.; Muiño, R. D.; Busnengo, H. F.; Salin, A. *Phys. Rev. Lett.* **2008**, *100*, 116102.
- [265] Zang, Y.; Pinkard, A.; Liu, Z.-F.; Neaton, J. B.; Steigerwald, M. L.; Roy, X.; Venkataraman, L. *J. Am. Chem. Soc.* **2017**, *139*, 14845–14848.
- [266] Jia, C. et al. *Science* **2016**, *352*, 1443–1445.
- [267] Jorn, R.; Seideman, T. *Acc. Chem. Res.* **2010**, *43*, 1186–1194.
- [268] Pluecker, T.; Wegewijs, M. R.; Splettstoesser, J. *Phys. Rev. B* **2017**, *95*, 155431.
- [269] Sarandy, M. S.; Lidar, D. A. *Phys. Rev. A* **2005**, *71*, 012331.
- [270] Tully, J. C. *Ann. Rev. Phys. Chem.* **2000**, *51*, 153.
- [271] Future work should also address the role of el-el interactions under nonequilibrium condition. In such a case, our approach of incorporating the total Hamiltonian (Eqs. 10.21-10.24) into a larger Hamiltonian with an outer bath (Eq. 10.51) may not be appropriate. That being said, the von Oppen NEGF approach<sup>[80]</sup> will also be difficult to apply with el-el interactions. Nevertheless, we have every reason to believe that the QCLE friction (Eq. 10.1) will be appropriate. A recent article might offer one approach to test this conjecture<sup>[272]</sup>; scattering theory<sup>[115]</sup> might offer another.
- [272] Hopjan, M.; Stefanucci, G.; Perfetto, E.; Verdozzi, C. *arXiv:1712.08061* **2017**,